TU Delft

Delft University of Technology

Numerical Analysis and Experimental Verification of Stresses Building up in Microelectronics Packaging

Rezaie Adli, Ali

DOI
10.4233/uuid:fc197d29-f9bd-4b0e-a4d5-485344d8d429

Publication date
2017

Document Version
Final published version

Citation (APA)
Rezaie Adli, A. (2017). *Numerical Analysis and Experimental Verification of Stresses Building up in Microelectronics Packaging*. [Dissertation (TU Delft), Delft University of Technology].
https://doi.org/10.4233/uuid:fc197d29-f9bd-4b0e-a4d5-485344d8d429

Important note
To cite this publication, please use the final published version (if applicable).
Please check the document version above.

Copyright
Other than for strictly personal use, it is not permitted to download, forward or distribute the text or part of it, without the consent of the author(s) and/or copyright holder(s), unless the work is under an open content license such as Creative Commons.

Takedown policy
Please contact us and provide details if you believe this document breaches copyrights.
We will remove access to the work immediately and investigate your claim.

This work is downloaded from Delft University of Technology.
For technical reasons the number of authors shown on this cover page is limited to a maximum of 10.

Numerical Analysis and Experimental Verification of Stresses Building up in Microelectronics Packaging

Proefschrift

Ter verkrijging van de grad van doctor
aan de Technische Universiteit Delft,
op gezag van de Rector Magnificus Prof. ir. K.C.A.M. Luyben
voorzitter van het College voor Promoties,
in het openbaar te verdedigen op donderdag 19 januari 2017 om 12:30 uur

door

Ali R. REZAIE ADLI

Master of Science in Mechanical Engineering, Boğaziçi University, Istanbul, Turkey
geboren te Tabriz, Iran

This dissertation has been approved by the
Promotors: Prof. dr. ir. K.M.B. Jansen and Prof. dr. ir. L.J. Ernst

Composition of the doctoral committee:

Rector Magnificus	chairman
Prof. dr. ir. K.M.B. Jansen	Delft University of Technology, promotor
Prof. dr. ir. L.J. Ernst	Delft University of Technology, promotor

Independent members:

Prof. dr. A. Wymyslowski	Wroclaw University of Science and Technology, Poland
Prof. dr. D. Yang	Guilin University of Electronic Technology, China
Prof. dr. U. Staufer	Delft University of Technology
Prof. dr. G.Q. Zhang	Delft University of Technology
Prof. dr. C.C.L. Wang	Delft University of Technology, reserve member

ISBN/EAN 978-94-6186-777-3
Copyright © 2017 by A.R. Rezaie Adli
All rights reserved. No part of this publication may be reproduced, stored in a retrieval system, or transmitted, in any form or by any means, electronic or mechanical, including photocopying, recording or otherwise, without the prior written permission of the author.
Cover by Ali R. Rezaie Adli
Printed by Ridderprint, the Netherlands

To my family

Summary

Thermosetting polymers are extensively used in packaging of microelectronic components due to their unique mechanical, thermal and electrical properties. The packaging is a term used for inter-filling and encapsulation of the integrated circuits. The process results in residual stress build-up both in the fabrication process and later due to the cyclic thermo-mechanical loading during the operation of the electronic or electromechanical devices in which the encapsulated package is placed. Here, in this study the encapsulation induced stresses are investigated by splitting the process in three stages: low viscous filling, isothermal curing and transient cooling. The residual stresses are initiated by the crosslinking (curing) of the epoxy polymer. Crosslink formation is a property of the thermosetting polymers which is accompanied by stiffness build-up and shrinkage. The encapsulation process is conducted at a high cure temperature (≈175^{o}C). The subsequent cooling to the ambient air temperature leads to further shrinkage of the cured polymer along with the other encapsulated package components. Furthermore, the mechanical properties of the cured polymer evolve from the rubbery state to the glassy state, passing through the transition region.

The encapsulation process is conducted using transfer molding such that the encapsulant epoxy compound melts at high mold temperature and is pushed by a plunger to cover the region that comprises the dies and interconnections.

Early studies on residual stress estimation rely on a cumbersome trial and error approach. These inefficient outdated methods have currently been replaced by the more reliable numerical methods which provide a cost effective and quick solution to predicting residual stresses. By performing a parametrical analysis these stresses may be reduced for each stage of molding. The key to a reliable virtual thermo-mechanical prototyping lies in a reliable representation of the material behavior of the polymer. In this thesis, the time, temperature and conversion dependent behavior of the epoxy molding compound (EMC) is determined experimentally. The kinetic characterization of the EMC is obtained after conducting multiple heating rate scans of initially uncured samples in the DSC (differential scanning calorimeter). The autocatalytic model of Kamal and Sourour is used to fit the calculated conversion rate of the detected data. Furthermore, the conversion and glass transition relation is established by constant heating rate scans of the isothermally cured

samples. The total volume shrinkage is determined using a PVT test set-up where a sample of the EMC is heated and cured isothermally at a temperature close to its glass transition temperature. The specific volume change between the start and end of the curing process is considered as the total cure shrinkage. Applying the previously obtained kinetic model to the volume shrinkage data showed that the shrinkage is quite linear with conversion. The coefficient of thermal expansion and bulk modulus of the same sample are also determined with the PVT equipment. A modified version of the Tait model is used to model the volume change as a function of pressure and temperature.

The aforementioned volume change characteristic of the thermosetting polymer is accompanied by variations in mechanical properties. The epoxy compound is initially a cylindrical piece of solid pellet which upon heating is transformed to a processable, low viscosity fluid. The linear growth of chains is followed by branching and crosslinking. And as the polymerization proceeds, the molecular weight of the EMC rises and at some point the polymer loses its ability to flow and is transformed into a rubbery gel. This stage is called the gel point and beyond this point some portion of the shrinkage stresses do no longer relax completely. The remaining stress in the cured epoxy is referred as the residual stress and it is accumulated during curing and subsequent cooling. The gel point and the viscosity of the EMC used in this study are measured in a parallel plate viscometer. Determination of the gel point is not based on the cross-over point of the storage and loss moduli but a new approach is proposed which is empirically based on the shape of the log viscosity conversion curve. This approach provides a reproducible gel point value, regardless of the test temperature.

A thermosetting polymer will behave differently under various processing conditions and initial conversion levels. Unfortunately, the material data sheets which are mostly provided by the suppliers lack the ability to show the whole picture. Therefore, the material models and parameters discussed so far are an essential part for any reliable numerical analysis comprising the various process parameters and stages. The transfer molding procss consists of a filling, curing and packing stage and in each of these steps the residual stresses need to be determined.

The shear stress of the epoxy melt during filling is determined numerically by assuming a Newtonian flow with conversion and temperature dependent viscosity. The flow front advancements for two different cavity geometries are investigated at selected nodal points. One of the geometries is based on the validation experiments used later in this study and the other is the double stacked die array configuration often used in industry to increase the IC packaging density. In the simulations the viscosity of the epoxy melt, shear rate and the shear stress at the surface of the die and board are calculated as well as conversion and pressure distribution at the end of filling. This shows that the thin gaps between the dies are

the weak spots which are vulnerable to air traps due to the extreme slow flow advancement in these regions. This local slow filling results in higher conversion and viscosity since the epoxy melt is accumulated at these regions.

Apart from this, a simplified analytical model is used to predict cure- and cooling induced residual stresses. In the cure stage material is assumed to be rubbery elastic with a conversion dependent modulus, which is modeled based on the Adolf and Martin scaling theory. In the cooling stage a constant modulus is assumed in combination with a temperature dependent expansion coefficient based on the aforementioned Tait model.

Next a simulation was performed of a two dimensional geometry of a real encapsulation process comprising a board, copper die pad, die attach, die and the epoxy molding encpasulant. In the cooling stage the material was modeled as viscoelastic based on the Generalized Maxwell model. A comparison showed that the thus calculated stresses were comparable to those obtained by the analytical model.

As an experimental validation a novel approach is used in which a stress chip is overmolded and the stresses were monitored in situ. It turned out that the stress chips could not produce reliable results at high curing temperatures but for the lower temperature tests were able to measure stresses during the molding and curing stages and continued to work after mold opening. The normal stress distributions at each stage are derived from the data and were seen to compare well with the analytically and numerically determined values.

Table of Contents

Abbreviations

IC	Integrated Circuit
1D	One Dimensional
2D	Two Dimensional
3D	Three Dimensional
SiP	System in Package
PCB	Printed Circuit Board
EMC	Epoxy Molding Compound
CTE	Coefficient of Thermal Expansion
DSC	Differential Scanning Calorimeter
MHR	Multiple Heating Rate
T_g	Glass Transition Temperature
DMA	Dynamic Mechanical Analysis
WLF	Williams-Landen-Ferry
TTS	Time-Temperature Superposition
VOF	Volume of Fluid
RIM	Reaction Injection Molding
PI	Polyimide
MEMS	Microelectromechanical Systems
nMOS	n channel MOSFET
pMOS	p channel MOSFET
MOSFET	Metal Oxide Semiconductor Field Effect Transistor

Chapter 1

Introduction

1.1. Introduction

This thesis comprises a thorough study of the electronic packaging process and application of various experimental and numerical methods to estimate the process induced residual stress. The electronic package is the term used to describe the housing that covers the integrated circuits and interconnections. The reliability of the package depends on the residual stresses built up during the packaging process.

The most widely implemented technique in electronic packaging is the encapsulation by the transfer molding process. In the transfer molding the integrated circuits and electronic components are placed in a mold cavity. The epoxy molding compound is loaded, heated and pushed by a plunger, passing through the runners and gates to the cavity in which it encapsulates the dies. The mold is released after the cure stage where the thermosetting epoxy cures until the opening of the cavity. The epoxy compound is usually cured to a conversion degree of higher than 90%. The whole process results in residual stress build-up which will deteriorate the mechanical properties of the encapsulated package.

The optimization of the encapsulation process by trial and error is not so easy due to the complex interrelation between various mechanical, physical, kinetic and thermal properties of epoxy material under different processing conditions. Moreover, the complex and thin geometry of the package and the interdependent filling, curing and subsequent cooling

stages of the transfer molding make this approach totally inefficient. Computer aided engineering, on the other hand, is an effective tool for numerical analysis of the residual stress building up in the packaging process. Realistic numerical simulation of the polymer encapsulation requires well-defined material models which can be obtained by a series of experimental characterization methods addressing the time and temperature dependent behavior of the compound.

The main purpose of this thesis is to predict the residual stresses evolving during the packaging process. Therefore, the residual stresses are analyzed numerically and experimentally.

1.2. Electronic Packaging

The first electronic packages were hermetic either with ceramic or metallic sealing material. After the introduction of various electronic equipments into the consumers daily life a cheaper and a faster method for packaging of electronic components in mass production was required. This new method is named plastic encapsulation in which the electronic components are encapsulated by an epoxy molding compound, EMC. The favorable mechanical properties of the encapsulant, along with lower cost, smaller shape, lighter weight and possibility of rapid fabrication of parts made the plastic encapsulation indispensable for the electronic industry.

After the introduction of plastic encapsulation in the 50s the market gradually shifted to this newly developed technique and by the new millennium 99% of the total ICs had being encapsulated by plastic packaging. The ceramic packaging which once used as a reliable packaging method for most of the electronics now is only used in some military and aerospace equipment where the harsh process conditions require the packaging materials other than epoxies.[1]

The main objective of the packaging is to protect the die, interconnections and the other exposed internal components from environmental and application resulted hazards. Some of the protections provided by the plastic encapsulation can be classified as;

- Mechanical support and dimensional stability
- Resistance to humidity
- Heat dissipation during operation
- Environmental protection
- Radiation protection
- Electrical insulation
- Protection from mechanical damage during handling

The types of electronic packaging are determined based on the interconnection of the die and board and other components. Zero level refers to the packaging in which the die is encapsulated after cutting out of wafer and attaching to a lead frame using an electrically insulated epoxy adhesive. When the die is connected to a PCB prior to packaging it is called second level packaging. Third level packaging is the encapsulation of PCB to a motherboard. The packaging of motherboard inside the electronic device like a tablet is called the fourth level.

1.2.1. 3D Packaging

The packaging technology has been evolved by the development of new IC schemes and technological advances in packaging. The market trend is shaping the consumer electronics nowadays much faster than previous decades due to the competition in the electronic industry. Consumer expectations are towards lighter and slimmer products like laptop computers, smartphones and digital cameras while the functionality should be kept up with another competition relying on an observational law named Moor's law [2], which acts as a driving force pushing the limits of the available transistor manufacturing technology. The latest advances in transistor production technology led to transistors each manufactured from a single molecule surrounded by 12 atoms [3].

The efficiency of the packaging is calculated by the ratio of the area of the silicon chip to that of the substrate. The term is called the silicon efficiency. The increasing demand for miniaturization of electronic devices with denser component structure had led to the new stacked chip scale packaging technologies that save space by stacking separate integrated circuits in a single package. Currently, electronic industry drives towards System in Package (SiP) which is a number of integrated circuits enclosed in a single package or module. Exceeding the 100% silicon efficiency can be achieved by this new 3D packaging technique in which the number of dies are stacked and interconnected vertically by fine off-chip wires or via solder ball arrays. The 3D package design provides a faster signal transfer and a denser and therefore a smaller package.

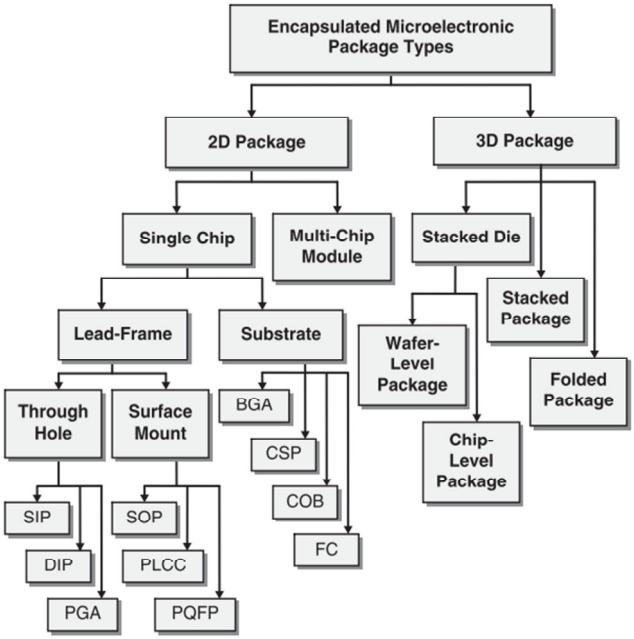

Figure 1.1 Microelectronic Packaging classification [1]

1.2.2. Encapsulant and Encapsulation

Polymers can be classified as thermoplastics, thermosets and elastomers. Although thermoplastics are environmentally sustainable due to recyclability when heated, they require high mold pressure and temperature for encapsulation. Elastomers, on the other hand, are easily deformable and therefore not suitable for protection purposes. Hence, thermosets are the most widely used polymers for encapsulation.

The thermosetting epoxies have some superior qualities over other plastic for encapsulation. A few of these properties can be given as;

- Resistance to heat
- High adhesion
- Resistance to solvents
- High fatigue resistance
- Ease of manufacturability due to lower viscosity at high temperature molding process
- Irreversibility of the crosslink mechanism (although it is a drawback considering the sustainability and environmental effects)
- Flame resistance

Epoxy compound

As the name implies the epoxy molding compound contains an epoxy resin but it is not the main ingredient as it is expected. Nonetheless, while the epoxy content accounts for less than 10%, the viscoelastic mechanical properties of the compound are shaped by it. Epoxy resin's core purpose is more structural such that it acts as a matrix to hold the filler particles together. Fused silica is generally used as a filler additive which contributes by improving the physical properties of the package. Flame retardants, stress relief agents, mold release agents, coloring agents, ion trapping agents, and coupling agents are the other additives contributing to enhance the attributed properties of the EMC.

Filler

The physical and electrical properties of the thermosetting epoxy molding compound, EMC, are determined by the percentage of filler content. Epoxy resin comprises 6 to 10% of a typical molding compound. The bulk part of the EMC is the filler which roughly covers the 60 to 90% of the EMC. Each additive in the molding compound has a certain function. The filler lowers the thermal shrinkage associated with the cooling after molding. Usually the epoxy compound has the highest thermal expansion in the package. So, the residual stress can be lowered by addition of filler to the epoxy compound. Some of the other crucial physical properties of the filler that enhances the EMC's mechanical behavior are; higher thermal conductivity after cure, lower water absorption, cost reduction, higher stiffness. The fluidity and moldability of the epoxy melt at high temperatures is affected by the quality of the fillers. The particle size and shape together with the molding cavity geometry determines the quality of the package and reliability of the final product. The higher the particle size the lower the stiffness. 3D packaging, for example, requires a finer particle size and a homogenous resin to be able to encapsulate the complex geometry without any undesirable reliability issue. The kinetic behavior of the resin is not affected by the filler content, on the other hand. The glass transition and heat of reaction are not changed significantly by the introduction of filler or other additives [1].

Polymerization

One phenomenon that distinguishes thermosets from thermoplastics is an irreversible process of crosslink formation such that the polymer is transformed from a liquid at high temperature to a solid state, gradually. During this transition the physical behavior of the material changes drastically. The curing mechanism is activated and accelerated by addition of other additives such as hardener and accelerator. The reaction mechanism can be classified as either addition or catalytic. At the start of crosslink formation monomer units react with a reactive free radical to form a reactive monomer. The reaction of monomers continues until collision of reactive monomer with another reactive monomer. In addition

type reaction the hardener behaves as a substance linking the monomers leading to a polymer network while in catalytic reaction it promotes the polymerization of the epoxy resin for crosslink formation.

The crosslinking of a thermosetting polymer is a process that consists of several steps. It starts with the formation of linear chains. As the reactions continues the linear chains begin to branch and these branches are irreversibly connected together forming a crosslink network. The molecular density accelerates that leads to a complete crosslinked polymer with an infinite molecular weight [4].

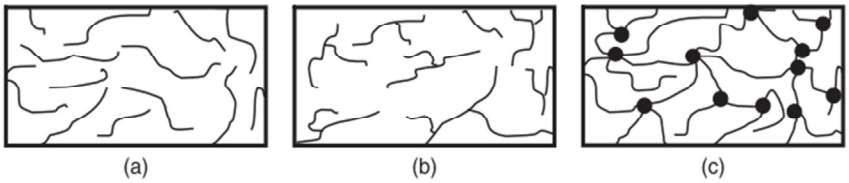

Fig a) Linear b) Branched c) Crosslinked

Residual stress build-up during molding

The stresses in multilayer structures can be decomposed into mechanical, thermal and cure induced parts. Among them, the thermal and the cure stresses can be defined as residual stresses. In curing epoxy systems, the cure induced stress refers to crosslinking originated stresses or more specifically it can be considered as the cure stress which arises as a result of curing shrinkage of the epoxy. Thermal stresses, on the other hand, are generated due to shrinkage mismatch of the adjacent layers when the multilayer structure is subjected to temperature variations.

During cure, under constrained boundary conditions the EMC shrinks which leads to a compressive force on the surface of the die beneath it. Furthermore, at the end of cure when the mold is opened, the resulted chemical shrinkage bends the multi-layered structure. Later, during cooling, the whole encapsulated package shrinks with different shrinkage levels for each component, due to the temperature drop. Hence, the mismatch between the strains of the adjacent layers leads to bending and stress build up under constrained boundary conditions.

Process Parameters

The factors that play a role in final package quality (for the same geometry and gate numbers and positions) can be investigated in two categories; Processing parameters and material parameters. Latter is about the composition of the EMC which determines the

mechanical and thermal behavior in various processing conditions. In this thesis the mechanical and physical behavior of the EMC is studied under various processing conditions.

The key processing parameters are time, temperature and pressure. Pressure is assumed constant during cure. Initially, after mold clamping the cavity pressure is close to the atmospheric pressure and when the filling starts the pressure rises maximum one order of magnitude to around 1MPa (see chapter 7). The rise in viscosity at this stage is negligible and does not affect the flow rate. Therefore, as the melt advances through the cavity the cavity pressure remains more or less stable. At the end of filling (packing) the pressure rises to force the melt to the cavity which is almost full. Later, during cure stage the pressure remains stable until the release of mold clamp. Hence, the cure time and the mold temperature are the essential independent process variables affecting the residual stresses. The viscosity, conversion, shrinkage and material stiffness all depend on these parameters.

1.3. Outline of the thesis

This thesis starts with material characterization of two epoxy molding compounds with slightly different filler contents. Then the viscoelasticity is introduced and the mechanical properties of the epoxy compounds are determined. The measured behaviors are modeled and the encapsulation stages are studied independently. The residual stresses generated during cure and cooling stages are estimated numerically using two approaches. Later, the numerical results are verified experimentally using a novel experimental technique.

Chapter 2 comprises the experimental techniques applied for the cure kinetics and volumetric characterization of the EMC. The measurements and the models are given in detail. The cure shrinkage, conversion rate, CTE and bulk modulus models are introduced and the two epoxy compounds are compared.

Chapter 3 covers the viscoelastic characterization of the epoxy compounds. The dynamic mechanical measurements are discussed and the models representing the viscosity and relaxation modulus of the EMC are given.

Chapter 4 focuses on the encapsulation. The governing equations of flow and the boundary conditions are given. The mesh model and the undertaken numerical approach are presented. The flow front advancement along with conversion, viscosity and shear stress distribution in the cavity are determined using a commercial software package Moldex3D.

Chapter 5 presents a simple 1D analytical approach for residual stress estimation in packaging. The incremental elastic approach is applied for cure induced and cooling induced stress determination. Conversion dependent cure stage and temperature dependent

cooling stages are studied independently. Four temperatures and 3 initial conversions are investigated.

Chapter 6 is about the 2D numerical study conducted for residual stress estimation during cure and cooling. The epoxy compound is assumed as elastic during cure and viscoelastic in cooling. The results were compared with the predicted stress obtained in chapter 5.

Chapter 7 covers the novel experimental method proposed for real time stress measuring during packaging. The piezoresistivity is described and the board designed specifically for this experiment is introduced. The resulted stress data are evaluated in detail and compared with the corresponding 1D and 2D numerical results.

Reference

[1] H. Ardebili and M. G. Pecht, *Encapsulation technologies for electronic applications*, First edit. 2009.

[2] G. E. Moore, "Cramming more Components onto Integrated Circuits," *Electronics*, vol. 38, no. 8, 1965.

[3] J. Martínez-Blanco, C. Nacci, S. C. Erwin, K. Kanisawa, E. Locane, M. Thomas, F. von Oppen, P. W. Brouwer, and S. Fölsch, "Gating a single-molecule transistor with individual atoms," *Nat. Phys.*, vol. 11, no. 8, pp. 640–644, 2015.

[4] E. A.Turi and R. B. Prime, "Thermal Characterization of Polymeric Materials, Thermosets." pp. 1380–1746.

Chapter 2

Cure Kinetics and Volumetric Characterization and Modeling of the Epoxy Molding Compounds

2.1. Introduction

The reliability of any numerical simulation containing polymers depends largely on the accuracy of the constitutive equations governing the mechanical behavior of the modeled system and also on the material models which are representing the changes in the physical properties as a result of thermo-mechanical processing conditions.

This chapter primarily comprises the applied experimental techniques and the associated models fitted for quantitative representation of thermo-mechanical and kinetic behavior of the epoxy thermosetting compounds used in this study. In this thesis, the data obtained by the developed numerical schemes are verified with the experimental study. The reliability of the numerical approach requires extensive quantitative information on material behavior under various processing conditions.

The main material parameters required for a reliable molding process are; conversion (crosslinking), viscosity, cure (chemical) shrinkage, thermal expansion coefficient and elastic and viscoelastic moduli of the thermosetting epoxy molding compound. Conversion is temperature and time dependent, while viscosity is conversion and temperature dependent. Thermal and chemical contractions are temperature and conversion dependent, respectively and furthermore, relaxation moduli functions are more complex and aside from

temperature and conversion dependency they acquire time dependent behavior for the transitional zone which is described in detail in chapter 3. The interrelation between various model parameters can be addressed by implementing the kinetic, physical and thermal characterization techniques which are investigated in detail in chapters 2 and 3. Among the parameters affecting the molding process, the conversion and volumetric variables are studied explicitly in this chapter.

In this thesis, the two fast curing epoxy polymers are evaluated based on the characterization techniques. One is a compound supplied by Hitachi with a filler content of 55% in volume and 69.5% in weight. The other compound is supplied by Sumitomo with a slightly higher filler content of 80% in weight. Both compounds are characterized and modeled, but one of them is selected to be used in the experimental molding study. The selection is based on the reproducibility of the measurements and the success in fitting of the models to the measured data.

The datasheets of both compounds provided by the suppliers are summarized in table 2.1. Note that none of the parameters in these datasheets are used in numerical studies. Instead, the material models obtained by the detailed characterization experiments are implemented for the corresponding material property.

Table 2.1 Material datasheet (the brand numbers are classified in this project*)
*** JEMSiP "Joint Equipment & Manufacturing for System in Package"**

		Hitachi [redacted]	Sumitomo [redacted]
Filler Content (in Ash)	weight%	69,5	80
Filler Content (in Ash)	vol%	55	Na
Gel Time	s	70	88
CTE-1	$x10^{-5}/^{o}C$	2,5	1,8
CTE-2	$x10^{-5}/^{o}C$	8	7,6
Young's Modulus	GPa	13	14,2
Specific Gravity	GPa	1,76	1,89
Water Absorption	%	0,55	0,24
Mold Shrinkage	%	0,8	0,38

2.2. Cure Kinetics

The chemical reaction of a thermosetting resin that results in the formation of a crosslinked network polymer structure is known as the conversion or curing process. The physical and mechanical properties of the epoxy polymer are dependent on the degree of cure. Therefore, understanding the kinetic behavior is important not only for modeling of the reaction rate

but also to optimize the process parameters and therefore to obtain and improve the mechanical quality of the end product.

There is substantial number of studies on the cure kinetics of thermosetting polymers. Although many of these studies have concentrated on the slow curing epoxy system, the necessity for characterization of fast curing epoxy compounds used in advanced electronics applications like underfill and encapsulation processes had led to in-depth experimental and numerical analysis of these fast curing epoxy compounds in the past decades [1]–[5]. The work of Fava can be considered as one of the pioneering studies in which the kinetic characterization of epoxy thermosetting polymers was investigated by comparing the three methods using Differential Scanning Calorimetry (DSC) [6]. The limitations and advantages of each method were investigated thoroughly in this work. A more recent study of Bilyeu is another work that covers the range of kinetic models and testing techniques for epoxy kinetic characterization [7].

The cure level has a significant effect on the mechanical behavior of the thermosetting polymer. Viscosity of the polymer melt during filling, viscoelastic moduli and chemical shrinkage all are affected by the degree of conversion of the epoxy compound. The molding temperature and cure time for the optimal package quality are reaction rate dependent aside from the epoxy polymer chemical composition. Therefore, a realistic modeling of the EMC curing reaction is an essential starting point for an accurate virtual representation of any molding process involving a thermosetting polymer.

Cure kinetics characterization can be performed in two ways: both mechanistic and phenomenological models have been used in the past. Mechanistic models are more cumbersome to implement since they require extensive knowledge of balance of species during reaction. Therefore, they require in-depth analysis of the chemistry of polymer crosslinking during cure. On the other hand, phenomenological models are generally preferred over the mechanistic ones due to the ease of measurements and faster evaluation of empirical data [1]–[5], [8]–[17]. DSC is the most widely accepted tool for phenomenological cure kinetics characterization of thermosetting polymers.

The transfer molding process of electronics encapsulation is conducted at relatively high isothermal temperatures (175^{o}C in most cases). Therefore, cure kinetic experiments should be able to predict the conversion rate at the specified process temperature. This is the temperature at which the actual transfer molding takes places. However, the measurements must sometimes be conducted at a lower temperature range since the high temperature experiments suffer from some drawbacks like fast curing of samples and losing the great portion of recordable data due to instrument sensitivity. Therefore, most of the isothermal cure kinetics measurements were conducted at lower temperatures where the recorded data

are more reliable. The accuracy is much higher for the tested temperatures and the data are later extrapolated and fitted to a kinetic model that covers the entire temperature range.

2.2.1. Differential Scanning Calorimetry

DSC is the most frequently utilized instrument in kinetic characterization of the polymeric compounds [1]–[6], [8], [9], [11], [16], [18], [19]. The basic working principle of DSC is based on indirect heat flow detection. The heat flow could be either to the sample (endothermic) or from the sample to the surrounding (exothermic) depending on the ongoing thermodynamic process, some of which are melting, glass transition, physical aging and polymerization.

Figure 2.1 shows a schematic of the DSC chamber where the heating takes place. The heating chamber, which is filled with nitrogen as a purge gas to avoid air oxidation and humidity, contains two heating plates. The cell containing a hermetically sealed epoxy compound is placed on the plate specified for the sample while the other plate is dedicated for an empty hermetically sealed cell. The empty cell is used as a reference such that the heat absorbed or released by the sample is obtained from the difference between the heating data of both cells. Sample weight is restricted to a minimum value of about 5mg due to limitation of instrument sensitivity and to a maximum sample weight of 15mg to minimize the thermal gradients inside the sample.

EMC cure is an exothermic process which leads to heat generation during the cross link network formation. The total heat generated by the epoxy curing is detected using DSC. The total heat generated up to time t is denoted by h. Then the degree of cure at time t is defined by

$$\xi(t) = \frac{h}{H_{tot}}, \qquad 2.1$$

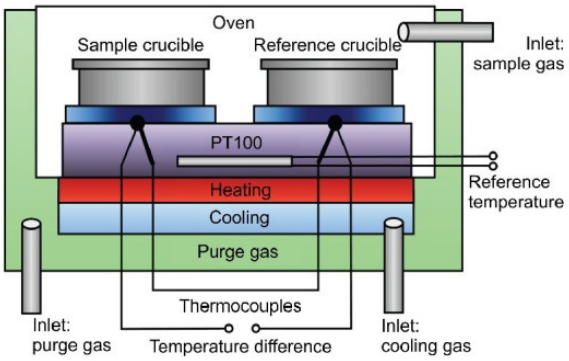

Figure 2.1 Schematic of a DSC heating chamber [20]

The framework of the analytical approach in DSC is based on the assumption that the heat released during the conversion of a sample is proportional to the conversion rate. In a fully reacted sample the integral of the exothermic heat flow gives the total heat of reaction which is considered as the basic property of a thermosetting polymer and should be determined experimentally, preferably by multiple heating rate measurements [21]. The described thermo-analytical approach can be expressed as a rate equation

$$\frac{d\xi}{dt} = \frac{1}{H_{tot}} \frac{dh}{dt}, \qquad 2.2$$

where dh is the heat flow from the sample and H_{tot} is proportionality constant representing the total heat released by the sample accompanying complete cure. ξ indicates the conversion level of a thermoset and $d\xi/dt$ denotes the rate of reaction.

2.2.2. Sample preparation

Prior to the experiments, samples had been stored in a freezer below -20°C to prevent any conversion. However, the effect of aging which was observed in some DSC measurements revealed that the samples had already been exposed to higher temperatures during transport. The storing temperature is well below the glass transition temperature (T_{g0}) of the uncured epoxy which is essential to avoid crosslink initiation.

The uncured samples were initially taken out to room temperature and pulverized or cut off into small sizes with a flat surface in order to assure a fully smooth contact area with the cell's wall in which they were placed. The higher the surface contact area, the faster the heat transfer to the sample, which results in smoother heat flow to the cells and hence a more precise measurement.

2.2.3. DSC methods

Reaction kinetics can be determined using three basic approaches: Two of these approaches involve isothermal curing of samples, either fully or partially. In the full reaction isothermal DSC method, the samples are rapidly heated to the specified isothermal temperature and cured until full conversion. During these experiments the heat flow is recorded as a function of time and later the total heat of reaction and the instantaneous heat of reaction are calculated by integrating the data with respect to time. The overall conversion degree can be obtained by using a range of isothermal cure temperatures covering the entire reaction region. There are some limitations in application of this method due to varying total heat data at different temperatures and unrecorded heat at low and high cure temperatures. That is why this technique is not used in the cure kinetics evaluations in this thesis. The second

isothermal method is the scanning of partially cured samples at a fixed heating rate such that the isothermal cure temperature and the cure time are predefined and an overall conversion pattern is obtained. The possibility to determine the glass transition of partially cured samples is another advantage of this method which will be described later. The most frequently applied method due to high accuracy of the recorded data is the non-isothermal multiple heating rate method. This approach requires a temperature scan of uncured samples at different heating rates.

In this study, the partially cured scanning method in conjunction with the multiple heating rate method were applied using a TA-Instruments DSC 2920. For simplicity, the second method is called the isothermal and the latter is named the Multiple Heating Rate (MHR) throughout this thesis.

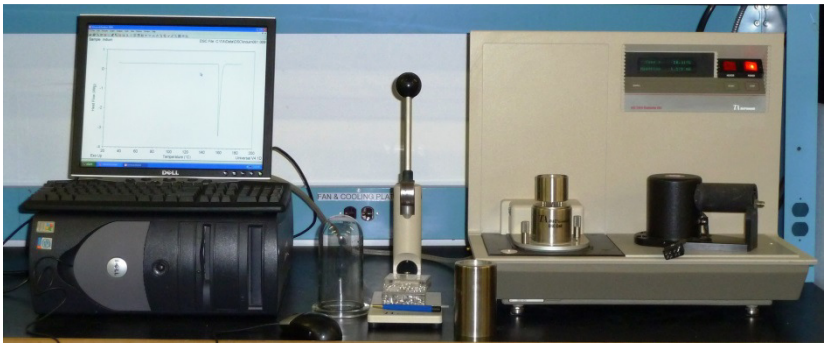

Figure 2.2 TA Instruments DSC 2920 and manual press for hermetic sealing

2.2.3.1. Isothermal method

In isothermal method the samples of the epoxy polymer are initially heated at various isothermal temperatures for preset durations. At the end of the specified cure time they are cooled down at a fast rate of 20°C/min to room temperature. Cooling down should be performed as quickly as possible to avoid any additional reaction. Especially at high cure temperatures the reaction rates are faster. The method proceeds by scanning of samples at a constant rate of 10°C/min such that the residual heat of reaction, that is, the remaining heat evolved for completion of cure, is obtained for each measurement. The difference between the total heat of reaction (which is obtained by the MHR method) and the residual heat of reaction gives the heat of reaction released by the sample during the preceding isothermal heating. Then, the degree of conversion for each isothermal test can be obtained by

$$\xi(t,T) = \frac{H_{tot} - H_{res}}{H_{tot}}. \qquad 2.3$$

Figure 2.3 shows a series of partially cured sample scans at 110°C for the selected time periods. The glass transition temperature can be observed as an endothermic shift in heat flow data. Theoretically, T_g increases towards a higher temperature at a higher degree of conversion and this phenomenon is clearly observable in figure 2.3 when the T_g of partially cured samples are compared.

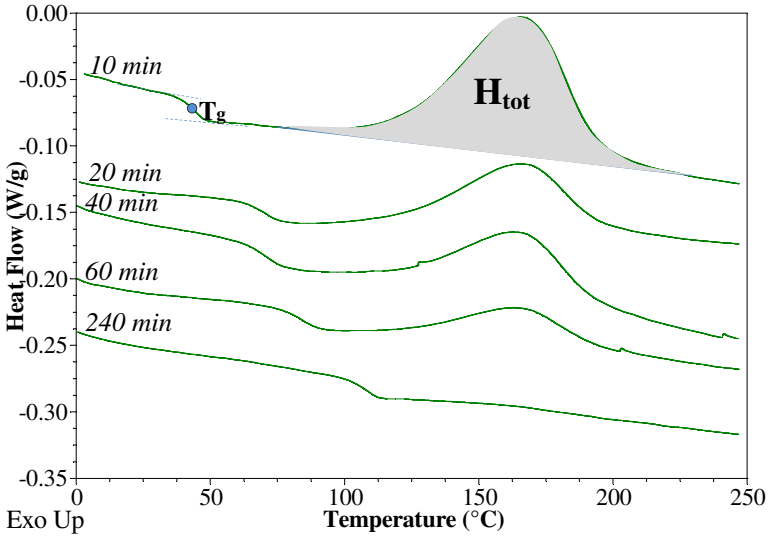

Figure 2.3 DSC scans of isothermally cured samples at 110°C for various cure times

Calculating the conversion using equation 2.3 is not reliable at high conversion levels, since the residual heat of reaction may not be detected above the conversion level of 95% [6]. At such higher conversion levels the recorded peak exotherm is small and it overlaps with the end portion of the highly rised T_g shift which makes it more difficult to detect the residual heat. Therefore, the residual heat data is not a reliable parameter for conversion detection at high conversion levels. However, T_g of partially cured samples can be used as a measure of conversion when the residual heat is not detectable. By definition, T_g is a transition of a polymeric material from a glassy state to a rubbery state while heating [21] and a direct relationship exists between the glass transition temperature and the degree of reaction. The glass transition temperature rises as the reaction approaches to full conversion and this relationship is independent of cure temperature. The increase of T_g as a result of crosslink formation is formulated by Di Benedetto in 1969 in his unpublished study and later

simplified by Couchman (1978) [22] and adapted by many other researchers [1]–[5], [8]–[17]. Plots of T_g data from the isothermal DSC measurements together with the numerical fit of the Di Benedetto equation (solid line) are given in figure 2.4.

$$\frac{T_g - T_{g0}}{T_{g\infty} - T_{g0}} = \frac{\lambda\,\xi}{1-(1-\lambda)\,\xi}, \qquad 2.4$$

Here T_{g0} and $T_{g\infty}$ represent the minimum and maximum values of T_g at uncured and fully cured stages, respectively. As can be seen in figure 2.3, T_g is not a single detectable point but rather a range representing a change in phase of the epoxy thermoset. The value of T_g is considered as a midpoint between the tangent line drawn to the start and end of endothermic transition region. λ is a structure dependent adaptable fitting parameter which is estimated as 0.55 for the Hitachi compound and 0.60 for the Sumitomo.

Table 2.2 Di Benedetto fitting parameters

Di Benedetto parameters	T_{g0}	$T_{g\infty}$	λ
Hitachi	31.33	113.9	0.55
Sumitomo	29.77	128.9	0.60

In figure 2.4 each marker represents a single T_g data point determined from a single partially cured isothermal DSC scan. As can be seen clearly, the conversion rise causes an increase in glass transition temperature regardless of the exposed cure temperature and cure time for the same epoxy based compound. As it is given in table 2.2 the range of glass transition region is wider for the Sumitomo compared to the Hitachi. This phenomenon can also be observed in figure 2.4 when the fit models are compared.

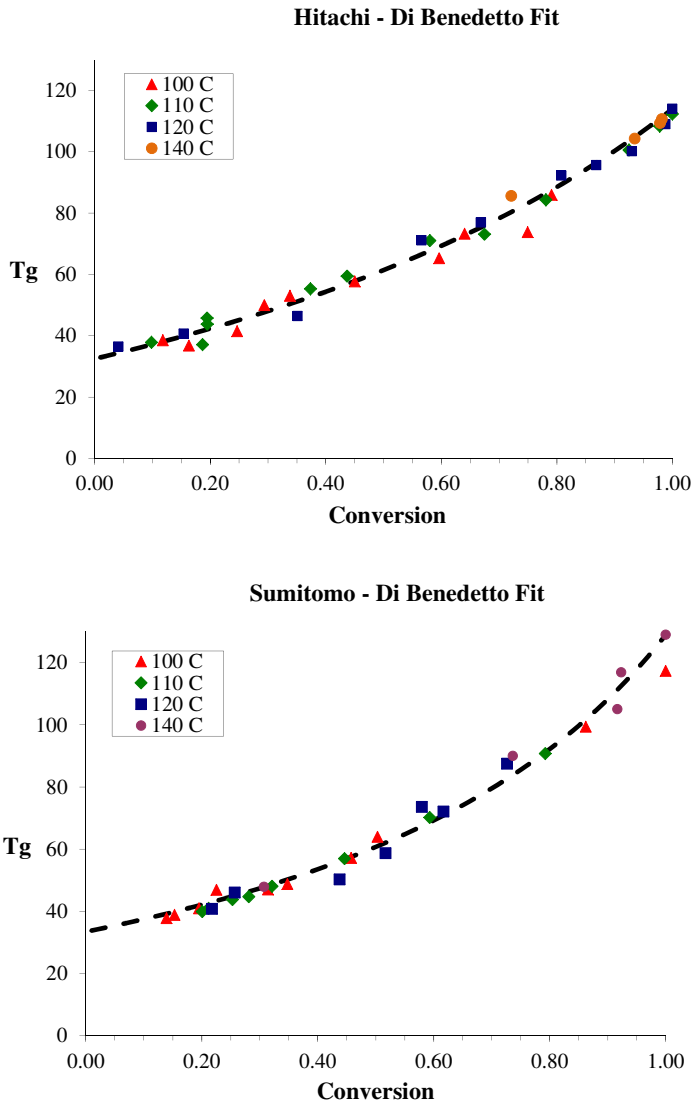

Figure 2.4 Isothermal DSC, Conversion - Glass Transition temperature relationship and the Di Benedetto fit for the Hitachi and the Sumitomo compounds

The degree of conversion with respect to time is given in figure 2.5 for the range of isothermal cure temperatures between 100 and 140°C and for various cure times. Each marker on these graphs represents a single cure test followed by a full scan at a constant rate. Conversion is obtained by applying equation 2.3 and later double checked and

corrected if necessary for the conversion values above 95%, using equation 2.4 of Di Benedetto. The solid lines, in this plot, represent the time and temperature dependent degree of conversion values based on the proposed model fit given in section 2.1.4. The experimental results are validated by comparing the two methods. This approach also provides a way of adjusting the model parameters by making slight changes, if it is required. As can be observed from the figures, the model parameters obtained for the Hitachi compound provided a better fit in all measured cure temperatures and cure times. It was rather difficult to fit the isothermal data obtained for the Sumitomo compound in line with the model fit which is based on the dynamic measurements.

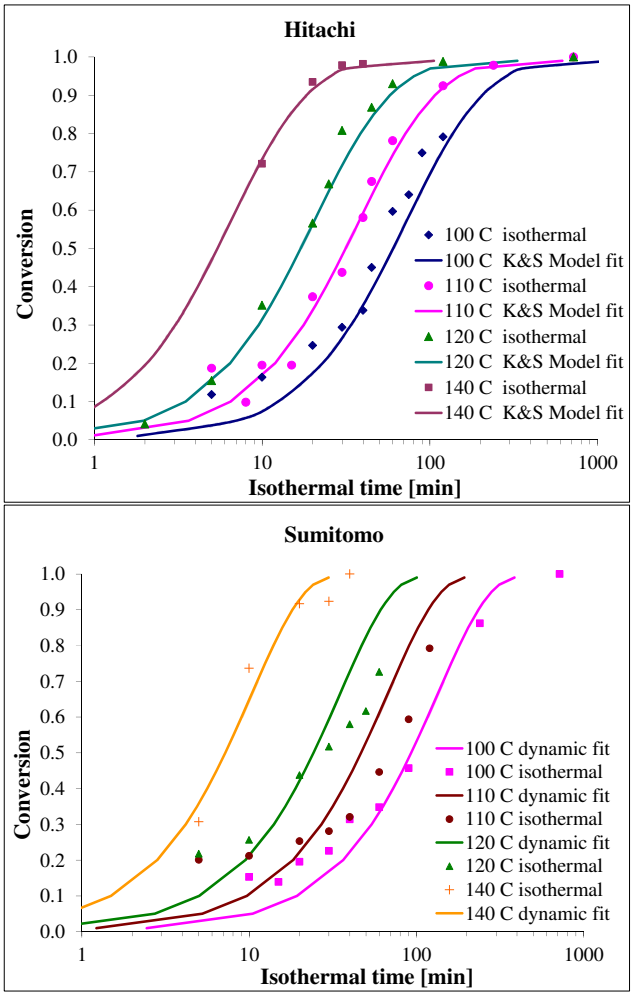

Figure 2.5 Isothermal DSC data and Kamal and Sourour kinetic model fit to MHR DSC

After the start-up of DSC the degree of reaction is rising at a decreasing rate. In other words, the rate of reaction is faster at the initial stages of the cure and it decelerates as the crosslink proceeds. Even though this phenomenon cannot be clearly observed in figure 2.5, since the graph is presented in a logarithmic time scale, one may refer to figure 2.6 which shows the DSC data along with the model fit for the isothermally cured Hitachi sample at 120^{o}C.

In all isothermal calorimetric scans the fastest available heating rate was applied to avoid any undesirable sample reaction prior to the thermal equilibrium. However, at shorter cure time experiments the unrecorded sample conversion during heating and cooling is not small compared to the measured conversion and for that reason during rescanning it leads to a lower residual heat of reaction detected by DSC. That is why the cure level sometimes is overestimated for the shorter isothermal cure times. Moreover, at high temperature experiments the heating up and cooling down periods take longer compared to low temperature tests and due to the higher temperature the reaction is faster. For these measurements the heating chamber was preheated before loading of the pans in order to minimize the sample cure before the start of the measurement such that the samples are placed inside the chamber at a temperature close to the test temperature.

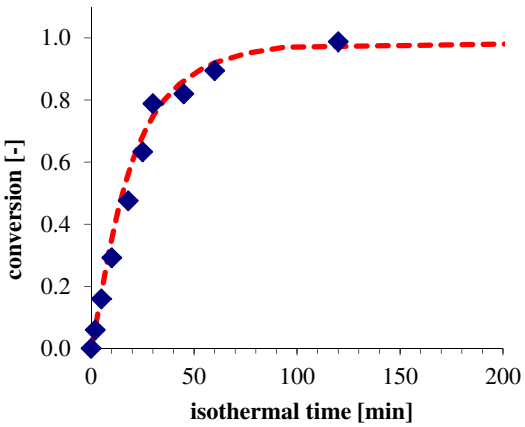

Figure 2.6 Degree of conversion with respect to isothermal cure time for cure temperature of 120^{o}C. The DSC data is represented by the blue square markers and the kinetic model by the dashed red line

2.2.3.2. Multiple heating rate method

There is an empirically accepted optimal range for the applied heating rate during sample scanning. Below and above this range may lead to underestimation of the total heat of

reaction. Essentially there are two factors affecting the lower value for H_{tot} at low heating rates below 1°C/min:

- First is the vitrification which is inevitable when the rising glass transition temperature reaches a value close to the scanning temperature. Vitrification, by definition, is the transition of a material into amorphous glassy state by supercooling [21]. Principally it would have the same effect if the epoxy is cured below the ultimate glass transition temperature. In this case the glass transition temperature will gradually rise to above the isothermal cure temperature, which results in vitrification and may lead to incomplete cure. Vitrification always proceeded with physical aging which is the characteristic of non-equilibrium state of vitrified polymer. Any amorphous polymer below its T_g is in non-equilibrium state and has a tendency towards a more stable equilibrium state. The aging has a significant impact on material behavior and leads to deterioration of properties like the stiffness, stress relaxation, enthalpy and dielectric constant [22].

  The physical aging and its effects on thermosetting resin's mechanical properties was studied by many researchers. Since the aging is not the scope of this thesis the interested reader may refer to the relevant studies on this subject [21]–[24].

- Second factor causing the underestimation of H_{tot} is the sensitivity of the scanning instrument at lower heating rates. On the other hand, higher heating rates may also cause to lower H_{tot} by initiating thermal degradation at high cure temperatures. It has to be highlighted that, the faster the heating rate, the higher the temperature required for achieving the full conversion. Thus, Based on empirical observations, for a temperature independent total heat of reaction, the heating rate must be restricted between 1 and 20°C/min [21].

In this study the samples are scanned at a range of heating rates between 1°C/min to 15°C/min each from -50°C to 280°C. The results of these measurements are shown in figure 2.7. The first heat flow shift around 40°C is the glass transition preceded by an enthalpic relaxation peak as a result of physical aging during sample storage. The effect of aging on DSC scans can be erased by heating the samples to slightly above T_g where the molecular mobility is higher. Then the sample is cooled down back to room temperature prior to the main scanning. Removing the effect of aging using this method results in negligible conversion of less than 1%. Note that in figure 2.7 the data are shifted on the vertical axis to provide a clearer picture for the reader.

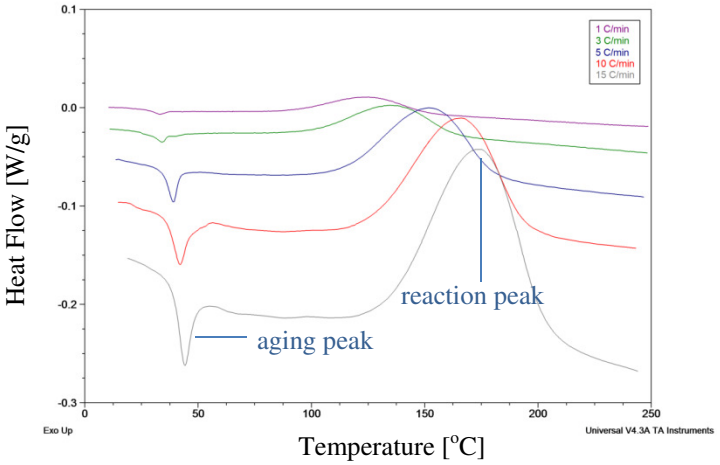

Figure 2.7 DSC Multiple heating rate scans of the Hitachi

The total heat of reaction is obtained from the area of the exothermic peak covering the temperature region of 110-220°C depending on the heating rate. A straight base line is drawn connecting the onset and the leveled off regions of the exothermic peaks. These tangent lines are shown in the top plots of figure 2.8. The area between the line and the exotherm gives the total heat of reaction for each measurement. The large differences between the measured exothermic peaks are due to the various heating rates applied during the scannings which can be corrected by dividing the heat flow values to the applied heating rates. The heat of reaction as a function of temperature is given in the second plots of figure 2.8.

The area representing the total heat of reaction can be obtained numerically using the trapezoidal integration method. Some part of the heat remains unrecorded at higher heating rates due to the instrument sensitivity. Hence, the largest area among the measurements is taken as the sample's total heat of reaction. The H_{tot} values of all measured heating rates which are determined by numerical integration, and the maximum H_{tot}, which is highlighted in bold are given in table 2.3.

Table 2.3 Total heat of reaction "H_{tot} [J/g]" obtained by the multiple heating rate method

heating rate [°C/min]	1	2	3	5	10	15
Hitachi	**43.86**	42.34	41.43	40.8	37.65	35.85
Sumitomo	**34.63**	33.50	33.34	32.21	31.70	30.46

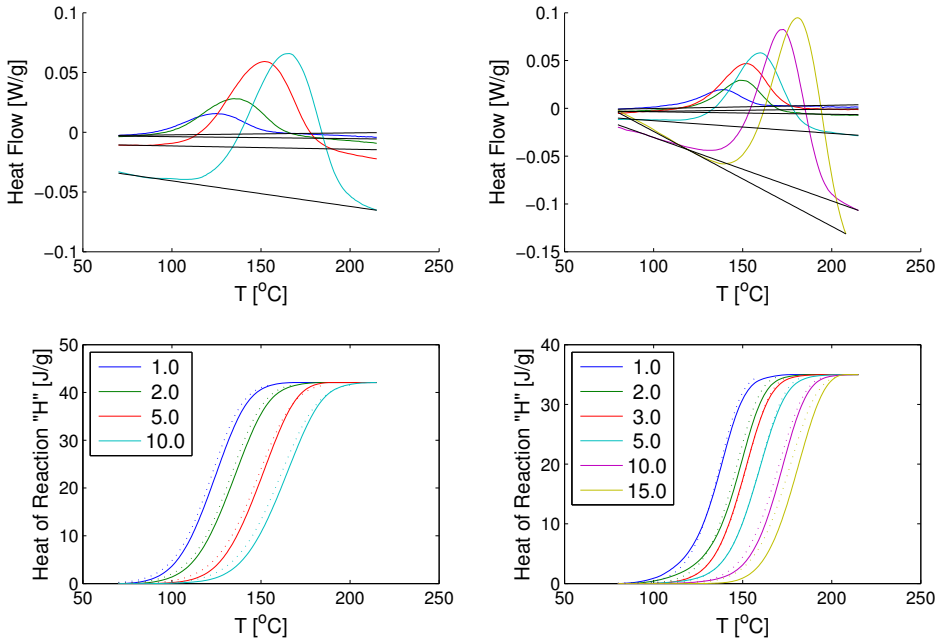

Figure 2.8 Heat flow to the samples at different heating rates (top) and the corrected (divided by the applied heating rate) heat of reaction corresponding to each heating rate (bottom) for the Hitachi compound (a) and the Sumitomo compound (b), Dotted lines are kinetic model fits (equations 2.5-2.7)

2.2.4. Kinetic Model

The crosslink mechanism in thermosetting polymers mostly described by the n^{th} Order or autocatalytic reaction models [1]–[5], [8]–[17] . In most of the early studies, the reactivity of thermosetting polymers are characterized by an n^{th} order kinetic expression governed by an Arrhenius model, $(K(T))$ which quantifies the speed of crosslinking [21]. Ryan showed that the n^{th} order kinetic model is insufficient in quantifying the maximum isothermal reaction rate and therefore, it is unable to provide an accurate description of the curing process [25]. Lu et al compared these two along with other kinetic models in his study of bisphenol A resin with methyline dianiline as hardener with different concentration of filler content in which he concluded that the autocatalytic model had the highest accuracy level [21]. Two autocatalytic models were proposed by Kamal and Sourour, one in 1973 and the other a year later [26], [27]. The first one was used to correlate the isothermal DSC data.

The latter is the more general expression which has commonly been used by many researchers. Among them Han et al. [28], Ryan and Dutta [5] were the early users of this approach. Among the other important models the work of Malkin and Kulichikhin was also worth to mention here [29] where a self-acceleration and self-inhibition effects were introduced to describe the separation and formation of partial microgel structure. According to this model, curing of reacting compounds not only comprises the mechanism of chemical reaction but also the effect of phase separation as a result of chemical conversion. The self-acceleration effect must not be mistaken for autocatalytic effect which is represented in equations 2.7.

The reaction kinetics in this study is modeled based on the simpler form of the autocatalytic Kamal & Sourour expression. The rate of reaction is defined as the product of two functions: the first one represents the temperature dependency and the latter states the reaction order.

$$\frac{d\xi}{dt} = K(T)\, f(\xi), \tag{2.5}$$

where $K(T)$ is the Arhenius temperature dependent term given by

$$K(T) = A\, exp(-E_a/RT)\,. \tag{2.6}$$

Here R stands for the gas constant which is 8.314 [$J.K^{-1}.mol^{-1}$] and T is the absolute temperature in Kelvin. A is the pre-exponential factor. The exponential term emphasizes the probability of the reaction by the collusion of atoms. The activation energy E_a represents the energy barrier that must be passed for the crosslink networking to take place. The Arrhenius law states that the energy to overcome the activation barrier is lower at higher cure temperatures.

The second function in equation 2.5,($f(\xi)$) is defined by the autocatalytic Kamal and Sourour model, which is expressed by

$$f(\xi) = \xi^m\,(1-\xi)^n. \tag{2.7}$$

ξ denotes the conversion level which is constrained between 0 and 1 representing the uncured and the fully cured states, respectively. $(1-\xi)$ is the concentration of remaining unreacted epoxide groups. m and n are reaction orders for the autocatalytic effect and the main reaction, respectively.

Equation 2.5 can be solved by arranging the terms at the left and right hand sides and integrating each with respect to conversion and temperature, respectively, which yields

$$\int_{\xi_0}^{\xi} \frac{d\xi}{\xi^m(1-\xi)^n} = \frac{A}{\beta}\int_{T_{\xi_0}}^{T_\xi} exp(-E_a/RT)\;\; dT. \tag{2.8}$$

Where β is the heating rate defined as $\beta = \frac{dT}{dt}$.

2.2.4.1. Determination of Model Parameters

The first step in parameter estimation for any kinetic model starts with determination of the activation energy. The most common methods are so called model-free iso-conversion methods which are classified by Ozawa [30] as:

- Flynn-Wall-Ozawa Method
- Friedman Method
- Kissinger-Akahira-Sunose Method

The most frequently used method that yields a simple relationship between activation energy, heating rate and temperature is based on the work of Ozawa [31] and Flynn and Wall [32]. The model requires an approximation either from a table proposed by Doyle [33] or implementation of a formula developed by Opfermann and Kaiserberger [34]. Friedman [35] derived a method for an n^{th} order reaction for various heating rates. The linear relationship between the conversion rate and the reciprocal of temperature at a specified degree of conversion was used to obtain the activation energy. Kissinger [36] developed a formula to estimate the activation energy of the reaction which he believed that it held only at maximum conversion rate. This was the earliest study among the iso-conversion techniques. Later, Akahira and Sunose showed that the relation proposed by Kissinger is valid at any conversion level [37]. The Kissinger and Ozawa methods both are based on constant heating rate assumption, $T = T_0 + \beta t$. In short, The Kissinger and Ozawa methods require determination of the temperature at which the same level of conversion is achieved in all of the heating rate analysis and each comes with an approximation technique, whereas in the Friedman method the conversion rate is also needed and moreover, the solution does not rely on any mathematical estimation.

The Activation energy determination in the Kissinger and Ozawa models starts with the integral of the kinetic model which is already given in equation 2.8, while for the Friedman method it begins with taking the natural logarithm of the reaction rate. As the term iso-conversion states, in all of the three methods mentioned above the temperature at the fixed conversion is obtained first in order to define a matching point in reaction level of the heating rate scans.

Activation Energy

The activation energy of the epoxy in this study was obtained based on multiple heating rate data and by implementing the Friedman method. As stated above Friedman used the rate of reaction to verify the activation energy of the reaction. This method does not require any integral approximation as opposed to the Kissinger and the Ozawa methods. Friedman derived this method for an nth order reaction but later the applicability of the method for much broader reaction rates was confirmed by other studies. Indeed, the applicability of this model is independent of the reaction order. Thus, it is called a model free method. The activation energy in equation 2.6 can be obtained by taking the natural logarithm of equation 2.5 which leads to

$$ln(\frac{d\xi}{dt}) = ln\big(A\, f(\xi)\big) - \frac{E_a}{RT_i}. \qquad 2.9$$

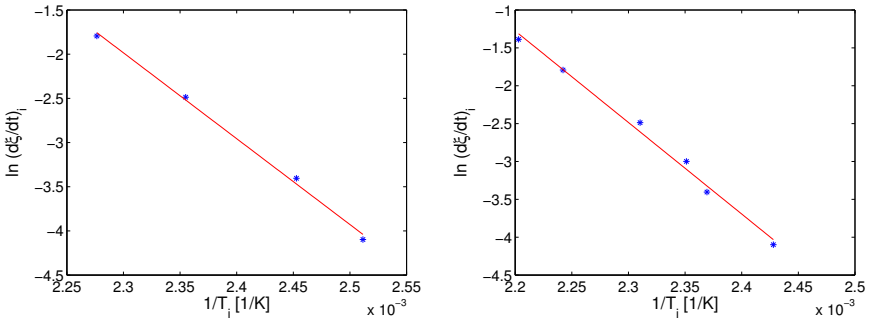

Figure 2.9 Determination of the activation energy using Friedman method from the slope of $ln(d\xi/dt)_i$ vs. $1 / T_i$ for the Hitachi compound (a) and the Sumitomo compound (b)

In order to implement the Friedman method one must define a fixed level of reaction for the range of applied heating rate measurements. Therefore, equation 2.9 becomes independent of the conversion function and can be simplified to

$$ln\left(\frac{d\xi}{dt}\right) = -\frac{1}{T_i}\frac{E_a}{R} + Constant. \qquad 2.10$$

Equation 2.10 can be rewritten to include the heating rate and incremental thermal variation as

$$ln\left(\frac{d\xi}{dT}\beta\right)\Big|_{T_i} = -\frac{1}{T_i}\frac{E_a}{R} + Constant. \qquad 2.11$$

Hence, the slope of $ln(d\xi/dt)_i$ versus $1 / T_i$ determines the activation energy.

$$E_a = R\,\frac{\Delta\left(ln\left(\frac{d\xi}{dT}\beta\right)\Big|_{T_i}\right)}{\Delta\left(\frac{-1}{T_i}\right)}. \qquad 2.12$$

Knowing the activation energy, the autocatalytic model order parameters can be obtained by applying a non-linear regression analysis to equation 2.5. The numerical discretization of the kinetic model is accomplished by implementing the forward time scheme to the heating rate data which results in

$$\xi_{i+1} = K(T)\,\Delta t\,\xi_i^m(1-\xi_i)^n + \xi_i. \qquad 2.13$$

The parameters determined by the Friedman method are given in table 2.4.

Table 2.4 Cure kinetic model fit parameters

Compounds	E_a [KJ.mol^{-1}]	A [10^7 s^{-1}]	m	n
Hitachi	77.5	1.95	0.216	1.267
Sumitomo	85.5	6.45	0.132	0.83

The reaction function based on the calculated model parameters multiplied by the pre-exponential constant is compared in figure 2.10 with the experimentally detected conversion rate divided by the Arrhenius term which contains the estimated activation energy. In other words, numerical $A\,f(\xi)$ is compared with the experimental $\dot{\xi}/\exp(-E_a/RT)$ and graphically shown over the conversion scale. The black solid line denotes $A\,f(\xi)$ and the data shown by the markers represents $\dot{\xi}/\exp(-E_a/RT)$ for the tested heating rate. Here $\dot{\xi}$ stands for reaction rate, $\frac{d\xi}{dt}$. For the Hitachi compound, the majority of the data are in good agreement with the numerical fit except the data at 10^{o}C/min which slightly deviates from the other measurements and the model. Note that the shapes of the curves are identical and the deviation is negligible and does not affect the overall cure kinetics behavior significantly, which are demonstrated in the subsequent plots. Based on the comparison plots, the numerical fit determined for the Hitachi agrees much better with the experimental data, compared to the Sumitomo.

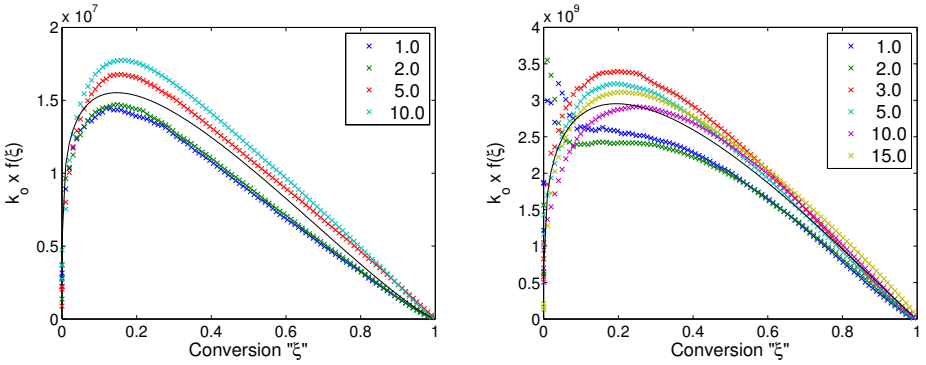

a **b**

Figure 2.10 Comparison of the f(α) based on empirically obtained activation energy and the numerical fit to the autocatalytic reaction function for the Hitachi compound (a) and the Sumitomo compound (b)

The conversion rate data measured indirectly by the MHR scanning method in DSC and the conversion rate representing the autocatalytic model are compared in figure 2.11. As it is clearly observed, the model is in good agreement with the DSC data for both compounds. The corresponding heat flow curves (integrated rate curves) were already shown in figure 2.8 (bottom plots) for both compounds.

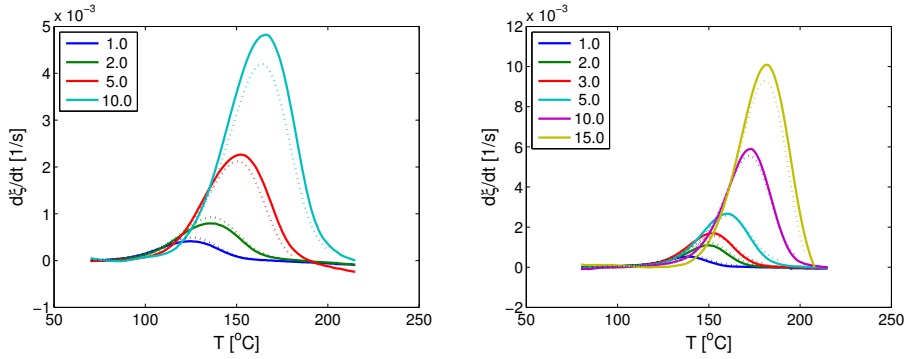

a **b**

Figure 2.11 Experimental (solid lines) and predicted (dotted lines) reaction rates for the Hitachi compound (a) and the Sumitomo compound (b)

2.3. Cure and Thermal Shrinkage

The shrinkage mechanism in epoxies can be either of chemical or thermal origin. The molecular structure of the epoxy resin changes by the reaction taking place during cure which results in transformation of liquid to a cross linked solid. During crosslinking the monomers link to the growing polymer network and are thereby restricted in their movement. This results in a decrease of free volume which is seen macroscopically as cure shrinkage. Therefore, the specific volume of the epoxy melt that experiences a molecular transformation to a more densely packed structure tends to decrease. The resulted shrinkage is called chemical or cure shrinkage which is the trigger for residual stress build-up. On the other hand, thermo-mechanical stress builds up as the molding compound starts cooling down to room temperature, primarily because of the thermal expansion mismatch between the epoxy polymer and the other internal components.

2.3.1. PVT test

The thermal and the chemical shrinkage are considered as the two main causes of warpage and residual stress in electronics packaging applications. In this study both of the shrinkage mechanisms are analyzed experimentally using the Gnomix high pressure dilatometer instrument and modeled accordingly. The working principle of the test setup is based on controlled temperature and hydrostatic pressure variations. The sample is immersed in mercury inside a cell which is confined by silicon oil. The applied pressure is transferred to the sample through the oil and then mercury, respectively and volume change is measured by a displacement sensor.

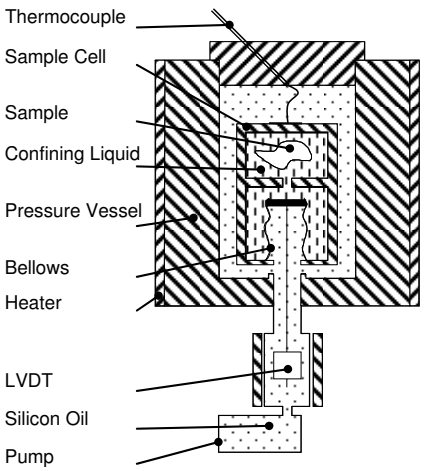

Figure 2.12 Schematic illustration of high pressure Dilatometer test setup [38]

The first step in the Dilatometry measurements is the cure shrinkage experiment where the volume change of the thermosetting epoxy compound during cure is recorded. In the second stage the fully cured sample is subjected to stepwise incremental pressure and temperature changes such that the isobaric thermal expansion and the isothermal bulk modulus data are obtained.

2.3.2. Cure Shrinkage

There are various experimental methods developed for cure shrinkage estimation. Some are mentioned in chapter 5. Therefore, no literature review is given on cure shrinkage at this point and the reader may refer to the relevant chapter.

Volume shrinkage because of the chemical shrinkage of the thermosetting compound during cure is evaluated experimentally and the results are discussed in this section. The thermal shrinkage study of the fully cured compounds is evaluated in the next section.

In order to predict the extent of cure shrinkage the Dilatometry PVT experiment with the following steps have been conducted:

- Epoxy pellets contain voids initially. Hence, prior to heating each compound is compressed at slightly above T_{g0} around 35^{o}C in order to get rid of voids.
- Samples are heated with a rate of 10^{o}C/min to 120^{o}C. The isothermal cure temperature is set lower than the actual molding process temperature to minimize the cure reaction during heating up.
- Samples are subjected to isothermal cure at 120^{o}C for 10 hours which is according to the DSC results discussed in chapter 2.1 is sufficient for a complete cure of the tested epoxy sample.
- This stage is completed by cooling down the sample to room temperature gradually with a constant cooling rate.

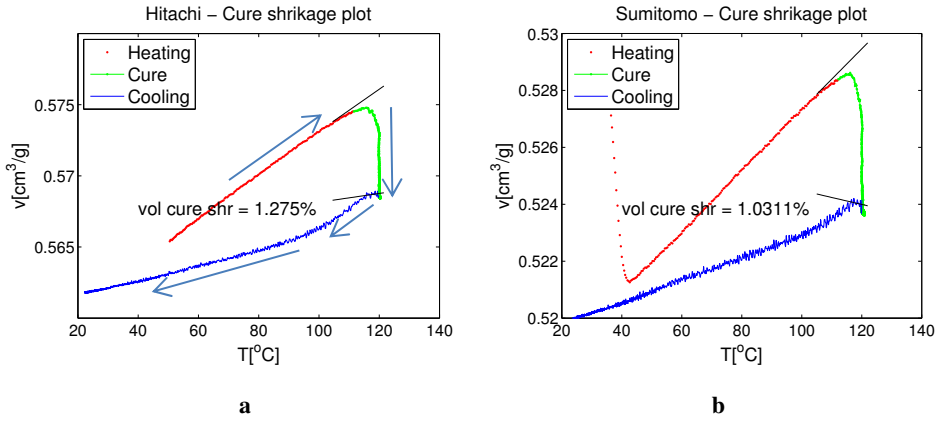

a **b**

Figure 2.13 Cure shrinkage experiment for the Hitachi (a) and the Sumitomo (b) compounds

The stages of the chemical shrinkage experiment are shown in detail in figure 2.13. The pre-compression is performed at a temperature just above T_{g0} where the sample's molecular mobility is less restricted. The pre-compression stage is not recorded for the Hitachi compound, but it is shown in the shrinkage data plot of the Sumitomo compound in figure 2.13. Expansion in volume after the initial pre-compression is resulted by heating the sample with a constant heating rate of 10°C/min until the preset isothermal cure temperature of 120°C. This volume expansion is dictated by the thermal expansion coefficient of the uncured epoxy melt. Upon reaching to the specified temperature of 120°C the isothermal cure stage starts at which the sample fully cures. Towards the end of the heating stage a slight drop in the linear volume change can be observed. This deviation prior to the isothermal stage can be attributed to the start of reaction before reaching to the isothermal temperature. The cure shrinkage experiment relies on the assumption that the epoxy is cured isothermally without any initial conversion of the test pellets. That is why the volume change is corrected by extrapolating the heating line to 120°C so the cure shrinkage of the epoxy as a result of complete cure is evaluated more accurately. The selected isothermal temperature is just above the ultimate glass transition temperature of the Hitachi and it is slightly below it for the Sumitomo compound. The cure temperature is a critical parameter and selecting any value below $T_{g\infty}$ may result in vitrification and incomplete cure. However, based on the analysis performed in section 2.3 no vitrification is expected for the Sumitomo compound at 120°C despite curing it below Tg_{∞}. Selecting a higher cure temperature, on the other hand, may contribute to a higher initial reaction which affects the accuracy level significantly. As mentioned before at the early stages of cure, the reaction rate is faster. Since longer time will be required for the equilibrium of the

instrument at higher cure temperatures the sample will react during heating and thus the deviation from a linear heating will be much higher than the one shown in figure 2.13.

The isothermal stage is shown in green in the figure above. At the end of isothermal curing the volumetric change between the uncured and the fully reacted stage is calculated. This value is considered as the experimentally obtained cure shrinkage or chemical shrinkage. Cure induced shrinkage of 1.275% and 1.0311% are recorded for the tested Hitachi and Sumitomo epoxy pellets, respectively. The higher Silica content used in the Sumitomo compound formulation leads to a lower shrinkage values compared to the Hitachi.

Cure shrinkage is interrelated to the conversion by implementing the time and temperature parameters of the shrinkage measurements into the autocatalytic kinetic model. The results are shown for both compounds in figure 2.14. The shrinkage as a function of conversion is rather linear for the Hitachi compared to the Sumitomo. This behavior of the Hitachi compound let us assume a simple linear model for the shrinkage mechanism in numerical analysis.

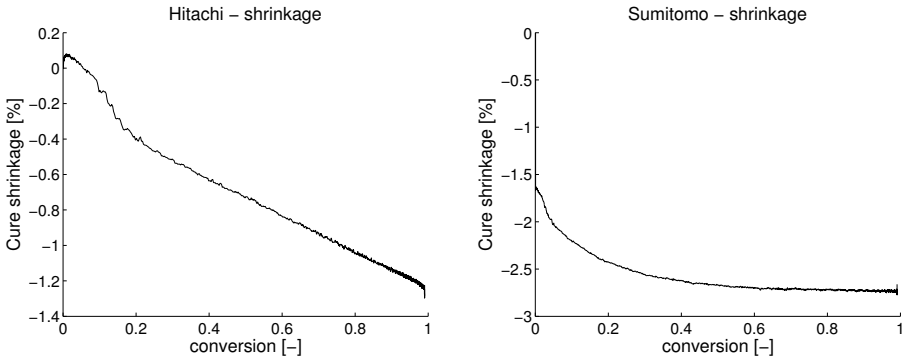

Figure 2.14 Cure shrinkage with respect to conversion based on the autocatalytic model (equation 2.7)

2.3.3. Thermal Shrinkage

The thermal expansion coefficient is a quantitative measure for the volume variation due to changes in temperature. The coefficient of thermal expansion of a curing system is difficult to detect directly by the existing experimental techniques. However, some indirect approaches have been applied. For example, a dielectric spectroscopy was used for indirect determination of CTE of a reacting system such that the conversion data was fitted to a modified WLF equation [39] and the rate of the model parameters were used to estimate the thermal expansion coefficient [17]. The CTE of an EMC with a low catalyst and different amount of filler content was studied by Jansen. The partially cured samples' thermal

expansion coefficient values were predicted using the rule of mixture that gives the CTE as a function of temperature and conversion [40]. Hence, various methods can be applied to determine the CTE of a curing epoxy. Nevertheless, during molding the curing process takes place at an isothermal temperature and ideally the encapsulated package is removed from the mold cavity after complete conversion of the epoxy. Hence, the thermal contraction is not required to be a function of conversion when the molding is the scope of study. Even if the epoxy is not cured completely still the cooling is fast due to the thin package geometry. Therefore, the conversion change during cooling down is negligible and its effect on contraction can be ignored.

The volume change of a fully cured epoxy material subjected to temperature variations at a constant pressure is characterized by the coefficient of thermal expansion coefficient, α, defined by

$$\alpha = \frac{1}{v_0}\left(\frac{\partial v}{\partial T}\right)_P, \qquad 2.14$$

where v_0 denotes the initial specific volume, $\partial v/\partial T$ signifies the specific volume gradient with respect to temperature and P stands for the applied constant pressure.

Polymers experience different thermal expansions below and above the glass transition temperature. Below T_g, the polymer is glassy and the molecules' mobility is lower in comparison with above T_g where the polymer is in its rubbery state and the polymer chains are mobile and slide over each other. The transition is gradual rather than a step change. The region in between the two states is a transition zone which covers the temperature range from slightly above T_{g0} to a temperature above $T_{g\infty}$, usually close to the temperature at which the peak exotherm is observed in DSC. This is the region where the time dependency of the mechanical properties of the thermosetting polymer should also be taken into account. The time and temperature dependent behavior is highly important in this region and both effects on the behavior of the thermoset were analyzed in this thesis, separately. The time dependent impacts on the behavior of the thermosetting epoxy will be discussed in detail in chapter 3.

At the volumetric measurement of the fully cured epoxy the temperature is raised at steps of 10^oC. After the thermal equilibrium at each step the pressure is increased incrementally stepwise from 10MPa to the maximum pressure of 80MPa. Therefore the volume change associated with the heating of the sample at the incremental constant pressures is recorded. The results of this measurement are given in figure 2.15. A bilinear transition separating the glassy and rubbery plateaus can be noticed at the glass transition region. Moreover, it is experimentally clear that the glass transition is also pressure dependent as the increase in pressure leads to a shift in glass transition region towards a higher temperature.

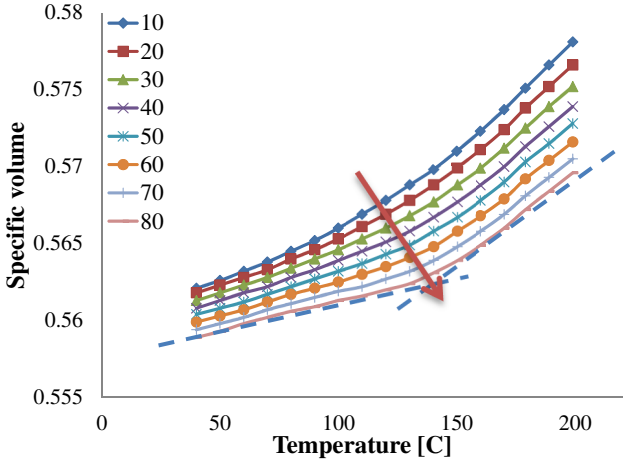

Figure 2.15 Heating scan of a cured Hitachi EMC at a range of pressure between 10 to 80MPa

2.3.4. Bulk Modulus

The bulk modulus can be described as the material's resistance to compression. Empirically it characterizes the volume response of an epoxy molding compound to the applied pressure under isothermal testing conditions which is represented by equation 2.15 and the plot at a fixed pressure is given in figure 2.16.

$$K = -v_0 \left(\frac{\partial P}{\partial v}\right)_T, \qquad 2.15$$

2.3.5. A volumetric model for fully cured epoxy

A modified form of Tait equation is implemented for modeling the volumetric response of the epoxy thermoset. Historically, Tait developed his model to model the compressibility of seawater. So far many modifications have been made to this empirical equation for specific purposes [41]. The Tait equation is given as [24]

$$V(p,T) = V_0(T)\left[1 - C\ ln\left(1 + \frac{p}{B(T)}\right)\right], \qquad 2.16$$

To approximate the pressure and temperature dependent specific volume of the epoxy thermoset a modified version of the Tait equation which allows for a gradual change of CTE and K during the glass transition was proposed as [38]

$$V_0(T) = v_0\left[1 + k_1(T - T_{gp}) + 0.5k_2\left((T - T_{gp}) + \ln\left(\frac{\cosh\left(C_1(T - T_{gp})\right)}{C_1}\right)\right)\right], 2.17$$

$$T_{gp=}T_{g0} + s_o p, \tag{2.18}$$

$$B(T) = b_1 + exp(-b_2 T), \tag{2.19}$$

where $V_0(T)$ is the temperature dependent specific volume at atmospheric pressure, B is the temperature dependent term and T_{gp} gives the pressure dependent glass transition temperature. C is the Tait constant with a constant value of 0.0894 and C_1, k_1, k_2, b_1, b_2 are the fit parameters. The proposed model provides a smoother transition rather than a step shift in glass transition region offering numerical advantage over the original Tait model.

The model for CTE is obtained by differentiating the modified Tait equation with respect to temperature [38], which yields

$$\alpha(T,P) = k_1 + 0.5\, k_2\big(1 + tanh\big[C_1\big(T - T_{gp}\big)\big]\big)\left(1 - C\, ln\left(1 + \frac{P}{B}\right)\right) - \frac{b_2 CP}{p+B}. \tag{2.20}$$

At atmospheric pressure the effect of pressure is low and hence, the terms containing pressure on the numerator can be neglected. The simplification gives

$$\alpha(T) = k_1 + 0.5\, k_2\big(1 + tanh\big[C_1\big(T - T_{g0}\big)\big]\big). \tag{2.21}$$

Taking the derivative of equation 2.21 with respect to pressure gives the compressibility (β) which is

$$\beta(T,P) = k_1 s_0 + 0.5\, k_2 s_0\big(1 + tanh\big[C_1\big(T - T_{gp}\big)\big]\big) + \frac{C(1-b_2 s_0 p)}{(B+P)}, \tag{2.22}$$

And according to equation 2.15 the bulk modulus can be obtained by

$$K(T,P) = \frac{1}{\beta(T,P)}. \tag{2.23}$$

The Tait model parameters for both compounds, obtained using the non-linear least square regression analysis are given in table 2.5.

Table 2.5 Tait fit parameters

Tait parameters	v_0	k_1	k_2	C_1	b_1	b_2	Tg_0	s_0	C
Hitachi	0.568	$8\ 10^{-5}$	0.00018	$2.34\ 10^{-2}$	$2.34\ 10^{3}$	$4.2\ 10^{-3}$	113	0.564	0.0894
Sumitomo	0.539	$3.2\ 10^{-5}$	0.000655	$7.67\ 10^{-3}$	$1.21\ 10^{3}$	$8.3\ 10^{-3}$	129	-0.406	0.0894

The CTE and bulk modulus based on the thermal expansion data obtained by PVT experiments at 10MPa are shown for a temperature range from 50 to 200°C with 10°C of increments, in figure 2.16. The smooth increase of α accompanying the heating of the sample can be observed during the glass transition region. The solid lines are the thermal expansion and bulk modulus calculated using the models given in equations 2.20 and 2.23,

which agree well with the experimental data. The graph shows that the volumetric CTE increases from $8x10^5$ in the glassy state to $2.5x10^4$ in the rubbery state. The Bulk modulus, on the other hand, decreases from 11GPa to 4GPa in the same temperature range.

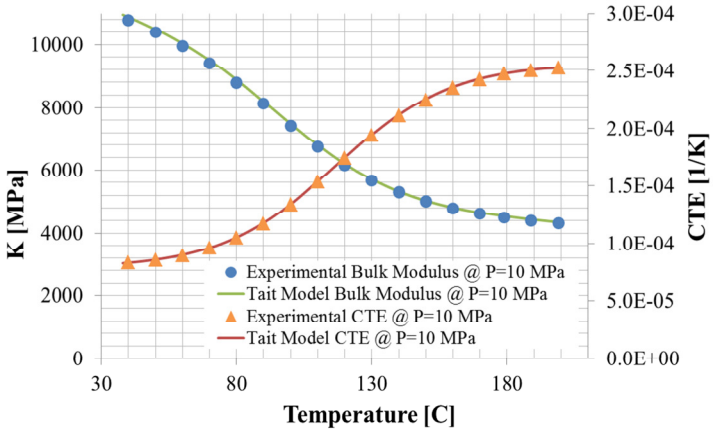

Figure 2.16 Coefficient of Thermal Expansion and Bulk Modulus of the fully cured Hitachi sample at 10MPa

2.4. Time-Temperature Transformation Diagram

The increase in glass transition temperature with respect to the applied isothermal cure temperature and the cure time is given in figure 2.17. The isothermal cure temperatures between 80 to 200°C are compared. In order to show the glass transition growth for each isothermal cure temperature the time logarithmic plot of 2.17b is also presented. The rate of rise in T_g is faster at the start of cure. Especially, $dT_g/dt_c\big|_{T_c}$ curves get steeper for the high cure temperatures. This behavior can be clearly observed in figure 2.17a. In other words, the higher the temperature, the faster the T_g rise, as expected.

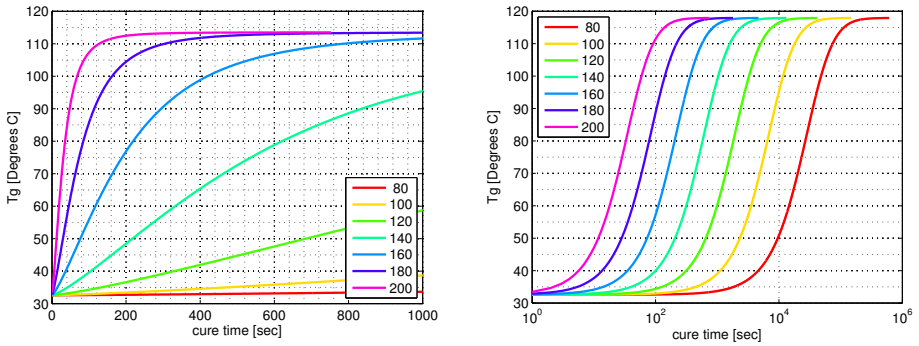

Figure 2.17 Variations in glass transition with respect to isothermal cure temperature and cure time for the Hitachi compound on a linear time scale (a) and logarithmic time scale (b)

The time-temperature transformation graph represented in figure 2.18 is obtained based on the glass transition data determined using calorimetric measurements and by implementing the autocatalytic kinetic model used to fit the kinetic data. This graph shows that the increase in cure temperature does not necessarily imply the same amount of decrease for cure time to achieve the same conversion level.

The time temperature transformation diagram shown in figure 2.18 demonstrates the gelation transition under exposed thermal conditions for the specified cure time. This line is obtained by calculating the time it takes to reach the conversion at gelation (here taken as 45%) for a specified isothermal temperature. For example, the gel time at 180^{o}C of cure temperature is around 50 seconds while almost 1000 seconds is required to get to the gel point at 120^{o}C, for the same compound. The time to gel point is important because generally the industry cure temperature standard for molding of electronics is 175^{o}C and hardly set lower than this value [42]. Incomplete filling may occur if the filling time set longer than the gel time for the selected cure temperature. Figure 2.18 also shows that for the cure temperature below the ultimate glass transition temperature of the substance vitrification will be observed either before or after the gel point depending on the cure temperature.

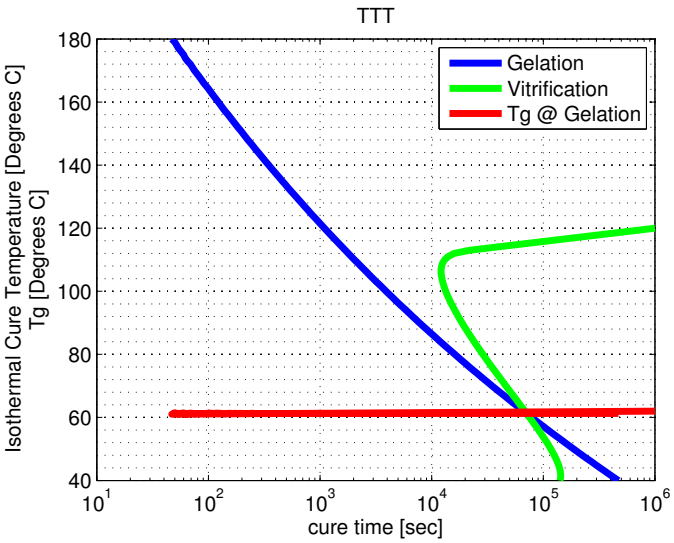

Figure 2.18 Time-Temperature Transformation of the tested Epoxy Compound

The red line in figure 2.18 is the glass transition temperature at the gel point for all cure temperature range which is constant and independent of cure time and temperature. The glass transition temperature at gelation (T_g^{gel}) is calculated as 62.5°C from the Di Benedetto equation 2.4 and $\xi_{gel} = 0.45$. Any isothermal cure temperature below T_g^{gel} results in vitrification before gelation and any cure temperature above T_g^{gel} may yield vitrification after gelation. This phenomenon is due to the slower evolution of glass transition below T_g^{gel}. Any cure temperature above T_g^{∞}, on the other hand, can be considered as free of vitrification until complete polymerization, independent of the duration of the cure. Moreover, any cure temperature below T_g^{∞} will lead to incomplete cure either vitrified or gelled, regardless of the cure time. So, if the isothermal T_{cure} set above T_g^{∞} there will be no vitrification but only gelation and if the epoxy cures isothermally at T_{cure} in between T_g^{gel} and T_g^{∞} then vitrification follows gelation. $T_{cure} = T_g^{gel}$ is the point at which the gelation and vitrification overlaps which is also confirmed previously by the experimental study of Enns [43].

Note that in the PVT cure shrinkage experiments 120°C is selected as the isothermal cure temperature which is just above T_g^{∞}.

2.5. Conclusion

This chapter comprises the experiments conducted for the kinetic and volumetric characterization of the EMCs. The cure kinetics is modeled based on autocatalytic Kamal and Sourour model using calorimetric measurements. Multiple heating rate scans of uncured samples are used for determination of the model parameters. The Friedman model is implemented for the activation energy determination and later the model parameters are adjusted by comparing the model based degree of conversion to the conversion data obtained by the DSC scans of partially cured samples. Therefore, the model is double checked by the two independent types of DSC measurements. Besides, the partially cured scanning method provided a relation between conversion level and the glass transition temperature independent of the applied cure time and temperature. The Di Benedetto model is used for numerical representation of this relationship.

Shrinkage during cure is tested using a PVT test setup. An uncured sample of epoxy, initially measured in weight, gradually cured at an isothermal temperature until full conversion. The volume change is obtained as the difference between the start and the end of isothermal section. Using the same test setup the fully cured sample is exposed to stepwise incremental pressure and temperature rise. From that, the isobaric volume change for a scanned temperature range is obtained indirectly which leads to coefficient of thermal expansion determination. Moreover, the volume change data based on the isothermal pressure increase gives the bulk modulus. Both CTE and Bulk modulus are modeled using a modified Tait equation.

In conclusion, it is shown that the selected material models offer an accurate representation of the material behavior under various processing conditions. Both compounds' models agree well with the experimental data. However, the model obtained for the Hitachi compound is verified to be a better fit than the Sumitomo model when compared with the isothermal DSC measurements. The cure shrinkage measured higher for the Hitachi compound due to the lower filler content compared to the Sumitomo. The cure shrinkage, conversion relationship is predicted to be almost linear for the Hitachi which is obtained by implementing the kinetic model. As a result, based on the kinetic and volumetric characterization measurements, the models obtained for the Hitachi compound provided a better fit and more realistic numerical applicability compared to the Sumitomo.

References

[1] K. M. B. Jansen, C. Qian, L. J. Ernst, C. Bohm, A. Kessler, H. Preu, and M. Stecher, "Kinetic Characterisation of Molding Compounds," *Int. Conf. Therm. Mech. Multi-Physics Simul. Exp. Microelectron. Micro-Systems. EuroSime*, pp. 1–5, 2007.

[2] G. Van Assche, a. Van Hemelrijck, H. Rahier, and B. Van Mele, "Modulated differential scanning calorimetry: isothermal cure and vitrification of thermosetting systems," *Thermochim. Acta*, vol. 268, pp. 121–142, Dec. 1995.

[3] M. Um, I. M. Daniel, and B. Hwang, "A study of cure kinetics by the use of dynamic differential scanning calorimetry," *Compos. Sci. Technol.*, vol. 62, pp. 29–40, 2002.

[4] V. M. Gonzalez-Romero and N. Casillas, "Isothermal and Temperature Programmed Kinetic Studies of Thermosets," *Polym. Eng. Sci.*, vol. 29, no. 5, pp. 295–301, 1989.

[5] A. Dutta and M. E. Ryan, "Effect of Fillers on Kinetics of Epoxy Cure," *J. Appl. Polym. Sci.*, vol. 24, pp. 635–649, 1979.

[6] R. a. Fava, "Differential scanning calorimetry of epoxy resins," *Polymer (Guildf).*, vol. 9, pp. 137–151, Jan. 1968.

[7] B. Bilyeu, W. Brostow, and K. P. Menard, "Epoxy Thermosets and Their Applications III. Kinetic Equations and Models," *J. Mater. Educ.*, vol. 23, no. 4–6, pp. 189–204, 2001.

[8] K. M. B. Jansen, L. Wang, C. V. H. Hof, L. J. Ernst, H. J. L. Bressers, and G. Q. Zhang, "Cure, temperature and time dependent constitutive modeling of moulding compounds," in *5th International Conference on Thermal and Mechanical Simulation and Experiments in Microelectronics and Microsystems, EuroSimE*, 2004, no. 4, pp. 581–585.

[9] S. L. Simon, G. B. Mckenna, and O. Sindt, "Modeling the Evolution of the Dynamic Mechanical Properties of a Commercial Epoxy During Cure after Gelation," *Appl. Polym. Sci.*, vol. 76, pp. 495–508, 2000.

[10] J. de Vreugd, K. M. B. Jansen, L. J. Ernst, C. Bohm, a. Kessler, and H. Preu, "Effects of Molding Compound Cure on Warpage of Electronic Packages," *2008 10th Electron. Packag. Technol. Conf.*, pp. 675–682, Dec. 2008.

[11] M. H. H. Meuwissen, H. a. de Boer, H. L. a. H. Steijvers, P. J. G. Schreurs, and M. G. D. Geers, "Residual stresses in microelectronics induced by thermoset packaging materials during cure," *Microelectron. Reliab.*, vol. 44, no. 12, pp. 1985–1994, Dec. 2004.

[12] S. Gan, J. C. Seferis, and B. Prime, "A viscoelastic description of the glass transition-conversion relationship for reactive polymers," *J. Therm. Anal.*, vol. 37, pp. 463–478, 1991.

[13] D. Adolf and J. E. Martin, "Calculation of Stresses in Crosslinking Polymers," *J. Compos. Mater.*, vol. 30, no. 1, pp. 13–34, 1996.

[14] D. Adolf and R. Chambers, "Verification of the capability for quantitative stress prediction during epoxy cure," *Polymer (Guildf).*, vol. 38, no. 21, pp. 5481–5490, 1997.

[15] V. Antonucci, a. Cusano, M. Giordano, J. Nasser, and L. Nicolais, "Cure-induced residual strain build-up in a thermoset resin," *Compos. Part A Appl. Sci. Manuf.*, vol. 37, no. 4, pp. 592–601, 2006.

[16] B. Boehme, K. M. B. Jansen, S. Rzepka, and K. Wolter, "Thermo Mechanical Characterization of Packaging Polymers," in *European Microelectronics and Packaging Conference (EMPC)*, 2009, pp. 1–10.

[17] E. Leroy, J. Dupuy, A. Maazouz, and G. Seytre, "Evolution of the coefficient of thermal expansion of a thermosetting polymer during cure reaction," *Polymer (Guildf).*, vol. 46, no. 23, pp. 9919–9927, Nov. 2005.

[18] Y. K. Kim and S. R. White, "Stress relaxation behavior of 3501-6 epoxy resin during cure," *Polym. Eng. Sci.*, vol. 36, pp. 2852–2862, 1996.

[19] S. Sourour and M. R. Kamal, "Differential Scanning Calorimetry of Epoxy Cure: Isothermal Cure Kinetics," *Thermochim. Acta*, vol. 14, pp. 41–59, 1976.

[20] W. Steinmann, S. Walter, M. Beckers, G. Seide, and T. Gries, *Thermal Analysis of Phase Transitions and Crystallization in Polymeric Fibers, Applications of Calorimetry in a Wide Context - Differential Scanning Calorimetry*. 2013.

[21] E. A.Turi and R. B. Prime, "Thermal Characterization of Polymeric Materials, Thermosets." pp. 1380–1746.

[22] J. D. Menczel and R. B. Prime, *Thermal Analysis of Polymers, Fundamentals and Applications*. .

[23] E. Suhir, Y. C. Lee, and C. P. Wong, *Micro and Opto Electronic Materials and Structures*. .

[24] D. W. Van Krevelen and K. Nijenhuis, *Properties of Polymers*. 2009.

[25] M. E. Ryan, "Rheological and heat-transfer considerations for the processing of reactive systems," *Polym. Eng. Sci.*, vol. 24, no. 9, pp. 698–706, Jun. 1984.

[26] M. R. Kamal and S. Sourour, "Kinetics and thermal characterization of thermoset cure," *Polym. Eng. Sci.*, vol. 13, no. 1, pp. 59–64, Jan. 1973.

[27] M. R. Kamal, "Thermoset Characterization for Moldability Analysis," *Polym. Eng. Sceince*, vol. 14, no. 3, pp. 231–239, 1974.

[28] C. D. Han and K.-W. Lem, "An Experimental Study on the Injection Molding of Thermosetting Polyester Resin," *Polym. Eng. Sci.*, vol. 24, no. 7, pp. 473–481, 1984.

[29] A. Y. A. Malkin and S. G. Kulichikhin, "Rheokinetics of Curing of Epoxy Resins Near the Glass Transition," *Polym. Eng. Sci.*, vol. 37, no. 8, pp. 1322–1330, 1997.

[30] T. Ozawa, "Estimation of activation energy by isoconversion methods," *Thermochim. Acta*, vol. 203, pp. 159–165, 1992.

[31] T. Ozawa, "Kinetic Analysis of Derivative Curves in Thermal Analysis," *J. Therm. Anal.*, vol. 2, pp. 301–324, 1970.

[32] J. H. Flynn and L. A. Wall, "A quick direct method for the determination of activation energy from thermogravimetric data," *Polym. Lett.*, vol. 4, pp. 323–328, 1966.

[33] C. D. Doyle, "Kinetic Analysis of Thermogravimetric Data," *J. Appl. Polym. Sci.*, vol. V, no. 15, pp. 285–292, 1961.

[34] J. Opfermann and E. Kaisersberger, "An advantageous analysis variant of the Ozawa-Flynn-Wall," *Thermochim. Acta*, vol. 203, pp. 167–175, 1992.

[35] H. L. Friedman, "Kinetics of thermal degradation of char-forming plastics from thermogravimetry. Application to a phenolic plastic," *J. Polym. Sci. Part C Polym. Symp.*, vol. 6, no. 1, pp. 183–195, 1964.

[36] H. E. Kissinger, "Reaction Kinetics in differential thermal analysis," *Anal. Chem.*, no. 1956, pp. 1702–1706, 1957.

[37] M. J. Starink, "The Determination of Activation Energy from Linear Heating Rate Experiments: A Comparison of the Accuracy of Isoconversion Methods," *Thermochim. Acta*, vol. 404, pp. 163–176, 2003.

[38] M. D. Patel, K. M. B. Jansen, L. J. Ernst, J. Zhou, and C. Bohm, "Study of Time and Temperature Dependency of Bulk Modulus for Moulding Compound by Transient Bulk Creep Experiments," in *ASME International Mechanical Engineering Congress and Exposition*, 2007, pp. 1–5.

[39] P. Bartolomeo, J. F. Chailan, and J. L. Vernet, "On the use of WLF equation to study resin curing by dielectric spectroscopy," *Polymer (Guildf).*, vol. 42, no. 9, pp. 4385–4392, 2001.

[40] K. M. B. Jansen, "Innovative Thermo-Mechanical Prediction and Optimization Methods for Virtual Prototyping of Miniaturised Electronic Packages and Assemblies - mevipro project," 2005.

[41] J. H. Dymond and R. Malhotra, "The Tait Equation : 100 Years," *Int. J. Thermophys.*, vol. 9, no. 6, pp. 941–951, 1988.

[42] H. Ardebili and M. G. Pecht, *Encapsulation technologies for electronic applications*, First edit. 2009.

[43] J. B. Enns and J. K. Gillham, "Time-Temperature-Transformation (Ttt) Cure Diagram: Modeling the Cure Behavior of Thermosets.," *J. Appl. Polym. Sci.*, vol. 28, no. 8, pp. 2567–2591, 1983.

Chapter 3

Dynamic Modeling of the Curing and the Fully Cured Epoxy Molding Compound

3.1. Introduction

The mechanical model for elastic solid materials is given by the classical theory of elasticity [1]. The stress strain relationship is represented by Hooke's law which states that the stress is directly proportional to the strain but independent of the strain rate. On the other hand, the stress is proportional to the strain rate for an ideal viscous fluid but, independent of the strain. The given relationships may apply for the ideal fluid and the ideal solid materials under infinitesimal strain rate and infinitesimal strain conditions, respectively. However, the mechanical behavior of polymeric materials is neither elastic nor viscous but somewhere in between, and depending on the thermo-mechanical loading conditions the one prevails over the other. Elasticity of solid materials and the viscosity of liquids are represented by different constitutive equations. Therefore, the model representing one end of the spectrum will not be applicable to the other end.

3.2. Stress Relaxation

In theory all materials are viscoelastic in nature, nonetheless, the degree of change of modulus with respect to time is small and can be ignored, generally. Furthermore, for most materials the time dependent behavior is difficult to be detected experimentally. Therefore, the classification of materials regarding their time dependent behavior is empirical rather

than theoretical. Polymers, on the other hand, are the main viscoelastic materials due to their strong time dependent behavior which can be clearly detected by dynamic measurements.

The stress response of a viscoelastic polymer under instantaneously applied constant strain condition is compared to the stress response of a Newtonian fluid and to an elastic Hookean solid in figure 3.1. In case of an elastic Hookean solid the resulted stress is constant as far as the strain remains constant and for a viscous Newtonian fluid the stress relaxes instantly to zero. However, a viscoelastic polymer shows stress relaxation which can be either back to zero for a liquid viscoelastic polymer or to an equilibrium stress level for a solid viscoelastic polymer [2]. Stress for a solid viscoelastic polymer may also relax to the initial zero stress state but a longer relaxation time is required for a viscoelastic material with dominant elastic character.

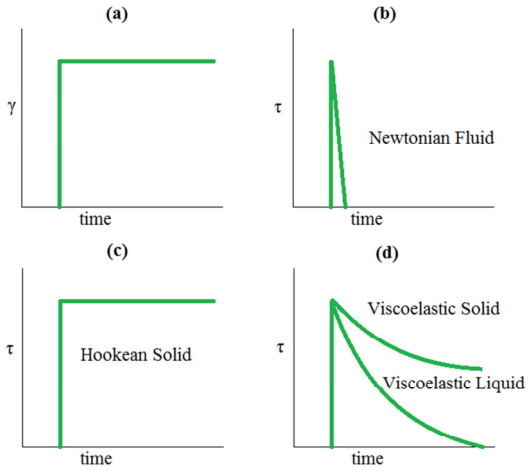

Figure 3.1 Stress response to an applied a) constant step strain for a b) Newtonian viscous fluid, c) Hookean elastic solid, d) Viscoelastic solid and viscoelastic liquid

Viscoelasticity can be defined as time and temperature dependent mechanical behavior of the material. The viscoelastic material is more elastic than viscous if they are exposed to shorter deformations at lower temperatures and they are more viscous rather than elastic if the deformation is applied for longer times at higher temperatures. In literature, for a fluid material with viscoelastic properties the term rheology is used instead of viscoelasticity. Throughout this chapter both terms can be used interchangeably depending on the material's physical state.

3.3. Theory of Linear Viscoelasticity

The Boltzmann Superposition Principle, proposed by Boltzmann in 1876 is the pillar of the linear viscoelastic theory [3]. It states that the deformation history affects the instantaneous response of the viscoelastic material to the applied loadings. Moreover, each incremental deformation is accumulated, independently. If a viscoelastic material is exposed to a constant stress then the addition of any incremental stress will build up to the creep of the previous loading. The same principle applies to the constant strain case in which an additional strain will lead to stress relaxation which starts after the previous loading as if the material is unloaded prior to the application of the load. The proposed principle is demonstrated in figure 3.2, and the mathematical description of the principle applied for the incremental stress relaxation can be given as

$$\sigma_t = \Delta\varepsilon_1 E(t-t_1) + \Delta\varepsilon_2 E(t-t_2) + \Delta\varepsilon_3 E(t-t_3) + \cdots \tag{3.1}$$

where σ_t is the time dependent stress and $\Delta\varepsilon_i$ is the incremental strain. E is the modulus and $E(t-t_i)$ is the relaxation modulus corresponding to the applied deformation period. The equation can be generalized to

$$\sigma_t = \int_{-\infty}^{t} E(t-\zeta)\,\dot{\varepsilon}(\zeta)\,d\zeta, \tag{3.2}$$

where $\dot{\varepsilon}(\zeta) = \frac{d\varepsilon_\zeta}{d\zeta}$. The integration is carried out from past times ζ to the current time t. It can be rewritten by replacing $t-\zeta$ by s:

$$\sigma_t = \int_{0}^{\infty} E(s)\,\dot{\varepsilon}(t-s)\,ds, \tag{3.3}$$

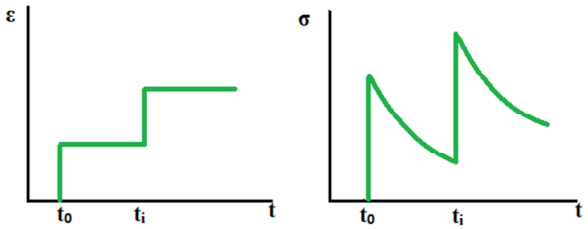

Figure 3.2 Step strain and the corresponding stress response

3.4. Dynamic Mechanical Analysis

The viscoelastic behavior of polymers requires special characterization techniques. Stress relaxation, creep and dynamic mechanical analysis are the main test methods. Dynamic mechanical measurements are the most widely conducted experimental techniques for the viscoelastic analysis of the polymers. Various test set-ups available, depending on the

sample physical state and the stiffness function for which the test is conducted. Dynamic measurements can be conducted either by applying a cyclic strain on a curing or cured sample and measuring the resulting stress or inversely, by applying the cyclic stress and measuring the resulting strain. The former method is more common than the latter. If the tested sample is in its solid state then the applied measurements are called viscoelastic analysis or dynamic mechanical analysis (DMA), and if the sample is in liquid state or will be liquidized during the experiment then the applied testing more commonly named as rheological measurement.

A sinusoidal measurement conducted at an angular frequency ω equivalent to a transient experiment at time t. As mentioned above in DMA measurements usually a sinusoidal strain is applied and the corresponding stress data is recorded. A sinusoidal oscillation of a strain in a shear deformation can be given by

$$\gamma_t = \gamma_0 sin(\omega t), \tag{3.4}$$

where γ_t is the time dependent strain and γ_0 stands for the strain amplitude. A same sinusoidal strain oscillation may also applied to a tensile deformation which yields

$$\varepsilon_t = \varepsilon_0 sin(\omega t), \tag{3.5}$$

where ε_t is the time dependent strain and ε_0 is the strain amplitude. The resulting time dependent stresses can be obtained by applying the Hooke's and Newton's laws:

$$\tau_t = \mu\dot{\gamma}_t = \mu\omega\gamma_0 cos(\omega t) = \mu\omega\gamma_0 sin\left(\omega t + \frac{\pi}{2}\right) \tag{3.6}$$

$$\sigma_t = E\varepsilon_t = E\ \varepsilon_0 sin(\omega t). \tag{3.7}$$

$\frac{\pi}{2}$ shows that the stress in a shear deformation is 90^o out of phase as opposed to the stress in tensile deformation which is in phase with the strain. The DMA working principle is based on this phase shift of viscous behavior. Such that a material with an in phase stress response shows elastic behavior and a sample with 90^o out of phase response shows completely liquid like behavior. A viscoelastic material will show a phase lag between 0 and 90^o which determines the relative degree of viscous character to elastic character. Therefore, the stress response for the applied strain will be out of phase with a phase angle of δ degrees.

$$\sigma_t = \sigma_0 sin(\omega t + \delta) \tag{3.8}$$

The most important time dependent material property that can be obtained using DMA is the complex modulus which shows the modulus associated with viscous and elastic character of the material. By combining equations 3.3 and 3.5 stress equation can be rewritten as

$$\sigma_t = \int_0^\infty \omega\, E(s)\, \varepsilon_0 \cos\big(\omega(t-s)\big)\, ds. \tag{3.9}$$

It can be extended by applying a trigonometric identity

$$cos(a-b) = sin(a)\, sin(b) + cos(a)\, cos(b), \tag{3.10}$$

that yields

$$\sigma_t = \varepsilon_0\Big[\sin(\omega t)\, \omega \int_0^\infty E(s) \sin(\omega s)\, ds + \cos(\omega t)\, \omega \int_0^\infty E(s) \cos(\omega s)\, ds\Big] \tag{3.11}$$

Both integral terms in equation 3.11 are frequency dependent and not time. Moreover, the first term is in phase while the second one is out of phase with the strain ε since $\cos(\omega t) = \sin(\omega t + 90^0)$. Equation 3.11 can be rewritten as

$$\sigma_t = \varepsilon_0[\sin(\omega t)\, E' + \cos(\omega t)\, E'']. \tag{3.12}$$

where E' and E'' are defined as the storage modulus and the loss modulus representing the two frequency dependent in phase and out of phase functions, respectively.

Equation 3.8 can be rewritten by expanding the sine function based on a trigonometric identity

$$sin(a+b) = cos(a)\, sin(b) + sin(a)\, cos(b), \tag{3.13}$$

which leads to

$$\sigma_t = \sigma_0[\sin(\omega t)\cos(\delta) + \cos(\omega t)\sin(\delta)] \tag{3.14}$$

By comparing equation 3.12 and 3.14 storage and loss moduli can be redefined as a function of phase angle and sinusoidal amplitudes.

$$E' = \frac{\sigma_0}{\varepsilon_0}\cos(\delta) \tag{3.15}$$

$$E'' = \frac{\sigma_0}{\varepsilon_0}\sin(\delta) \tag{3.16}$$

Trigonometric sine and cosine functions can be defined as complex exponential:

$$e^{i\theta} = \cos\theta + i\sin\theta \tag{3.17}$$

where $i = \sqrt{-1}$. Using the complex exponential definition 3.17 the complex modulus can also be represented in terms of complex stress and strain terms as

$$E^* = \frac{\sigma_0\, e^{i(\omega t+\delta)}}{\varepsilon_0\, e^{i\omega t}} = \frac{\sigma_0}{\varepsilon_0}\,[cos(\delta) + i\, sin(\delta)] = E' + iE'' \tag{3.18}$$

So, E' is the real part of the complex modulus corresponding to the elastic behavior and the imaginary part, E'', refers to the viscous character of the viscoelastic material. For an ideal elastic material where the phase lag is zero, E' becomes the tensile modulus and E'' becomes zero. On the other hand, for an ideal liquid where the phase lag is 90°, E' becomes zero and E'' will be a function of viscosity. The magnitude of the complex modulus is defined as

$$|E^*| = \sqrt{E'^2 + E''^2} \tag{3.19}$$

Another useful property that can be obtained by DMA is loss tangent, $tan(\delta)$ showing the ratio of energy lost to energy stored:

$$\tan(\delta) = \frac{E''}{E'} \tag{3.20}$$

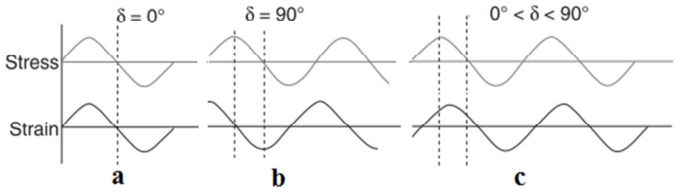

Figure 3.3 Sinusoidal stress strain curves for a) ideal solid, b) ideal liquid and c) viscoelastic materials

The aforementioned DMA technique is particularly important when the sample material is a viscoelastic solid and therefore, the dynamic tensile experiment is applicable and provides valuable data. However, there are times that the tensile test cannot be applied, for instance because of the liquid like behavior of the tested sample. Then shear deformation can be applied to determine the mechanical properties of a liquid-like material. Therefore, by applying a sinusoidal shear strain, γ, and the measured shear stress, τ, the complex shear modulus can be obtained. The derivation used for the complex tensile modulus can also be applied directly to obtain the complex shear modulus. Then, we have

$$G^* = \frac{\tau_0}{\gamma_0}\,[cos(\delta) + i\,sin(\delta)] = G' + iG'' \tag{3.21}$$

Here, G' and G'' refer to the shear storage modulus and shear loss modulus, respectively.

For rheological measurements the main interest is to obtain the viscosity. The complex viscosity is expressed by

$$\mu^* = \tau/\dot{\gamma}, \tag{3.22}$$

where $\dot{\gamma}$ is the applied shear rate. The same derivation method used for the complex tensile and shear moduli can also be applied to obtain the complex viscosity, μ^*.

$$\mu^* = \frac{\tau_0\, e^{i(\omega t+\delta)}}{\omega\, \gamma_0\, e^{i\omega t}} = \frac{\tau_0}{\omega\gamma_0}\,[sin(\delta) + i\, cos(\delta)] = \mu' - i\mu'', \tag{3.23}$$

The relationship between the components of the complex shear modulus and complex viscosity can be derived from equations 3.21and 3.23 such that it provides a basis for viscosity analysis using the dynamic mechanical analysis shear setup. The real part of the complex viscosity can be represented in terms of the loss modulus of the complex shear modulus while the imaginary component is associated with the storage modulus [4].

$$\mu' = G''/\omega \tag{3.24}$$

$$\mu'' = G'/\omega \tag{3.25}$$

$$\mu^* = G^*/i\omega \tag{3.26}$$

Then, the viscosity of an ideal liquid will have the real component only and the viscosity of an elastic solid will be based on the imaginary component. Furthermore, the magnitude of the complex viscosity is defined by

$$|\mu^*| = |G^*|/\omega \tag{3.27}$$

3.5. Constitutive models

The spring and dashpot analogy is often used to describe the basic mechanical modeling of elastic and viscous materials where the Hookean solid is characterized by a spring and the Newtonian fluid is represented by a dashpot. Therefore the elastic modulus, E, in Hooke's formula is used for the spring constant and the viscosity, μ, represents the damping coefficient. The corresponding models are given as

$$\sigma = E\varepsilon \qquad \text{Hooke's Elastic Solid} \tag{3.28}$$

$$\sigma = \mu\dot{\varepsilon} \qquad \text{Newtonian Viscous Fluid} \tag{3.29}$$

The spring element exhibits instantaneous extension or instantaneous recovery upon step loading or unloading. The dashpot element, on the other hand, symbolizes a piston moving in a viscous fluid and is used to describe the time dependent behavior.

The viscoelastic models are developed by combining the two aforementioned elements in various forms. The most basic combinations are the series and the parallel connections of a single spring and a single dashpot elements which are known as Maxwell and Kelvin-Voigt models, respectively.

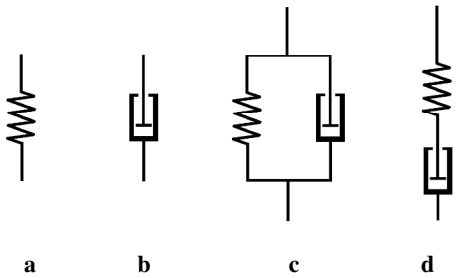

Figure 3.4 a) Spring element, representing the elastic behavior, b) Dashpot element, representing the viscous behavior, c) Voigt-Kelvin element (parallel combination of spring and dashpot), d) Maxwell element (in series arrangement of spring and dashpot elements)

For the Maxwell model where the spring and dashpot are in series arrangement, the elastic and viscous strains are additive. Hence, the total strain gives

$$\sigma + \lambda\dot{\sigma} = \mu\dot{\varepsilon}, \tag{3.30}$$

where λ is μ/E, signifying the relaxation time of the material. The Maxwell model is not suitable for creep modeling of a viscoelastic material since it exhibits a typical viscous behavior by being deformed unlimited for a constant external stress. Furthermore, the expected recovery upon removing of the stress cannot be modeled by the Maxwell model.

In Voigt-Kelvin model where the spring and the dashpot elements are combined in parallel, the elastic and viscous stresses are additive. Hence, the total stress gives

$$\sigma = E\varepsilon + \mu\dot{\varepsilon}, \tag{3.31}$$

In parallel arrangement for the uniaxial tension, the spring extension is restricted by the dashpot. Therefore, it exhibits decelerating creep dominated by the dashpot extension. Upon stress release the extended spring will compress the dashpot back to the original position providing a full strain recovery after unloading. This contraction effect cannot be modeled by the Maxwell model. It is apparent that the Voigt model is quite effective in predicting creep but, inadequate in stress relaxation since the stress due to constant step strain relaxes immediately. Moreover, the relaxation will not be completed.

The standard linear model and the Burgers model are the other two important viscoelastic models. The former is known as the three element model, while the latter as the four element model. The standard model is a combination of a Voigt-Kelvin and a spring elements in series. And the Burgers model comprises a Maxwell and a Voigt-Kelvin elements which are connected in series. The following equation is derived for the standard linear model

$$\sigma + \lambda\dot{\sigma} = E_1\varepsilon + (E_1 + E_2)\lambda\dot{\varepsilon}. \tag{3.32}$$

And the Burgers model can be defined by

$$\sigma + a_1\dot{\sigma} + a_2\ddot{\sigma} = b_1\varepsilon + b_2\dot{\varepsilon} + b_3\ddot{\varepsilon}. \tag{3.33}$$

A detailed study of the these models will not be given in this thesis and an interested reader may refer to the relevant references [2], [3], [5]–[8].

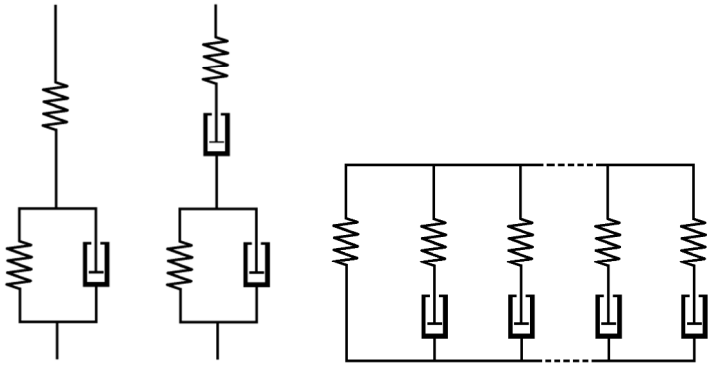

Figure 3.5 a) The standard linear (three element), b) Burgers (four element) and c) Generalized Maxwell models

A more sophisticated model is required to simulate the complex time dependent mechanical structure of a real viscoelastic polymer. Combining a number of Maxwell elements in series does not make any change in characteristic behavior. Thus, multiple Maxwell elements in series, mechanically is the same as a single Maxwell element [9]. On the other hand, Maxwell models connected in parallel with addition of a single spring element perfectly represents the viscoelastic behavior such as elasticity with different retardation times and stress relaxation with various relaxation times corresponding to each individual Maxwell element. The emerged model is the most general form of the linear model and accordingly named as the generalized Maxwell model.

The relaxation modulus function of the generalized Maxwell model is given by

$$E(t) = \sum_{i=1}^{N} E_i \exp(-t/\lambda_i). \tag{3.34}$$

And the storage and loss moduli are defined by

$$E'(\omega) = \sum_{i=1}^{N} \frac{E_i\,\omega^2\lambda_i^2}{1+\omega^2\lambda_i^2}, \tag{3.35}$$

$$E''(\omega) = \sum_{i=1}^{N} \frac{E_i \omega \lambda_i}{1+ \omega^2 \lambda_i^2}, \tag{3.36}$$

where E_i is the pre-exponential factor and λ_i is the time constant for each branch such that

$$\lambda_i = \frac{\mu_i}{E_i}. \tag{3.37}$$

The series in equation 3.34 is also known as the Prony series and is often used to implement viscoelastic material behavior in FEM calculations.

3.6. Rheological modeling of reacting systems

The viscosity is an important parameter in thermoset processing, which is not only affected by the temperature and time like in thermoplastics, but it is also directly affected by the curing reaction of the polymer. This correlation between conversion and viscosity must be clearly identified and modeled. The processing temperature during molding affects the flowing resin in two opposite ways. Viscosity rises quickly as a result of higher cure rate at a higher temperature. On the contrary, higher temperature results in lower initial viscosity. Moreover, at the same conversion level the viscosity is lower for a higher temperature.

A detailed overview of chemorheological characterization methods and models is given by Ryan [10].According to Ryan the viscosity of an epoxy can be modeled as a function of time, temperature, pressure, filler content and shear rate;

$$\mu = \mu(t, T, P, F, \dot{\gamma}). \tag{3.38}$$

Although the conversion is not stated explicitly as a variable, yet, the time and the temperature parameters indirectly determines the epoxy's degree of cross-link. The effect of each parameter on viscosity can be determined by various measurement methods. Therefore, it is difficult to establish a single comprehensive model taking into account all of the influencing parameters. Based on the process conditions and the material properties the most significant variables can be determined. For a non-Newtonian fluid the main characteristic of the flow is a variable viscosity which mostly depends on the shear rate. Therefore, the majority of the non-Newtonian fluid models are classified as shear dependent. These models which are mainly applied to thermoplastics, used in injection molding, can be classified as; Power Law, Ellis, Carreau, Cross and Cross-Carreau. These are all strain rate dependent models. However, they do not take into account the effect of conversion which is essential in thermoset rheology modeling. The temperature effect is introduced as an independent Arrhenius multiplication term [11].

Viscosity characterization of thermosetting polymers should be interrelated to their conversion level. Kamal studied the isothermal viscosity variations of thermosetting epoxy

at a fixed reaction level [12]. An early work of Flory suggested a correlation between the average molecular weight and viscosity during cure [13]. Macosko and Miller developed a simplified approach based on Flory's formula such that they determined the weight averages directly rather than the indirect method of Flory [14]. The viscosity was found to be independent of shear rate by some studies conducted using Rheometrics Mechanical Spectrometer, in cone and plate setup for reacting Poly Urethane systems [15], [16]. In another important study Perry et al designed a parallel plate viscometry for fast polymerizing polyurethane system, which is fitted directly to a reaction injection molding machine. The viscosity was assumed to be independent of strain rate [17].

Although this is not true for most thermosetting epoxy compounds, still it may apply under certain processing conditions and for specific thermosetting polymers. Nguyen, for example, claimed that at high mold temperature during the initial stages of cure, strain rate dependency may be ignored for the die encapsulation epoxy compound [18]. A simple time dependent exponential growth and a time dependent power law formulas were used by Malkin and Kulichikin [19], which were applied on low and high conversion levels, accordingly. A dual Arrhenius temperature and time dependent model was developed by Martin and Tungare at which the model parameters were derived from the non-isothermal viscosity data obtained using dynamic oscillatory parallel plate rheometry [20], [21]. The logarithm of viscosity rate which is the instantaneous viscosity divided by the minimum viscosity of the polymer was related to the WLF equation by Enns et al. [22]. Then a formulation was developed from a combined Arrhenius, weight average molecular weight and WLF equations. The same formula was also adapted by Kadijk to define the zero shear rate viscosity parameter, where the shear thinning viscosity behavior was formulated by the generalized Cross-Carreau model [23].

A viscosity model must meet the following requirements [11]:

- The higher the temperature, the lower the viscosity at the same conversion level.
- The viscosity decreases at a deceasing rate with increasing temperature.
- The iso-shear rate curves never cross over.

A model taking into account the effects of temperature as well as the degree of conversion and the gel point was introduced by the Castro and Macosko [24]. The proposed model was later used by many of researchers for reacting systems. Nguyen and Halley studied fast curing epoxy molding compounds used specifically in IC encapsulation [25], [18]. Nguyen showed that the Castro Macosko model provided the best fit for fast curing systems.

In this thesis, the viscosity data were modelled by Castro Macosko model based on isothermal parallel plate rheometry experiments and correlated with the autocatalytic

Kamal and Sourour kinetic model in order to determine the gel point. The equation is given as

$$\mu = \mu_0 \left[\frac{\xi_g}{\xi_g - \xi}\right]^{(J_1 + \xi J_2)}, \tag{3.39}$$

where μ_0 is the initial or zero shear rate viscosity and ξ_g represents the degree of conversion at gelation. J_1 and J_2 are fitting parameters.

3.6.1. Viscosity measurements

Thermosetting epoxy processability is determined by its viscosity during filling. In polymerizing systems the viscosity at the high molding temperature increases in a rapid rate. Due to fast crosslinking of the commercially available encapsulants only the first few minutes are suitable for cavity filling. Depending on the cure kinetics of the epoxy, the conversion rises rapidly at the high mold temperature which results in an increase in viscosity. The higher the viscosity the more pressure is required for filling which would be detrimental for the wire connections and the other vulnerable components. A high viscosity may also lead to high shearing stress values. Furthermore, upon passing the gel point where the flow is inhibited, residual stresses start to build up (under constrained boundary conditions) which additionally may result in warpage of the package. The failure types associated with high viscosity are incomplete filling, air trap, paddle shift and wire sweep. Therefore, material behavior during filling should be characterized experimentally and a model representing the viscosity change as a function of conversion and temperature is essential for a reliable encapsulation simulation.

Figure 3.6 is a schematic plot of a typical viscosity change during molding. Initially the viscosity is low because of the high molding temperature. Then by the start of polymerization the viscosity rises first gradually in a slow rate and later at a rapid rate until the gel point. The gel point restricts any further flow. In this thesis, it is assumed that any stress relaxes fully below the gel point where the polymer is essentially in a liquid phase. Therefore, the relaxation modulus is taken zero below the gel point and any modulus increase associated with the phase change from a highly viscous melt to a viscoelastic solid should be formulated beyond this point. The details of the modulus formulation depending on the process conditions are given in chapters 5 and 6.

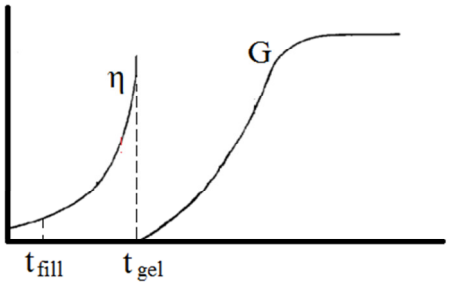

Figure 3.6 Schematic of the viscosity and the relaxation modulus during cure

3.6.2. Cox-Merz Rule

The sinusoidal data obtained by dynamic shear experiments can be converted to steady state viscosity using an empirical relationship developed by Cox and Merz [26]. The proposed rule which is known as the Cox-Merz rule relates the complex viscosity to the steady state shear viscosity at angular frequency ω and a shear rate, $\dot{\gamma}$= ω. Although the theoretical basis of the rule has not been explained so far, the dynamic measurements showed that it is accurate at low frequencies and low shear rates for most polymeric systems. However, there are studies questioning the applicability of the rule to thermoplastic melts [27].

The low frequency assumption can be expressed by

$$\mu'(\omega)|_{\omega\to 0} = \mu(\dot{\gamma})|_{\dot{\gamma}\to 0} \,. \tag{3.40}$$

The equation is based on the fact that the material is more viscous in nature at lower frequency rates. Therefore, the elastic behaviour is mostly negligible. Then, equation 3.40 can also be given as

$$\mu^*(\omega)|_{\omega\to 0} = \mu(\dot{\gamma})|_{\dot{\gamma}\to 0} \,. \tag{3.41}$$

Empirically proven that it provides a high accuracy at low frequency when $\dot{\gamma}$= ω [27].

$$|\mu^*(\omega)| = \mu(\dot{\gamma})|_{\dot{\gamma}=\omega} \,. \tag{3.42}$$

3.6.3. Gel point

A crucial phenomenon in curing of the thermosetting resins is the gelation which is considered as the physical transformation of an epoxy polymer from a high viscous liquid state to a solidified viscoelastic gel where no further flow is possible. This transition occurs due to a rapid rise in viscosity as a result of entangled polymer network formation of the curing thermoset. Gelation can be achieved at different times depending on the applied cure

temperature. The gel point which is the curing material's intrinsic property is defined as the conversion level at the gelation and it indicates the processability limit of the EMC. The epoxy below the gel point is considered as liquid where the generalized Newtonian model defines the dynamics of the flow. At this stage the stress depends on viscosity and the viscosity is considered as a function of time, temperature and conversion. Hence below the gel point the elastic definition for the mechanical response of the strain is not valid and the viscous character dominates. Therefore, in this study, it is assumed that the stress relaxes fully below the gel point. As a result, the stress contribution to the residual stress below the gel point is essentially zero. The cure induced stress building up inside the package is taken into account above the gel point until the maximum degree of conversion is reached at the end of molding (see chapter 5).

Various techniques can be implemented for gel point determination. Different gel points would be obtained if different test methods are applied. Gel point is the most studied rheological parameter and in literature various testing techniques have been conducted so far. The simplest is the manual testing of the bulk material under various isothermal conditions [15]. The experiment can be conducted by an ice pick, a screw driver or a similar tool. The sample can be probed continuously and the time at solidification is assumed as the gel time. Although it is the simplest of the gel point experiments it yielded reproducible results [15]. This method was also attempted in this study by heating the EMC pellets in the oven. The solidification of the samples was tested manually by probing them continuously; initially in longer time intervals and later close to the expected gel point, more frequently. The thermal fluctuation during the sample inspection was the main drawback of the method, which led us to looking for another technique. It was difficult to keep the temperature of the oven and the sample at a pre-set cure temperature. The isothermal temperature of the oven dropped when the samples were checked. Although the temperature drop did not affect the sample temperature much, yet the associated heating of the oven to preserve the pre-set oven temperature resulted in an extra rise of the sample temperature over the oven temperature. This phenomenon increased the degree of conversion of the epoxy without giving any clue about the sample thermal history. At the higher cure temperatures a few degrees of temperature fluctuation may cause to significant variation in the EMC's degree of crosslink reaction. Hence, it can be concluded that the gel point was difficult to detect and almost impossible to be linked to the degree of conversion experimentally. Theoretically, the viscosity of a high polymer melt should jump to infinity at the gel point where the fluid to solid transition occurs. However, experimentally it is impossible to record the infinity. Therefore, in some studies the instantaneous relative viscosity of 10^3 or 10^4 Pa.s was assumed as an indication for gelation [28][29]. The most frequently adopted method for gel point determination is multi-frequency dynamic oscillatory measurement. The cross-over of storage modulus and loss modulus is

considered as the point where the gelation starts [30]. Yang showed that the gel point obtained by dynamic measurements is smaller than the predetermined relative viscosity value set for gelation [28]. Other than the mechanical experimental techniques explained here, the gel point can also be predicted using the chain branching theory of Flory [13] or as an onset of molecular insolubilization [22].

3.6.4. Parallel plate rheometry

The conversion dependent shear modulus and viscosity of the epoxy molding compound are tested using the parallel plate Rheometrics RSA 2. The parallel plate setup gives the ability to perform torsional dynamic measurements starting from the liquid state of the epoxy to the gel state where the further flow of the sample is restricted by the infinite network of the crosslink build-up during cure. The tests were performed at isothermal cure temperatures of 130,140,150 and 160^{o}C.

Figure 3.7 Rheometrics RSA2

The sample preparation starts by pulverizing the EMC pellets and compressing the resulting powder into a cylindrical shape with 3 ±0.25mm of thickness. The dimensions of each sample are constrained to the plate diameter which is 2.5cm. Nonetheless, the sample diameter is set smaller than the plate diameter to compensate for the radial expansion when the samples are squeezed by the parallel plates at the start of the measurements. The chamber with the parallel plates set-up was initially heated to the predetermined test temperature. The cylindrical samples are loaded into the test chamber. The sample melts when it touches the stationary bottom disc inside the chamber. The sample melting rate is directly related to the isothermal chamber temperature in which it is loaded. It is much faster for the higher isothermal pre-set temperatures. The elapsed time between the sample

loading and the start of each measurement is a few seconds. Upon loading of the samples, the chamber opening lid is closed immediately to avoid any temperature loss, yet a short temperature fluctuation can be observed. Then the top disc which was raised prior to the sample loading is lowered slowly by the operator. The gradual lowering of the top lid is essential at this point since the liquefied epoxy viscosity is at the lowest level which makes the polymer melt extremely vulnerable to the pressure applied by any external force. The top disc is brought to a point at which the epoxy melt is pressed slightly. At this stage the operator feels a resisting viscous epoxy melt under the top disc and stops pushing further. Due to the adhesive nature of the epoxy the top disc sticks to the epoxy surface and the pre-set oscillation starts immediately. The thickness of the epoxy disc is measured and used as a parameter in the measurements each time, which it is found that the thickness is only changed 0.25mm at most. As can be observed in figure 3.8 the disc shape epoxy compound diameter is in agreement with the discs and no overflow is observed from the sides after the tests.

Figure 3.8 Parallel plates with the epoxy sample in between, after a dynamic viscosity measurement

3.6.5. Determination of steady state viscosity and gel point

The steady state viscosity is derived from the dynamic data by applying the Cox-Merz rule explained in 3.6.2. Isothermal viscosity data with respect to time are given in figure 3.9. The plot does not clearly show the viscosity change at the start. Therefore, a logarithmic plot of the viscosity versus time is also given in figure 3.13. The minimum viscosity values at each isothermal cure temperature are shown in figure 3.11. A decaying exponential trend can be observed. Although this exponential decay is an expected behavior of polymeric compounds at higher cure temperatures, some portion of the initial viscosity, μ_0 is unrecorded due to the instrument sensitivity. Furthermore, especially towards the higher cure temperatures μ_0 would be attained before the start of experiment, for instance, during

sample loading to the chamber. Therefore, the minimum viscosities would be slightly underestimated at higher temperatures but the overall trend will not be different.

Viscosity model fit

The following Arrhenius equation is used for μ_0 determination and the resulted fit is given in figure 3.11.

$$\mu_0(T) = b \exp \frac{T_b}{T_c}, \tag{3.43}$$

where b is fitting constant, T_b is the activation energy dependent variable and T_c refers to the cure temperature in K. T_c is considered to be isothermal during the measurements. However, heat loss is inevitable during the sample loading to the chamber which leads to the thermal fluctuations as it is shown in figure 3.10. Note that, the legends in figures 3.9 to 3.14 represent the average of the applied cure temperatures. The calculations including the viscosity and kinetic models are based on the recorded temperature data and not on the average values. The viscosity model parameters are given in table 3.1.

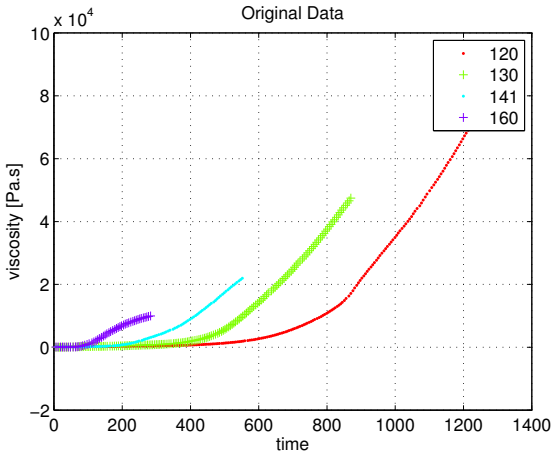

Figure 3.9 Viscosity data obtained by the isothermal constant frequency oscillatory parallel plate rheometry measurements

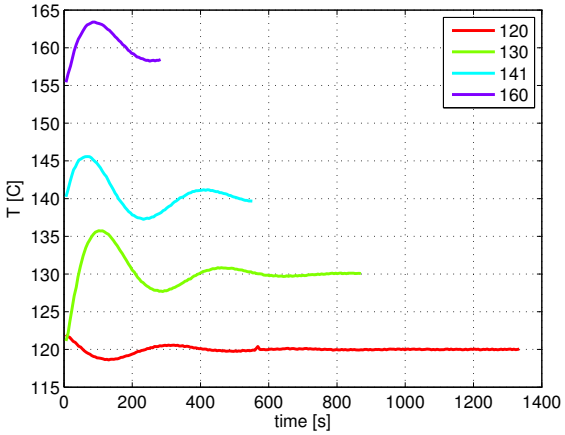

Figure 3.10 Recorded cure temperature during viscosity measurements by parallel plate rheometry

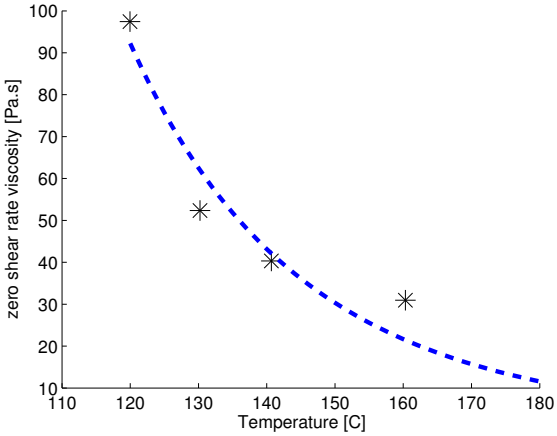

Figure 3.11 Zero shear rate viscosity obtained from each isothermal rheometry experiment and the model representing the variations as a function of temperature (dashed line)

Table 3.1 The Castro Macosko model constants

Castro Macosco Parameters	**J_1** [-]	**J_2** [-]	**b** [Pa.s]	**T_b** [K]
Hitachi	3.5	-4	$3x10^{-8}$	8800
Sumitomo	20	-23	$16x10^{-8}$	2250

The predicted degree of cure for the measured time range at each isothermal experiment is represented in figure 3.12. The autocatalytic Kamal and Sourour model (equation 2.4) is used for the conversion estimation based on the measured temperature profile. The kinetic model parameters are provided in table 2.3. Figure 3.12 shows the conversion degrees until the times at which the tests were stopped or ended.

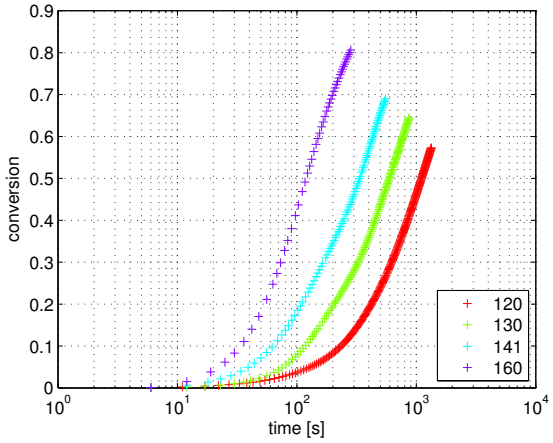

Figure 3.12 Conversion for the tested time range

The logarithmic viscosity plot of 3.13 shows the initial variations of viscosity with respect to the applied cure temperature, in detail. As expected, the higher the temperature, the lower the initial viscosity. Another important phenomenon that can be observed by this graph is the viscosity rate variations. All curves show a slightly “S” shaped behavior with a slower start and end sections and acceleration in between. This acceleration may reflect the reaction peak observed during the cure kinetics measurements in chapter 2.

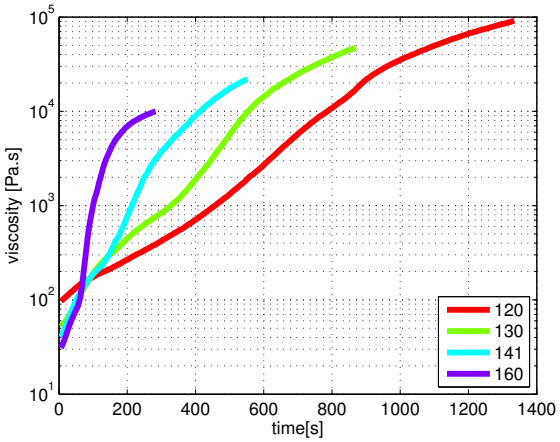

Figure 3.13 Viscosity (log) vs. time data obtained by the isothermal constant frequency oscillatory parallel plate rheometry measurements

Gel point determination

The majority of the gel point determination techniques explained in 3.6.3 are not readily applicable for the single frequency isothermal rheometry experiments conducted in this study. Therefore, the proposed method for the gel point prediction in this study is based on the empirical observations explained for figure 3.13. For a comprehensive understanding of the viscosity data, it is plotted versus the conversion using the kinetic model (equation 2.5). The results are shown in figure 3.14. By increasing the cure temperature the viscosity becomes lower for the same degree of cure. The "S" shaped behavior as explained in figure 3.13 can also be observed in this conversion plot. The points where the steep viscosity rate switches to a milder viscosity change are marked by circles. These are the points where the samples are gelled and the instrument is unable to continue the same torque for the rest of the experiment. Two phenomena may have occurred after this point. Either the contact between the disc and the sample is broken partially or the disc still connected to the epoxy and the rheometer tries to keep up with the imposed stress by increasing the input force. However, it is not as effective as it should be and therefore, the viscosity apparently drops after these points, while the expected behavior is a rapid increase in viscosity. The conversion at these points varies between 42 and 50%. The average of these values is assumed to be the gel point of the tested EMC and is 45%.

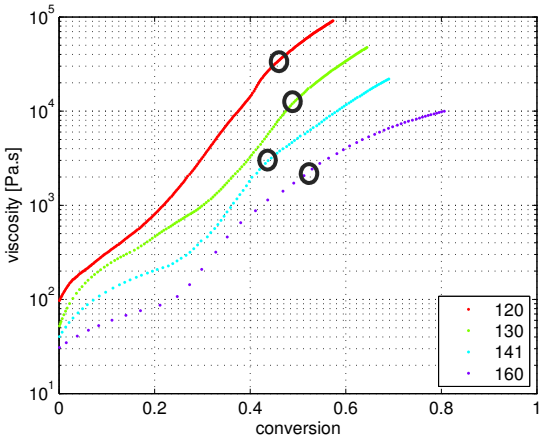

Figure 3.14 Correlated viscosity (log) data vs. conversion. The circles indicate the end of the steep viscosity sections

3.7. Dynamic modeling of fully reacted EMC

The Dynamic Mechanical Analysis TA-Instruments Q800 is used for the dynamic tensile measurements of the fully cured EMC. First, a single frequency dynamic measurement is conducted to obtain a temperature dependent storage modulus. This method provides a fast determination of the modulus to be used later in pseudo-viscoelastic approach undertaken in chapter 5. Besides, a more complete time-temperature superposition DMA study is conducted in section 3.7.3 to obtain the frequency and temperature dependent behavior of the compound.

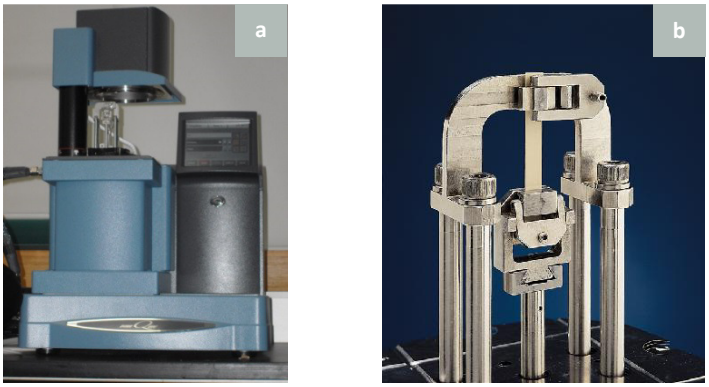

Figure 3.15 a) Dynamic Mechanical Analyzer TA-Instrument Q800, and b) the tensile test set-up

3.7.1. Tensile dynamic measurements

The storage modulus E', loss modulus E'' and $\tan\delta$ data are obtained using a single frequency, DMA heat scan of a fully reacted epoxy sample. A thin rectangular specimen with 17 mm in length, 4.5 mm in width and 0.35 mm in thickness is used for the measurement. Figure 3.16 shows that at room temperature the storage modulus of 9GPa is detected for the Hitachi compound while the gradual heating of the sample to 225°C decreases the storage modulus to 190MPa. On the contrary, the modulus values at the specified temperature range are 17GPa and 500MPa for the Sumitomo compound. The midpoint of the transition region or more precisely a maximum in the loss modulus can be considered as the glass transition temperature of a fully cured epoxy which is 125°C for the Hitachi. This temperature is slightly higher than the glass transition temperature of 113.5°C determined from the DSC scans. For the Sumitomo compound, on the other hand, the glass transition temperature of 128°C agrees well with the one obtained using the DSC measurement.

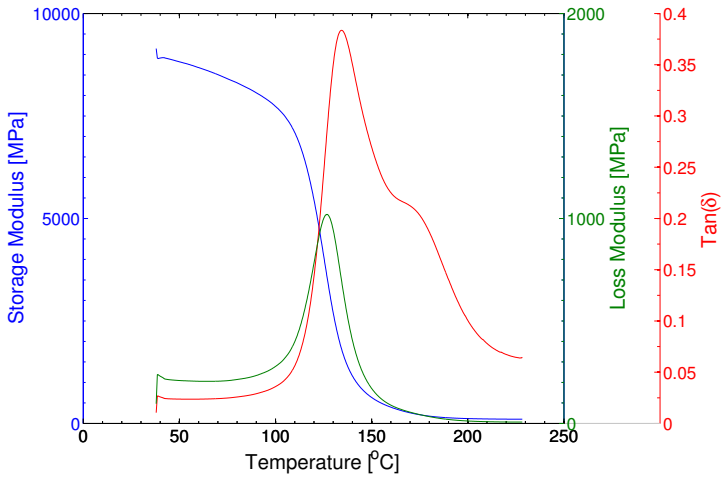

(a)

Figure 3.16 DMA temperature scan of a cured Hitachi (a) and Sumitomo (b) samples at 1Hz

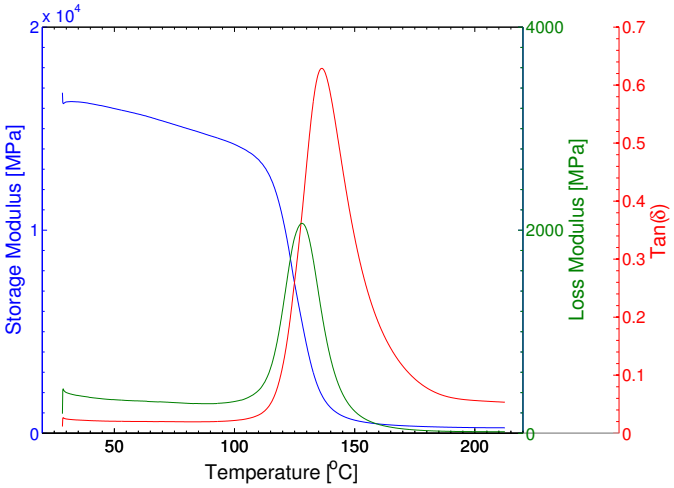

(b)

Figure 3.16 (Continued)

3.7.2. Time dependent behavior

In order to determine the time dependent behavior a similar heating scan experiment was performed but now at multiple frequencies. The applied frequencies are 0.3, 1, 3, 10, 30 and 60Hz. The resulting E', E'' and $\tan\delta$ are shown in figure 3.17. The lower frequencies do not provide a noticeable change in behavior of the tested epoxy and the frequencies higher than 60 Hz are unreliable and noisy due to the instrument sensitivity and low stiffness of the sample.

3.7.3. TTS

The time-temperature superposition (TTS) principle states that the effect of temperature on a time dependent mechanical property is determined by a shift along the time axis. a_T is the multiplication factor which will be referred to as the shift factor. The materials displaying this behavior are named as the thermo-rheologicaly simple (TRS) materials [31]. Mathematically this can be expressed as

$$E(t,T) = E(t_{red},T_r), \tag{3.44}$$

$$E'(\omega,T) = E'(\omega_{red},T_r), \tag{3.45}$$

where $t_{red} = a_T t$ and $\omega_{red} = a_T^{-1}\omega$. $E(t_{red}, T_r)$ and $E'(\omega_{red}, T_r)$ are the so-called "master curves" which only depend on one, reduced, curve at a reference temperature T_r.

The raw data comprising the storage and loss moduli together with the corresponding tan δ determined from this measurement are given in figure 3.17. The shift in glass transition region to a higher temperature range is observed by increasing the frequency.

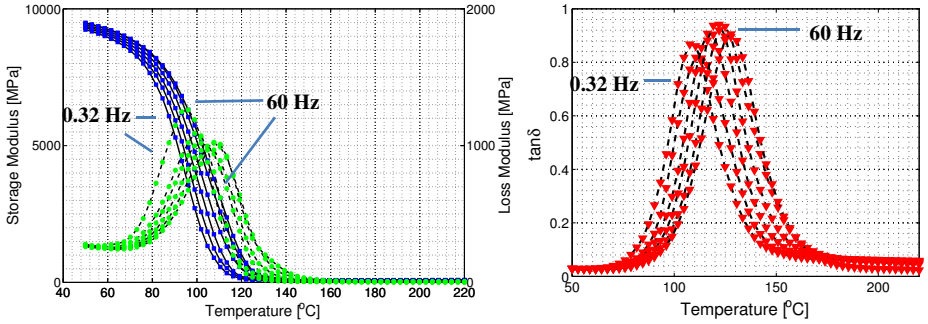

Figure 3.17 Relaxation modulus and tan δ data obtained from a tensile DMA multiple frequency TTS measurement using a fully cured Hitachi sample

In figure 3.18 the storage modulus data of figure 3.17 is plotted versus frequency. The figure clearly shows the glassy and rubbery moduli at 40°C and 250°C, respectively. Using this figure the master curve can be obtained by shifting the isothermal individual curves along the horizontal axis either to a lower frequency (longer deformation time) or to a higher frequency (shorter deformation time) until they all overlap at a point. As a reference temperature usually the glass transition temperature is chosen. The shifting may also be applied to the loss modulus or tan(δ) curves. However, the change of several decades in storage modulus data through the transition region makes the storage modulus favorable due to easier detection and application of the shifting.

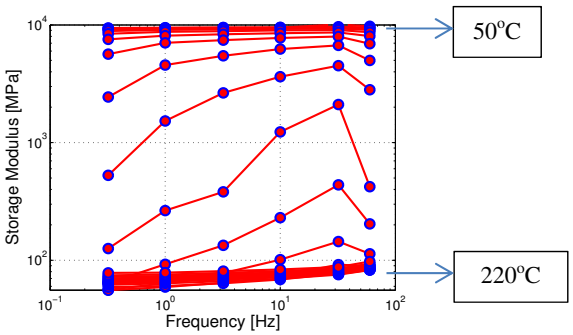

Figure 3.18 Storage Modulus vs. frequency for the range of isothermal measurements

The shifted storage modulus is shown in figure 3.19. T_g is selected as the reference temperature for the shifting such that the data generated above the T_g are shifted towards the left and the data below T_g are shifted to the right. This new derived curve is the master curve of storage modulus for the reference temperature of T_g. Hence, at T_g the shift factor is unity.

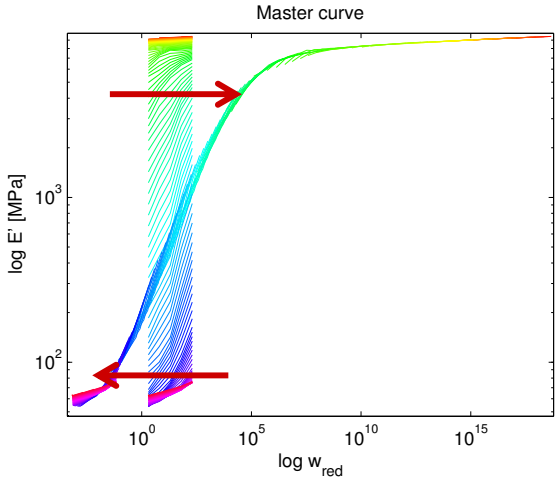

Figure 3.19 TTS and the resulted master curve after shifting, T_r=115°C

Prony series

The Generalized Maxwell model in equation 3.34 is fitted to the determined master curve using a non-linear least square analysis in MATLAB. The Prony terms that cover the range of 25 decades are given in table 3.2.

Table 3.2 The Generalized Maxwell model relaxation time and the stiffness parameters

Generalized Maxwell Branch	Relaxation Time [s]	Stiffness [MPa]
1	1.00E-18	16
2	1.00E-17	99
3	1.00E-16	100
4	1.00E-15	111
5	1.00E-14	116
6	1.00E-13	121
7	1.00E-12	130
8	1.00E-11	136
9	1.00E-10	147
10	1.00E-09	153
11	1.00E-08	179
12	1.00E-07	186
13	1.00E-06	196
14	1.00E-05	367
15	1.00E-04	498
16	1.00E-03	1088
17	1.00E-02	1685
18	1.00E-01	1757
19	1.00E+00	1186
20	1.00E+01	722
21	1.00E+02	303
22	1.00E+03	148
23	1.00E+04	78
24	1.00E+05	10
25	1.00E+06	5
26	1.00E+07	2

Shift Factor

In figure 3.20 the logarithm of shift factor data as a function of temperature is given. A model representing the shift factor is useful when dealing with different temperatures and deformation times. Shift factor models often used in literature are the WLF and the Arrhenius models which are expressed as

$$\log a_{WLF} = \frac{C_1(T-T_r)}{C_2+T-T_r}, \tag{3.46}$$

$$\log a_{Arh} = \frac{-E_a}{2.303\,R}\left[\frac{1}{T}-\frac{1}{T_r}\right], \tag{3.47}$$

where C_1 and C_2 are the fit parameters. R is the gas constant of 8.314 [J/mol/K] and E_{at} [J/mol] refers to the activation energy. T_r is the reference temperature which is chosen as T_g.

The Arrhenius model have been used mostly for the shift factor below the glass transition temperature. The Williams-Landel-Ferry or more simply WLF which is derived based on the effect of temperature on viscosity using the free volume definition above T_g, is used in literature for various material properties modeling including the viscosity and the shift factor. Since the model is derived based on the macroscopic mobility of the polymer above T_g, the applicability of it for the entire tested temperature range is rather restricted. This phenomenon is also clearly visible in figure 3.20 where it is used for the transition plateau and for the temperatures above T_g, respectively. The latter is more precise, while the former is accurate for a constrained transitional region and deviates from the shift factor data by decreasing the temperature close to T_{g0}. The Arrhenius model seems to fit the region below the glass transition better than WLF, as it is expected, yet it deviates faster towards the rubbery plateau when compared to WLF. Both models are applicable with a reasonable accuracy in the glass transition region. The main concern is the transitional region and the change of modulus in glassy and rubbery plateaus is considered as negligible.

A simple second order polynomial model is used instead of the Arrhenius model for the temperatures below the glass transition temperature. Then, the entire tested temperature range is covered by the specified models. The fittings shown in figure 3.20b confirm that the models are in good agreement with the data.

The polynomial model is defined by

$$\log a_{Poly} = \sum_{i=1}^{3} a_i T^{i-1} , \tag{3.48}$$

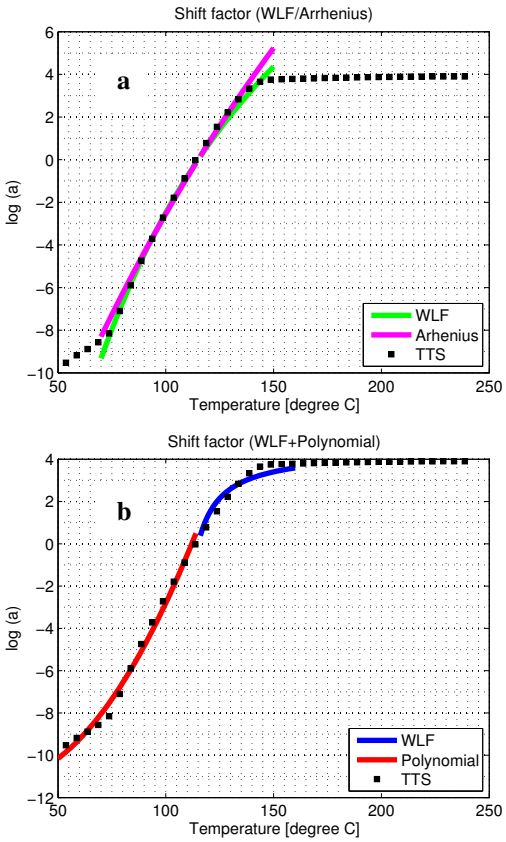

Figure 3.20 Shift factor log(a) vs temperature for the transition region with the reference temperature T_g=115^{o}C based on a) the WLF and Arrhenius models, b) the WLF and the Polynomial models, comparison with the TTS DMA data

In literature, it is shown that C_1 and C_2 values generally provide a good fit for the polymeric systems when chosen 17.44 and 51.60 [K], respectively [5]. However, it is also observed that these parameters may deviate from the general fitting values depending on the physical properties of the epoxies [32]. Therefore, in the linear regression analysis these values were set as an initial estimate for the WLF model but as it can be seen, at the end, the WLF constants are not close to these values. The fit parameter for the WLF, the Arrhenius and the polynomial models are given in table 3.3.

Table 3.3 Shift factor models parameters

WLF $\langle T_{transition} \vert T > T_g \rangle$		Polynomial			Arrhenius
C_1	C_2	a_1	a_2	a_3	E_{at}
[-]	[K]	[-]	[1/K]	[1/K^2]	[J/mol]
25 / 4.43	165 / 10.64	121	-0.88	1.48 10^{-3}	4.7 10^5

3.8. Conclusion

In this chapter the dynamic analysis are intoroduced. The multifrequency tensile DMA measurements are conducted to quantify the viscoelastic behavior of the fully cured Hitachi compound. The data are fitted to the Generalized Maxwell model. The WLF, a second degree polynomial and an Arrhenius models are implemented to model the time-temperature superposition shifting. The combination of the WLF and the polynomial models are provided the best fit for the viscoelastic transition region. The viscosity is determined using the parallel plate rheometry. The conversion dependent Castro Macosko model is used to fit the viscosity data. The gelation is determined to be at 45% conversion based on the implementation of the kinetic model to the viscosity results. The modeling of the Sumitomo compound failed in several terms:

- In reproducibility of the data at the same process conditions.
- In fitting to a model representing the conversion dependent viscosity behavior.
- In fitting to a model representing the viscoelastic behavior.

References

[1] L. D. Landau and E. M. Lifshitz, *Theory of Elasticity, Course of Theoretical Physics, Volume 7*. 1970.

[2] W. Macosko , Christopher, *Rheology Principles, Measurements, and Applications*. 1993.

[3] J. D. Ferry, *Viscoelastic Properties of Polymers*. 1961.

[4] S. H. Dillman and J. C. Seferis, "Kinetic Viscoelasticity for the Dynamic Mechanical Properties of Polymeric Systems," *J. Macromol. Sci. Part A - Chem.*, vol. 26, no. 1, pp. 227–247, Jan. 1989.

[5] D. W. Van Krevelen and K. Nijenhuis, *Properties of Polymers*. 2009.

[6] N. Phan Thien, *Understanding Viscoelasticity An Introduction to Rheology*. .

[7] E. A.Turi and R. B. Prime, "Thermal Characterization of Polymeric Materials, Thermosets." pp. 1380–1746.

[8] J. D. Menczel and R. B. Prime, *Thermal Analysis of Polymers, Fundamentals and Applications*. .

[9] W. N. Findley, J. S. Lai, and K. Onaran, *Creep and Relaxation of Nonlinear Viscoelastic Materials with an Introduction to linear Viscoelasticity*. .

[10] M. E. Ryan, "Rheological and heat-transfer considerations for the processing of reactive systems," *Polym. Eng. Sci.*, vol. 24, no. 9, pp. 698–706, Jun. 1984.

[11] J. Koszkul and J. Nabialek, "Viscosity models in simulation of the filling stage of the injection molding process," *J. Mater. Process. Technol.*, vol. 157–158, pp. 183–187, Dec. 2004.

[12] M. R. Kamal, "Thermoset Characterization for Moldability Analysis," *Polym. Eng. Sceince*, vol. 14, no. 3, pp. 231–239, 1974.

[13] J. Flory, "Molecular Size Distribution in Three Dimensional Polymers. I. Gelation," *J. Am. Chem. Soc.*, vol. 63, no. 11, pp. 3083–3090, 1941.

[14] C. W. Macosko and D. R. Miller, "A new derivation of average molecular weights of nonlinear polymers.," *Macromolecules*, vol. 9, no. 2, pp. 199–206, 1976.

[15] E. B. Richter and C. W. Macosko, "Viscosity changes during isothermal and adiabatic urethane network polymerization," *Polym. Eng. Sci.*, vol. 20, no. 14, pp. 921–924, 1980.

[16] S. D. Lipshitz and C. W. Macosko, "Rheology Changes During a Urethane Network Polymerization," *Polym. Eng. Sceince*, vol. 16, no. 12, pp. 803–810, 1976.

[17] S. J. Perry, J. M. Castro, and C. W. Macosko, "A Viscometer for Fast Polymerizing Systems," *J. Rheol. (N. Y. N. Y).*, vol. 29, no. 1, pp. 19–36, 1985.

[18] L. T. Nguyen, "Reactive Flow Simulation in Transfer Molding of IC Packages," in *Electronic Components and Technology Conference*, 1993, pp. 375–390.

[19] A. Y. A. Malkin and S. G. Kulichikhin, "Rheokinetics of Curing of Epoxy Resins Near the Glass Transition," *Polym. Eng. Sci.*, vol. 37, no. 8, pp. 1322–1330, 1997.

[20] A. V. Tungare, G. C. Martin, and J. T. Gotro, "Chemorheological Characterization of Thermoset Cure," *Polym. Eng. Sci.*, vol. 28, no. 16, pp. 1071–1075, 1988.

[21] G. C. Martin and A. V. Tungare, "Modeling the Chemorheology of Thermosetting Resins During Processing," *Polym. Eng. Sci.*, vol. 29, no. 18, pp. 1279–1285, 1989.

[22] J. B. Enns and J. K. Gillham, "Time-Temperature-Transformation (Ttt) Cure Diagram: Modeling the Cure Behavior of Thermosets.," *J. Appl. Polym. Sci.*, vol. 28, no. 8, pp. 2567–2591, 1983.

[23] S. E. Kadijk and B. H. a. a. Van Den Brule, "On the pressure dependency of the viscosity of molten polymers," *Polym. Eng. Sci.*, vol. 34, no. 20, pp. 1535–1546, Oct. 1994.

[24] J. M. Castro and C. W. Macosko, "Studies of mold filling and curing in the reaction injection molding process," *AIChE J.*, vol. 28, no. 2, pp. 250–260, Mar. 1982.

[25] P. J. Halley, "A New Chemorheological Analysis of Highly Filled Thermosets Used

in Integrated Circuit Packaging," *John Wiley Sons*, no. June, pp. 95–106, 1996.

[26] P. W. Cox and E. H. Merz, "Correlation of Dynamic and Steady Flow Viscosities," *J. Polym. Sci.*, vol. 28, no. 118, pp. 619–622, 1958.

[27] T. S. R. Al Hadithi, H. A. Barnes, and K. Walters, "The Relationship between the Linear Oscillatory and Nonlinear Steady State Flow Properties of a Series of Polymer and Colloidal Systems," *Colloid Polym. Sci.*, no. 270, pp. 40–46, 1992.

[28] Y. Yang and L. Suspene, "Curing of Unsaturated Polyester Resins: Viscosity Studies and Simulations in Pre-Gel State," *Polym. Eng. Sci.*, vol. 31, no. 5, pp. 321–332, 1991.

[29] V. M. Gonzalez-Romero and N. Casillas, "Isothermal and Temperature Programmed Kinetic Studies of Thermosets," *Polym. Eng. Sci.*, vol. 29, no. 5, pp. 295–301, 1989.

[30] C. M. Tung and P. J. Dynes, "Relationship between Viscoelastic Properties and Gelation in Thermosetting Systems," *J. Appl. Polym. Sci.*, vol. 27, no. I, pp. 569–574, 1982.

[31] F. Schwarzl and A. J. Staverman, "Time Temperature Dependence of Linear Viscoelastic Behavior," *J. Appl. Phys.*, vol. 23, p. 838, 1952.

[32] C. a Angell, "Why C-1=16-17 in the WLF equation is physical - and the fragility of polymers," *Polymer (Guildf).*, vol. 38, no. 26, pp. 6261–6266, 1997.

Chapter 4

Numerical Modeling of Flow Front and Shear Stresses during Die Encapsulation

4.1. Introduction

Transfer molding is the most extensively used process for electronic encapsulation [1] and the filling is an important stage in transfer molding. For a comprehensive optimization of the encapsulation the effect of epoxy melt flow on package properties should be studied. The mechanical properties of EMC mainly develops during the cure and the subsequent cooling stages, however improper filling may lead to process induced failures as well. Longer filling times, for instance, may result in short shots due to high viscosity of the epoxy molding compound after the gel point. On the contrary, shorter time requires higher filling pressure which would be detrimental to the wires and connections inside the cavity and it would also cause filling stresses, air traps or epoxy anisotropy [2]. At low viscosity, flow instabilities may develop affecting the properties and the appearance of the molded package [3]. Therefore the filling time and temperature must be determined such that a cost effective packaging is guaranteed without any undesirable filling issue.

The failure modes associated with the filling stage of the packaging process are generally known as: air trap, short shot, wire sweep and paddle shift [4]. An improperly selected epoxy molding compound or processing conditions, or a flaw in a gate or mold design leads to these failures which can be prevented effectively prior to molding by numerical investigation of the process. Therefore, the filling stage of the encapsulation molding is

simulated in this chapter in a 3D model, using MOLDEX 3D® software package. Rhinoceros® is used for the design and meshing of the cavity and the encapsulated parts.

The electronic encapsulation is basically a package to house the microelectronics including the interconnections. The design parameters like the thickness of the mold cavity and the complexity of the integrated parts make the encapsulated package vulnerable to flow induced failures. The novel packaging techniques like the chip scale package or the system in package described in chapter 1 which are based on die stacking, provide a smaller and denser packaging size while improving the speed, power and functionality [1]. The die stacking technique integrates the various ICs and memory modules into a single package in which they are wire bonded and encapsulated. Shear stresses are very important for stacked die encapsulation. The densely stacked structure generates a very thin space and a wide area to be encapsulated in between the dies, which results in flow retardation in those narrow regions. This phenomenon leads to air traps and voids due to the unbalanced filling. The stacked die array configuration makes the problem more difficult to overcome due to flow retardation consecutively. This repetitive pattern in stacked die arrays is also studied in this chapter after the initial study using the same numerical scheme.

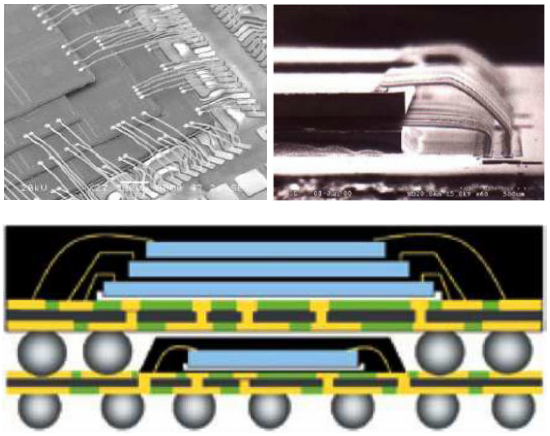

Figure 4.1 Some examples for stacked die configuration: vertical die to die bonding (top left), TSV (through silicon via) and wire bonding (top right), PoP (Package on package) (bottom) [courtesy of imec]

4.2. Flow modeling in literature

The early works on the encapsulation molding of microelectronics were based on a general assumption which states that the inertia and lateral velocity components can be neglected in thin cavities. This formulation is known as the Hele-Shaw approximation which has some limitations inherent in the simplicity of the formulation. The flow in the complex parts, for

example, may not be effectively simulated due to the existence of lateral streamlines which are ignored in the Hele-Shaw approximation.

Thanks to the advances in computational power and introduction of the reaction injection and transfer molding process specific software packages, the two and three dimensional encapsulation simulations of the microelectronics have been the subject of many studies during the last decades [5]–[12]. Various numerical schemes and approaches have been implemented. Finite difference [5]–[7], [13], [14], finite volume [8], [9] and finite element [9]–[16] based schemes were used to solve the governing flow equations. The Hele-Shaw approximation [4], [12]–[20], stokes formula [21] or fully applied Navier Stokes equations [5]–[12], [16], [22] were implemented in these studies. The analytical approaches were also presented and compared with the existing models [17], [20].

Castro and Macosko used the Hele-Shaw approximation to numerically predict the flow advancement in a rectangular shape cavity [18], [19]. The numerical results were compared with the experimental shots performed using a transparent plaque mold. They observed flow front instabilities at high flow rates. The flow in a tube was also studied by Castro and Macosko using a simple analytical model and a three dimensional Navier Stokes model by implementing the explicit forward time and backward space finite difference scheme [17]. The models were tested using the two flow cases of constant flow rate and constant pressure. The finite difference found to be accurate at early stages of filling and the analytic approximation was determined to be more reliable at longer times. The viscosity was assumed to be constant due to the limited polymerization of the thermosetting polymer during flow. An important observation was the build-up of polymer layer on the tube boundaries due to the crosslink formation and a higher flow resistance. Nguyen studied the isothermal reactive flow in a multi-cavity mold [4].The initial pellet conversion was assumed to be negligible but effective prior to the start of molding and hence, the epoxy flow with various conversion levels between 0 and 0.06 was simulated. The underfill of a flip chip package was studied numerically using a two dimensional Hele-Shaw model with the temperature field determined by a finite difference scheme and the pressure field solved using the finite element method [14]. The gate position and size were investigated by Lee et al. The center, corner and in between the two positions were analyzed in an encapsulation of a stacked die array package and the center gate location was found to be the optimal one leading to a lesser void trap [23].

4.3. Numerical Approach

In this paper, the constitutive equations of melt flow are constructed based on incompressibility assumption of both melt and air during filling. This assumption can be

justified for the filling stage only. The packing stage is assumed compressible. Hence, the following assumptions were made:

a. The viscoelastic, time dependent character of the molding compound is considered to be negligible as long as the degree of conversion remains below the gel point. Therefore the flow is assumed to be Newtonian [24].
b. As a result of a low Reynolds number the flow is laminar.
c. The thermal conductivity and heat capacity were assumed to be constant during filling.
d. The entrance runner and gate lengths are excluded from the filling time.
e. The flow rate is constant and it is based on the measurements of the molding experiments.
f. The shear thinning effect (non-Newtonian pseudo-plastic behavior such that the viscosity decreases with increasing shear rate) was neglected mostly in literature and the flow is found to be independent of the shear rate below the viscosity of 10^2N.s/m^2 [25]. Therefore, the epoxy melt exhibits a Newtonian characteristic with a temperature and conversion dependent viscosity term.
g. The flow is non-isothermal. The transfer pot temperature is assumed to be lower than the cavity temperature.
h. The velocity profile is symmetric about the center of the cavity.

4.3.1. Governing Equations of Epoxy Melt Flow

The conservation of mass, momentum and energy equations (Navier-Stokes equations) of the flow for the filling stage can be given by [26]

$$\nabla.\bar{u} = 0, \tag{4.1}$$

$$\frac{\mathrm{D}\bar{u}}{Dt} = -\nabla P + \rho\bar{g} + \mu\nabla^2\bar{u}, \tag{4.2}$$

$$\rho c_p \frac{\mathrm{D}T}{Dt} = \dot{\alpha}\Delta H + \mu\dot{\gamma}^2 + k\nabla^2\mathrm{T}, \tag{4.3}$$

where, $\bar{u} = u_i\hat{\imath}, u_j\hat{\jmath}, u_k\hat{k}$. $\hat{\imath}$, $\hat{\jmath}$ and $\hat{k}$ are the unit vectors representing the coordinate axes. ρ is the density. c_p and k are the specific heat constant and thermal conductivity, respectively. $\dot{\alpha}\Delta H$ is the conversion induced heat generation due to the exothermic heating of the epoxy compound and $\mu\dot{\gamma}^2$ is the viscous heat generation term. $\underline{\dot{\gamma}}$ is the strain rate tensor, which is defined by

$$\underline{\dot{\gamma}} = \frac{1}{2}\underline{\dot{\gamma}}:\underline{\dot{\gamma}} = \frac{1}{2}[\nabla.\bar{u} + (\nabla.\bar{u})^T]. \tag{4.4}$$

4.3.2. Hele-Shaw Approximation

The encapsulation process is a flow in a narrow gap which is dominated characteristically by the pressure gradient and the viscous forces [13]. Hence, the effect of inertial and gravitational forces on the flow dynamics is rather restricted. Therefore, most of the time further simplification of the governing equations yields satisfactory results. The simplification of the momentum equation gives

$$\frac{\partial P}{\partial x} = \frac{\partial}{\partial z}\left(\mu \frac{\partial u_i}{\partial z}\right), \tag{4.5}$$

$$\frac{\partial P}{\partial y} = \frac{\partial}{\partial z}\left(\mu \frac{\partial u_j}{\partial z}\right), \tag{4.6}$$

$$\frac{\partial P}{\partial z} = 0. \tag{4.7}$$

The resulted equations are called the Hele-Shaw approximation and used extensively for modeling of the injection molding and transfer molding of the thermosetting resins in literature [4], [12]–[20]. The momentum and the continuity equations are combined into a single equation with a pressure gradient and a fluidity parameter, $S = \int_0^h \frac{z^2}{\mu} dz$.

$$\frac{\partial}{\partial x}\left(S \frac{\partial P}{\partial x}\right) + \frac{\partial}{\partial y}\left(S \frac{\partial P}{\partial y}\right) = 0 \tag{4.8}$$

Note that, in this study the full 3D Navier-Stokes equations are used. For that reason the thin cavity approximation is only mentioned shortly. However, since the flow is viscous dominated and the inertial effects are relatively small, it can be expected that the Hele-Shaw approximation may lead to a similar flow profile for the thin gap flow. In flow modeling of complicated geometries like lead-frames where it is difficult and even in extreme cases impossible to model and mesh the openings, the Hele-Shaw approximation may provide a fair prediction of the flow pattern [20]. However, the stacked die filling is more complicated and the Hele-Shaw approximation will be inadequate in truly representing the flow pattern. Therefore, a three dimensional flow analysis is essential in order to be able to visualize the cross flow effect and voids which are generated due to the flow retardation during the stacked die encapsulation.

4.3.3. Packing Stage Modeling

The melt compressibility effect should be included for the packing phase. Hence, equation 4.1 is replaced by

$$\frac{\partial \rho}{\partial t} + \nabla . \rho \bar{u} = 0, \tag{4.9}$$

4.3.4. Flow front tracking

The flow front position representing the interface between air and epoxy melt can be detected by various techniques. The most widely used model is the volume of fluid (VOF) method which first used by Hirt and Nichols in 1981 [27]. Hence, using the VOF method, the interface is located by the following advection equation

$$\frac{\partial \varphi}{\partial t} + \bar{u}.\nabla\varphi = 0, \tag{4.10}$$

where φ defines the volume fractional function such that $\varphi = 0$ defines the vacuum or air and $\varphi = 1$ indicates the presence of epoxy compound at the specified element. Then, the interface comprises the elements providing $0 < \varphi < 1$. The following boundary and initial conditions are assumed

$$\varphi(\bar{X}, t)|_{x=0} = 1, \tag{4.11}$$

$$\varphi(\bar{X}, t)|_{t=0} = 0. \tag{4.12}$$

The density and viscosity values at each element can be interpolated by [28]

$$\rho = \varphi\rho_a + (1-\varphi)\rho_m, \tag{4.13}$$

$$\mu = \varphi\mu_a + (1-\varphi)\mu_m, \tag{4.14}$$

where ρ_a and μ_a are the density and the viscosity of air, respectively and ρ_m and μ_m is the corresponding values of epoxy melt.

4.4. Process and material parameters

In this study, the flow advancement pattern of the epoxy molding compound is numerically analyzed in MOLDEX 3D® software package using the Reaction Injection Molding, RIM, module. Essentially, RIM and transfer molding are based on the same principles and numerically no difference exist between the two molding types, despite the differences in processing. Note that in some software packages the boundary conditions may not be applicable to transfer molding if the package is intended for RIM process only [4].

The material variables affecting the flow behavior are the viscosity, conversion, specific heat, thermal conductivity and the volume change. The viscosity and cure kinetics were determined previously in the corresponding sections in chapters 2 and 3. The process parameters are the filling time, filling speed, mold pressure, packing pressure profile and mold temperature.

4.4.1. Material variables

Chemo-rheology

The crosslink progress of the EMC is modeled by the autocatalytic Kamal and Sourour formula [29] given by equation 2.5. The viscosity increase is determined by the Castro Macosko model [18], [19] represented by equation 3.39. The original formula is strain rate, conversion and temperature dependent. But, in this study the viscosity is assumed to depend only on the degree of conversion and temperature.

Volumetric

Previously in equations 2.16 to 2.19 the Tait model with modified terms is presented to accurately represent the volume change behavior of the epoxy compound under various process temperature and pressure conditions. However, this model was not directly applicable in MOLDEX 3D®. Therefore, the model is adapted to the already existing form of the Tait model in the software which is named "the modified Tait model 2". The Tait model is already given by equation 2.16, but the parameters introduced by the software are redefined as

$$V_0 = \begin{cases} b_{1s} + b_{2s}\bar{T} & for\ T \le T_t \\ b_{1m} + b_{2m}\bar{T} & for\ T > T_t \end{cases} \quad 4.15$$

$$B = \begin{cases} b_{3s}\exp(-b_{4s}\bar{T}) & for\ T \le T_t \\ b_{3m}\exp(-b_{4m}\bar{T}) & for\ T > T_t \end{cases} \quad 4.16$$

where $\bar{T} = T - b_5$ and $T_t = b_5 + b_6 P$.

The model constants which are determined using nonlinear regression analysis in Matlab are given in table 4.1.

Table 4.1 Modified Tait model parameters

b_1 [cm^3/gr]	b_{2s} [$cm^3/gr/^oC$]	b_{2m} [$cm^3/gr/^oC$]	b_{3s} [MPa]	b_{3m} [MPa]	b_{4s} [$1/^oC$]	b_{4m} [$1/^oC$]	b_5 [^oC]	b_6 [^oC/MPa]
0.568	$6.78\ 10^{-05}$	$1.2\ 10^{-04}$	674.50	447.15	$5.7\ 10^{-03}$	$1.7\ 10^{-03}$	111	0.42

4.4.2. Process variables

In this study, the encapsulation simulations of the two different models were investigated: One is based on the molding experiment described in chapter 7 and the other is a model of a stacked chip array package. Both models will be studied independently in the following sections.

Experimental study (chapter 7)

The cavity geometry as well as the process and material parameters all are based on the experimental molding conditions studied in chapter 7. Four different mold temperatures of 120, 140, 160 and 175°C with the initial degree of conversions of 0.5, 2 and 6% are studied. 175°C is the standard molding temperature and 120, 140 and 160°C are the experimentally tested mold temperatures. A study comparing the effect of mold temperature at a constant initial conversion is also presented. The process parameters applied in the simulations are given in table 4.2.

Table 4.2 Molding experiment conditions

Temperature [°C]	120	140	160	175
Initial Conversion [%]	0.5	2	6	6
Filling time [s]	30.5	30.5	30.5	30.5

Packing

In transfer molding the filling can be controlled by one of the two methods: Velocity control or pressure control. If the transfer piston speed is set constant, then the pressure is adapted accordingly during filling to compensate for the flow retardation or slowing down due to the viscosity rise. On the contrary, a pressure profile may be selected with a varying velocity. Most of the time the combination of both methods is used in which the plunger injects the epoxy with a constant velocity, whereas after the switch-over point the pressure control method is activated such that the process switches over to the packing stage as soon as the plunger pressure reaches a preset value [30]. In this case the switch-over point is 98% of the filling time. If the velocity control to pressure control switch is made too early the melt would stop suddenly due to the viscosity rise and if it is made too late then a non-uniform density may occur. The standard switch over point is used in this study for all the simulations. In the velocity control stage a constant velocity based on the value in the corresponding experiment is used. After the switch point the pressure is increased gradually and the packing is stopped when the pressure reaches to 4MPa. This is the pressure limit set in the molding experiments.

Stacked double die array

The encapsulation of a two layer stacked die array of 4 by 4 at 175°C of mold temperature and filling time of 40 seconds with the initial conversion of 2% is simulated. The flow pattern causing voids and air traps is studied incrementally.

4.5. Models

The meshes are generated in Rhinoceros® with boundary layer solid meshes generated for the cavity and tetrahedral meshes for the components.

4.5.1. Molding Experiment Model

The maximum dimensions of the whole model used in the molding study are 75.6mm in lateral, 71.5mm in longitudinal directions and 1.09mm in thickness. Figure 4.2a shows the cavity model including the chip, substrate, gates, runners and transfer pots. The two transfer pots loaded with the EMCs are designed to fill the entire cavity through four rectangular gates, connected by short runners in between. In order to cut the computational load only the left side of the model is meshed and simulated. Considering the large mesh size which consists of around $6x10^8$ linear tetrahedral elements in total due to the wide filling area and thin gap, implementing the symmetry feature that connects the front and back sides of the model lowers the simulation time considerably. The mesh for the cavity is generated in three steps. Initially the mesh is generated for the bottom half of the cavity and later for the top half. Then they joined together and defined as a single cavity mesh. This provided more flexibility in defining the sensor nodes, such that some sensors are generated at nodes on the mid-plane of the cavity. The number of elements in thickness direction in the free region of the cavity is designed to be four major and two boundary layers. Above the die the element number is set to two major and two boundary layer elements. The chip itself is modeled by a single layer mesh in thickness direction since it is not considered as the part of the flow.

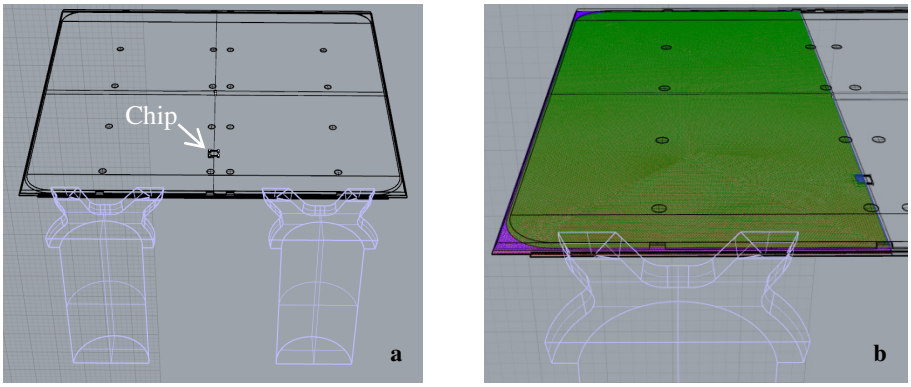

Figure 4.2 Molding experiment model comprising the substrate, chip, cavity, gates, runners and the transfer pots

The whole meshed model consisting of a substrate, a single chip over the midline of the board and the cavity enclosed by the moldbase is shown in figure 4.3a. In figure 4.3b the two gates at the left side which are meshed in red are clearly observable. Figure 4.3c shows the midplane of the cavity and the top surface of the chip. The sensor nodes locations in the cavity and on the chip surface are shown in figures 4.3c and 4.3d. The sensor nodes which are specified with the numbers are investigated later in figure 4.8 for the shear stress distribution during filling.

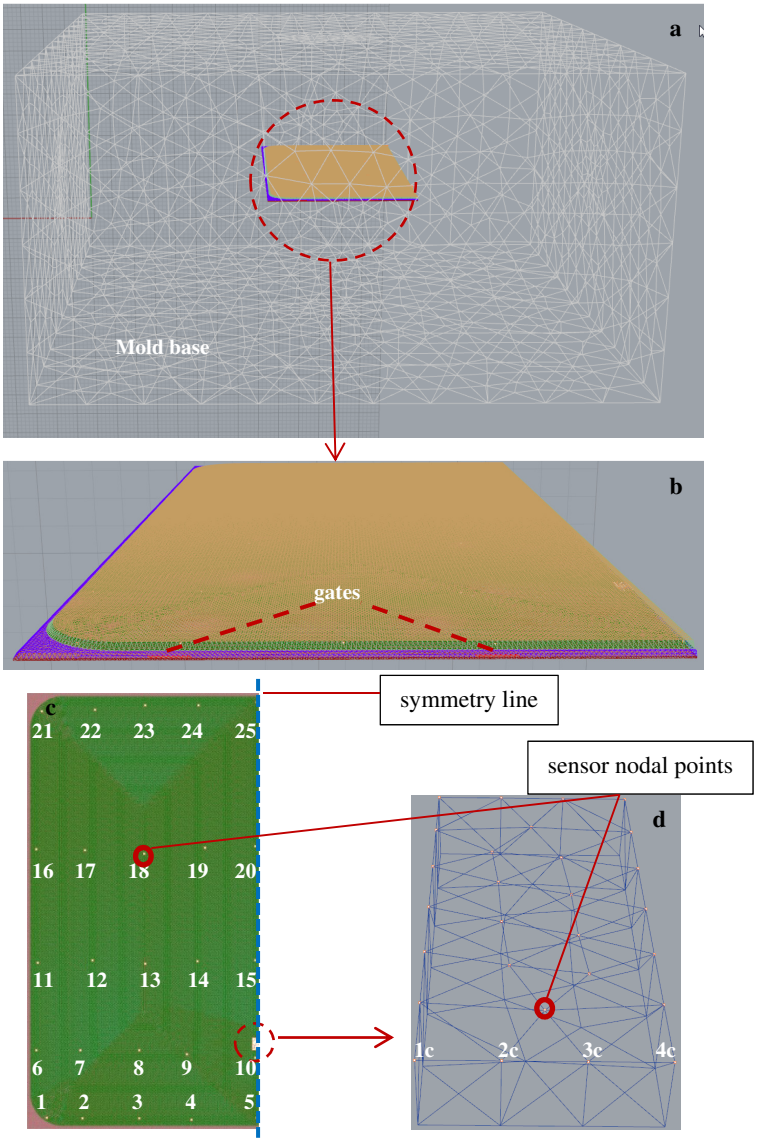

Figure 4.3 Molding experiment model & meshing

4.5.1.1. Flow Pattern

The melt advancement for the experimental model is shown in figure 4.4 in increments of 10% on the left half of the cavity. The flow entering through four gates, equally distributed at the front panel provides a discrete pattern of semicircular melt distribution at the start of filling. The flow front reaches to the die attached on the midline of the cavity at 28% of filling and covers it at 30%. A uniform flow front after about 40% filling can be observed and since there is no obstacle to pass through, the flow progresses smoothly until the end, after that point. A slightly faster flow front near the edge can be attributed to a little bit higher temperature or to the gate position near the mold wall.

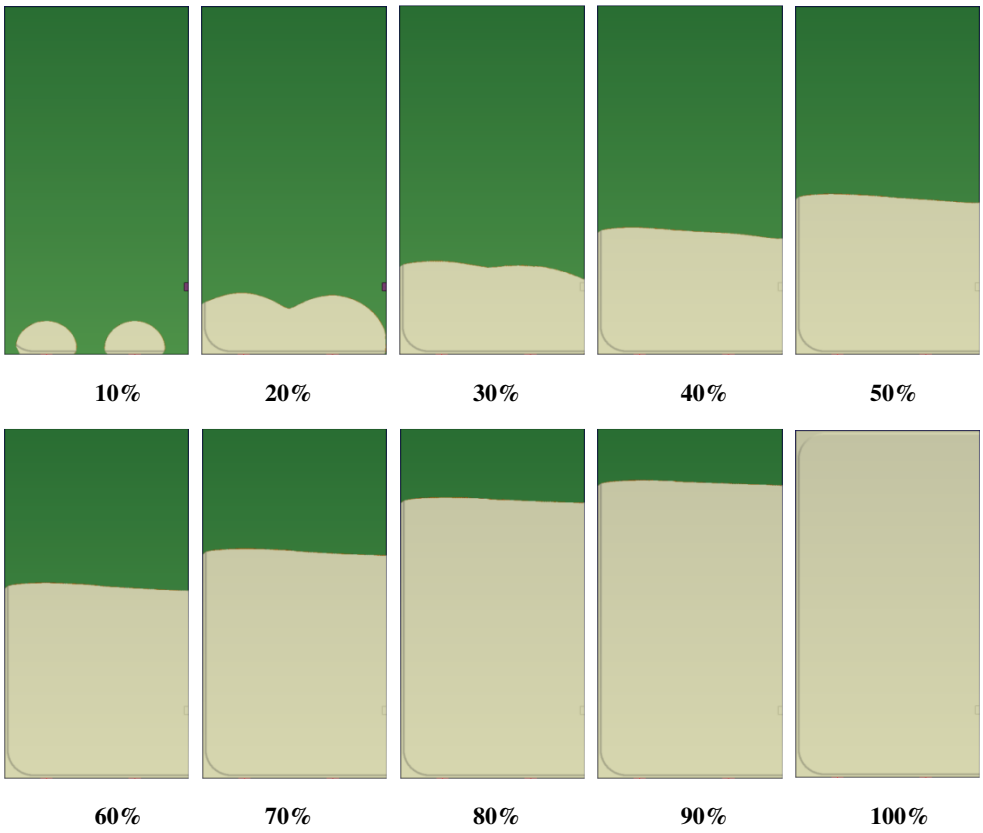

Figure 4.4 Mold filling pattern for the experiment study

4.5.1.2. Results

The pressure, degree of conversion, viscosity, shear rate and shear stress on the surface of the chip during filling is investigated for the range of tested conditions and compared in the

following sections. Each condition specifies a conducted experiment. Figures from 4.5 to 4.7 are obtained from a single sensor node located at the surface of the chip which is indicated in figure 4.3.

Figure 4.5 shows the change in pressure from the start of filling to the end of packing. It is clear that, the lower the temperature, the higher the pressure, and this is directly related to the viscosity of the epoxy melt given in figure 4.6b. The interesting behavior here is the change in viscosity which is more dominated by the mold temperature rather than the degree of conversion. Although the experiment at 120°C has the lowest initial conversion, the viscosity is the highest. The cure progress is given in figure 4.6a for the three cases. The initial cure level of 6% at a highest temperature of 160°C (see chapter 7 for detailed explanation) results in a faster conversion until the end of filling. The conversion rises to 11.5% at 160°C while the rise is limited to 1.5% at 140°C and it almost remains the same at 120°C with a slight increase from 0.35% to 0.85%. The impact of viscosity on the shear stress can be observed in figure 4.7. In spite of the same shear rate values at 140°C and 120°C, the shear stress is more than two fold higher in 120°C due to the higher viscosity. 0.3, 0.5 and 1.3kPa are the shear stresses obtained at 160, 140 and 120°C, respectively. The peaks observed at the onset of the melt-sensor interface in shear rate values, depend on several factors such that they can be minimized by decreasing the convergence tolerance or increasing the element number in the region close to the defined nodal sensors. The small thickness and the large surface area of the cavity results in unhealthy mesh distribution when a much denser mesh is applied in a small region, and it causes to considerably higher computational load and time which is found not to be efficient. Nonetheless, the maximum applicable mesh density allowed by the software is generated in this study. The peak sizes are reduced by this method. The smaller peaks are also observed at the corresponding sensor nodal points in figures 4.8 and 4.12.

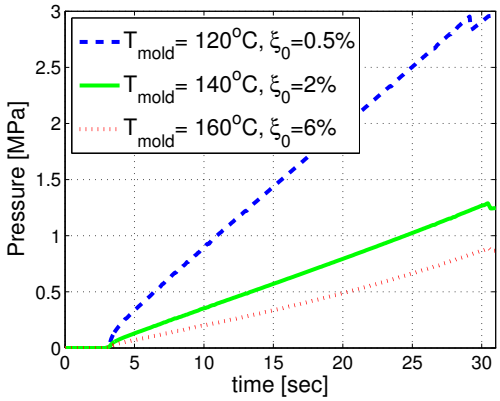

Figure 4.5 Pressure during filling

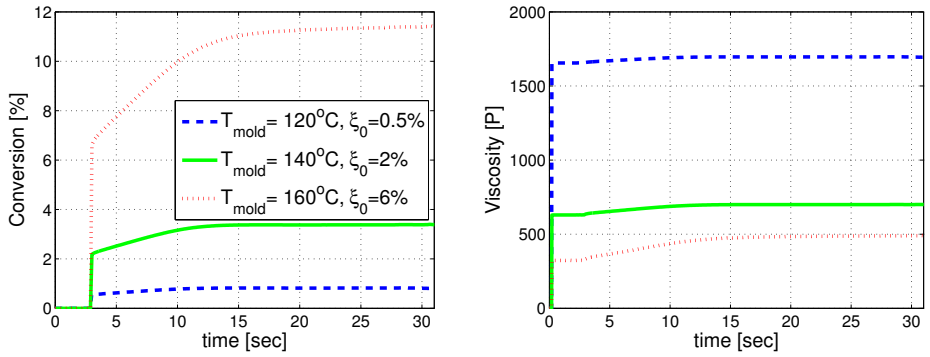

Figure 4.6 Conversion and viscosity during filling

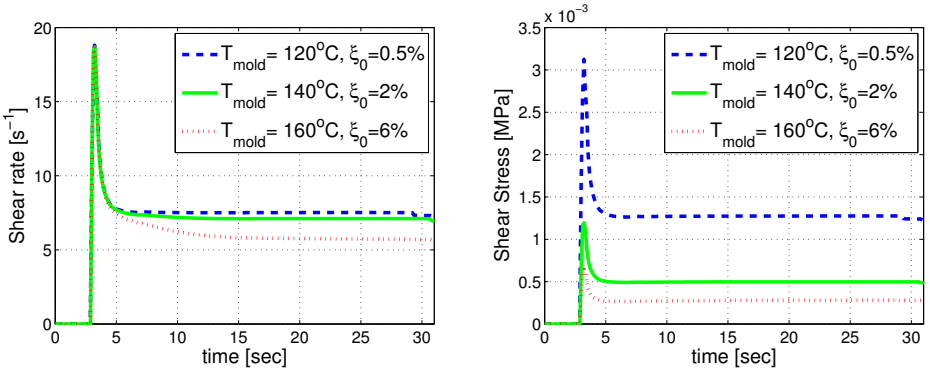

Figure 4.7 Shear rate and shear stress during filling

The shear stress patterns during filling based on the locations of the compared sensors are investigated in figure 4.8. The sensor positions are shown previously in figure 4.3c and 4.3d. The studied simulation is the one with temperature of 140°C and the initial conversion of 2%. In figure 4.8a the shear stress values at the entrance of the cavity are compared. The black and green lines indicate the sensors located at the front of the two gates and the others represent the sensors in between the gates. The stronger melt front leads to a higher shear stress at these points. In figure 4.8b the shear stress distribution of the sensors at the chip surface are compared. The arrow shows the positions starting from the symmetry line at the center to the corner of the chip. Hence, the closer to the gate, the higher the stress values are. The shear stress on the selected sensor points on a diagonal line from the center to the back corner is given in figure 4.8c. The dashed blue line is the node at the symmetry line close to the inlet side (no. 5 in figure 4.3c). The lower flow rate at this node compared to

the other nodes yields a lower shear stress value. When the nodes extending from the gate front to the back on a linear path are compared, it is observed that the gate front sensor node (no. 4 in figure 4.3c) results in a maximum shear stress and the others give almost the same values regardless of their distance from the gate.

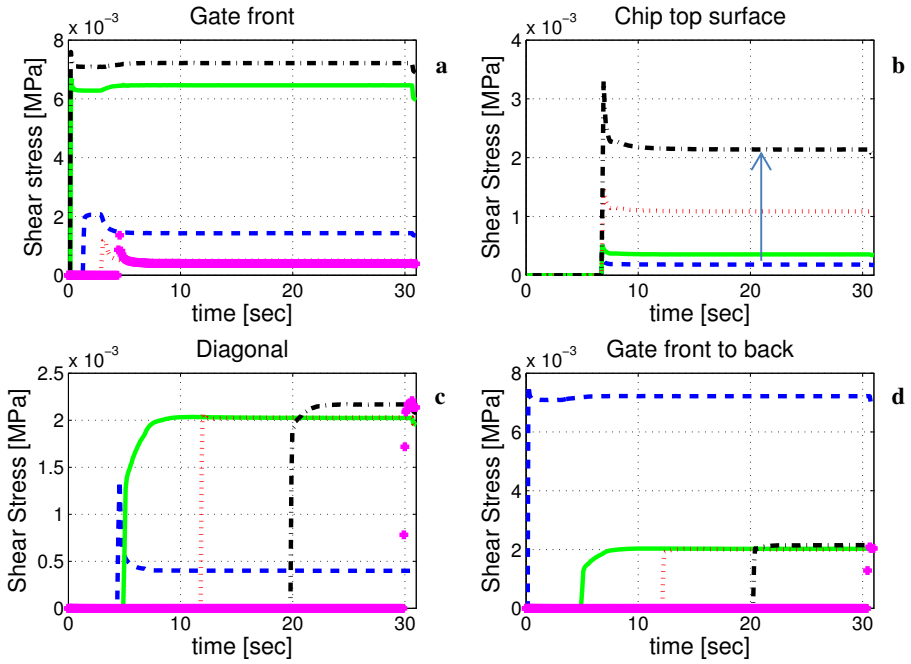

Figure 4.8 Shear stress distributions of the sensor nodes shown in figure 4.3c and 4.3d: a) first row [1, 2, 3, 4, 5], b) chip top surface front edge [1c, 2c, 3c, 4c], c) from the mid front to the back corner [5, 9, 13, 17, 21], d) center gate front [4, 9, 14, 19, 24]

The pressure and conversion distribution on the mid-plane surface at the end of filling is plotted in figure 4.9 for 175°C filling temperature with initial conversion of 6%. The pressure is highest at the gate front and lowest at the end of the cavity. The maximum end conversion is determined to be 27.5% on the symmetry line towards the back side of the cavity and in between the two gates. The melt is accumulated at these regions due to the locations of the gates, which leads to higher conversion values.

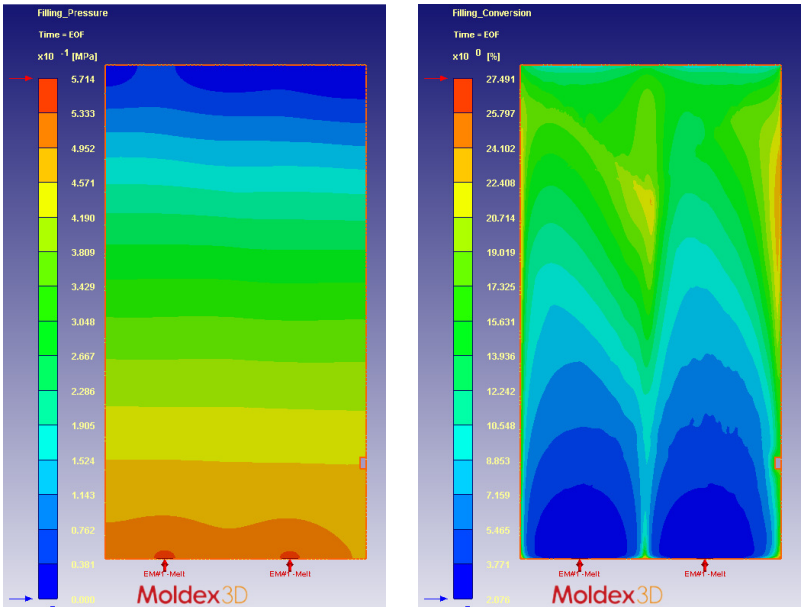

Figure 4.9 Pressure (left) and conversion (right) distribution at the end of filling in the midplane at 175°C

4.5.1.3. Constant initial conversion

In figures 4.10 to 4.12 the pressure, conversion, viscosity, shear rate and shear stress values at four different mold temperatures are given. The initial conversion is assumed as 2% in all of the tested temperatures. The end conversion is maximum at 175°C which is around 17% on the chip surface. The faster rise in conversion at 175°C compared to 160°C leads to a higher viscosity at the end of filling. However, the higher viscosity does not yield a higher shear stress due to the lower shear rate at the higher temperature. A similar phenomenon can be observed when 120°C and 140°C are compared. Despite the same shear rate values, almost a threefold higher viscosity at the lower temperature results in a higher shear stress. This comparison reveals the complexity of interdependent material and mechanical behaviors.

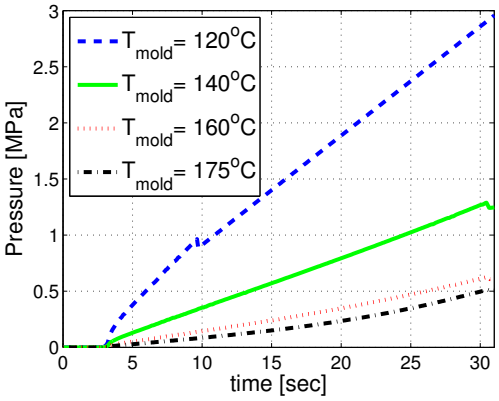

Figure 4.10 Pressure during filling with the initial conversion of 2%

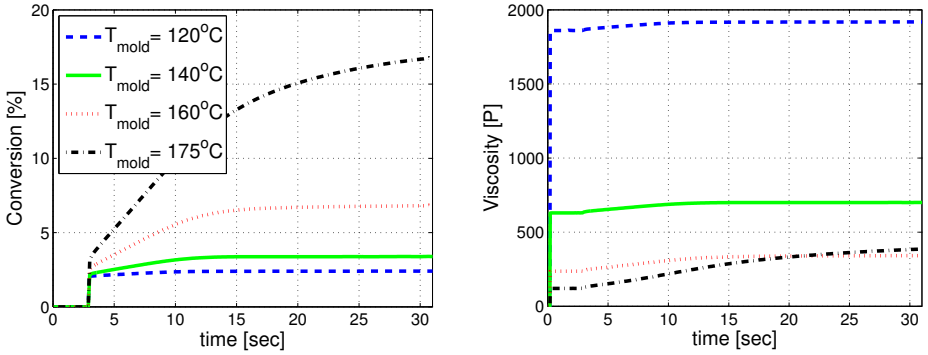

Figure 4.11 Conversion and viscosity during filling with the initial conversion of 2%

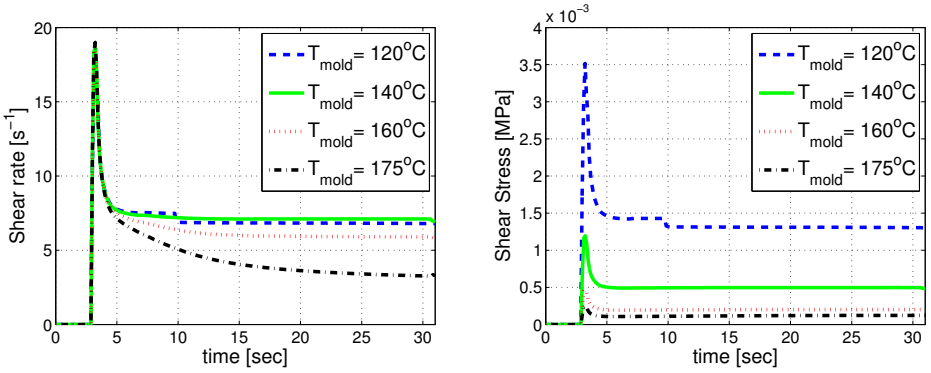

Figure 4.12 Shear rate and shear stress during filling with the initial conversion of 2%

4.5.2. Stacked double die array model

A package with a two layer stacked die, designed in a 4x4 matrix array, is studied. The mold cavity thickness is 0.6mm. The surface area of the top and the bottom chips are 5.93x5.45 mm^2 5.10x4.70 mm^2, respectively, and the whole package volume is 51x51x0.6mm^3. The thickness of the top die is 175µm and the bottom die is 120 µm. The die to die gap is 40µm, while the die to substrate gap is 60µm. The gap at the top between the cavity platen and the top of surface of the top die is 200 µm. The schematic of the stacked die design is shown in figure 4.13 including the substrate and interconnections.

The gate is located at the center, covering a wide rectangular entrance area. The processing time is 40 seconds for the filling stage and the temperature of the mold is set to be 175°C which is the standard encapsulation temperature. The whole strip design is represented in figure 4.14. The cavities at both sides are designed to be filled by 4 separate EMC pellets, each filling two cavities. Each cavity contains 16 stacked die arrays. In this study only the left half of the cavity is simulated using the symmetry feature.

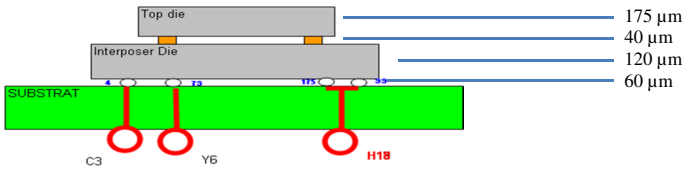

Figure 4.13 Schematic of the stacked die array including the substrate

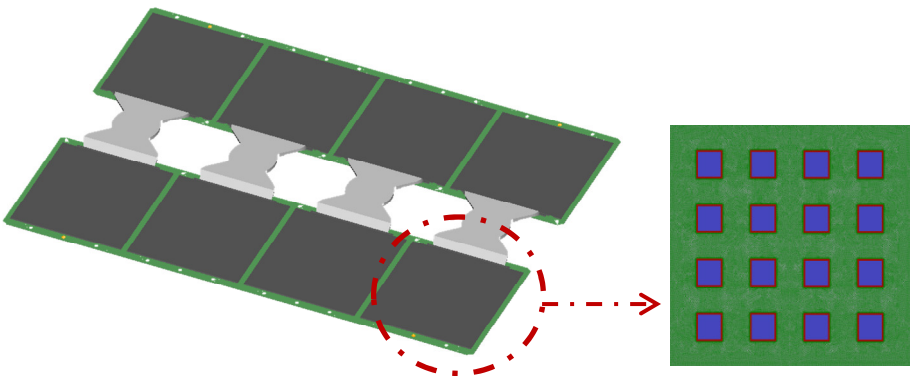

4.14 Encapsulation model for the stacked die array

Figure 4.15 shows the grid model of the moldbase, the cavity and the stacked dies which are generated in Rhinoceros® and later exported to MOLDEX 3D®. The total created mesh

consists of around $4.5x10^8$ tetrahedral elements. The symmetry feature is used to decrease the number of elements and so the computational time. Due to the small gap sizes around the dies and in between them a much denser mesh is generated compared to the free cavity region. The number of elements in thickness direction in the cavity is 5 at the edges and 12 where the stacked dies are located.

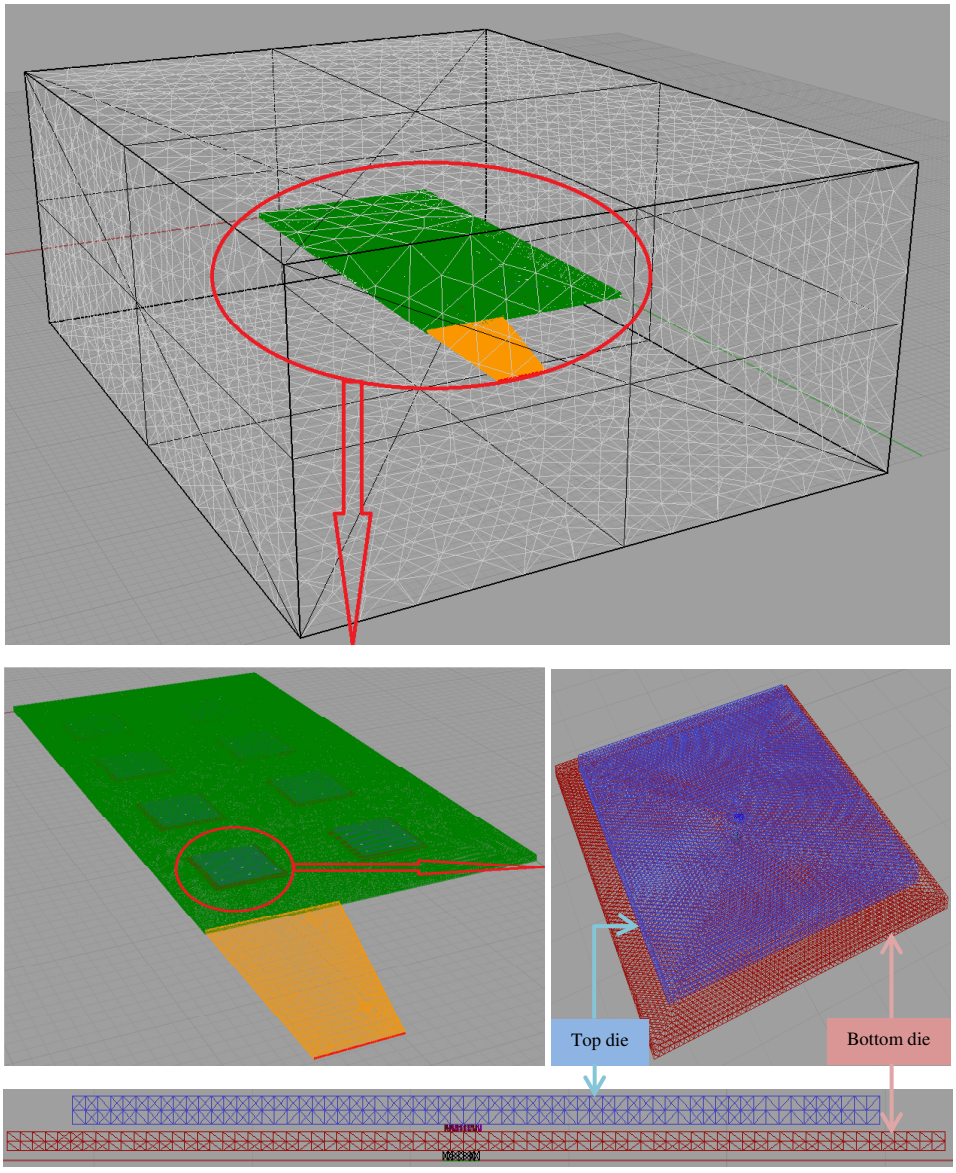

Figure 4.15 Computational mesh generated for the moldbase, the cavity and the stacked dies

4.5.2.1. Flow Pattern

Figure 4.16 shows the melt advancement in increments of 10% filling intervals. The resin flows and expands into the cavity through the single gate designed at the center. It tends to accelerate in the free region between the stacked units. Flow retardation is observed on top of the die stacks as well as in between the two dies and at the bottom in the gap between the die and the substrate due to the thin spacing. The degree of conversion rises fast due to the high mold temperature which directly leads to a higher viscosity. Hence, the flow front nearly stops at those regions but it proceeds faster in the obstacle-free paths at the sides.

The flow retardation is indicated at 30% filling and the resulted void formation is shown in a zoomed in view at 35% filling snapshot in figure 4.16. The voids will remain in the package after complete conversion of the epoxy compound. These are the weak regions of the package which are considered detrimental and affect the lifespan of the microelectronics.

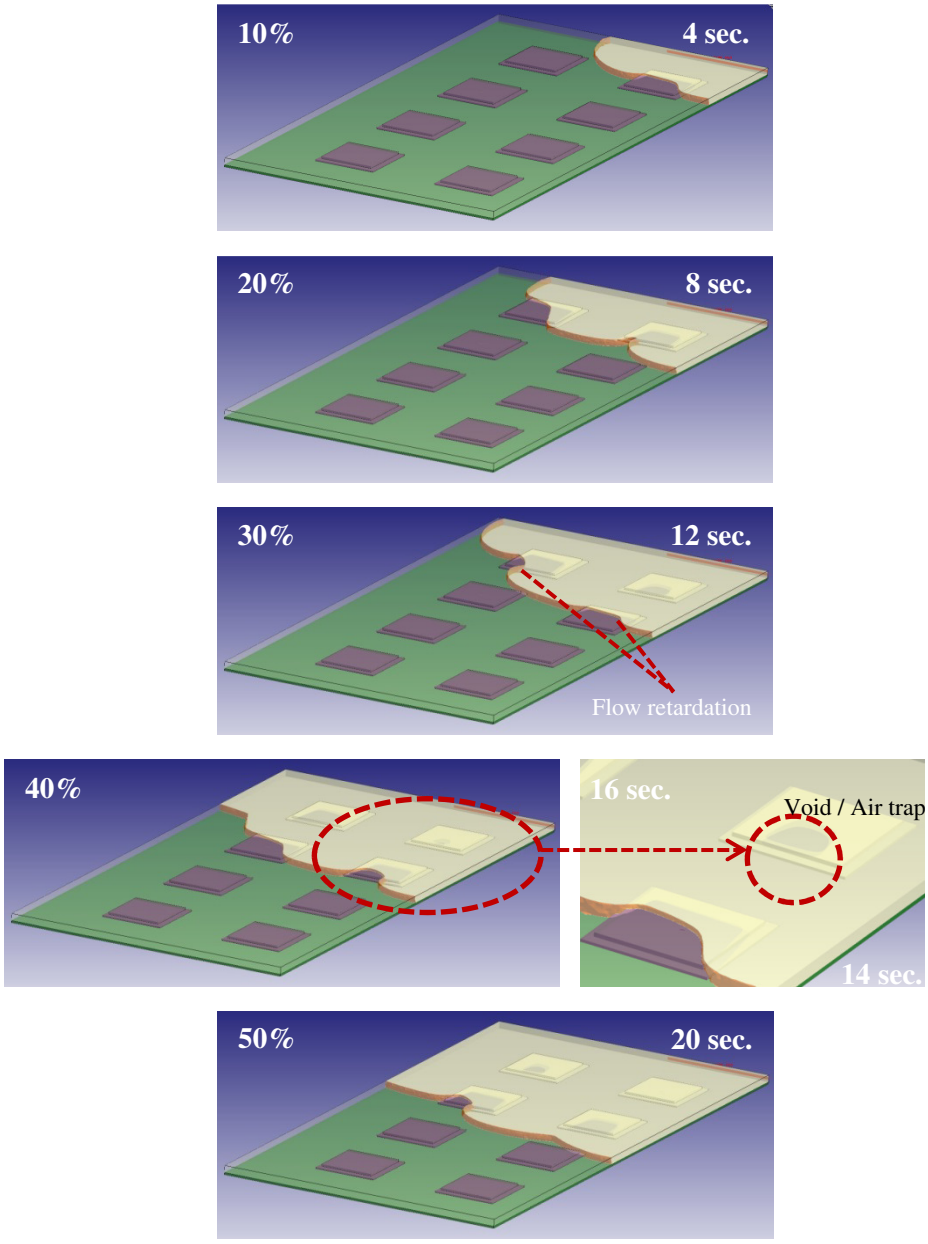

Figure 4.16 Epoxy melt advancement from 0 to 100% mold filling times in a stacked die array

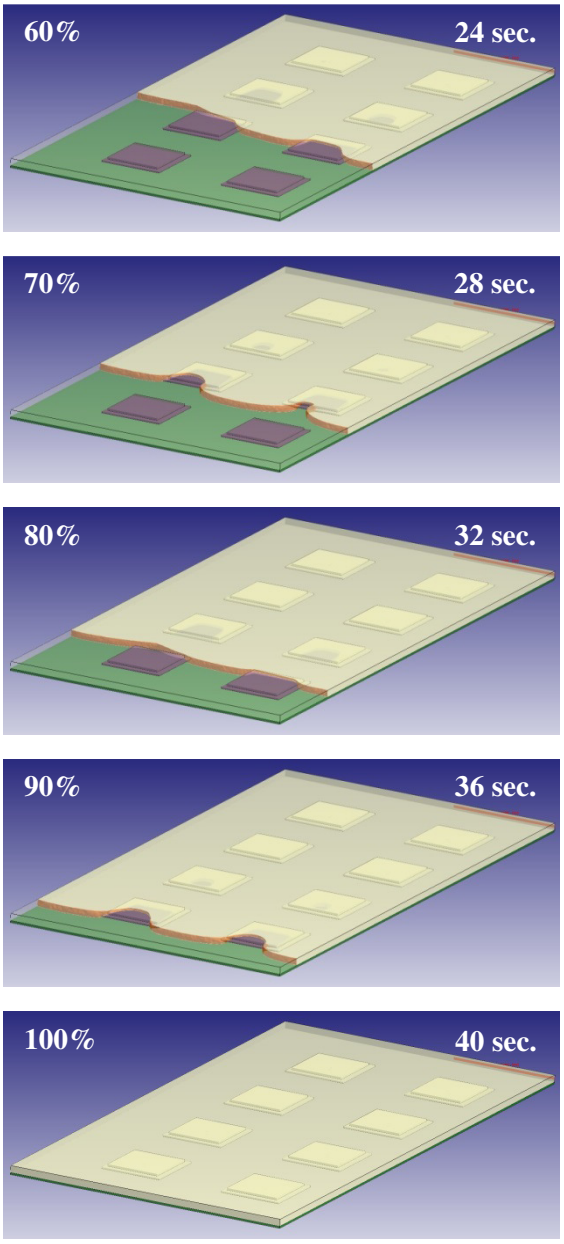

Figure 4.16 (Continued)

4.5.2.2. Results

The EMC degree of conversion and viscosity at the end of filling is given in figure 4.17. The plot represents the top surface of the cavity. The conversion after 40 seconds at 175°C reaches close to 40% at the front corners and in thin spacing between the top die and the cavity top. This is a critically high conversion level due to the risk of gelation at 45% conversion of the used epoxy compound. The minimum conversion region is at the gate front and between the stacked die arrays in flow direction and specifically on the symmetry line which is subjected to continuous epoxy melt flow through the gate. The maximum calculated viscosity is 370Pa.s which is corresponding to the maximum polymerization of 39.3%. The minimum viscosity is obtained as 200Pa.s.

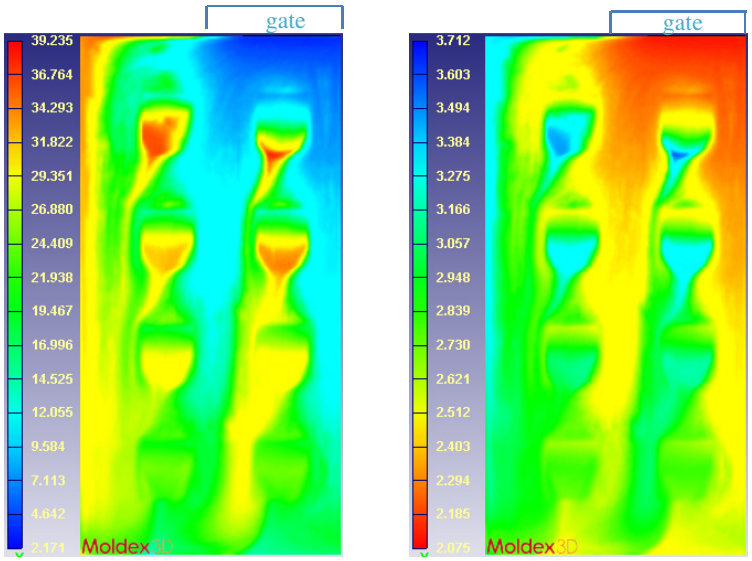

Conversion **Viscosity**

Figure 4.17 Filling-end conversion and viscosity pattern of the stacked die (gate position at the top)

The viscosity and conversion patterns are shown in figures 4.18 and 4.19 respectively representing the vertical sections of the flow plane. Starting from the left side they indicate the plane:

i. between the substrate and the bottom die,
j. comprising the bottom die,
k. between the bottom die and the top die,

l. comprising the top die,
m. between the top die and the substrate.

In these pictures the effect of gap thickness on the encapsulated part can be observed clearly. The conversion level and the viscosity are directly related to the thickness of the filling part. The gap between the bottom and the top dies are the smallest which leads to a slower flow and larger accumulation of the EMC in those regions. Besides, the stacked dies closer to the gate, which are filled earlier, result in higher conversion degrees and viscosities. Nonetheless, the dies toward the end of the array, which are filled later, are more vulnerable to air traps and void formations. This phenomenon can be observed in figures 4.18 and 4.19 in which unlike the front stacked dies, close to the vents at the back side the low crosslinked epoxy melt find its path to the thin spacing between the dies and substrate. The melt slows down in those regions but it is faster at the free sides which may get to the vents before the complete filling of the cavity. The melt at the end may constrain the further escape of air which will result in trapped air and voids.

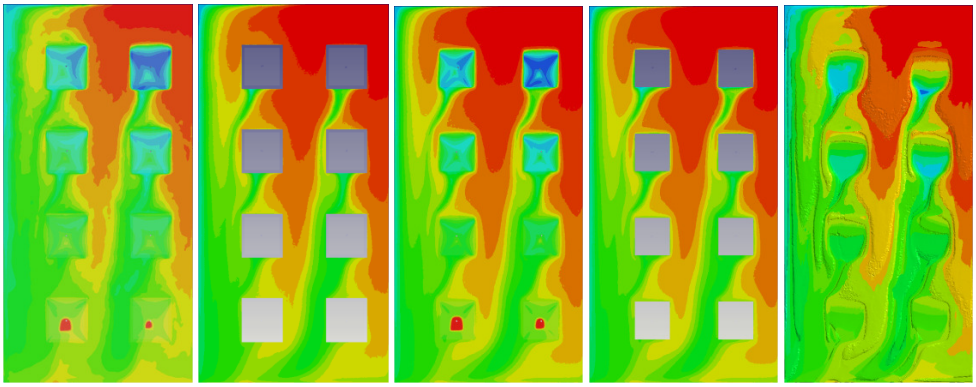

Figure 4.18 Horizontal layers showing the viscosity distribution pattern

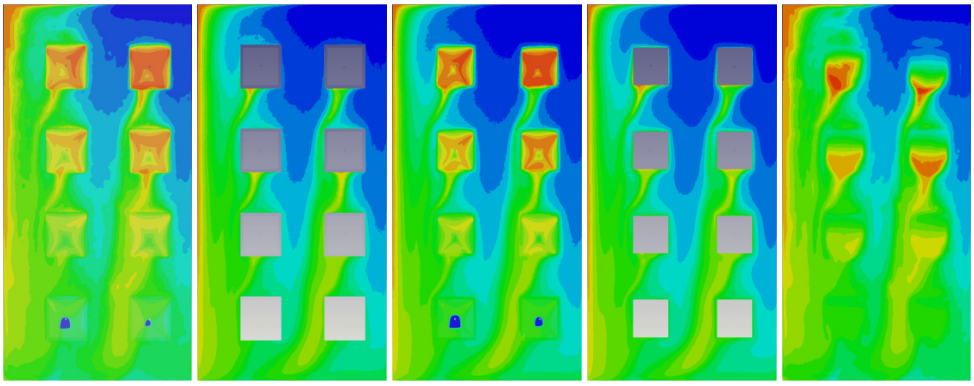

i **j** **k** **l** **m**

Figure 4.19 Horizontal layers showing the conversion distribution pattern

The shear stress with respect to the filling time on the surface of the top dies as a function of time is given in figure 4.20. Shear stress values between 200 and 700Pa are obtained which are expected to be low enough to avoid any damage to the die stack structure.

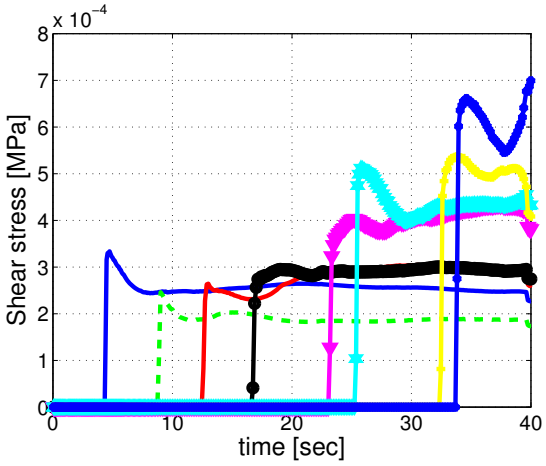

Figure 4.20 Surface shear stress on the surface of the top dies

4.6. Analytical stress estimation

An exact solution for a steady state flow between the parallel plates can be obtained in two dimensional coordinate system using the simplification of the Navier-Stokes equations [31], which yields

$$\frac{dP}{dx} = \mu \frac{d^2u}{dy^2}. \quad 4.17$$

If the pressure gradient is taken constant in flow direction then the velocity can be given by

$$u(y) = -\frac{1}{2\mu} \frac{\Delta P}{\Delta x} (b^2 - y^2). \quad 4.18$$

This equation states that the velocity profile is parabolic. The shear stress at the wall of the plates is determined by

$$\tau_{xy}\big|_w = \mu \left(\frac{\partial u}{\partial y}\right)_w \approx -\mu \frac{U_m}{b}. \quad 4.19$$

Here U_m is the maximum velocity obtained at the center of the channel. The negative stress acts in a positive x direction.

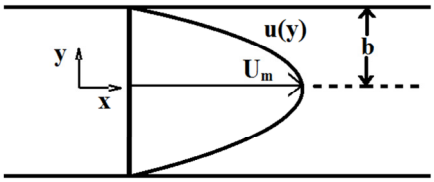

Figure 4.21 Parallel plate flow layout

In the experimental model the filling time is set to be 31 seconds and the length of the cavity is 71.5mm. If a constant flow rate is applied then the average velocity should be 2.3mm/s and if the flow case of 140°C is considered with the average viscosity of 70Pa.s then, the required pressure gradient of 0.14MPa can be easily calculated using the average velocity in the approximation equation 4.20.

$$u_{avg} = \frac{b^2}{3\mu} \frac{\Delta P}{\Delta x}. \quad 4.20$$

As a result, the maximum velocity becomes 3.5mm/s at the center of the cavity which leads to a shear rate of $7s^{-1}$. Hence, the wall shear stress is determined as 0.5kPa. This value matches the result obtained using the full 3D numerical analysis as it can be compared in figure 4.7. Therefore, for a simple cavity without a complex geometry of the internal components a simple two dimensional analytical model would provide a satisfactory estimate of the maximum strain and stress on the cavity wall. However, this approximation cannot be applied to a more complex board with the stacked dies on it.

4.7. Conclusion

The numerical studies of the three dimensional mold cavity filling based on two different models are presented. The flow is assumed to be non-isothermal and Newtonian with pseudo non-Newtonian characteristics determined by the conversion and temperature dependent viscosity. The chemo-rheological behavior of the epoxy compound is simulated by the previously determined autocatalytic Kamal and Sourour and Castro Macosko models. The effect of initial EMC conversion and mold temperature are investigated in a simple thin gap model. The model geometry is based on the molding experiment study which is explained in detail in chapter 7. Due to the simplicity of the model and a well-designed gate distribution a smooth melt transition is observed. The pressure distribution, conversion, viscosity, shear rate and shear stress are studied on a single node for various process conditions and are later compared to those of a series of the selected nodes for the position wise study of the parameters. As expected from a reacting flow, the shear stress is affected by the viscosity change. However, the effect of temperature is much more dominated. The highest shear stress is obtained at the gate front regions where they are fed with continuous melt flow. No significant shear stress change is observed towards the back of the cavity. The minimum values are obtained at the front corners at which they are filled by the lateral viscous flow.

The flow retardation pattern is studied in encapsulation of a stacked die array package. It is observed that the epoxy flow slows down when the flow front reaches the stacked units. The continuous array of stacked dies results in a repeated flow retardation pattern. On the other hand, the flow is accelerated in the free region. Hence, the melt covers the stacked unit from the sides and top which at the end leads to void and air trap formation. It is also determined that the smaller the gap between the dies, the slower the filling and hence the higher the conversion and viscosity values. This pattern is studied by investigation of the horizontal sections of the cavity.

Further study may be conducted on the stacked die arrays with larger number of dies and smaller gaps and by taking into account the effect of copper pillars, wire sweeps and the other interconnections. Note that a much larger computational power will be required to conduct such a simulation.

References

[1] H. Ardebili and M. G. Pecht, *Encapsulation technologies for electronic applications*, First edit. 2009.

[2] M. R. Kamal and M. E. Ryan, “The Behavor of Thermosetting Compounds in Injection Molding Cavities,” *Polym. Eng. Sceince*, vol. 20, no. 13, pp. 859–867, 1980.

[3] S. J. Perry, J. M. Castro, and C. W. Macosko, "A Viscometer for Fast Polymerizing Systems," *J. Rheol. (N. Y. N. Y).*, vol. 29, no. 1, pp. 19–36, 1985.

[4] L. T. Nguyen, "Reactive Flow Simulation in Transfer Molding of IC Packages," in *Electronic Components and Technology Conference*, 1993, pp. 375–390.

[5] M. K. Abdullah, M. Z. Abdullah, M. A. Mujeebu, S. Kamaruddin, and Z. M. Ariff, "A Study on the Effect of Epoxy Molding Compound (EMC) Rheology During Encapsulation of Stacked-CHIP Scale Packages (S-CSP)," *J. Reinf. Plast. Compos.*, vol. 28, no. 20, pp. 2527–2538, 2009.

[6] M. K. Abdullah, M. Z. Abdullah, M. A. Mujeebu, Z. M. Ariff, and K. A. Ahmad, "Three-Dimensional Modelling to Study the Effect of Die-Stacking Shape on Mould Filling During Encapsulation of Microelectronic Chips," in *IEEE Transactions on Advanced Packaging*, 2010, vol. 33, no. 2, pp. 438–446.

[7] M. K. Abdullah, M. Z. Abdullah, S. Kamarudin, and Z. M. Ariff, "Study of flow visualization in stacked-Chip Scale Packages (S-CSP)," *Int. Commun. Heat Mass Transf.*, vol. 34, no. 7, pp. 820–828, Aug. 2007.

[8] R. Chang, W. Yang, S. Hwang, and F. Su, "Three-Dimensional Modeling of Mold Filling in Microelectronics Encapsulation Process," in *IEEE Transactions on Components and Packaging Technologies*, 2004, vol. 27, no. 1, pp. 200–209.

[9] C. Y. Khor and M. Z. Abdullah, "Modelling and analysis of the effect of stacking chips with TSVs in 3D IC package encapsulation process," *Maejo Int. J. Sci. Technol.*, vol. 6, no. 02, pp. 159–185, 2012.

[10] T. Mitani and H. Hamada, "A flow simulation for the epoxy casting process using a 3D finite-element method," *Polym. Eng. Sci.*, vol. 45, no. 3, pp. 364–374, Mar. 2005.

[11] L. Nguyen, C. Quentin, W. Lee, S. Bayyuk, B. S. A. Allen, and S. Wang, "Computational Modeling and Validation of the Encapsulation of," *Trans. ASME*, vol. 122, no. June, pp. 138–146, 2000.

[12] H. Zhou and D. Li, "A Numerical Simulation of the Filling Stage in Injection Molding Based on a Surface Model," *Adv. Polym. Technol.*, vol. 20, no. 2, pp. 125–131, 2001.

[13] C. a. Hieber and S. F. Shen, "A finite-element/finite-difference simulation of the injection-molding filling process," *J. Nonnewton. Fluid Mech.*, vol. 7, no. 1, pp. 1–32, 1980.

[14] Y. K. Shen, S. H. Chen, and H. C. Lee, "Analysis of the Mold Filling Process on Flip Chip Package," *J. Reinf. Plast. Compos.*, vol. 23, no. 4, pp. 407–428, Mar. 2004.

[15] H. H. Chiang, C. A. Hieber, and K. K. Wang, "A unified simulation of the filling and postfilling stages in injection molding. Part I: Formulation," *Polym. Eng. Sci.*, vol. 31, no. 2, pp. 116–124, 1991.

[16] Y. Chou, H. Yeh, H. Chiu, C. Yu, R. Chang, and C. City, "A three-dimensional cae molding of microchip encapsulation," pp. 1–6.

[17] J. M. Castro, S. D. Lipshitz, and C. W. Macosko, "Laminar Tube Flow with a Thermosetting Polymerization," *AIChE J.*, vol. 28, no. 6, pp. 973–980, 1982.

[18] J. M. Castro and C. W. Macosko, “Studies of mold filling and curing in the reaction injection molding process,” *AIChE J.*, vol. 28, no. 2, pp. 250–260, Mar. 1982.

[19] J. M. Castro, C. W. Macosko, F. E. Critchfield, E. C. Steinle, and L. P. Tackett, “Reaction Injection Molding: Filling of a Rectangular Mold,” *J. Elastomers Plast.*, vol. 12, no. 1, pp. 3–17, Jan. 1980.

[20] S. Han and K. K. Wang, “Flow analysis in a chip cavity during semiconductor encapsulation,” *J. Electron. Packag.*, vol. 122, no. 2, pp. 160–167, 2000.

[21] A. M. K. Reddy, R. Han, and M. Gupta, “Numerical and Experimental Investigation of Microchip Encapsulation,” *J. Reinf. Plast. Compos.*, vol. 17, no. 1, pp. 70–93, 1998.

[22] A. J. Chorin, “The numerical solution of the Navier-Stokes equations for an incompressible fluid,” *Bull. Am. Math. Soc.*, vol. 73, no. 6, pp. 928–932, Nov. 1967.

[23] M. W. Lee, J. Y. Khim, M. Yoo, J. Chung, and C. H. Lee, “Rheological Characterization and Full 3D Mold Flow Simulation in Multi-Die Stack CSP of Chip Array Packaging,” in *56th Electronic Components and Technology Conference 2006*, 2006, pp. 1029–1037.

[24] R. B. Bird, R. C. Armstrong, and O. Hassager, *Dynamics of polymeric liquids, vol 1 Fluid mechanics*. .

[25] S. D. Lipshitz and C. W. Macosko, “Rheology Changes During a Urethane Network Polymerization,” *Polym. Eng. Sceince*, vol. 16, no. 12, pp. 803–810, 1976.

[26] L. D. Landau and E. M. Lifshitz, *Fluid Mechanics*, vol. 6, no. 1. 1987.

[27] C. . Hirt and B. . Nichols, “Volume of fluid (VOF) method for the dynamics of free boundaries,” *J. Comput. Phys.*, vol. 39, no. 1, pp. 201–225, Jan. 1981.

[28] M. Renardy, Y. Renardy, and J. Li, “Numerical Simulation of Moving Contact Line Problems Using a Volume-of-Fluid Method,” *J. Comput. Phys.*, vol. 171, no. 1, pp. 243–263, Jul. 2001.

[29] M. R. Kamal and S. Sourour, “Kinetics and thermal characterization of thermoset cure,” *Polym. Eng. Sci.*, vol. 13, no. 1, pp. 59–64, Jan. 1973.

[30] L. T. Manzione, *Plastic Packaging of Microelectronic Devices*. 1990.

[31] H. Schlichting, *Boundary layer theory*. 1978.

Chapter 5

Instantaneous Linear Elastic Approach for 1-D Analytical Estimation of Residual Stresses in a Bilayer Model

5.1. Introduction

The mechanical behavior of polymeric materials is known as viscoelastic [1]. Therefore, for a reliable prediction of deformation and stresses a constitutive model representing the time dependent response of the polymer is essential. The reliability of the constitutive model, on the other hand, is provided via the data obtained by the dynamic measurements of several decades covering the entire range of process (molding) temperature. The complexity of the mechanical behavior and the requirement for extensive and time consuming experiments and their complicated evaluation techniques lead to a search for some alternative methods. The simplest method would be the elastic mechanical modeling of the entire deformation history. Yet, for curing systems the modulus is rising continuously and it increases by polymerization from as low as a few Pa to as high as 100MPa after full conversion at the rubbery state inside the mold. Later during cooling down the modulus evolves further until the glassy plateau where it is almost two orders of magnitude of the starting rubbery modulus value. Moreover, the polymer in liquid state does not contribute to the stress build-up. But above the gel point the shrinkage of the EMC and the increase of modulus affect the total stress level. These phase transitions and corresponding mechanical variations are difficult to be described precisely by an elastic constitutive model.

The classical plate theory has been a common approach for residual stress prediction in composite materials [2]–[8]. The majority of these studies assumed a stress free state prior to cooling [6]–[11]. One of the early elastic mechanical models developed for composite laminates is the work of Hahn and Pagano [6] where the cure stage was assumed as stress free. Yet, the cooling stage after full crosslink formation was studied based on an incremental linear elastic model with a temperature dependent mechanical behavior. The material properties were considered to be independent of the crosslinking reaction during cooling. Bogetti [3] adopted the incremental linear elastic model in which the cure dependent modulus was formulated based on uncured and fully cured equilibrium states data. The isotropic interrelation was used for the elastic moduli determination. Antonucci numerically investigated a non-isothermal resin cure by adopting the Cauchy-Navier approach [2].

The effect of warpage during cure is taken into account analytically for the stress prediction by some studies [5], [12]–[14]. In an experimental bilayer study of Hu et al. at which the results are verified by a finite element analysis it is proven that without considering the effect of cure shrinkage, warpage was underestimated. This study concluded that, implementing the cure shrinkage together with a temperature dependent thermal expansion coefficient and a temperature dependent elastic modulus provides a more realistic estimation for warpage in comparison to a viscoelastic study with no cure shrinkage effect [15]. The warpage in bilayer and multilayer thin plates during curing reaction were studied by Jansen et al, assuming an elastic mechanical model [12], [13]. In these studies an analytical model was also developed for the stress-free temperature and strain. The residual stress was studied numerically using classical plate theory during the cooling stage by Harper and Weitsman and verified experimentally by curvature measurement [7]. Verification of the stress and warpage data by bending technique have been conducted by others as well [8], [16], [17]. Some special solutions had been proposed for the layered composites like the study of Townsend in which the warpage due to the thermal mismatch of a thin film over a thick substrate was investigated analytically [8]. Another important example is the work of Bogetti who particularly studied thick composite layers [3], [4].

The crosslinking mechanism of thermosetting epoxy polymers has been well-defined quantitavely [1], [18], [19]. The cure reaction progress of an epoxy polymer directly affects the physical properties such as stiffness, viscosity or CTE. Nonetheless, the effect of curing reaction on such mechanical properties are not characterized effectively in the literature, and most of the time the proposed experimental methods and numerical techniques are either too complex and time consuming to apply or not reliable for the processing cure time or temperature range. This can be clearly observed in the viscoelastic superposition for master curve determination of some studies. The time temperature superposition models are

mostly restricted to some portion of the viscoelastic region and beyond a certain temperature value the resulting modulus deviates from the real experimental results and is not reliable anymore. Therefore, some researchers preferred to apply two distinct models by separating the working temperature range such that the entire transition region is covered effectively [5], [12], [13]. Therefore, introducing the third variable to an already complicated phenomenon brings about additional reliability concern and numerical complexity to an already multivariably dependent process. There is no doubt that in order to better understand the viscoelastic mechanical behavior of the thermosetting polymers the effect of all process variables should be taken into account. Hence, an accurate and verified model comprising the interdependent time, temperature and conversion variables are indispensable.

The shift in relaxation time, based on the degree of conversion can be considered as the stiffness response variation of an epoxy with a highly crosslinked density at a short response time to a lower crosslinked level with a longer response time or vice versa. Plazek used this method for the first time as a retardation mechanism that shifts the creep time of natural rubber vulcanizates, which were crosslinked to different degree [20]. In literature, there are some other well-established numerical and experimental approaches such that the cure dependent viscoelastic mechanical behavior is defined successfully and the models are verified with great accuracy [5], [12], [13], [21]–[25]. However, the need for predicting a mechanical property or the stress value under certain deformation history with the limited experimental data is also vital. Moreover, a simple model may facilitate the complexity of the optimization procedure when a faster prediction for a process parameter is needed.

5.2. Shrinkage

Cure Temperature

During a typical transfer molding process the EMC experiences cure and thermal shrinkage, consecutively, as shown schematically in figure 5.1. The red line shows the cure stage where the package is encapsulated and solidified completely at the mold temperature (for the present compound it is advised to be molded at 175^{o}C). This temperature is selected based on several criteria. A fast curing epoxy at higher cure temperatures results in physical degradation of the molding compound as a result of overheating. Moreover, a higher temperature means a shorter cure time which may lead to incomplete filling of the cavity. Therefore, a higher cure temperature is not favorable for both the molding material and the package. On the other hand, the acceptable limit for the minimum temperature for the encapsulation is the ultimate glass transition temperature. As mentioned in chapter 2 any temperature below $T_{g\infty}$ may lead to vitrification. Then, any isothermal cure temperature

above $T_{g\infty}$, which is around 113°C for the measured EMC provides a polymerization close to complete cure. However, the lower the temperature, the longer the molding time for a complete polymerization. This is the point at which the feasibility of mass fabrication of microelectronics should be considered by taking into account many aspects, including the cost. The tradeoff between molding duration and material degradation due to overheating which is a consequence of high cure temperature of the epoxy, determines the accepted range for the isothermal molding cure temperature.

Effective shrinkage

The gel point is attained almost at the half of complete polymerization of the tested epoxy polymer. The cure shrinkage is considered to be effective, starting from the gel point. The schematic of the proposed assumption is given in figure 3.6. Thus, this point is crucial for determination of the effective cure shrinkage and the start of stiffness build-up. The cure shrinkage is followed by the thermal shrinkage as a result of cooling to room temperature which is illustrated in green. Initially the slope is steeper since the epoxy is in the rubery state with a high thermal expansion coefficient, α, resulting in a larger volume change for each incremental temperature drop. At T_g the molecular freedom of the cured epoxy becomes restricted due to the transition to a glassy state with a lower α. The volume change between the mold temperature and the room temperature at the gel point determines the total thermal shrinkage.

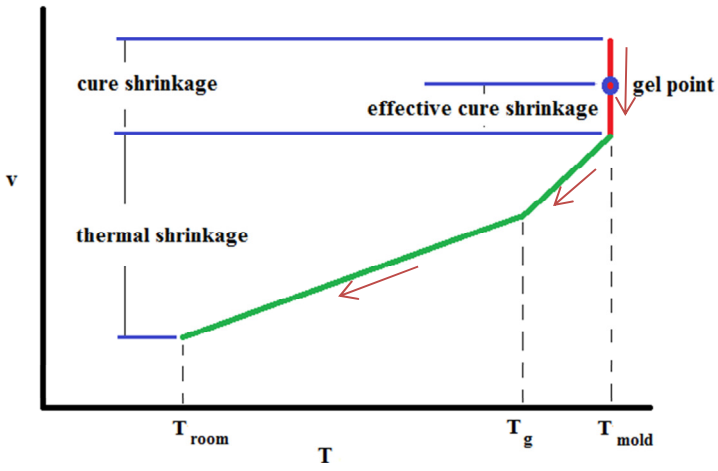

Figure 5.1 Schematic illustration of cure and thermal shrinkage during transfer molding

Instantaneous linear elastic approach

The mechanical model proposed in this chapter is originated from the bilayer study of Jansen [12] including the model applied for the estimation of warpage which was originally developed based on Stoney's formula for bending of layers. [26] The residual stresses at each layer were studied by implementing the in-plane stress equation independently from the rest of the process for each stage. The present study takes into account the effect of moduli change and volume change as a function of cure for the entire cure stage and as a function of time and temperature, independently, for the cooling stage. The methodology proposed for estimation of residual stress was verified by numerical and experimental studies given in chapters 6 and 7.

For the epoxy curing the cure hardening instantaneous linear elastic method is applied such that the modulus of elasticity is formulated as a function of conversion only. And for the cooling down stage the temperature dependent instantaneous linear elasticity is used to determine the stresses. So, the applied model is essentially elastic with a defined constant modulus at each increment but changing as a function of conversion and temperature. This method sometimes is defined as pseudo-viscoelastic [27]. The epoxy polymer is a viscoelastic material and in order to use an elastic model, the elastic modulus should be defined properly. Besides, the modulus will be a function of the selected frequency. There has been no general consensus about the frequency that should be applied in this model. For example, the predetermined frequencies in the relevant studies are 0.1, 1 and 10 Hz or not indicated at all [28]–[30]. A monotonically increasing cure dependent elastic modulus was used by Johnston et al. [28]. Bogetti and Gillespie implemented a formula based on the glassy and rubbery moduli [3]. As Zobeiry emphasized in his study the selection of the predetermined frequency is rather arbitrary [30]. Hence, in this thesis a dynamic mechanical analysis is performed at a single frequency (see chapter 3 section 3.7.1) and the storage modulus is taken as the elastic modulus of the EMC as a function of temperature.

There is a trade-off of time versus accuracy as we go from a more complex viscoelastic model to a simpler elastic model. The instantaneous linear elastic approach offers higher accuracy than a simple elastic model and it is economical compared to a viscoelastic method. In a comparative study the results obtained using the instantaneous linear elastic approach were determined to be reasonably accurate and reliable when compared with the fully viscoelastic approach [31].

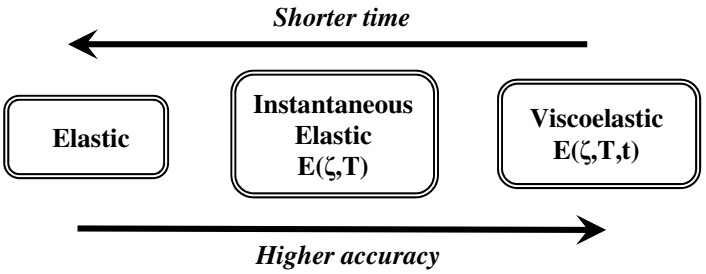

5.3. Bilayer in-plane stress calculation

As described in detail in chapter 2 the epoxy molding compound is solidified during molding which causes the variations in mechanical, kinetic and physical properties. The high production volume of the electronics requires accurate stress estimation techniques prior to fabrication to reduce the failure rates and improve the product reliability. Therefore, a well-established, comprehensive viscoelastic model comprising the process dependent variations of the EMC's physical properties is essential. On the other hand, a well-defined simplified method will save cost and time and may provide a quick prediction of residual stresses for fast process optimization, if the model is defined properly. The method defined in this chapter is an answer for this need. The model is based on independent evaluation of the cure and the cooling down stages such that the stiffness variation, shrinkage and boundary conditions are treated accordingly. The warpage contribution to the deformation is included by implementing the curvature in the constitutive equation. Furthermore, the conversion dependent stiffness, thermal behavior, the resulted volumetric variations and cure mechanism are introduced by the relevant models given in chapter 2.

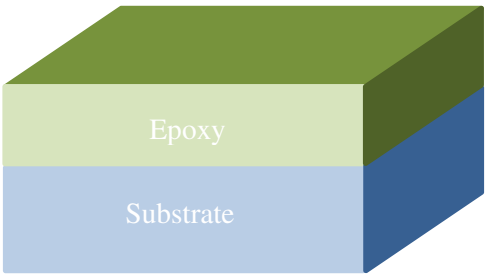

Figure 5.2 Schematic of the bilayer model

An instantaneous elastic model was used for the stress prediction on the interface of a bilayer package illustrated in figure 5.2. Bottom layer is a substrate and the top layer is the epoxy compound with the mechanical properties evolving by the progress of the

crosslinking. The incremental material properties are assumed homogeneous. The planar biaxial stresses in layer i are defined by

$$\varepsilon_{xx_i} = \frac{1}{E_i}\left[\sigma_{xx_i} - \nu\sigma_{yy_i}\right], \tag{5.1}$$

$$\varepsilon_{yy_i} = \frac{1}{E_i}\left[\sigma_{yy_i} - \nu\sigma_{xx_i}\right]. \tag{5.2}$$

Strains are isotropic $\left(\varepsilon_{xx_i} = \varepsilon_{yy_i}\right)$, and the deformations are considered uniform through the thickness. Then the planar biaxial stresses can be given by

$$\sigma_{xx_i} = \sigma_{yy_i} = \frac{E_i}{1-\nu}\varepsilon_{yy_i}. \tag{5.3}$$

Then the instantaneous planar stress can be expressed by

$$d\sigma_i = E_i' \, d\varepsilon_i, \tag{5.4}$$

where E_i' is the ith layer reduced elastic modulus at the time of strain increment, defined as $E_i' = \frac{E_i}{1-v_i}$. v_i is the Poisson's ratio for the ith layer. The effect of Poisson's ratio variations on mechanical properties of the epoxy polymer was found to be negligible by O'Brian [32]. In this study, the Poisson's ratio is taken to be constant at 0.45, which is the Poisson's ratio value of the fully reacted sample, calculated by implementing the experimental data of compression and tensile measurements in the interrelation function $\nu = \frac{1}{2} - \frac{E}{6K}$, given in table 5.1.

ε_i in equation 5.4 stands for the mechanical strain in ith layer, which is given in terms of the total incremental strain $d\varepsilon_{tot_i}$ and the shrinkage induced strain ε_{sh} by

$$d\varepsilon_i = d\varepsilon_{tot_i} - d\varepsilon_{sh_i}. \tag{5.5}$$

It is assumed that the stress is generated due to the bending of the whole package and the shrinkage of the both or one of the layers. Some portion of the resulted stress relaxes while some remains in the package in the form of residual stress. Determination of these residual stresses is the main purpose of this chapter.

The total strain ε_{tot_i} comprises a common planar strain of adjacent layers and a deflection resulted parts

$$d\varepsilon_{tot_i} = d\bar{\varepsilon} + d\phi(z - z_b), \tag{5.6}$$

where ϕ denotes the curvature, z is the height through the thickness in the ith layer and z_b refers to the neutral plane of the both layers.

Application of equilibrium of forces and moments to the given bilayer model yields

$$dF_{tot} = \sum_{i=1}^{2} F_i = W\left[\int_0^{h_1} d\sigma_1\, dz + \int_{h_1}^{h_1+h_2} d\sigma_2\, dz\right], \tag{5.7}$$

$$dM_{tot} = \sum_{i=1}^{2} M_i = W\left[\int_0^{h_1} z\, d\sigma_1\, dz + \int_{h_1}^{h_1+h_2} z\, d\sigma_2\, dz\right], \tag{5.8}$$

where W is the layers' width, and h_1 and h_2 are the thicknesses of the die and EMC layers, respectively.

5.4. Modulus for cure and cooling

As mentioned before thermosetting polymers are essentially viscoelastic in nature and detailed material characterization is required for the realistic representation of the mechanical behavior under the exposed thermo-mechanical loading in transfer molding. However, in this chapter instead of a complete time, temperature and conversion dependent characterization of the transition region, the temperature or conversion dependent models are used to calculate the deformation and stress. Similar pseudo-viscoelastic approach has been implemented by some researchers in various forms [2], [6], [8], [12], [13], [33], [34].

Except the filling stage where the average melt temperature is slightly below the pre-set mold temperature, the overall temperature of the epoxy melt in a standard encapsulating experiment is above the viscoelastic region. Therefore, the time and temperature dependent viscoelastic behavior can be ignored and a constant elastic moduli may be used for the entire cure stage. However, using the elastic modulus of the fully cured compound, even at the rubbery end of the spectrum, leads to overestimation of the stresses since the modulus develops gradually as a result of crosslinking of the epoxy polymer. Therefore, even though, the complex time-temperature dependent behavior is negligible, the conversion effect should be taken into account for an accurate cure induced stress determination. Hence, the modulus should be implemented as a function of conversion. Some conversion dependent models have been proposed by some researchers. For example, a linear interrelation function was proposed by Kim and Hahn, based on the tensile test they performed on partially cured samples. The initial values were overestimated and this behavior was attributed to the neglected viscoelastic characteristic of the resin [35]. In an important study by Martin and Adolf a useful prediction for the rubbery equilibrium modulus was proposed, which is expressed by [21]

$$G_\infty = G_\infty^f \left(\frac{\xi^2 - \xi_{gel}^2}{1 - \xi_{gel}^2}\right)^{8/3}, \tag{5.9}$$

where G_∞^f is the rubbery shear modulus of the fully cured epoxy. This model is implemented in this study to calculate the modulus during cure.

Moduli during cure evolve from zero at the beginning of the filling stage where the epoxy melt is initially uncured to the highest equilibrium value at full conversion. Experimental monitoring of cure dependent moduli is complex and requires specific test set-ups for the intended modulus. The EMC is liquid below the gel point and moreover, at the initial stage of filling it can be considered as a low viscous Newtonian fluid. Measuring the tensile viscoelastic modulus of a curing compound is almost impossible due to the physical state of the EMC below the gel point which is liquid with varying viscosity depending on the degree of conversion. Therefore, the tensile measurements like the study of Kim and Hahn [35] is not applicable to the early stages of polymerization, since the samples cannot be hold by the clamps of the tension test set-up. Viscosity gradually increases starting from as low as 10Pa.s depending on the applied temperature and reaches to its peak value at the gel point. Epoxy is no more a fluid beyond the gel point where the viscous dominated behavior is superseded by the viscoelastic response.

The most preferred test method is the dynamic parallel plate measurement of the shear relaxation modulus [16], [17], [25], [36]. Nonetheless, some modeling techniques have been also proposed for determination of the conversion dependent bulk modulus. Meuwissen et al proposed a linear time dependent bulk modulus based on uncured and fully cured equilibrium moduli. However, the proposed model relied on estimation of the equilibrium modulus rather than an empirical or theoretical approach [25].

The experimental measurement of hydrostatic pressure induced deformation of a curing polymer is always accompanied by the chemical cure shrinkage. That is why the bulk modulus measurements are mostly restricted to temperature or time varying studies at the fully cured state.

The simplification of the cooling induced stress model requires the elastic temperature dependent properties of the epoxy molding compound which can be obtained from a single experiment at a fixed frequency. Although the dynamic analysis can be performed using a frequency sweep DMA experiment, the complexity of the test and the requirement for further interpretation of the test data, makes the modeling more complex. On the other hand, elastic moduli are already provided by the suppliers of the EMCs which can be used directly in a linear incremental model for a simple stress analysis. Figure 5.3 shows the fixed frequency DMA heating rate experiment. The accuracy of a linear assumption for the shift in elastic modulus may not replicate the same results obtained by a more complete assumption of viscoelastic moduli. However, the room temperature and the mold temperature are respectively lying on glassy and rubbery plateau of the tested EMC which makes the pseudo-viscoelastic analytical approach represented in this study relatively accurate and comparable to the viscoelastic model.

The isotropic mechanical behavior leads to simplified interdependent material functions such that any modulus can be determined as a function of two other moduli or by using a predetermined modulus and a Poisson's ratio obtained under the same process conditions. These interdependent material functions are given in the following table. The related equations are used in this and other chapters of this thesis to obtain the shear or the tensile moduli, based on the already known Poisson's ratio, bulk modulus or shear modulus data.

Table 5.1 Inter-relation of the isotropic elastic mechanical functions [37]

Elastic constant	Expressed as function of:					
	G* and *E	***G* and *ν***	***E* and *ν***	***K* and *E***	***K* and *ν***	***K* and *G***
K	$\frac{GE}{9G-3E}$	$\frac{2G(1+\nu)}{3(1-2\nu)}$	$\frac{E}{3(1-2\nu)}$			
G			$\frac{E}{2(1+\nu)}$	$\frac{3KE}{9K-E}$	$\frac{3K(1-2\nu)}{2(1+\nu)}$	
E		$2G(1+\nu)$			$3K(1-2\nu)$	$\frac{9KG}{3K+G}$
ν	$\frac{E}{2G}-1$			$\frac{1}{2}-\frac{E}{6K}$		$\frac{3K-2G}{6K+2G}$

The bulk modulus data obtained by a PVT test set-up is explained in detail in chapter 2. The model proposed for the bulk modulus is already given in equations 2.22 and 2.23. Moreover, the single frequency heating rate tensile DMA experiment was performed at 1 Hz. The results of both experiments as a function of temperature are shown together with the shear modulus obtained using the interrelation between the moduli. The PVT measurements do not cover the whole temperature range since the samples are preheated slightly to just above the T_g to be compressed at the start of the measurements. Besides, due to the instrument sensitivity the maximum recordable temperature is around 200°C. However, the unrecorded region mostly lies on the equilibrium plateau. Therefore, the data beyond the range are extrapolated numerically. The Poisson's ratio given in figure 5.4 is determined based on the dynamic mechanical analysis performed in chapter 3 and using the interrelation of the isotropic elastic functions. Hence, it is 0.38 below T_g at the glassy end and 0.5 above T_g at the rubbery end. The recorded tensile and bulk moduli data are 9200 and 11000 MPa, respectively and the rubbery equilibrium data for the tensile and bulk moduli are 100 and 4300 MPa, respectively. The apparent decrease in the Poisson's ratio below the glass transition can be attributed to small inconsistencies between $E(t,T)$ and $K(T)$, since both measurements are conducted at different time scales.

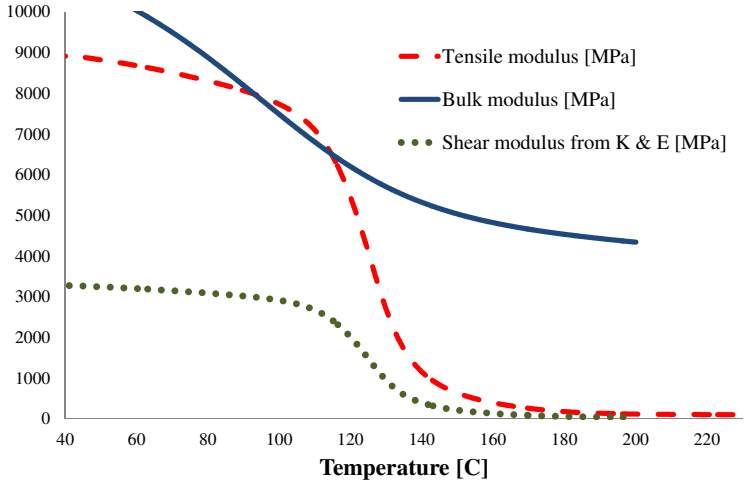

Figure 5.3 Single frequency constant shear rate DMA Tensile modulus and the hydrostatic bulk modulus data using PVT

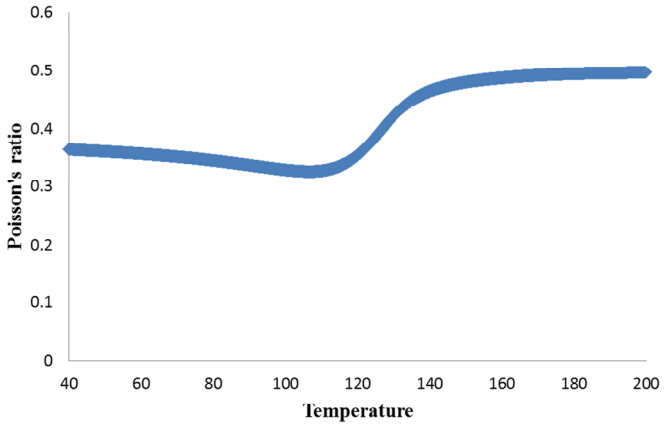

Figure 5.4 Poisson's ratio based on interrelation functions among the moduli

Based on the aforementioned assumptions, the temperature dependent elastic modulus $E(T)$ for the fully cured epoxy can be determined using the isotropic relation among the moduli. On the other hand, the cure dependent modulus is predicted by implementing the fully cured rubbery shear modulus into the Martin and Adolf model given in equation 5.9. Then, equation 5.4 can be rewritten for the cure stage as

$$d\sigma_i = E_i'(\xi)\, d\varepsilon_i, \tag{5.10}$$

and for the cooling stage as

$$d\sigma_i = E_i'(T)\, d\varepsilon_i. \tag{5.11}$$

5.5. Constitutive Modeling

The analyzes in this section largely parallels that of Jansen's bilayer bending study [12]. First, a formula for the cure induced stress will be developed and later the same approach will be used to derive the equation for the cooling induced stress.

5.5.1. Isothermal curing

During cure the mold cavity is closed and hence the encapsulated substrate is constrained inside the cavity. The warpage is restricted by the cavity walls and therefore any in-plane or out-of-plane deformation and curvature defined in equation 5.6 is restricted. The total force at the end of cure can be obtained by applying equations 5.4 through 5.7 and based on the aforementioned boundary condition it results in zero curvature and strain change during cure ($d\phi = d\bar{\varepsilon} = 0$). As a result, the cure-end total force, F_c, experienced by the mold walls is obtained as

$$F_c = -\int_{h_1}^{h_1+h_2} E_2'\, d\varepsilon_{sh_2} dz. \tag{5.12}$$

ε_{sh_2} is the cure induced strain of the epoxy. The thermal shrinkage is an intensive property of all materials but, the cure shrinkage is characteristic of thermosetting polymers. Since the process temperature during cure is constant, there is no thermal shrinkage during cure. The substrate neither cures like the reactive thermosetting epoxy nor experiences any thermal shrinkage. As a result, the substrate does not shrink during cure ($\varepsilon_{sh_1} = 0$).

For the total cure-end force, equation 5.12 reduces to

$$F_c = -h_2 \int_{\varepsilon_0}^{\varepsilon_c} E_2'\, d\varepsilon_{sh_2}. \tag{5.13}$$

As mentioned before the equilibrium modulus is considered as cure dependent. So, equation 5.13 can be rewritten in terms of incremental conversion as

$$F_c = -h_2 \int_0^{\xi_c} E_2' \frac{d\varepsilon_{sh_2}}{d\xi} d\xi\,, \tag{5.14}$$

where $\frac{d\varepsilon_{sh_2}}{d\xi}$ is the incremental change in cure induced strain with respect to the degree of cure. The lower bound of the integral takes the zero initial conversion while the conversion at the end of cure may depend on molding duration and the applied cure temperature. The

theoretically expected ideal value for ξ at the cure-end is unity representing the full conversion, yet the kinetic characteristic of the epoxy resin under isothermal molding condition may result in a lower value represented by ξ_c.

The negative sign indicates that the stress is compressive as a result of contraction of epoxy during cure. The total force balance of the whole system comprising the mold cavity surface, the epoxy encapsulated substrate and die assembly requires a positive force with the same magnitude applied on mold wall boundaries. At the end of cure when the mold cap is detached, the restricting opposite force on wall boundaries will vanish and the package will shrink freely with the calculated force in equation 5.14. At this stage the board is still inside the mold cavity and the temperature is at the isothermal temperature. So, the addition of the total cure-end force to the force balance equation 5.4 results in

$$\int_0^{h_1} \Delta\sigma_1 \, dz + \int_{h_1}^{h_1+h_2} \Delta\sigma_2 \, dz + F_c = 0, \tag{5.15}$$

where $\Delta\sigma$ defines the stress change between the start and the end of cure. However, the incremental change in stress $d\sigma$ is used in this study to provide a comparative way of stress evaluation in any point of cure, such that, the cure end is considered as the last evaluated incremental change in stress.

Inserting in-plane stress defined in equation 5.10 and taking the integral through the thickness of the layers leads to

$$\begin{aligned} dF_{tot} = {} & (E_1' h_1 + E_2' h_2) d\bar{\varepsilon} \\ & + \left[\frac{1}{2}\left(E_1' h_1^2 + E_2'(h_2^2 + 2h_1 h_2)\right) - z_b(E_1' h_1 + E_2' h_2)\right] d\phi + F_c = 0. \end{aligned} \tag{5.16}$$

Equation 5.16 must be valid independent of the curvature change $d\phi$. Then, the planar strain can be defined by

$$d\bar{\varepsilon} = -\frac{1}{1+ab} \, \frac{F_c}{E_1' h_1}, \tag{5.17}$$

in which a and b are the dimensionless parameters representing the thickness ratio h_2/h_1 and the moduli ratio E_2'/E_1' of the layers, respectively. Each incremental time step not only changes the modulus but also shifts the neutral plane to a new position. Based on the assumption stated above the neutral plane becomes

$$z_b = \frac{h_1\left(1+ab(a+2)\right)}{2(1+ab)}. \tag{5.18}$$

The same procedure can be applied to the moment balance for the cure stage such that the incremental moment constrained in the package denoted by M_c is determined by

$$dM_c = \int_0^{h_1} \Delta\sigma_1 \, z \, dz + \int_{h_1}^{h_1+h_2} \Delta\sigma_2 \, z \, dz, \tag{5.19}$$

which results in

$$dM_c = -h_2\left(h_1 + \frac{h_2}{2}\right)\int_{\xi_0}^{\xi_c} E_2' \frac{d\varepsilon_2}{d\xi} d\xi. \tag{5.20}$$

M_c can be considered as the moment applied at the end of cure when the mold cap is released. Then, the moment balance at the end of cure becomes

$$\int_0^{h_1} \Delta\sigma_1\, z\, dz + \int_{h_1}^{h_1+h_2} \Delta\sigma_2\, z\, dz + M_c = 0. \tag{5.21}$$

Expansion of the integrals yields

$$dM_{tot} = \frac{E_1'h_1^2 + E_2'h_2\left(2h_1h_2 + h_2^2\right)}{2} d\bar{\varepsilon} + \left[\frac{h_1^3E_1' + \left(h_2^3 + 3h_1^2h_2 + 3h_1h_2^2\right)E_2'}{3} - \frac{E_1'h_1^2 + E_2'\left(h_2^2 + 2h_1h_2\right)}{2} z_b\right] d\phi + dM_c = 0. \tag{5.22}$$

The curvature for the cure-end can be obtained by combining equations 5.17, 5.18, 5.20 and 5.22.

$$\phi = -\frac{6a}{h_1}\int_0^{\xi_c} \frac{\left[1 + \left(a^2 + 2a\right)b\right]}{N} \frac{d\varepsilon_2}{d\xi}\, d\xi, \tag{5.23}$$

in which N is defined by

$$N = 1 + b(4a^3 + 6a^2 + 4a) + a^4b^2. \tag{5.24}$$

As stated before, the stress and the warpage at any point in time are both functions of degree of conversion and temperature. Curing of epoxy comprises a phase change from a low viscous fluid, to a high viscous liquid and then to a solid above the gel point by forming a strong 3D structure with a high viscoelasticity effect. As a result, for the duration of cure, the modulus grows and the chemical shrinkage progresses until the clamp release. Therefore, the b parameter representing the modulus ratio is a function of conversion. Although the cure-end is a single point in time stating the highest equilibrium value, the exact cure-end is not determined experimentally and the analytical study given in this chapter is based on a fact that any point on conversion can be the cure end. So, instead of a theoretical predefined cure-end of unity, the equations derived above cover the conversion scale of the corresponding study. This approach provides the flexibility of the experimental analysis which is studied in detail in chapter 7.

A simplification can be done for the stress and warpage study by taking $\xi = 1$ and assuming the elastic modulus for the EMC accordingly. However, in this chapter the stress study covers the entire cure and cooling time, incrementally.

5.5.2. Transient cooling

It is assumed that at the end of cure the conversion of the epoxy reaches to its maximum value for the specified encapsulation process. This maximum value is defined as ξ_c in equation 5.14. After the cure, the mold top platen is removed and the encapsulated package is taken out to room temperature where the transient cooling accompanied by the resulted shrinkage. Unlike the cure stage where the shrinkage is effective only for the epoxy compound while the other internal components preserve their shapes, in cooling stage all components are exposed to shrinkage. However the degree of contraction may differ for each component and as a result, warpage and residual stress evolves in the package.

The transient cooling takes place from the isothermal mold temperature T_m to room temperature T_r of 24°C. Unlike the cure stage where the boundaries are constrained, during cooling the package is free to warp. Then, by applying the force balance equation of 5.7 we can get the equations for the planar strain and the curvature as we did for the cure stage which yields

$$d\bar{\varepsilon} = \frac{\frac{d\varepsilon_1'}{dT}+ab_T\frac{d\varepsilon_2'}{dT}}{1+ab_T}, \tag{5.25}$$

$$d\phi = -\frac{6a(a+1)}{h_1}\int_{T_m}^{T_r}\frac{b_T}{N_T}\Delta\alpha_T\, dT, \tag{5.26}$$

where b_T is the temperature dependent elastic modulus ratio, $\Delta\alpha_T$ refers to the temperature dependent coefficient of thermal expansion and $\frac{d\varepsilon_i'}{dT}$ denotes the strain change with respect to incremental temperature variation of i^{th} layer. The integral boundaries of the curvature equation refers to the temperature limits, set for the cooling stage.

The N_T term in the curvature equation is also temperature dependent now as opposed to the cure dependent one defined for the cure-end. Hence, it is expressed by

$$N_T = 1 + b_T(4a^3 + 6a^2 + 4a) + a^4b_T^2, \tag{5.27}$$

while the neutral plane is defined by

$$z_b = \frac{h_1\left(1+ab_T(a+2)\right)}{2(1+ab_T)}. \tag{5.28}$$

Note that the elastic modulus is considered as conversion dependent for the cure stage while it is temperature dependent for the cooling stage. Therefore, the constitutive model proposed in this chapter should be solved for each stage, independently.

5.5.3. Warpage

The deflection of the bilayer assembly in out of neutral plane direction with respect to its undeformed flat initial geometry is considered as warpage. The analytical definition of the warpage can be obtained by using the following relation between the deflection and curvature [12].

$$d = R\left[1 - \cos\left(\frac{2L}{R}\right)\right] \cong \frac{\phi L^2}{8}, \tag{5.29}$$

where R is the radius of the curvature given as $1/\phi$ and L is the length of the both layers.

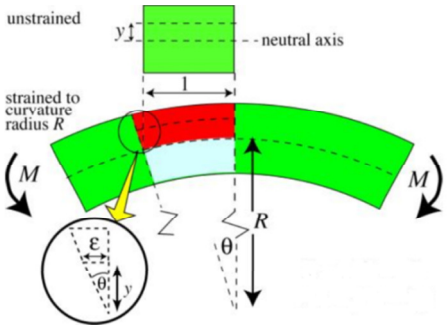

Figure 5.5 Curvature and deflection

5.5.4. Modeling approach

The material models implemented in this chapter are based on the extensively studied epoxy molding compound characterization measurements which are given in detail in chapter 2. The EMC material models' parameters are given in relevant sections of chapter 2 and will not be repeated here.

The residual stress is studied based on the tested molding process conditions. The gradual cooling transition started just after the end of cure. The duration of the molding affects the stress values due to the coupling of implemented kinetic model. The details about the experiment and process conditions can be found in chapter 7.

The cooling stage is modeled based on two approaches. The first one is the instantaneously elastic temperature dependent model and the second one is calculated by using the viscoelastic model.

During the cure stage the cure shrinkage prevails which is measured by the PVT experiment described in detail in chapter 2. A simple model can be applied to determine the strain experienced by the molding compound as

$$\varepsilon_{ch} = \frac{\Delta V_{ch}}{3V_0} \int_{\xi_0}^{\xi} d\xi \cong \varepsilon_{ch}^{\infty}\, \xi, \tag{5.30}$$

where ΔV_{ch} is the total volume change and V_0 is the initial volume of the uncured epoxy. Therefore, ε_{tot}^{ch} refers to the total strain of the epoxy layer determined by the PVT measurement.

Analytical stress model implementation

The incremental linear formula is implemented as

$$\sigma_i(t + \Delta t) = E_i' \, \Delta\varepsilon_i + \sigma_i(t)\,. \tag{5.31}$$

The conversion degree and temperature is determined at each time step. Then based on the model variables described above, the stress at the interface can be approximated by

$$\sigma_i(\xi) = E_i(\xi)\left\{\left[\frac{ab}{1+ab} + \left(\frac{S}{2(1+ab)} - 1\right)\, 6a\,\frac{S}{N}\right]\, \varepsilon_{ch}^{\infty}\, \xi - \int \mathrm{d}\varepsilon_{ch_i}\right\}, \tag{5.32}$$

and for the first layer where the cure shrinkage is ineffective, equation 5.32 becomes

$$\sigma_1(\xi) = E_1\left[\frac{ab}{1+ab} + \left(\frac{S}{2(1+ab)} - 1\right)\, 6a\,\frac{S}{N}\right]\, \varepsilon_{ch}^{\infty}\, \xi, \tag{5.33}$$

where $S = 1 + a(a+2)b$. E_1 is independent of the degree of cure and taken as constant.

The cooling induced stress simplifies to

$$\sigma_i(T) = E_i(T)\left[\frac{\alpha_1 + ab\alpha_2}{1+ab} + \frac{S}{N}(\alpha_2 - \alpha_1)\,\left(1 - \frac{S}{2(1+ab)}\right) - \alpha_i\right]\, dT. \tag{5.34}$$

Hence, the stress at the first layer surface can be estimated by

$$\sigma_1(T) = E_1(T)\left[\frac{\alpha_1 + ab\alpha_2}{1+ab} + \frac{S}{N}(\alpha_2 - \alpha_1)\,\left(1 - \frac{S}{2(1+ab)}\right) - \alpha_1\right]\, dT. \tag{5.35}$$

The proposed equations developed in this thesis provide a fast and reliable stress estimation method in a bilayer model with a curing layer. The results obtained by these equations are evaluated for the first time in this thesis by comparing the results to the numerically obtained values in chapter 6 and the experimentally measured data in chapter 7.

5.5.5. Viscoelastic model

As it is mentioned before, the aim of this chapter is to provide a method for a quick overview of the stresses building up in a bilayer package and the results can be compared with the subsequent chapter 6 where a two dimensional viscoelastic approach is presented. However, although it is not the main purpose of this chapter to introduce the viscoelasticity, the stress evolution in the cooling stage is evaluated using both the instantaneous elastic

and the viscoelastic approaches to provide a comparative study for the reader. Hence, the viscoelastic stresses during cooling down is determined incrementally as well by

$$\sigma_i(t) = \sum E_i'(t - t')\,\Delta\varepsilon_i(t'). \tag{5.36}$$

The stiffness parameters and the corresponding relaxation times of each Maxwell branch are previously determined in chapter 3 and given in table 3.2. The relaxation modulus imposed on the epoxy layer was obtained by taking into account the remaining relaxation time and incremental strain at each time step. The shift factor for the studied temperature range is obtained based on the WLF/Polynomial model proposed in chapter 3 (see equations 3.43 and 3.45). The horizontal shift factor, $\log(a_T)$, of the tested temperature range (25-140°C) is shown in figure 5.6.

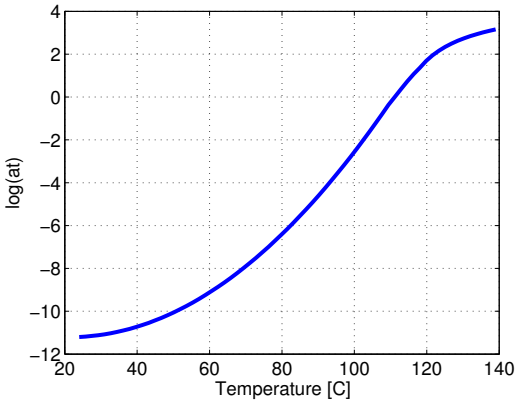

Figure 5.6 $\log(a_T)$ covering the temperature range of the cooling period of the 140°C test temperature

5.6. Computational Results

5.6.1. Simulation conditions

The bilayer model studied in this chapter consists of a die and an EMC on top. As mentioned earlier the Hitachi compound is taken as the encapsulant layer in the present and the subsequent chapters. The cure shrinkage as well as cure kinetics are already determined in chapters 2 and 3. Therefore, these properties will not be repeated in this chapter again and the reader may refer to the corresponding chapters. The cure shrinkage is assumed as conversion dependent and the change in thermal expansion is taken into account by the temperature dependent Tait function (equation 2.21).

Three different cure conditions are studied numerically using the instantaneous linear elastic approach. Note that the test parameters are based on the process conditions of the

corresponding experiment given in chapter 7. The process conditions are provided in table 5.2 for an overview.

Table 5.2 Process conditions and calculated final conversion for the four experimental studies of chapter 7

Cure temperature	[^{o}C]	120	140	160
Cure time	[s]	2800	1100	400
Cure-end Conversion	[%]	83.5	88.5	91

The main discussion and detailed analyses will be focused on the test temperature of 140^{o}C with the cure time of 1100s. The results of the other studies will be given briefly in this chapter and all can be compared with the corresponding 2D numerical simulations given in chapter 6 in which the epoxy behavior is assumed as viscoelastic during cooling, or with the measured stress data of the molding experiment which will be discussed in chapter 7 in detail.

5.6.2. 140^{o}C

The cure temperature is set to 140^{o}C and the cure time is 1100 seconds. The epoxy compound is not completely cured after the molding experiment. It can be observed in figure 5.7 that based on the implemented kinetic model the cure-end conversion rate is expected to be 88.5%. A consequence of an under-cured system is an underdeveloped modulus which leads to a lower stress. The modulus growth starts after the gel point and continues with an increasing rate. The ratio of the cure dependent shear modulus to the modulus of a fully cured epoxy is given as a function of time in figure 5.6. Although the epoxy cure reaction is close to full conversion, the equilibrium shear modulus ratio is less than half of the maximum value that can be attained under complete polymerization. The equilibrium modulus progress gets faster as the conversion degree rises over 90%. This phenomenon can be observed by studying figures 5.7, 5.10 and 5.13.

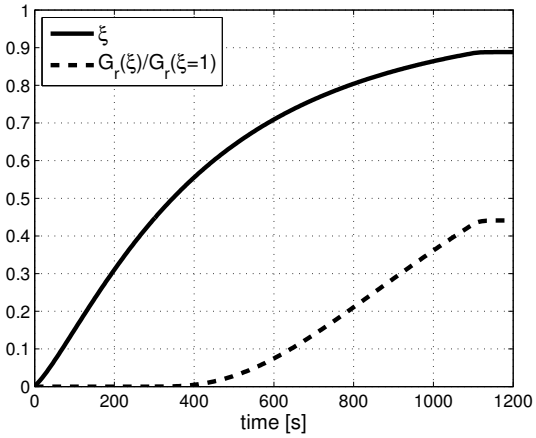

Figure 5.7 Conversion dependent rubbery shear modulus and the degree of conversion for 140^{o}C mold temperature

The one dimensional stress estimation on the surface of the die-epoxy interface, calculated based on the aforementioned homogenous strain distribution assumption, results in a single stress value at each incremental time step for each stage independently. It is a simple approach when it is specifically aimed for a stress at a point as a function of time. One dimensional evaluation of the residual stress in a more complex geometry may look insufficient. However, the simplicity of the layered geometry proposed in this study provides a fast and relatively accurate method for prediction of deflection and residual stresses at each stage.

As mentioned earlier the stress for the cure stage is based on several assumptions including the constrained boundary conditions that prevent any warpage induced deformation prior to the mold opening (1100 sec). This leads to a single stress value representing the cure induced residual stress at the end of cure stage. However, the range of cure stress data representing the shorter cure reaction levels are also given in this graph in order to have a general overview about the possible variations in stress magnitude if the cure reaction time is taken shorter than the compared experimental cure time. On the other hand, in case of a complete polymerization by extending the cure time, the expected cure induced stress for the epoxy used in the experiment will be close to 2MPa. This is based on a fact that the modulus is not developed to its fully reacted equilibrium state in this study which can be clearly observed in figure 5.7. Therefore, the cure-end in-plane stress is calculated to be 1MPa.

A thermal induced stress of 18MPa is obtained for the cooling stage when the temperature dependent modulus is implemented (blue dashed line in figure 5.8). Then, in total, the predicted residual stress is 19MPa. Moreover, if the time dependent behavior of the epoxy, based on the Generalized Maxwell Model with the Prony terms given in table 3.2 is taken into account, the estimated total residual stress becomes 13MPa (green dash-dotted line in figure 5.8). The fact that in the viscoelastic calculation the stress decreases after reaching the glass transition region (at about 1140 seconds in figure 5.8) is partly caused by stress relaxation and partly by stress reduction due to warpage.

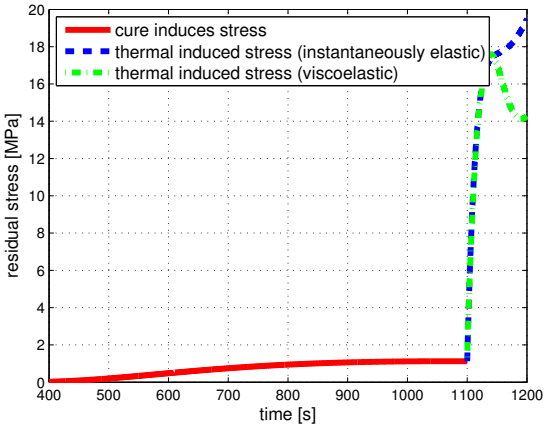

Figure 5.8 Calculated cure and thermal induced stresses for 140^{o}C molding

The warpage obtained by equation 5.29 takes into account the variations in epoxy modulus. The rise in modulus during cure and thermal stages were affected by the conversion and the temperature changes, as stated before. Therefore, the analytically calculated deflection rate for each stage is independent from each other, as can be observed in figure 5.9. Need to emphasize that the deflection as a result of cure strain is a single value obtained at the end of cure reaction, because the boundary conditions at this stage is constrained and does not let any warpage to occur before the detachment of the clamp. But again as it is done in this study for the stress analysis, the warpage is also given for a range of time covering the entire cure time. Therefore, the deflection at any point can be considered as if the cure reaction is ended at a shorter time or degree of conversion. The estimated midpoint deflection for the cure stage increases rather linear with the progress of polymerization and at the cure-end the maximum bending becomes 0.2mm and at the end of cooling stage the bilayer package bends 1.45mm at the center. Hence, the total deflection is estimated to be 1.65mm.

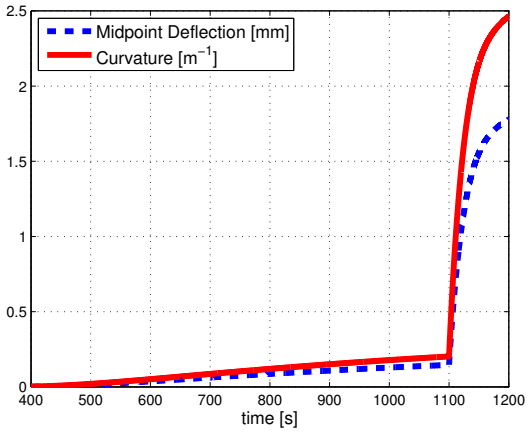

Figure 5.9 Midpoint deflection and curvature estimation for 140°C molding

5.6.3. 120°C

The cure temperature of 120°C is the lowest studied temperature. The temperature is slightly below the rubbery end at the onset of the viscoelastic transition region which makes the assumption made for the cure stage rather difficult to apply. However, the results match well when compared with the other tested conditions. The cure-end degree of conversion is 83.5% which results in $G_r(\xi)/G_{r\infty}$ ratio of 0.28 at the end of cure. The cure induced stress is obtained as 0.85 which is slightly lower than the value predicted for the 140°C case. The cooling induced stress using the instantaneous linear elastic model at the interface is calculated as 15MPa and using the viscoelastic model as 11MPa. The total mid-point deflection at the end of molding is 1mm and the total curvature is obtained as 1.35m^{-1}.

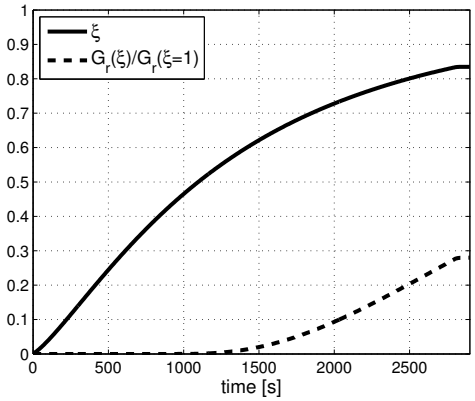

Figure 5.10 Conversion dependent shear modulus and the degree of conversion for 120°C molding

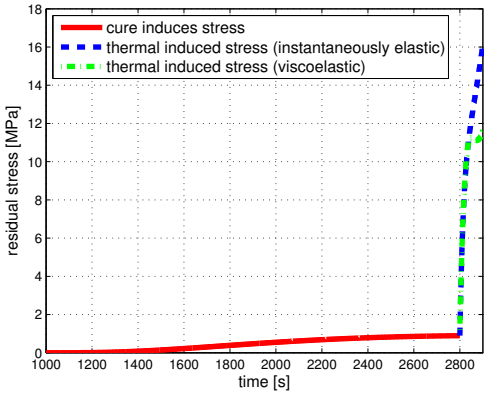

Figure 5.11 Cure and thermal induced stress profile for 120°C molding

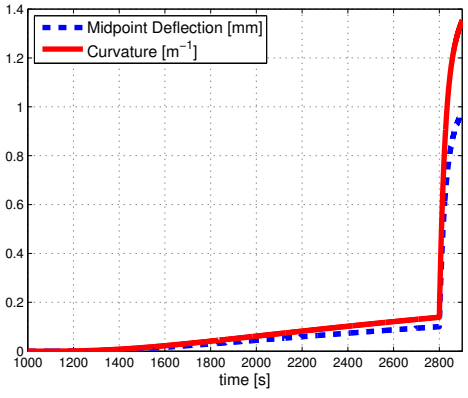

Figure 5.12 Midpoint deflection and the resulted curvature estimation for 120°C molding

5.6.4. 160°C

160°C is the highest cure temperature studied for validation of the numerical approach. The cure time is 400s which leads to 91% cure-end conversion and $G(\zeta_{cure\text{-}end})/G_\infty$ ratio of 0.52. As a result, the cure induced stress is obtained as 1.2MPa and the cooling induced residual stress is determined as 29MPa based on the instantaneous elastic approach and 15MPa by adapting the viscoelastic behavior in the model. The estimated total midpoint deflection is 2.5mm.

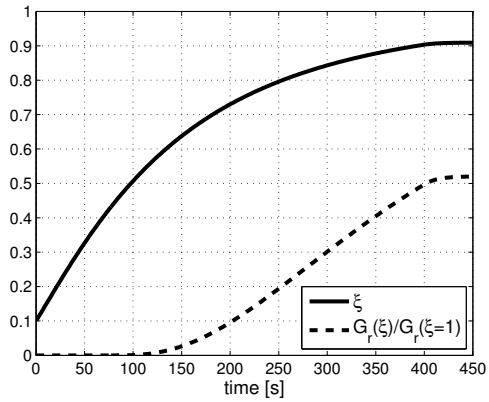

Figure 5.13 Conversion dependent shear modulus and the degree of conversion for 160°C molding

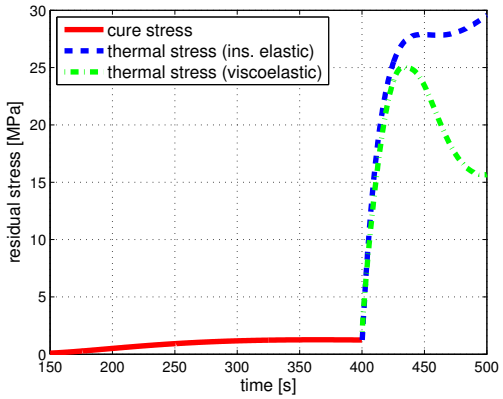

Figure 5.14 Cure and thermal induced stress profile for 160°C molding

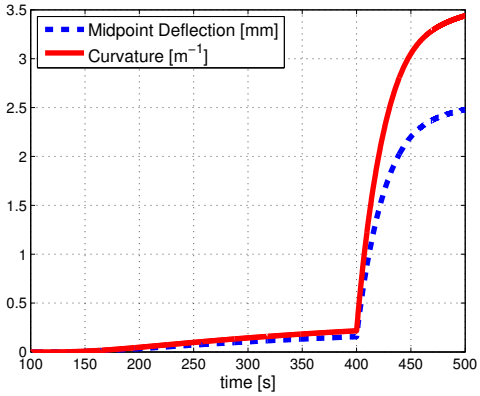

Figure 5.15 Midpoint deflection and the resulted curvature estimation for 160°C molding

5.7. Conclusion

A simple analytical in-plane stress estimation model for the bilayer plate structure is presented in this chapter. The model consists of a layer of epoxy on top of a polyimide substrate. The geometry of the layers is given according to the dimensions of the components used in the experimental study given in detail in chapter 7. The stress in between the two layers is analyzed by evaluating the process in two stages as it is done for the numerical simulation in chapter 6. Therefore, the deformation and the moduli are modeled and the boundary conditions are applied at each stage, accordingly.

Table 5.3 Estimated cure-end and cooling-end stress values for the tested molding conditions

	Cure temperature	[°C]	120	140	160
	$G(\zeta_{cure\text{-}end})/G_\infty$	[%]	28	44	52
	Cure stress	[MPa]	0.85	1	1.2
	Cooling (ins. elastic) stress	[MPa]	15	18	29
	Cooling (viscoelastic) stress	[MPa]	11	13	15
Cure stage	**Curvature**	[m^{-1}]	0.15	0.2	0.25
	Midpoint deflection	[mm]	0.1	0.15	0.2
Cooling stage	**Curvature**	[m^{-1}]	1.2	2	3.5
	Midpoint deflection	[mm]	0.9	1.5	2.3

In most of the existing studies the effect of cure on total residual stress was neglected and the cure stage assumed as a stress free stage of molding [6]–[11]. The results in this chapter

does not entirely contradict those assumptions but a pattern showing a consistent relation between the cure and cooling induced stress values for the studied epoxy at various mold temperatures can be observed. Table 5.3 shows the cure and cooling induced in-plane stresses as well as the resultant deflection and curvature values. It can be concluded that the stress at the end of cure is a factor of 15 to 20 lower than the stress increase during cooling.

The residual stress during the curing polymerization where the polymer stiffness and shrinkage starts developing after the gel point is calculated using the conversion dependent model (equation 5.32). The cure shrinkage mechanism is particularly effective after the gel point where the stress relaxation is restricted more and more after each incremental time step. The cure-end means the transition from a constrained boundary condition to an unconstrained boundary due to unclamping of the mold and releasing of the encapsulated package. The conversion dependent stress model now is replaced by the temperature dependent one (equation 5.34). The temperature dependent CTE is used to estimate the shrinkage during cooling of the package. In reality, the polymerization continues as far as the temperature remains above the glass transition temperature but the cooling rate is fast and therefore, no considerable curing reaction takes place upon this point. Therefore, it is assumed that the reaction is terminated at the start of cooling.

An incremental viscoelasticity was also studied along with the instantaneously elastic model. The model is based on the Generalized Maxwell equation. The cooling induced in-plane residual stresses which are determined using both models are shown for each studied case. In the corresponding figures the curve representing the stress variation in cooling stage reveals that the stress build-up is fast and the pattern is relatively linear both in instantaneously elastic and viscoelastic calculations. However, after passing almost half of the cooling time a relaxation pattern is observed. In the viscoelastic model the relaxation is much sharper while in the instantaneous elastic model the effect is slightly weaker. Therefore, it is shown that the relaxation pattern is simulated successfully by the proposed instantaneous elastic stress model but the effect remains weaker when compared to the viscoelastic approach.

A full viscoelastic finite element analysis provides a deeper understanding of residual stress formation by taking into account the whole geometry of the package as it is the subject of the following chapter. This is specifically true in case of a need for more sophisticated stress analysis. The detailed numerical study always delivers a deeper insight about the distribution of the loads and gives a broader knowledge for process optimization. Nonetheless, the presented method provides an efficient and practical way for rapid prediction of one-dimensional homogenous stress build-up.

The proposed model reveals that the maximum residual in-plane stresses can be estimated quite realistically if the implemented material models match the interdependent material behavior under the exposed process conditions. The bilayer geometry may also be extended to a more detailed multilayer structure covering the whole range of internal components.

References

[1] J. D. Ferry, *Viscoelastic Properties of Polymers*. 1961.

[2] V. Antonucci, a. Cusano, M. Giordano, J. Nasser, and L. Nicolais, "Cure-induced residual strain build-up in a thermoset resin," *Compos. Part A Appl. Sci. Manuf.*, vol. 37, no. 4, pp. 592–601, 2006.

[3] T. A. Bogetti and J. W. Gillespie, "Process-Induced stress and deformation in thick section thermoset composite laminates," *U.S. Army Ballist. Res. Lab*, 1990.

[4] T. A. Bogetti and J. W. Gillespie, "Two-dimensional cure simulation of thick thermosetting composites," *J. Compos. Mater.*, vol. 25, no. March 1991, p. 409, 1991.

[5] J. de Vreugd, K. M. B. Jansen, L. J. Ernst, C. Bohm, a. Kessler, and H. Preu, "Effects of Molding Compound Cure on Warpage of Electronic Packages," *2008 10th Electron. Packag. Technol. Conf.*, pp. 675–682, Dec. 2008.

[6] H. T. Hahn and N. J. Pagano, "Curing Stresses in Composite Laminates," *J. Compos. Mater.*, vol. 9, no. January, pp. 91–106, 1975.

[7] B. D. Harper and Y. Weitsman, "Residual Thermal Stresses in an Unsymmetrical Cross-Ply Graphite/Epoxy Laminate," *Am. Inst. Aeronaut. Astronaut.*, pp. 325–332, 1981.

[8] P. H. Townsend, D. M. Barnett, and T. a. Brunner, "Elastic relationships in layered composite media with approximation for the case of thin films on a thick substrate," *J. Appl. Phys.*, vol. 62, no. 1987, pp. 4438–4444, 1987.

[9] K. Y. Lin and I. H. Hwang, "Thermo-Viscoelastic Analysis of Composite Materials," *J. Compos. Mater.*, vol. 23, pp. 554–569, 1989.

[10] L. W. Morland and E. H. Lee, "Stress Analysis for Linear Viscoelastic Materials With Temperature Variation," *Trans. Soc. Rheol.*, vol. 4, pp. 233–263, 1960.

[11] F. Schwarzl and A. J. Staverman, "Time Temperature Dependence of Linear Viscoelastic Behavior," *J. Appl. Phys.*, vol. 23, p. 838, 1952.

[12] K. M. B. Jansen, J. De Vreugd, and L. J. Ernst, "Analytical Estimate for Curing-Induced Stress and Warpage in Coating Layers," *Appl. Polym. Sci.*, vol. 126, no. December 2011, pp. 1623–1630, 2012.

[13] K. M. B. Jansen and B. Öztürk, "Warpage Estimation of a Multilayer Package Including Cure Shrinkage Effects," *IEEE Trans. Components, Packag. Manuf. Technol.*, vol. 3, no. 3, pp. 459–466, Mar. 2013.

[14] D. G. Yang, K. M. B. Jansen, and ErnsfL.J., "Modeling of Cure-Induced Warpage of

Plastic IC Packages," in *Proceedings of the 5th International Conference on Thermal and Mechanical Simulation and Experiments in Microelectronics and Microsystems*, 2004, pp. 33–40.

[15] G. Hu, S. Chew, and B. Singh, "Cure shrinkage analysis of green epoxy molding compound with application to warpage analysis in a plastic IC package," in *Proceedings of the Electronic Packaging Technology Conference, EPTC*, 2007, pp. 7–11.

[16] J. Lange, S. Toll, J.-A. E. Månson, and A. Hult, "Residual stress build-up in thermoset films cured above their ultimate glass transition temperature," *Polymer (Guildf).*, vol. 38, no. 16, pp. 809–815, 1997.

[17] J. Lange, S. Toll, J.-A. E. Månson, and A. Hult, "Residual stress build-up in thermoset films cured below their ultimate glass transition temperature," *Polymer (Guildf).*, vol. 38, no. 4, pp. 809–815, 1997.

[18] D. W. Van Krevelen and K. Nijenhuis, *Properties of Polymers*. 2009.

[19] E. Suhir, Y. C. Lee, and C. P. Wong, *Micro and Opto Electronic Materials and Structures*. .

[20] D. J. Plazek, "Effect of crosslink density on the creep behavior of natural rubber vulcanizates," *J. Polym. Sci. Part A-2*, vol. 4, pp. 745–763, 1966.

[21] D. Adolf and J. E. Martin, "Calculation of Stresses in Crosslinking Polymers," *J. Compos. Mater.*, vol. 30, no. 1, pp. 13–34, 1996.

[22] D. Adolf and R. Chambers, "Verification of the capability for quantitative stress prediction during epoxy cure," *Polymer (Guildf).*, vol. 38, no. 21, pp. 5481–5490, 1997.

[23] D. Adolf and J. E. Martin, "Time-cure superposition during cross-linking," *Macromolelcules*, vol. 23, no. 18, pp. 3700–3704, 1990.

[24] D. B. Adolf, J. E. Martin, R. S. Chambers, S. N. Burchett, and T. R. Guess, "Stresses during thermoset cure," *J. Mater. Res.*, vol. 13, no. 3, pp. 530–550, Jan. 2011.

[25] M. H. H. Meuwissen, H. a. de Boer, H. L. a. H. Steijvers, P. J. G. Schreurs, and M. G. D. Geers, "Residual stresses in microelectronics induced by thermoset packaging materials during cure," *Microelectron. Reliab.*, vol. 44, no. 12, pp. 1985–1994, Dec. 2004.

[26] C. a. Klein, "How accurate are Stoney's equation and recent modifications," *J. Appl. Phys.*, vol. 88, no. 9, p. 5487, 2000.

[27] N. Zobeiry, "Viscoelastic constitutive models for evaluation of residual stresses in thermoset composites during cure," 2006.

[28] A. Johnston, R. Vaziri, and A. Poursartip, "A Plane Strain Modelfor Process-Induced Deformationof Laminated Composite Structures," *J. Compos. Mater.*, vol. 35, no. 16, pp. 1435–1469, 2001.

[29] A. a Johnston, "An Integrated Model of the Development of Process Induced Deformation in Autoclave Processing of Composite Structures," 1997.

[30] N. Zobeiry, R. Vaziri, and A. Poursartip, "Computationally efficient pseudo-viscoelastic models for evaluation of residual stresses in thermoset polymer composites during cure," *Compos. Part A Appl. Sci. Manuf.*, vol. 41, no. 2, pp. 247–256, 2010.

[31] A. Ding, S. Li, J. Sun, J. Wang, and L. Zu, "A comparison of process-induced residual stresses and distortions in composite structures with different constitutive laws," *J. Reinf. Plast. Compos.*, vol. 35, no. 10, pp. 807–823, 2016.

[32] D. J. O'Brien, P. T. Mather, and S. R. White, "Viscoelastic Properties of an Epoxy Resin during Cure," *J. Compos. Mater.*, vol. 35, no. 10, pp. 883–904, 2001.

[33] A. Plepys, M. S. Vratsanos, and R. J. Farris, "Determination of residual stresses using incremental linear elasticity," *Compos. Struct.*, vol. 27, pp. 51–56, 1994.

[34] R. J. Farris and M. S. Vratsanos, "Impulse viscoelasticity: a new method to study polymerization of thermosets," *Int. J. Fract.*, vol. 39, no. 1–3, pp. 93–102, 1989.

[35] K. S. Kim and H. T. Hahn, "Residual stress development during processing of graphite/epoxy composites," *Compos. Sci. Technol.*, vol. 36, no. 2, pp. 121–132, 1989.

[36] S. L. Simon, G. B. Mckenna, and O. Sindt, "Modeling the Evolution of the Dynamic Mechanical Properties of a Commercial Epoxy During Cure after Gelation," *Appl. Polym. Sci.*, vol. 76, pp. 495–508, 2000.

[37] K. M. B. Jansen, *Thermomechanical modelling and characterisation of polymers, "Course book, Delft University of Technology, WB1433."* 2007.

Chapter 6

Viscoelastic Simulation of Residual Stresses Building up in Die Packaging

6.1. Introduction

The residual stresses growing during the encapsulation process affect the mechanical properties of the encapsulated packages. The durability of the product is negatively affected and the reliability becomes a major issue for the manufacturers and consumers. Determination of the source of these stresses which may either have a material origin or be process resulted, is significant. In this chapter the molding process parameters, playing a role in physical, mechanical and thermal properties of the EMC, are addressed and a numerical methodology for stress estimation as a function of these variables is introduced. The residual stresses as a result of change in physical and mechanical properties during die encapsulation are investigated numerically. The material models and the constitutive equations were determined using the applied experimental characterization techniques provided in detail in chapter 2 and chapter 3.

The presented study will show the stress distribution profile within the encapsulated package during the cure and the cooling stages independently. However, the main purpose of the simulation is to estimate the stress distribution on the chip surface which is experimentally measurable and hence verifiable (see chapter 7). The process variables are selected based on the molding experiments as presented in chapter 7. The isothermal cure temperatures of 120, 140 and 160^{o}C with the known cure time, cooling range and conversion degrees are simulated to validate the corresponding experimental stress data

which are determined using the piezoresistive chips in chapter 7. The details of this experiment are described in the following chapter. After the validation studies which are conducted for different cure times and temperatures a simulation representing the ideal die packaging with the cure time letting to 98.5% EMC conversion at 175°C mold temperature is conducted. Note that the stress results which are presented in this chapter will be compared with the experimental stress data in chapter 7.

This chapter is more comprehensive compared to chapter 5 in many ways. In chapter 5 the whole purpose is to simplify the mechanical behavior and geometry to come up with a working analytical model for quick stress determination in transfer packaging process. Therefore, in chapter 5 the whole encapsulated package is simplified to a one-dimensional bilayer geometry with a stress formula effective only in thickness direction. Whereas in this chapter the model comprising the substrate, copper pad, die attach, die and the epoxy is introduced with viscoelastic stress relaxation applied in the cooling stage. An incremental elastic approach is used for the cure stage stress analysis which is the same assumption as imposed in chapter 5. The boundary conditions are assumed as constrained for the cure and unconstrained for the cooling stages.

6.2. Thermal modeling

During molding, the curing epoxy is heated both by the isothermal cure temperature, externally, which is kept constant during the process, and by the heat emitted due to the exothermic reaction taking place, internally. In general, the heat balance of the analyzed system can be given by [1], [2]

$$\frac{\partial}{\partial x_i}\left(k\frac{dT}{dx_i}\right)+\dot{Q}=\rho c_p\frac{dT}{dt}, \tag{6.1}$$

where the first term on the left side is the energy transfer by conduction and the term at the right side states the change in internal energy. k denotes the thermal conductivity, ρ is the density and c_p states the specific heat capacity. The second term on the left side, $\dot{Q}$, refers to the energy generated per unit volume by the exothermic epoxy cure which is already given in equation 2.2 $\left(\frac{d\xi}{dt}=\frac{1}{H_{tot}}\frac{dh}{dt}\right)$ as the rate of enthalpy of the curing reaction.

$$\dot{Q}=\rho H_{tot}\frac{d\xi}{dt}. \tag{6.2}$$

A high thermal conductivity is a preferred feature for an EMC to overcome the heat generated by the chip and other internal electrical components during operation. The thermal conduction as well as other mechanical properties of the epoxy compound is enhanced by the silica content which is used as the filler material in the EMC. Moreover,

the package features like the small size and the thin geometry of the epoxy layer let us to assume the EMC in this study as a perfect conductor. Besides, the curing epoxy and the layers beneath it are constrained by the highly conductive cavity walls. Therefore, it can be expected that the temperature is steady and uniform during the curing stage, $T(t,\xi) = T_c$ and as a result the conversion gradient across the thickness is also neglected for the EMC. Then, the time-temperature-conversion relationship can be constructed easier by the numerical integration of the inverse time function $t(\xi)$ derived from equation 2.5, which yields

$$t(\xi) = \int_{\xi_0}^{\xi} \frac{d\xi}{Aexp(-E_a/RT_c))\,\xi^m(1-\xi)^n}\,. \tag{6.3}$$

Considering the algorithm efficiency, this simplification effectively reduces the computational cost. In case of a negligibly conductive material, on the other hand, the heat balance yields

$$\dot{Q} = \rho c_p \frac{dT}{dt}, \tag{6.4}$$

which leads to

$$T(t) = T_c + \frac{H_{tot}}{c_p}\xi(t), \tag{6.5}$$

and the conversion dependent time is obtained as [3]

$$t(\xi) = \int_{\xi_0}^{\xi} \frac{d\xi}{Aexp(-E_a/RT(t))\,\xi^m(1-\xi)^n}\,. \tag{6.6}$$

Equation 6.3 and 6.6 can be solved by applying a numerical trapezoidal integration. Note that in this numerical study the epoxy is assumed as a perfect thermal conductor and the temperature fluctuations are ignored. As it is assumed for the isothermal cure stage the differences in thermal gradients during cooling are neglected as well. Therefore, monotonically decreasing temperature with homogenous distribution is assumed for the cooling stage.

6.3. Mechanical modeling during cure and cooling

The mechanical constitutive modeling of the curing polymer involves complex interrelations of time, temperature and conversion variables [4]. The stress generation during encapsulation process is affected mainly by the strain due to cure and thermal shrinkage, and by the increase in modulus accompanying both isothermal polymerization and transient cooling.

6.3.1. Elasticity of the EMC in the cure stage

Figure 6.1 shows a typical elastic modulus of a fully cured EMC, which was obtained in DMA using the tensile test set-up at a high constant frequency and under infinitesimal strain. In this measurement a strip of fully cured EMC sample was heated with a constant rate starting from room temperature to 230°C, covering the entire transition region. Using this method, one can easily determine the maximum tensile modulus data for the tested temperature range. As it can be observed clearly in figure 6.1 the modulus is in equilibrium rubbery state at temperatures above 140°C. At the equilibrium state, the deformation times as well as the temperature variations do not have strong influence on the modulus level. Therefore, for the isothermal cure stage of the molding for which the cure temperature is usually set above the viscoelastic transition region, it can be assumed that the epoxy behaves elastically and the viscoelastic behavior can be ignored. For that reason, during polymerization the elastic constitutive model provides a satisfactory description of the mechanical behavior and therefore, the viscoelastic variations can be neglected as far as the temperature remains constant at the predefined mold temperature. Note that, this assumption can only be valid for the isothermal cure stage and not applicable in cooling study where the temperature of the epoxy drops to room temperature gradually.

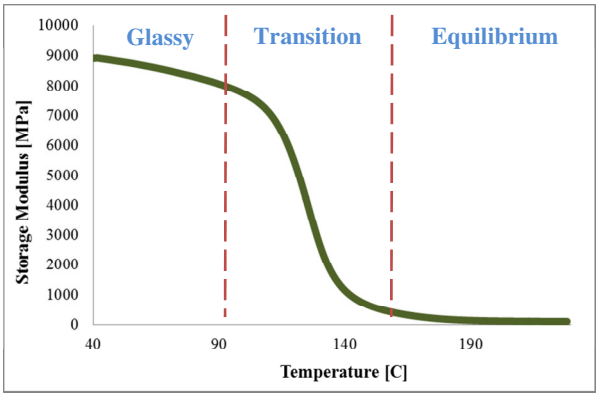

Fig 6.1 Storage modulus in a heat ramp scan of a fully cured EMC at a high frequency and low strain

6.3.2. Conversion dependent equilibrium modulus

The effect of crosslink polymerization on the rubbery modulus of the epoxy can be seen in figure 6.2. An uncured sample of the EMC is cured isothermally and the rubbery shear modulus is monitored in DMA. The isothermal temperature is set above the transition temperature to determine the rise in equilibrium modulus. An oscillatory displacement at a constant frequency is applied using the shear sandwich test setup. The high glassy modulus

of the epoxy instantly drops close to zero at the start of the measurement when the sample melts. The lower modulus is associated with the viscous fluid behavior of the epoxy melt before gelation. The modulus starts rising upon passing the gel point. Close to complete conversion, the modulus levels off. This is the time when the cure shrinkage is almost completed and the glass transition is close to its maximum value. Furthermore, the viscosity and the equilibrium stiffness of the sample are at the highest attainable levels for the determined cure temperature. The rubbery shear modulus is obtained as 250MPa at the end of conversion. Based on the experimental observations of figures 6.1 and 6.2 the mechanical behavior of the epoxy resin during the cure stage is considered as elastic and conversion dependent. Note that the onset of gelation as seen in figure 6.2 agrees well with the observations in section 3.6 that the conversion at gelation ranges between 0.42 and 0.50.

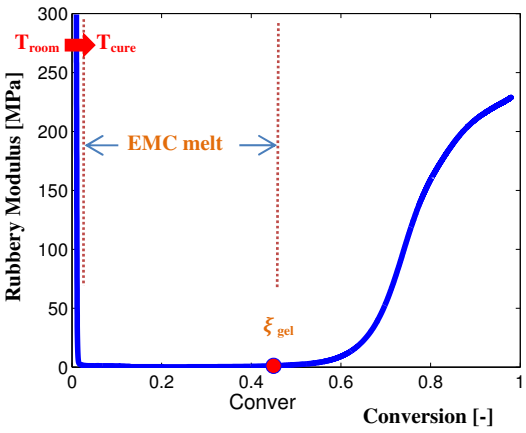

Fig 6.2 Rubbery shear modulus with respect to degree of conversion during isothermal curing of an initially uncured resin

6.3.3. Viscoelastic constitutive modeling in cooling

The total residual stress during packaging can be considered as the sum of stresses building up during cure and cooling stages of the molding. Hence, the cure induced and thermal induced stresses are simulated independently because of the different mechanical behavior of the thermosetting epoxy compound at each stage. Moreover, it helps cutting down the computational load by applying the time dependency only in the cooling stage and assuming an elastic response for the cure induced deformation. Therefore, the cure stage is modeled elastically with a conversion dependent equilibrium modulus which is estimated by equation 5.6 [5], [6]. During cooling, on the other hand, the viscoelastic behavior is taken into account. It is assumed that the stress is isotropic and can be expressed as the sum of shear and compressive parts as [7]

$$\sigma_{ij}(t) = 2\int_{-\infty}^{t} G(t-t')\dot{\varepsilon}_{ij}\, dt' + \int_{-\infty}^{t}\left[K(t-t') - \frac{2}{3}G(t-t')\right] trace(\dot{\varepsilon}_{tot})\delta_{ij}\, dt', \quad (6.7)$$

where $G(t)$ is the shear relaxation modulus and $K(t)$ is the Bulk modulus. The trace of total strain rate, $\dot{\varepsilon}_{tot}$, is

$$trace(\dot{\varepsilon}_{tot}) = \sum_{k=1}^{3} \dot{\varepsilon}_{tot_{kk}}, \quad (6.8)$$

and the δ_{ij} is the Kronecker delta defined as

$$\delta_{ij} = \begin{cases} 0 & if\ i \neq j \\ 1 & if\ i = j \end{cases}$$

The hydrostatic pressure is given by

$$P = K\, trace(\varepsilon_{tot}). \quad (6.9)$$

Using the definition given in equation 6.9, equation 6.7 can be rewritten as

$$\sigma_{ij}(t) = 2\int_{-\infty}^{t} G(t-t')\dot{\varepsilon}_{ij}\, dt' - P(t)\delta_{ij}\frac{2}{3}\int_{-\infty}^{t} G(t-t')trace(\dot{\varepsilon}_{tot})\delta_{ij}\, dt'. \quad (6.10)$$

The bulk modulus is much higher than the shear modulus in viscoelastic fluids. Hence, it can be assumed that the viscous part of the deformation is incompressible and the volume change is elastic. Therefore, the second term of equation 6.10 can be simplified and thereby the equation becomes

$$\sigma_{ij}(t) = 2\int_{-\infty}^{t} G(t-t')\dot{\varepsilon}_{ij}\, dt' - P(t)\delta_{ij}. \quad (6.11)$$

where ε in equation 6.11 stands for the deviatoric part of the deformation tensor which is given by

$$\varepsilon = \varepsilon_{tot} - \frac{1}{3}trace(\varepsilon_{tot}). \quad (6.12)$$

The total strain is defined as the sum of mechanical and contraction parts.

$$\varepsilon_{tot} = \varepsilon_{mec} + \varepsilon_{th} + \varepsilon_{ch}, \quad (6.13)$$

where ε_{mec} is the Cauchy strain tensor and ε_{th} and ε_{ch} stand for the thermal and intrinsic chemical shrinkage strains, respectively.

6.4. Epoxy shrinkage modeling

6.4.1. Cure strain

The cure induced stress starts to evolve above the gel point due to the effective chemical shrinkage which can be represented analytically as a function of conversion by [8]

$$\varepsilon_{ch} = \sqrt[3]{1 + \xi . \varepsilon_{ch}^{\infty}} - 1 \tag{6.14}$$

where $\varepsilon_{ch}^{\infty}$ denotes the total cure shrinkage. Considering the thin epoxy thickness compared to the other dimensions, the cure shrinkage can be assumed to be uniform and homogeneous through the thickness. Then, the simpler linear cure shrinkage model given in equation 5.27 can be applied. No considerable difference between the strain estimation by these methods was detected.

6.4.2. Thermal strain

The stress during cooling is modeled using the time and temperature dependent viscoelastic model such that the strain at each time step is evaluated based on the temperature dependent coefficient of thermal expansion. It is assumed that during cooling the temperature drops monotonically to room temperature. Therefore, the temperature dependent cooling strain is given by

$$\varepsilon_{th} = \frac{1}{3}\int_{T_{iso}}^{T_{room}} \alpha(T)\, dT, \tag{6.15}$$

where $\alpha(T)$ is the temperature dependent thermal expansion coefficient which is modeled in chapter 2 by equation 2.21.

6.5. Modeling approach and process conditions

6.5.1. Constitutive model implementation

A two dimensional model for numerical simulation of the package is developed based on the dimensions of the components used in the molding experiment. Comsol Multiphysics software package was adopted for mesh generation and numerical simulations.

The dynamic storage and loss moduli as a function of radial frequency, ω, can be represented in terms of rubbery, G_r, and glassy, G_g, moduli by the Maxwell model [9];

$$G'(\omega) = G_r + \left[G_g - G_r\right] \sum_{k=1}^{N} g_k \frac{\omega^2 \lambda_k^2}{1+\omega^2 \lambda_k^2}. \tag{6.16}$$

$$G''(\omega) = \left[G_g - G_r\right] \sum_{k=1}^{N} g_k \frac{\omega\, \lambda_k}{1+\omega^2 \lambda_k^2}. \tag{6.17}$$

And the relaxation modulus as a function of time $G(t)$, defined using the Generalized Maxwell model by [9]

$$G(t) = G_0 \left[\mu_\infty + \sum_{k=1}^{N} \mu_k \exp(^{-t}/_{\lambda_k})\right], \tag{6.18}$$

where G_0 is the instantaneous absolute stiffness, λ is the relaxation time and μ_∞ is the relative stiffness defined by $\mu_\infty = G_\infty^f / G_0$, and for each branch of the Generalized Maxwell model it is given by $\mu_k = G_k / G_0$. The relative stiffness and the branch stiffness is related by

$$\mu_\infty + \sum_{k=1}^{N} \mu_k = 1. \tag{6.19}$$

$G_k \; and \; \mu_k$ denote the absolute and the relative stiffness parameters, respectively, for the branch k of the spring in the Generalized Maxwell model and G_∞^f is the equilibrium modulus of the fully cured epoxy.

Inserting the relaxation modulus defined by equation 6.18 to the deviatoric part of 6.11 yields

$$\sigma_{dev} = 2G_0 \varepsilon \left[\mu_\infty + \sum_{k=1}^{N} \mu_k \exp(^{-t}/_{\lambda_k})\right], \tag{6.20}$$

For the numerical simplicity, equation 6.20 can be rewritten by defining a new variable q_k, representing the extension of the spring in branch k of the generalized Maxwell model:

$$\sigma_{dev} = 2G_0 [\varepsilon \mu_\infty + \sum_{k=1}^{N} \mu_k \, q_k]. \tag{6.21}$$

q_k can be solved using the following differential equation [10]:

$$\dot{q}_k + \frac{1}{\lambda_k} q_k = \dot{\varepsilon}. \tag{6.22}$$

The temperature dependent shift factor is determined using the combined WLF-polynomial model given in section 3.7.3. For the temperature values above the glass transition, shift function modeled by the Williams-Landen-Ferry (WLF) [11] and for the temperatures below the glass transition a polynomial of a third degree is used. The shift function fit is shown in figure 3.20 and the model parameters are given in table 3.3. Besides, the Generalized Maxwell model parameters (Prony terms) are provided in table 3.2.

The solution of equation 6.22 is carried out in Comsol Multiphysics by the implicit backward difference discretization. The explanation of the solution procedure is not the scope of this thesis. For further information the reader may study the documentation of the software [12], [13].

6.5.2. Model and meshing

The in-plane cure and thermal stresses are analyzed in a two dimensional multi-layered model which is based on the molded package dimensions of the experiment which is studied in detail in chapter 7. The schematic of the model is given in figure 6.3a which consists of five layers. In the real-time molding test which is used as a verification study, the stress measuring sensors are embedded on the surface of the chip. For that reason the main purpose of the numerical study is to compare the stresses on the die surface (epoxy interface) with the ones obtained by the molding test experiment.

The 2D model is meshed by the unstructured triangular grid. High mesh density is used with a higher resolution for thin regions of the domain. Note that the model is longer sideways (see figure 6.10).

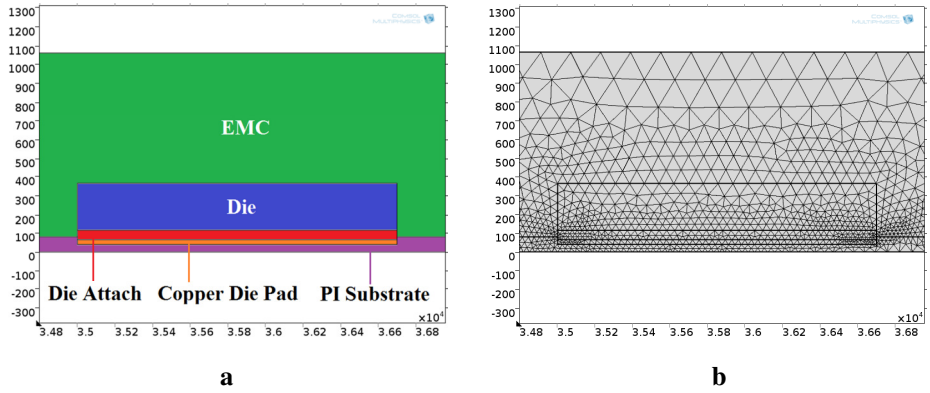

Fig 6.3 a) Schematic of the numerical model representing the transfer molding measurement, b) Unstructured triangular mesh model for the entire domain

6.5.3. Boundary Conditions

During the epoxy cure the cavity is constrained due to the clamped mold. The cavity top platen is released after the cure end and hence, the package surface boundaries are assumed free to warp. Starting from the cure-end, a bottom corner node of the PI flex-board is assumed to be constrained and the other corner at the symmetric end is numerically limited to move only in horizontal direction. The proposed boundary condition will give a bending of the board in a realistic manner. The proposed boundary condition also provides numerical stability and the model symmetry. Otherwise, the chip will be shifted inside the epoxy as the shrinkage proceeds and the direction of the shift will be depending on the assumed fixed boundary point of the EMC. For instance, if the mold boundaries are set constrained on one corner starting from the cure-end and the other corner node assumed

free, then the chip and the other layers will be moving towards the constrained edge and the symmetry will be lost. Therefore, full surface constraint for the curing and the two point constraint at two edges of the board are applied for the cooling simulations.

6.5.4. Material parameters

The mechanical properties of the components are assumed elastic except the EMC which is assumed elastic for the cure stage but viscoelastic for the cooling stage. Therefore, all the other components are modeled in an elastic manner for the entire molding. The thermal and mechanical properties of the package components are given in table 6.1.

Among the package layers the die attach and polyimide board are polymeric compounds. The properties of the die attach is comparable to the EMC. The adhesive has a lower stiffness and a larger difference between its glassy and rubbery CTE values compared to the epoxy compound. Therefore, a linear model is used for numerical representation of the die attach's CTE at the transition region.

Table 6.1 Thermo-mechanical properties of the package layers

	E [GPa]	**ρ [Kg/m^3]**	**ν [-]**	**α [10^{-6}/K]**
Chip	150	2330	0.17	2.6
PI Substrate	2.1-3.1*	1300	0.35	18**
Cu Pad	110	8700	0.35	17
Die Attach	5.3	1800	0.35	47-115*
EMC(cured)	0.1-9***	1760	0.35-0.45	27-75

***A linear transition model is used.**

****The PI substrate α is 1.8 10^{-6}/K within 35-323^{o}C temperature range** [14], [15]**.**

*****the values presented here are the tensile and the rubbery values obtained by DMA at a fixed frequency. The viscoelastic relaxation modulus as given in section 6.5.1 is used in simulations.**

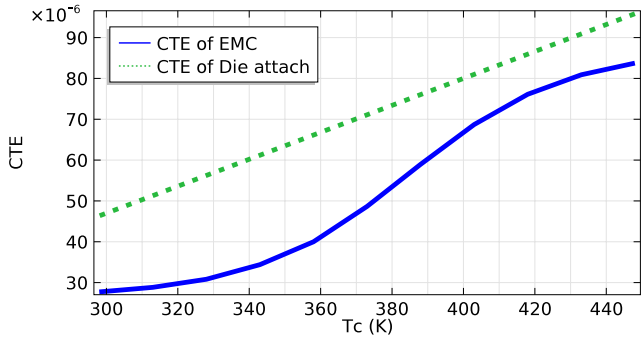

Fig 6.4 Incremental variation of coefficient of thermal expansion of the die attach (green dotted line) and epoxy (blue solid line) based on the temperature dependent linear (die attach) and Tait (EMC) models for the exposed temperature range in cooling stage as a function of temperature

6.6. Simulation results

Four simulations at 120, 140, 160 and 175°C were conducted. The purpose of the first three simulations is to validate the proposed method by comparing the stress results with the experimental data, which are studied in chapter 7. Therefore, the conversion and the cooling times are defined based on the experimentally pre-determined ones. The following table summarizes the process parameters and the numerically estimated stress results in each simulation, accordingly.

Table 6.2 Simulation parameters and the simulated maximum in-plane normal stresses

	Simulation #	[-]	1	2	3	4
	Cure temperature	[C]	120	140	160	175
	Cure time	[s]	2800	1100	400	350
	Expected cure-end Conversion	[%]	83.5	88.5	91	98.5
Max. Compressive planar stress	**Cure**	[MPa]	0.65	0.73	1.25	1.8
	Cooling	[MPa]	14	16	21	29

The simulations indicated by numbers from 1 to 4 in table 6.2 refer to the process and material conditions of the corresponding experiments. Each simulation is investigated in detail in the following sections. The final stresses are compressive as it is confirmed by the negative sign in the figures showing the stress profiles. However, note that the negative sign is dropped in the results given in table 6.2.

6.6.1. Simulation no. 2

The in-plane normal stress at the cure-end is shown on the 2D model in figure 6.6. The stress in the epoxy layer is tensile due to the cure shrinkage in a constrained cavity. As a result, a compressive stress is induced in the die and in PI board beneath the epoxy layer. The higher stress values compared to the epoxy can be attributed to the higher rubbery modulus of both compounds. The substrate develops a tensile stress at the region below the copper pad as opposed to the compressive stress imposed on the copper layer. The tensile stress in this region is almost the same as the tensile stress of the die attach beneath the chip. The chip surface stress profile is in a range of 0 to 0.73MPa which matches the data detected by the stress chip in figure 7.9.

The cooling stage stress distribution for the whole package is given in figure 6.7. After the cure-end the package is free to warp. Hence after cooling down to room temperature the cured epoxy layer shrinks and bends. A low compressive stress of 0.7MPa is imposed in the thin PI layer due to the bending. Hence, the largest interface which is in between the epoxy and the PI is in a low stress state on both sides. The tensile stresses of 30 and 25MPa are calculated for the copper pad and the die attach, respectively. The in-plane normal stress on the chip surface is determined as compressive which is between 3 to 16MPa.

Note that in both stages the maximum values are obtained at the chip edges. These maximum stresses compare well with the values obtained by the incremental elastic method in chapter 5, which is 1MPa at the end of cure stage and 18MPa at the end of cooling. Figure 5.8 is the corresponding stress graph in chapter 5.

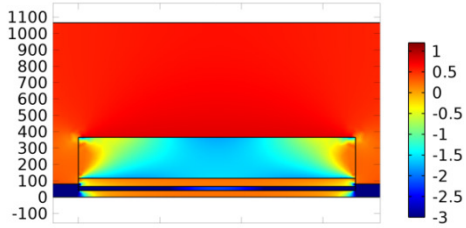

Fig 6.6 Cure induced planar stress profile after 88.5% EMC conversion

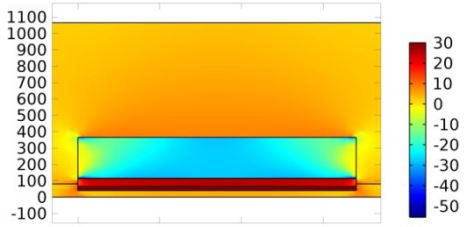

Fig 6.7 Cooling induced planar stress after cooling from 140^{o}C to room temperature

Figures 6.6 and 6.7 provide a general understanding of the normal in-plane stress distribution in the package for both stages, but it is still difficult to be able to visualize the chip surface stress distribution quantitatively, from these figures. Therefore, the progress of stress build-up on the surface of the chip is shown in figures 6.8 and 6.9 for the cure and cool stages, respectively. The stress build-up after the gel point is shown in time intervals of

100 seconds in figure 6.8. 400 seconds is the time just after the gel point at which the epoxy mechanical properties starts to develop. For the progress of the degree of conversion with respect to the cure time of the studied process one may refer to figure 5.7. 1100 second is the end of the cure stage based on the corresponding molding experiment. The cooling stage is given in 20 seconds time intervals in figure 6.9 since the cooling time is considerably shorter compared to the cure time.

The planar stress profile is symmetric, as expected. Two compressive stress peaks are obtained on the chip surface, one at the corner and the other at the chip center. At the end of both stages the maximum compressive stresses are obtained at the chip surface corners. The maximum cure-end stress is 0.73. This is the cure shrinkage induced stress corresponding to 88.5% degree of cure. The maximum thermal shrinkage induced stress, on the other hand, is calculated as 16MPa. The stress pattern observed in the cure stage is repeated in the cooling stage as well. The maximum value is determined at the chip top surface edge which drops to 4MPa by moving slightly towards the center and then rises again at the center to around 10MPa at the end of cooling stage. Compared to the cure stage no tensile stress is observed on the surface of the chip.

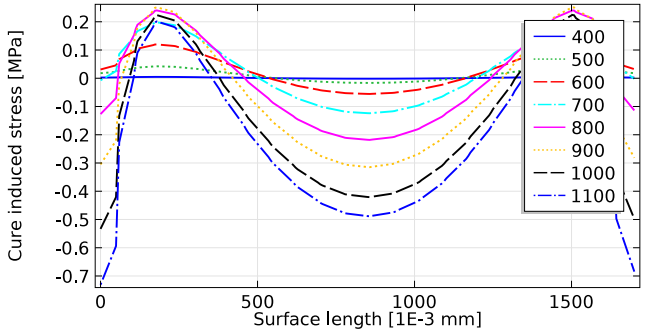

Fig 6.8 Simulation no. 2, cure induced in-plane normal stress on the chip surface (The legend refers to the cure time in seconds)

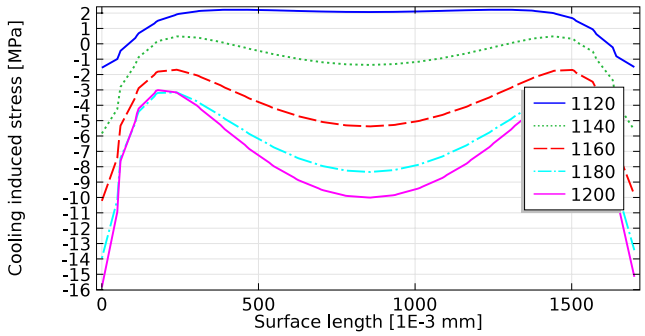

Fig 6.9 Simulation no. 2, cooling induced in-plane normal stress on the chip surface (The legend refers to the cooling time in seconds)

The shrinkage of the epoxy during cure forces the PI board to bend inward (concave up). This behavior was observed by the experiments as well. The total bending of the board at the center is calculated as 3.5mm. The total deformation at the end of cooling is shown in figure 6.10.

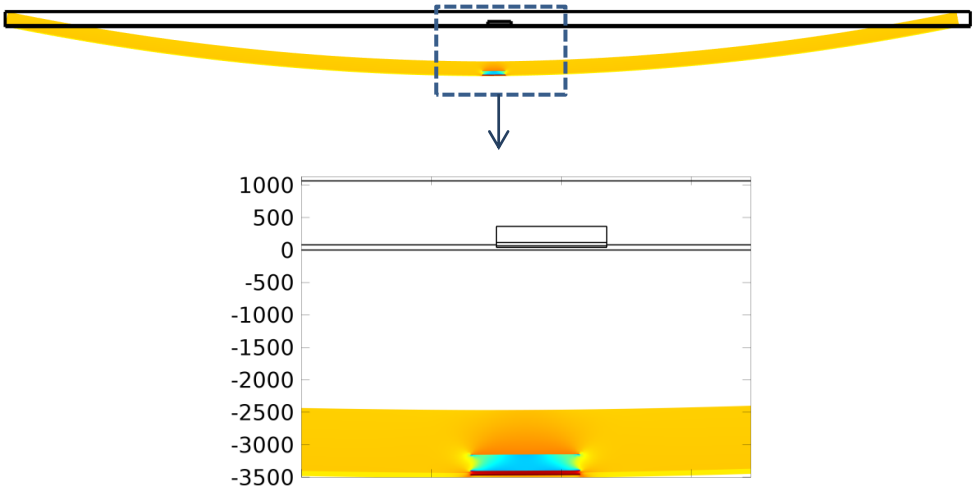

Fig 6.10 Deflection of 3.5mm after the EMC cure at 140°C and cooling down to room temperature determined by the simulation (The color scale related to residual stresses in figure 6.7)

6.6.2. Simulation no. 1

The EMC conversion is expected to be 83.5% at the end of 2800s at mold temperature of 120°C. The stress profiles in the package are given in figure 6.11 for the cure-end and in figure 6.12 for the cooling-end.

The stress distribution on the chip surface represented in time intervals for each stage can be observed in figures 6.13 and 6.14. The time intervals are 400s for the cure and 10s for the cooling stages. The stress evolution starts after the gel point which is reached after 1200 seconds at the pre-determined test conditions. At the end of cure 83.5% degree of conversion leads to a maximum cure induced compressive in-plane normal stress of 0.65MPa at the chip surface edges and 0.45MPa at the center of it. After cooling from 120°C to room temperature the compressive stress at the surface becomes 14MPa at the edge and 11.5MPa at the center. The maximum stress values compare well with the analytically determined results of chapter 5.

The maximum stress values are less than the previous study (simulation no.1) because of the 5% lower conversion degree at the end of cure stage and the lower thermal gradient when cooled down from the mold temperature to room temperature.

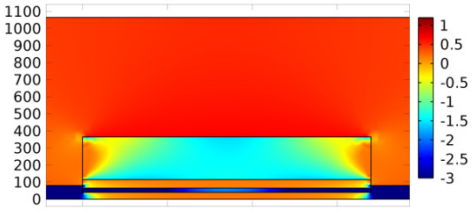

Fig 6.11 Cure induced planar stress profile after 83.5% EMC conversion

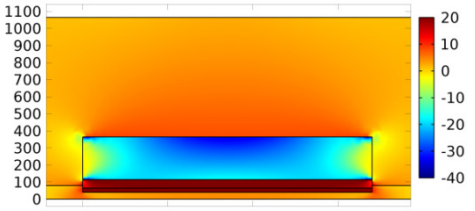

Fig 6.12 Cooling induced planar stress after cooling from 120°C to room temperature

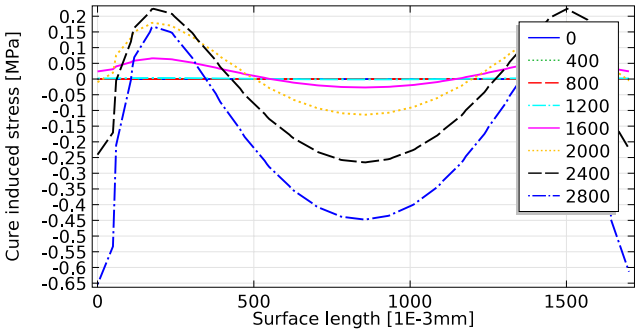

Fig 6.13 Simulation no. 1, cure induced in-plane normal stress on the chip surface

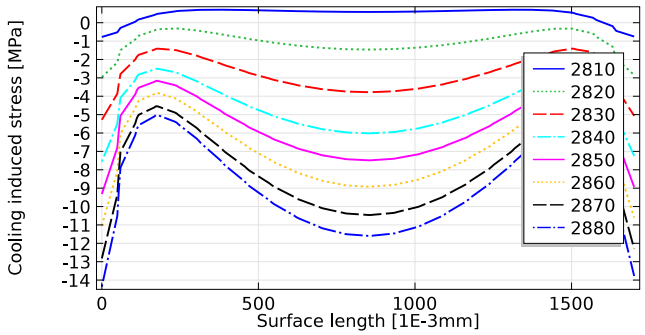

Fig 6.14 Simulation no. 1, cooling induced in-plane normal stress on the chip surface

6.6.3. Simulation no. 3

The validation test number 3 is the closest condition to an industry standard chip encapsulation process. In this simulation it is assumed that the epoxy cures at isothermal temperature of 160^{o}C for 400s with an initial conversion degree of 6%. The stress profiles for the cure and cooling stages are given in figures 6.15 and 6.16 and the chip top surface stress distributions are shown in figures 6.17 and 6.18, respectively. The maximum compressive cure-end normal stress becomes 1.25MPa after 91% conversion and like the previous studies it is obtained at the chip top corners. This value agrees well with the 1.25MPa cure-end stress of the bilayer model. At the chip center the stress is 0.65MPa and between the two maxima it reduces to an almost stress-free state with a 0.02MPa tensile stress. As can be observed in figure 6.18 the maximum cooling induced stress is 21MPa at the end of cooling which is slightly lower than the stress obtained using the analytical approach in chapter 5.

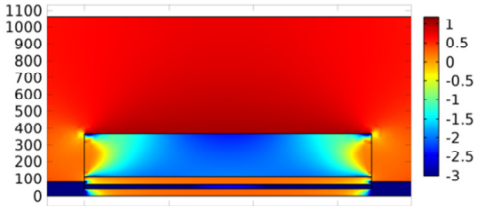

Fig 6.15 Cure induced planar stress profile after 91% EMC conversion

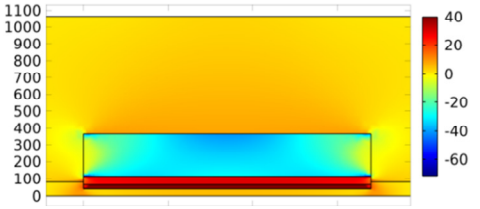

Fig 6.16 Cooling induced planar stress after cooling from 160^{o}C to room temperature

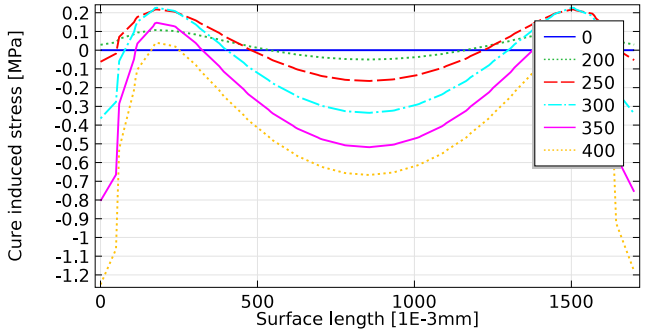

Fig 6.17 Simulation no. 3 cure induced in-plane normal stress on the chip surface

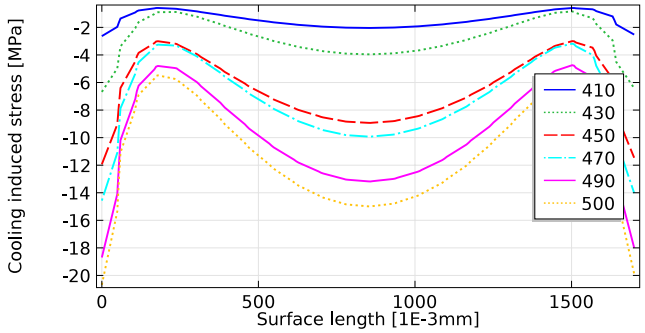

Fig 6.18 Simulation no. 3, cooling induced in-plane normal stress on the chip surface

6.6.4. Simulation no. 4

The simulation number 4 is conducted to estimate the residual stresses if the standard process conditions are applied. The cure temperature is set to 175°C and the cure time is defined such that the total epoxy conversion reaches above 98%. Therefore, the cure time is defined as 350s and the resulted degree of conversion based on the kinetic model (equation 2.5) becomes 98.5% with an initial conversion of 20%. Note that, this study could not be verified using the experimental technique proposed in chapter 7. The capability of the model to replicate the experimental results with a high accuracy under various process parameters is verified by the test cases which are the first three studies.

The maximum in-plane normal stresses are determined at the edges of the chip, as expected. These values are 1.8 and 29MPa respectively for the cure-end and cooling-end stages.

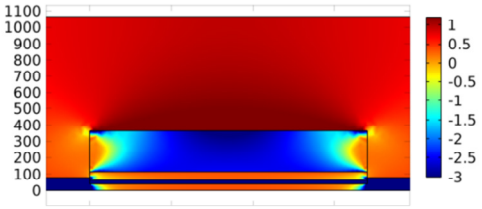

Fig 6.19 Cure induced planar stress profile after 98.5% EMC conversion

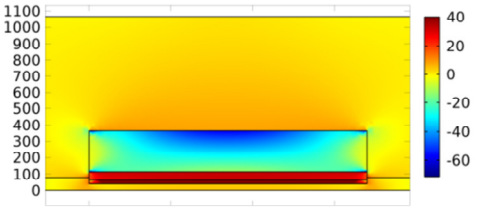

Fig 6.20 Cooling induced planar stress after cooling from 175°C to room temperature

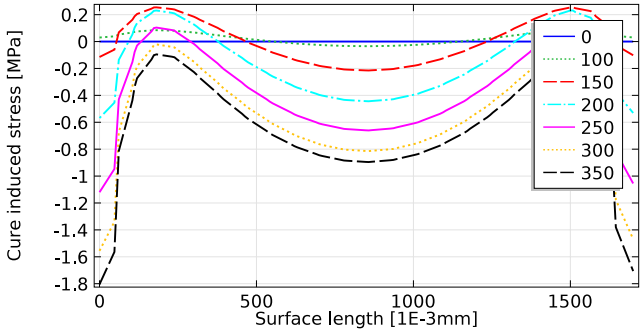

Fig 6.21 Simulation no. 4, cure induced in-plane normal stress on the chip surface

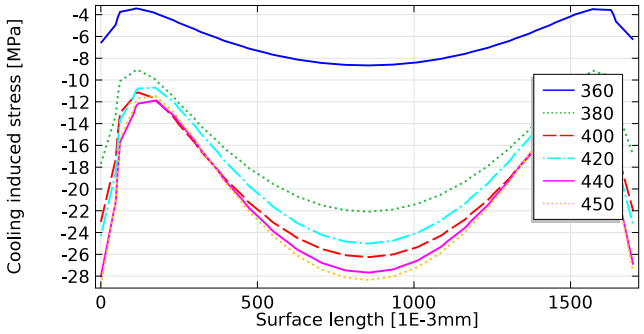

Fig 6.22 Simulation no. 4, cooling induced in-plane normal stress on the chip surface

6.7. Conclusion

The in-plane residual stresses on the surface of the chip during die encapsulation are analyzed numerically using Comsol Multiphysics. A two-step constitutive model is developed which is based on the thermo-mechanical state of the EMC in the cure and the

cooling stages of the molding. Material properties are implemented from the kinetic, dynamic and volumetric models derived using characterization tests that are explained in detail previously in chapters 2 and 3. The process parameters like the cure temperature, the cure time, the initial epoxy conversion and the model parameters like the cavity dimensions and the thicknesses of the package layers are designed based on the corresponding experiments given in chapter 7.

The stress after cure and cooling stages are calculated independently. The three essential differences between the two stages are: the free boundary condition set in cooling stage compared to the constrained exterior boundaries during cure, the shrinkage of the package components as opposed to the cure shrinkage of the epoxy in cure, and the constitutive equations that included a viscoelastic behavior of the epoxy layer in the cooling stage.

The highest stresses on the chip surfaces in all of the simulations are compressive. At the end of both stages, the cure and the cooling induced stresses are highest at the chip corners and range from 0.65MPa at 83.5% degree of conversion to 1.8MPa at 98.5%. This is not due to cure temperature but is a result of the final conversion degree of the epoxy. The stress profile at the end of cure stage is compressive at the entire chip surface in 160 and 175^{o}C cure simulations, but in 120 and 140^{o}C cases it is tensile at a small portion of the chip surface close to the corners. These tensile peaks are less than 0.2MPa.

The calculated stresses at the end of cooling stages are much larger than the cure induced stresses. Even at 98.5% epoxy conversion where it leads to a maximum stress of 1.8MPa, the cooling induced stress is larger by a factor of 16. The cure induced stress can be comparable and significant only if the cure temperature is reduced and the cure time is increased. Hence the thermal shrinkage is lowered and the conversion gets close to 100%. However, this does not match the industry standards and not feasible.

The cure and cooling induced stresses calculated in this chapter can also be compared with the values obtained based on the analytical model presented in chapter 5. Considering the complexity of the material behavior and the interdependency of the processing parameters, it can be clearly concluded that the model proposed in chapter 5 provided a fair prediction of residual stresses.

References

[1] J. P. Holman, *Heat Transfer*. 2002.

[2] Y. C. Fung, *A first course in continuum mechanics*. 1994.

[3] C. Heinrich, M. Aldridge, A. S. Wineman, J. Kieffer, A. M. Waas, and K. W. Shahwan, “Generation of heat and stress during the cure of polymers used in fiber composites,” *Int. J. Eng. Sci.*, vol. 53, pp. 85–111, 2012.

[4] J. D. Menczel and R. B. Prime, *Thermal Analysis of Polymers, Fundamentals and Applications*. .

[5] D. Adolf and J. E. Martin, "Calculation of Stresses in Crosslinking Polymers," *J. Compos. Mater.*, vol. 30, no. 1, pp. 13–34, 1996.

[6] D. Adolf and R. Chambers, "Verification of the capability for quantitative stress prediction during epoxy cure," *Polymer (Guildf).*, vol. 38, no. 21, pp. 5481–5490, 1997.

[7] S. Timoshenko and J. N. Goodier, *Theory of Elasticity*. 1951.

[8] T. A. Bogetti and J. W. Gillespie, "Process-Induced stress and deformation in thick section thermoset composite laminates," *U.S. Army Ballist. Res. Lab*, 1990.

[9] J. D. Ferry, *Viscoelastic Properties of Polymers*. 1961.

[10] W. Macosko , Christopher, *Rheology Principles, Measurements, and Applications*. 1993.

[11] M. L. Williams, R. F. Landel, and J. D. Ferry, "The Temperature Dependence of Relaxation Mechanisms in Amorphous Polymers and Other Glass-forming Liquids.," *J. Am. Chem. Soc.*, vol. 77, no. 12, pp. 3701–3707, 1955.

[12] "Comsol Documentation - The MEMS Module User's Guide." 2013.

[13] *Comsol Multiphysics Reference Guide*. 2012.

[14] DuPont ™, "Technical Data Sheet, Kapton ® Polyimide film," 2011.

[15] DuPont, "Kapton properties," 2014.

Chapter 7

Experimental Analysis of Residual Stresses Building up in Die Encapsulation

7.1. Introduction

There are many factors affecting the lifespan of microelectronics. However, all electronic devices, regardless of their reliability, will fail at some stage, some sooner than others. The working conditions like the temperature and humidity and the cyclic thermo-mechanical loading are the main factors affecting the lifetime of the electronic components during their operation. On the other hand, the residual stress built-up during the encapsulation of microelectronics is an equally significant factor that contributes to the decline in lifetime of the products in which the encapsulated packages are installed. The cyclic thermo-mechanical stresses may not be reduced, but the fabrication induced stresses can be decreased. A lower residual stress may be achieved by changing the molding parameters like the process temperature, the filling time or the cavity design like the number of inlets, the gate dimensions and positions, or the runner length. Apart from the process and design parameters, the composition of the EMC can also be optimized to achieve a lower residual stress. Basically, if the total shrinkage of the molding compound after encapsulation becomes equal to the total shrinkage of the substrate then the encapsulated package will not experience any stress and as a result it will not warp. To achieve the optimum condition of zero residual stress there should not be any shrinkage associated with the EMC cure. Besides, the thermal shrinkage of the epoxy should be the same as the one of the substrate and the glass transition must be just above the cure temperature [1]. This ideal condition

may not be achievable but the process can be optimized to lower the degree of the residual stresses.

The outdated trial and error methods for prediction of these stresses have been replaced by the numerical simulation methods over the time. Moreover, the commercially available software packages which are easy to implement to particular needs and dedicated specifically to the molding process, encourages the industry for investment on virtual modeling and simulation tools. A well-designed numerical simulation performed prior to mass production provides a convenient way in estimation of production resulted stresses. However, the computational study should not be the only tool used in a reliability study of the packaging process. Accuracy of the numerically predicted stress values should also be validated by consistent experimental results.

The novel experimental technique proposed in this paper is capable to record the residual stress generated on the chip surface during the encapsulation process. The continuous real time stress measurement can be adapted to any package and parametrical optimization measurements can be conducted by testing various process conditions.

In this chapter the stress during and after die encapsulation is investigated using the stress measuring chips. The working principle of the chip is based on piezoresistivity effect. The resistivity of silicon changes with the applied stress. This property of the silicon is called the piezoresistivity effect and have been used in various sensors [2]–[8]. In this study, the new generation of stress measuring chip is used for experimental real time analysis of residual packaging stresses during cure. The stress chips have been implemented in several studies successfully [9]–[11]. In these studies the chips were first attached to a board and encapsulated and the external electrical connections were established afterwards. The chips were used to monitor the stress changes during subsequent thermal and mechanical tests. But the stress generated during the encapsulation process could not be recorded. The application of the proposed measurement technique in this study to monitor the stresses during the molding process is new and was developed by the author [12]–[14].

7.2. Piezoresistivity effect

The resistivity change of doped silicon by stress application was discovered by Bell laboratories in 1954 and this property of silicon had been implemented to the sensors which are considered among the first microelectromechanical system (MEMS) manufactured for various sensing purposes.

The majority of sensors are based on metal gauges. However, the piezoresistive sensors have wider application areas and some advantages over the metal strain gauges which make

them suitable for this study. The resistance change in metal sensors is mainly based on deformation, while in silicon it is a function of both deformation and strain dependent resistivity change. The resistivity change is more dominant than the deformation effect, which gives a higher sensitivity to the silicon sensor compared to the metal sensors. The resistivity change of semiconductors, under stress, is several orders of magnitude larger than the resistivity change due to deformation. With no piezoresistivity effect the bulk resistivity is assumed to be constant during the applied stress. Thus, the term piezoresistivity is used for silicon sensors and not metals. The other important feature of the piezoresistive sensors is that they are fabricated into dies by microelectronic fabrication technologies and as a result they offer nonintrusive detection of stresses.

7.2.1. Theory of Piezoresistivity

The working principle of the stress measuring chip is based on the change in electrical resistivity of silicon under the subjected mechanical strain. This resistivity is affected not only by the stress direction with respect to the transistor orientation but also by the doping type and doping concentration [4]. The resistance is described by

$$R = \varrho \frac{l}{a}, \tag{7.1}$$

where l and a are the length and the cross sectional area of the semiconductor and ϱ refers to the bulk resistivity defining the intrinsic electrical resistance property of the material. The piezoresistivity of a semiconductor is related to stress, σ, through the piezoresistivity coefficient, Π by

$$\Pi = \frac{\Delta R/R}{\sigma}. \tag{7.2}$$

The numerator in equation 7.2 can be expressed in terms of relative changes in dimensions and resistivity, which yields

$$\frac{\Delta R}{R} = \frac{\Delta l}{l} + \frac{\Delta w}{w} + \frac{\Delta h}{h} + \frac{\Delta \varrho}{\varrho}. \tag{7.3}$$

w and h refer to the width and height of the piezoresistive material. The first three terms represent the change in resistivity ratio due to the deformation, while the last term expresses the piezoresistivity effect.

Both stress and resistivity are second order tensors. Hence, they are interrelated by a fourth order tensor, Π_{ijkl}.

$$\Delta \varrho_{ij}/\varrho = \sum_{kl} \Pi_{ijkl} \sigma_{kl}. \tag{7.4}$$

Using the symmetry feature of the stress and resistivity tensors, the piezoresistivity coefficient can be described as a second order tensor. Then, equation 7.4 can be rewritten as

$$\Delta\varrho_i/\varrho = \sum_j \Pi_{ij}\sigma_j. \tag{7.5}$$

where Π_{ij} has only three independent elements in case of a crystal cubic symmetry structure such as silicon. So, Π_{ij} is expressed in a matrix of 6x6 by

$$\Pi_{ij} = \begin{bmatrix} \Pi_{11} & \Pi_{12} & \Pi_{12} & 0 & 0 & 0 \\ \Pi_{12} & \Pi_{11} & \Pi_{12} & 0 & 0 & 0 \\ \Pi_{12} & \Pi_{12} & \Pi_{11} & 0 & 0 & 0 \\ 0 & 0 & 0 & \Pi_{44} & 0 & 0 \\ 0 & 0 & 0 & 0 & \Pi_{44} & 0 \\ 0 & 0 & 0 & 0 & 0 & \Pi_{44} \end{bmatrix}. \tag{7.6}$$

Π_{11} and Π_{12} refer to the piezoresistivity effects for longitudinal and transverse directions, respectively, and Π_{44} states the piezoresistivity coefficient for the out of plane electric field.

The basics of the piezoresistivity theory and how it is implemented for stress sensors are briefly described in this chapter. However, the details of the subject covering the metal oxide field semiconductor field effect transistors (MOSFETs), energy bands, crystallographic sensor orientation, wafer coordinates, and the doping concentration will not be discussed in this thesis. The specified studies are beyond the knowledge required for the application and evaluation of the stress-chip data which is the essential purpose of this chapter. An interested reader may refer to the detailed studies on the related fields [2]–[9], [11], [15]–[17].

7.2.2. The stress measuring chip

The piezoresistive silicon chip used in this study was developed by Robert Bosch GmbH as a part of European joint project called iForceSens, in cooperation with several other institutes and companies including IZM, TZM, PTB, Sensitec and MEAS [11]. These chips consist of sensing cells which are capable of measuring the temperature variations as well as the in-plane stresses.

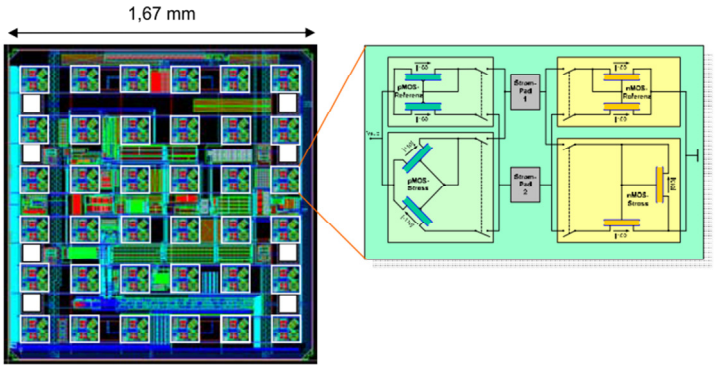

Fig 7.1 Layout of the stress sensor with a 6 by 6 measuring cells and 1.67 by 1.71 mm^2 chip area, and the circuit diagram of the measuring cell with nMOS and pMOS current mirrors [13]

The change of resistance under the applied stress largely depends on the crystallographic direction of the resistors and also on the wafer orientation. The sensor layout is demonstrated in figure 7.2. The current mirrors are designed orthogonally such that the nMOS transistor channels are set along [010] and [100] silicon crystal directions and measures the in-plane shear stresses while the pMOS transistors are oriented in [-110] and [110] crystallographic directions and they determine the difference in in-plane normal stresses. Furthermore, an npn transistor embedded in each cell is used to determine the temperature variations.

The subjected stress results in a change of resistance due to the relative change of the mirror currents at each transistor which can be approximated linearly by

$$\Delta\varrho/\varrho \approx -\Delta I/I. \qquad 7.7$$

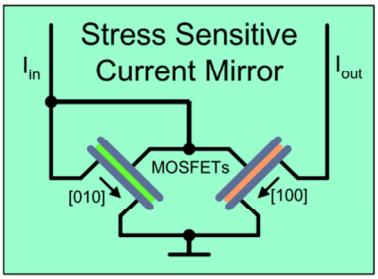

Fig 7.2 Orthogonal oriented MOSFET channels with stress sensitive current mirrors [9]

The change of current ratio for each transistor can be expressed in terms of piezoresistive coefficients as

$$\frac{\Delta I}{I}\Big|_{[100]} = -\Pi_{11}\sigma_x - \Pi_{12}\sigma_y - \Pi_{12}\sigma_z, \tag{7.8}$$

$$\frac{\Delta I}{I}\Big|_{[010]} = -\Pi_{12}\sigma_x - \Pi_{11}\sigma_y - \Pi_{12}\sigma_z, \tag{7.9}$$

$$\frac{\Delta I}{I}\Big|_{[110]} = -0.5(\Pi_{11} + \Pi_{12})(\sigma_x + \sigma_y) - \Pi_{12}\sigma_z - \Pi_{44}\tau_{xy}, \tag{7.10}$$

$$\frac{\Delta I}{I}\Big|_{[-110]} = -0.5(\Pi_{11} + \Pi_{12})(\sigma_x + \sigma_y) - \Pi_{12}\sigma_z + \Pi_{44}\tau_{xy}. \tag{7.11}$$

Note that the stress difference sensitivity of the nMOS channel is higher than the pMOS, whereas the shear stress sensitivity of pMOS is substantially higher than the nMOS channel. Therefore, $\Pi_{11} + \Pi_{12}$ are the piezoresistive coefficients of the n channel and Π_{44} is the coefficient of p channel.

Using the current ratio definition for each transistor given in equations 7.8 through 7.11 one can determine the in-plane stress difference, σ_D, and the in-plane shear stress, τ_{xy}, values. For the coordinate system of the chip with the x axis along [-1-10] and the y axis along [-110] direction, the stress values can be expressed by

$$\tau_{xy} = \frac{1}{2\,\Pi_{44}}\left[\frac{I_{out}-I_{in}}{I_{out}+I_{in}}\right], \tag{7.12}$$

$$\sigma_D = \sigma_x - \sigma_y = \frac{1}{\Pi_{11}-\Pi_{12}}\left[\frac{I_{out}-I_{in}}{I_{out}+I_{in}}\right]. \tag{7.13}$$

Where the currents I_{in} and I_{out} in equation 7.12 refer to $I_{[010]}$ and $I_{[100]}$ and in equation 7.13 to $I_{[-110]}$ and $I_{[110]}$, respectively.

The piezoresistive coefficients of the silicon chip were determined at Robert Bosch by the four point bending tests performed along the transistors orientations. As a result the in-plane difference coefficient Π_D=Π_{11}-Π_{12} and the in-plane total coefficient Π_S=Π_{11}+Π_{12} of the n channel transistors were obtained as -8.1x10^{-4} MPa^{-1} and -5.95x10^{-4}, respectively and the p channel piezoresistivity coefficient Π_{44} was calculated as 10MPa^{-1} [11].

If the temperature between the time steps does not change significantly, then an approximate equation for the total stress, σ_S can be derived. Hence, the accuracy of the total stress value can be improved by taking the measurement intervals as small as possible such that the temperature change between the steps is minimized. Then, σ_S can be determined by

$$\Delta\sigma_S = \sigma_x + \sigma_y \approx \frac{2}{\Pi_{11}+\Pi_{12}}\left[1 - \frac{I'_{out}+I'_{in}}{I''_{out}+I''_{in}} - \Pi_{12}\Delta\sigma_z\right]. \tag{7.14}$$

Here I'_{out} and I'_{in} express the last recorded output and input current values and I''_{out} and I''_{in} refer to the same current data from the previous step [11].

If the out-of-plane-stress is assumed to be much smaller than the in-plane stresses then the last term in equation 7.14 can be neglected. Hence, it can be rewritten as

$$\Delta\sigma_S = \frac{2}{\Pi_{11}+\Pi_{12}}\left[1 - \frac{I'_{out}+I'_{in}}{I''_{out}+I''_{in}}\right]. \quad 7.15$$

Then, the in-plane normal stresses, σ_x and σ_y can be determined by

$$\Delta\sigma_x = \frac{(\Delta\sigma_S+\Delta\sigma_D)}{2}, \quad 7.16$$

$$\Delta\sigma_y = \frac{(\Delta\sigma_S-\Delta\sigma_D)}{2}. \quad 7.17$$

7.3. Board design and test setup

The chip surface area is 1.67 by 1.70 mm. 36 piezoresistive sensing elements shown in figure 7.4 are located on the surface of the chip forming a 6 by 6 grid. The board is designed such that the copper interconnections which are wire bonded to the stress measuring chip at one side are connected to a PC for continuous data acquisition at the other end. The sensing signals are obtained by an analog interface. The whole hardware system consists of three interface parts. The stress measurement chip and the ASIC unit of the constant current source card (CS-card) and the national instrument card (Ni-card) plugged to the PCI slot of the PC. Hence, there are three interfaces. The cabling between the Chip and the CS-card provides an analog read out. The CS-card/Ni-card interface is cable connected and the Ni-card is connected to the PC providing the analog/digital conversion as well as digital input/output operations. The power to the chip is provided by the CS-card with a maximum current supply of ±1.5 mA and the power of the CS-card is supplied by the Ni-card (5V, max. 1A). Additional cell information like the cell address and the chip ID is transmitted via the current interface.

The layout of the board and the interconnections are illustrated in figure 7.3. The design provides instantaneous data recording capability during molding when the mold cap is still closed. Therefore, the length of the board is designed longer than the length of the cavity such that the copper connections are extended to the outside of the mold to be connected to the CS-card. Instead of a traditional rigid board like the glass epoxy FR4, a Polyimide, film layer is used as a substrate. As a result, the copper connections are sandwiched in between the polyimide layers. The thickness of the copper connections is 25µm and each PI layer is 45µm in thickness. Therefore, the total board thickness is 115µm.

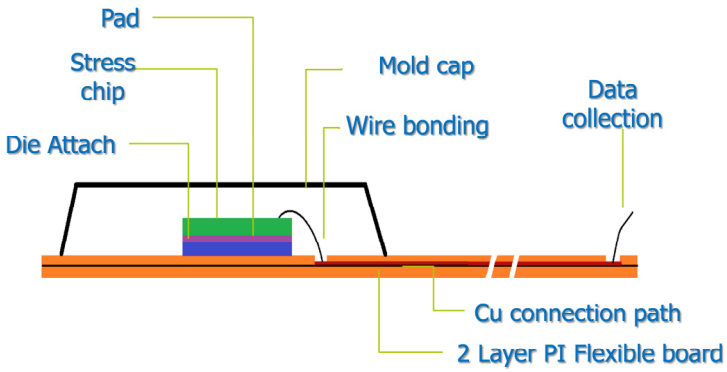

Fig 7.3 Schematic of the designed board and the interconnection

The main concern of the design was the force applied on the cavity edges during the clamping where the board and interconnections pass over. The clamping force would have broken the board or cut the connections extending to the outside of the mold. If the connections were broken or the board was torn off by the applied force, the whole experiment would have failed. Therefore, an uninterrupted, continuous data acquisition during molding was one of the key points taken into account during the design of the board, which was achieved by using a flexible board material. Besides, the board thickness was also an important factor in board material selection. However, the flexibility of the board resulted in buckling during filling due to the viscous melt flow. Hence, the polyimide boards were reinforced inside the cavity by a rigid copper layer taped to the bottom to keep the board flat during filling.

There are four connection pads on each side of the surface of the chip. However, the chip should be wire bonded to the board only on one side through four of the connections. Therefore, four connection pads are designed at the end of the longitudinal axis of the board. The chip pad is designed to be over the cavity midline in transfer direction, close to the front edge towards the inlet. In this way, the melt front contact with the chip surface takes place just a few seconds after the start of molding. Then, the stress data can be collected for a longer time during filling. The melt advancement is already discussed in chapter 4 where the direction of the flow front and the chip/melt contact time is simulated for the designed cavity model.

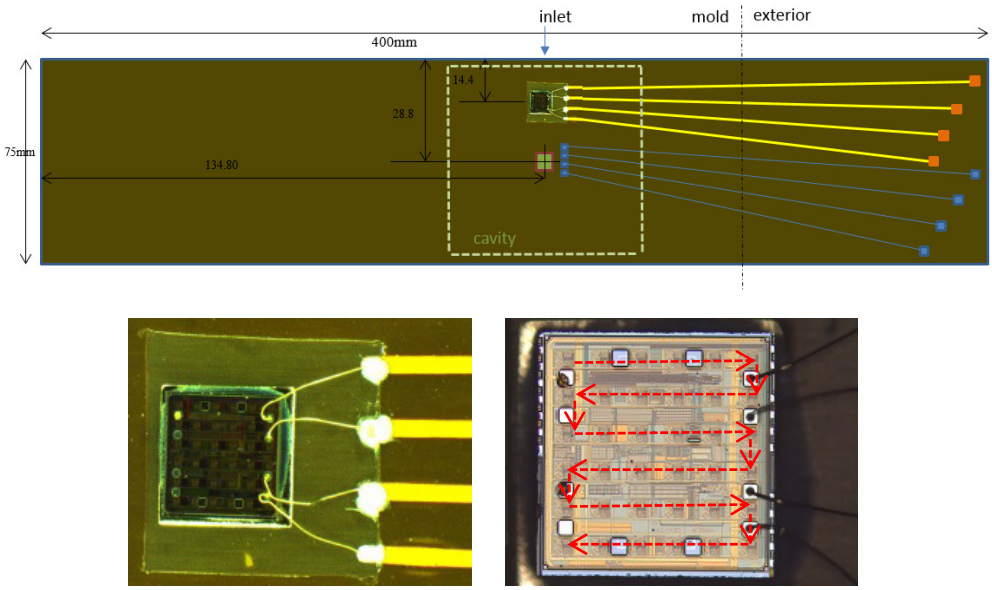

Fig 7.4 The board layout (top), the stress chip wire bonding (bottom left) and the chip showing the sensors and the pattern used in data reading (bottom right)

7.4. Selected processing conditions

The molding temperature for the IC encapsulation is standardized at 175°C [18]. However, the preliminary experiments showed that the stress measuring chips are not responsive above 160°C and even at 160°C occasional interruptions of data acquisition were experienced. This temperature sensitivity of the chips was observed regardless of the cavity filling speed and cavity height. Therefore, the test temperatures had to be set at $T \leq 160$°C. Hence, the measurements were conducted at cure temperatures of 120, 140 and 160°C. 160°C is critically high but since it is important to determine the residual stresses at a temperature as close as possible to the standard molding temperature, several attempts have been made to obtain a continuous data series at this temperature. 5 out of 6 measurements failed to provide a continuous data set. Therefore, the analysis of the cure temperature of 160°C, in this study, is based on the 6th shot which is highlighted in table 7.1. Another equally crucial test temperature is 120°C which is on the viscoelastic transition region but it is an important test temperature to evaluate the validity of the numerical approach.

In this chapter, the data detected from the encapsulation experiment with the cure temperature of 140°C was investigated in detail and can be verified with the numerical and analytical results obtained using the approaches explained in chapters 5 and 6. The results of the measurement conducted at 120 and 160°C are also given briefly for comparison

purpose after the in depth analysis of 140°C. All of the conducted molding experiments with the initial conversion degrees prior to the start of filling and the corresponding expected viscosity values are shown in table 7.1. The measurements with continuous and complete data sets which are studied in this chapter are highlighted. The conversion degrees are estimated using the autocatalytic model 2.5.

Table 7.1 Molding experiments (the measurements with the continuous data acquisition are highlighted)

Isothermal Cure Temperature	Cavity Filling Speed	Estimated Initial Conversion	Filling Time	Expected Viscosity	Expected max. Filling Shear Stress	Expected Conversion Range
°C	mm/s	%	s	Pa.s	Pa	-
160	1.1	6	30.5	27-68	75-187	0.05-0.2
160	1.1	26	30.5	68-200	190-600	0.2-0.38
160	0.6	6	49	27-150	40-200	0.05-0.33
160	2	6	15	27-45	150-240	0.05-0.13
160	1.1	6	-	27-68	75-187	0.05-0.2
160	1.1	6	30.5	27-68	75-187	0.05-0.2
140	1.1	22	30.5	180-300	500-900	0.2-0.3
140	1.1	2	30.5	17-45	160-250	0.02-0.08
120	1.1	0.5	30.5	100-200	400-500	0.005-0.02

With this experiment we wanted to find out the stresses during and after encapsulation of a die and to focus on the following processing parameters:

Molding Temperature: At lower molding temperature the curing is slower which leads to slow increase in viscosity as well, but the viscosity is higher, such that the forces imposed on the chip would also be higher. 175°C which is the recommended molding temperature of the characterized epoxy compound could not be chosen due to the already mentioned sensor issue. Hence, the initial tests were performed at 160°C and later two shots were done at 140°C and the last one conducted at 120°C.

Injection speed: With higher filling speed the forces on the die are higher but the recorded contact time is shorter. The selected plunger speeds of 0.6, 1.1 and 2mm/s were applied but only the shots performed at 1.1mm/s provided reliable data.

Initial conversion: At higher initial conversion, which is a result of longer time interval between loading and start of filling or simply just because of the higher mold temperature

the viscosity is higher which results in a larger surface friction. Therefore, various initial conversions are aimed at the same mold temperature to compare the effect of conversion by prolonging the filling initiation until the desired initial conversion achieved.

The stress chips were limited in number and more than half damaged during the difficult wiring process which had to be carried out manually at NXP. Some others failed during transportation and a few were not responsive at all which has been realized after the wire bonding during the calibration procedure undertaken by ENAS Fraunhofer. Therefore, the limited number of working chips restricted us from repeating the tests to obtain data for all planned test conditions we set previously.

7.5. Detailed molding steps and measurement procedure

The measurements were conducted by applying the following steps:

- The mold was heated to the cure temperature. Meanwhile, the EMC pellets were taken out of the freezer to be equilibrated to room temperature.
- A copper layer was taped to the bottom of the board such that the chip was adjusted to be at the mid-plane of the cavity which is shown in picture 7.5d and the board was connected to the Ni-card via a clamp plug.
- The board with the wire bonded chip was placed into the cavity. The process can be detected as a temperature rise. The sensors temperature shifted from room temperature of 26^{o}C to the mold temperature of 140^{o}C. A dummy copper plate is inserted at the adjacent cavity since the EMC melt is forced symmetrically into the both cavities at the same time.
- Then the epoxy pellets were inserted using the loading equipment shown in figure 7.5i into the chamber called transfer pot shown in figure 7.5f. The pots were already preheated to the cure temperature. Therefore, the EMC temperature starts rising upon loading.
- The mold top platen was clamped over the mold cavity covering the whole rectangular area designed to be encapsulated. Mold clamping can be determined from the temperature drop due to the contact of the mold with the colder top platen. Need to emphasize that at this point the extended section of the board is compressed between the edges of the mold bottom part and top platen. The pressure applied in clamping should be high enough to ensure a complete tight closure of the mold cavity during filling and curing stages. Insufficient clamping may result in mold flashing. In our test set-up the part of the board laying through the one side of the cavity to the outside results in an unbalanced clamping and

hence the complete closure was not ensured in all tests which led to melt flash in one measurement as can be seen in the picture 7.5k.

- Then the injection was started. In filling stage the plunger pushes the pellets by applying the preset speed through the runners and gate to the cavity. The epoxy melt temperature gradually increased to the mold temperature while passing through the runners. However, the board temperature after clamping is around $10^{o}C$ lower than the mold temperature. When the melt passes over the chip surface the temperature of the chip rises to the epoxy melt temperature which is equilibrated to the mold temperature. This can be observed in detail in figure 7.7. The transfer pressure which is the pressure applied by the plunger is less than 1MPa. During the filling the low transfer pressure ensures the slow progress of the melt in the cavity and the molding problems like wire sweep that may be resulted due to the high pressure in the cavity is avoided.
- The filling stage was followed by the packing. At the end of filling the cavity is already filled completely but, the plunger pushes more epoxy melt to the cavity to compensate for the epoxy shrinkage. The aim is to minimize the warpage and the residual stress after the mold release. The increase in plunger pressure is limited to 5MPa but its effect on the cavity pressure is much larger and cannot be measured directly.
- When the mold pressure reached to the preset maximum pressure of 5MPa the packing stopped and the curing of the epoxy continued at the isothermal mold temperature until the complete cure (or to the desired preset degree of cure) of the epoxy. The stress rise due to a high hydrostatic pressure does not provide any information for a direct comparison of the in-plane stresses. Furthermore, the offset values in the stress data in packing are different for each sensor.
- At the end of cure the mold was opened and the heating stopped immediately. The mold detachment is detected in data by the decrease in the stresses close to the levels prior to filling.
- The temperature of the chip dropped to room temperature gradually when the encapsulated board was taken out from the mold cavity. This temperature drop was accompanied by the rapid change in the in-plane stresses.

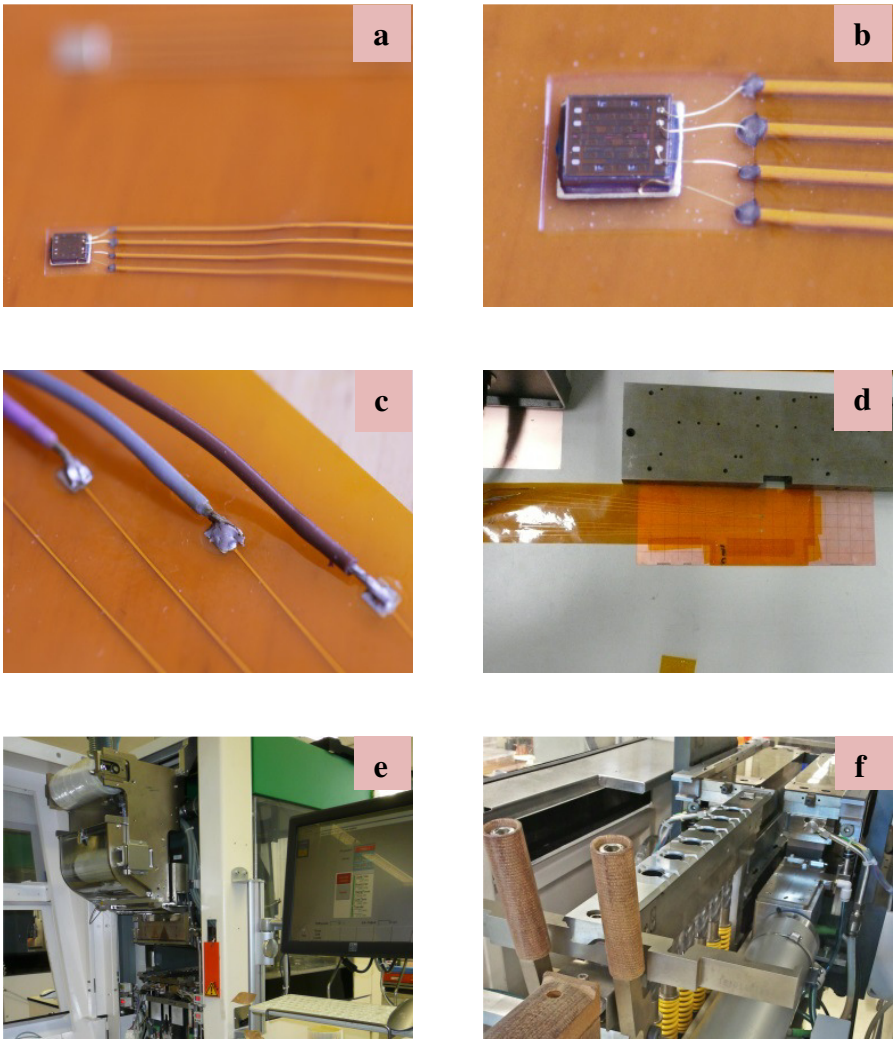

Fig 7.5 Pictures showing the various steps of the encapsulation experiment
a) & b) wire bonded stress measuring chip,
c) board end connections which are bonded to a CS-card for data acquisition,
d) package enhancement (attachment of a copper plate to the board's bottom surface, and positioning the chip with respect to the mold gate), e) mold, f) transfer pot,

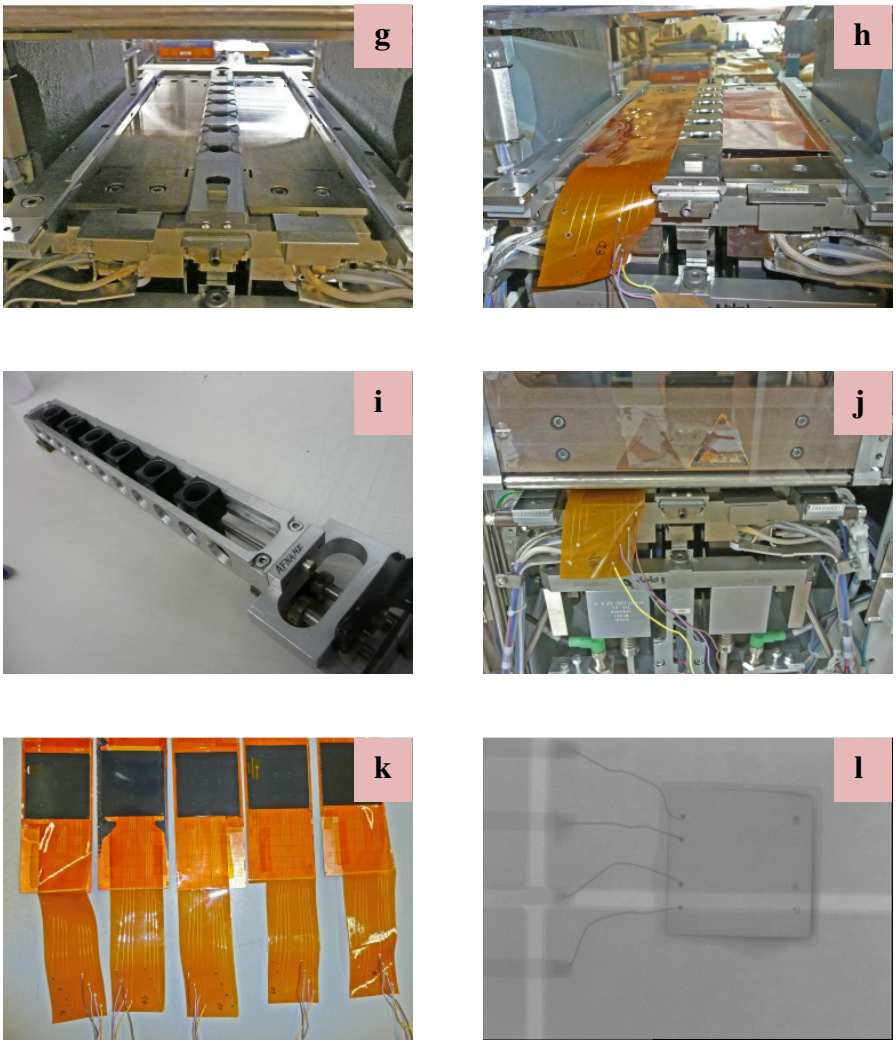

Fig 7.5 (Continued)

g) empty mold cavity,

h) board with the piezoresistive chip at the left side and a dummy board at the right side

i) EMC pellet loading device,

j) cavity after mold clamping (part of the board is outside the cavity for connection)

k) encapsulated substrates,

l) x-ray shot of a chip inside the epoxy showing the wires are not damaged

7.6. Results

The data derived by the stress chips are: in-plane normal stress difference, in-plane shear stress and temperature. The data from the sensors are recorded by stepwise scanning through the sensors (as shown in figure 7.4). The time gap between the adjacent sensor's readings is 16ms. That is why the recorded data are not aligned at the same point in time and are slightly shifted with a consistent pattern repeated during the entire measurements. Besides, this is the shortest interval for data acquisition which provides the highest accuracy.

The sensors taken into account are defined by their positions on the chip as if they are positioned in a 6 by 6 grid. The position of each sensor is given by two numbers such that the first one is showing the vertical (flow direction) position and the second number stating the horizontal position of the sensors. The sensor [1,4] for instance, displays the stress data for the sensor at the first row and the fourth column from the back side on the chip's surface. The same definition applies to the other points as well. The selected sensors' positions are shown in figure 7.6 over the schematic picture of the chip surface by the red markers. As a result, the numbers [6,1] through [6,6] are assigned to the sensor row that first detects the moving melt front.

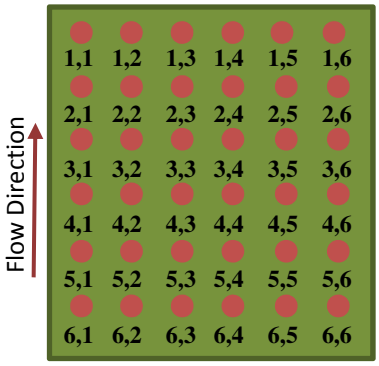

7.6 Sensor numbering on the surface of the chip

7.6.1. Molding measurement conducted at 140°C cure temperature

7.6.1.1. Temperature and stress data

Figure 7.7 shows the temperature data detected by the piezoresistive sensors during the molding experiment conducted at 140°C. The stages of the molding are determined by interpretation of the temperature and the stress data. The start and the end temperature values of each stage are shown in figure 7.7. The temperature rises as soon as the board is

placed inside the cavity and it equilibrated at 250s. The mold closing is detected as a decrease in temperature and the first minima after this point which happens due to the higher temperature of the melt compared to the sensor states the beginning of over-molding of the chip. The temperature drop in figure 7.7 shows the time when the heating stops and the board is being removed from the mold cavity. The other stages cannot be determined from the temperature data and is explained in figure 7.8 by considering the variations in the in-plane stress data.

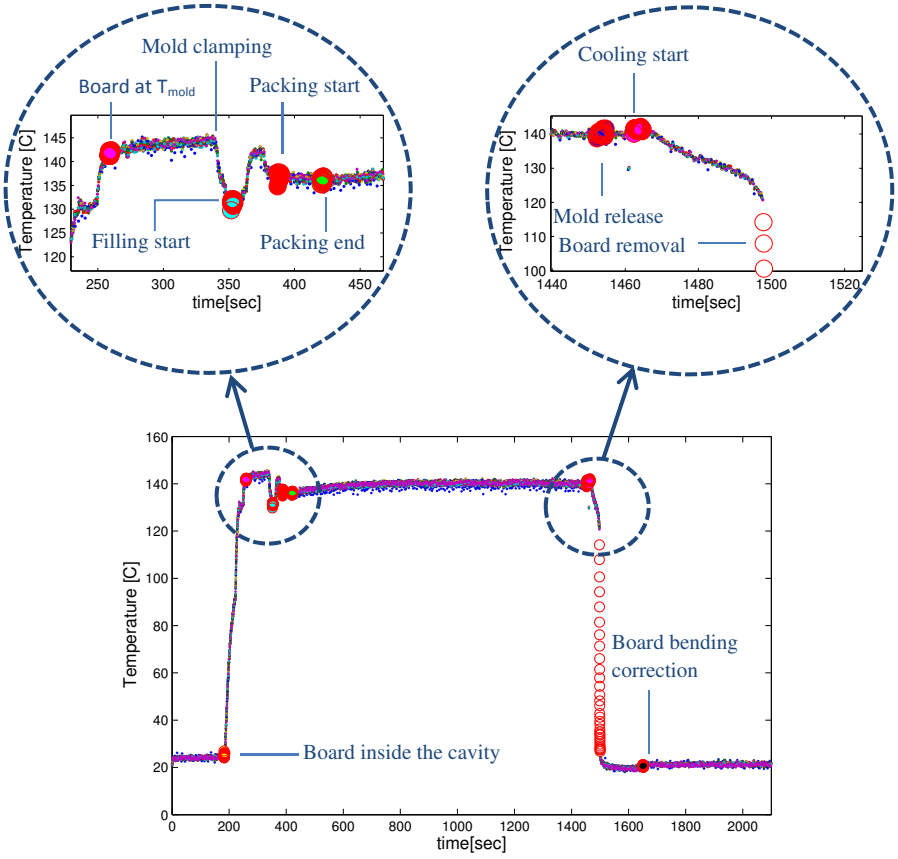

Fig 7.7 Temperature data from the 36 piezo-resistive sensors with the markers showing the various stages of the molding experiment (140°C) based on readings from all sensors

The in-plane normal stresses determined by the 36 sensors are shown in figure 7.8a. On the other hand, in figure 7.8b a selection of this data is shown representing a single column on the sensor chip (see figure 7.6). The central part of this measured in-plane stress plot shows

the signal change during the curing phase (≈400-1500 sec). The steep stress rise at 400s coincides with the moment the cavity is completely filled and the holding pressure is applied (≈50 bar). This pressure should not affect the in-plane stresses. Yet figure 7.8 clearly shows that it has a quite a large effect on the recorded in-plane stress signals (apparent signal change up to 50MPa). These stress levels are much larger than the expected in-plane cure induced stresses of about 1MPa (see chapters 5 and 6). We thus have to conclude that we cannot use the in-plane stress data of the stress chip when the chip is in compression. After mold opening (≈1450 sec) the pressure returns to atmospheric and the stress signals turn back close to their original lower values. This suggests that we should exclude the high pressure part from the data analysis. The reason for this unexpected pressure effect is the fact that the algorithms are optimized to evaluate signals under atmospheric pressure only and the assumption to neglect the $\Pi_{12}\Delta\sigma_z$ term in equation 7.14 cannot be justified for the cure stage in our experimental conditions.

At the end of molding measurements a heavy block is placed over the board to prevent the possible further warpage of the package. This is mainly done to keep the boards straight for further thermal cycling analyses which are conducted independently from the present study. The last markers (black) in figure 7.8b show the effect of the extra weight on the sensors. This is done after the equilibration of the data at the end of cooling stage. Therefore, the cure and cooling induced stresses are not affected by the added weight.

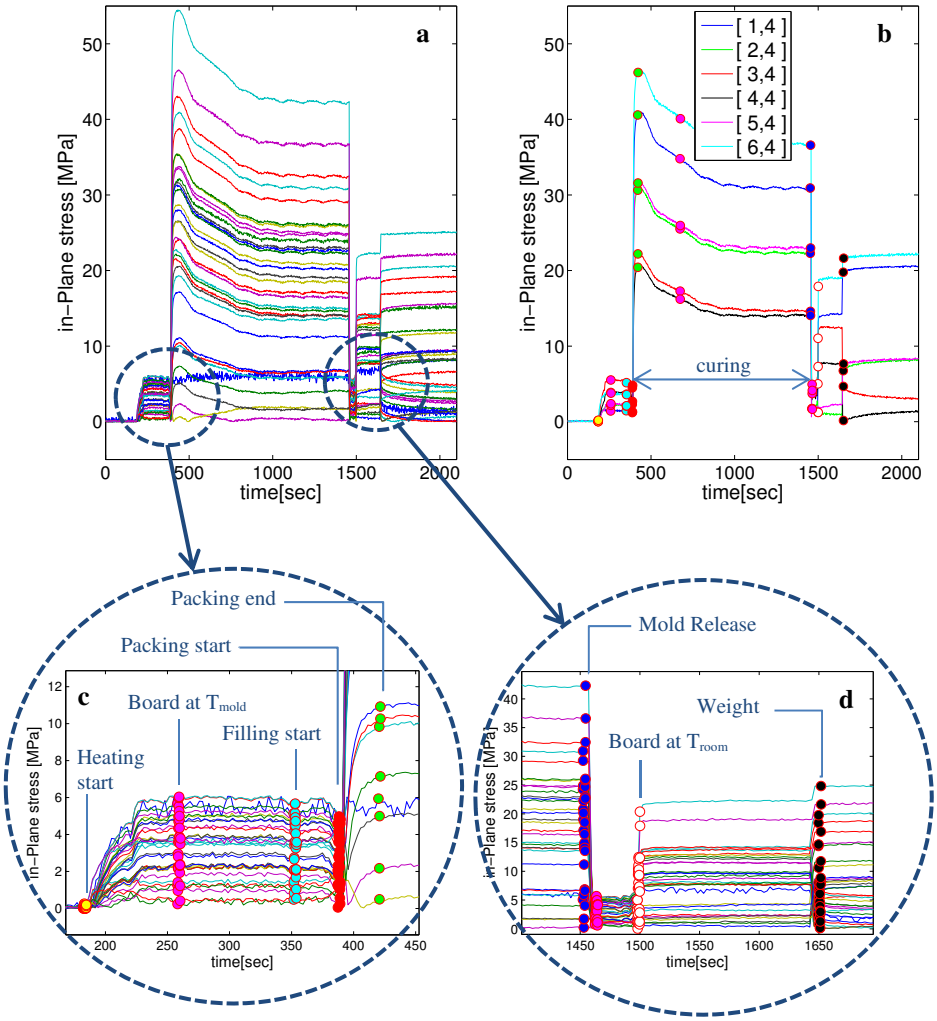

Fig 7.8 In-plane normal stresses detected by the all 36 sensors (a) and by the selected sensors (b) and more detailed plots of the selected regions (c & d)

7.6.1.2. Filling

During filling (355-385 sec) insignificant changes in the in-plane shear and in-plane normal stress data are detected (typically less than 1MPa) which may be attributed to the chip surface friction caused due to the viscous melt flow over it. The wall shear stress of the fluid had been studied in the past using vertical floating piezoresistive sensors, cantilever or tactile sensors or using methods like oil films, liquid crystal coating or by implementing the

hot wire technology [2], [19]–[22]. Determination of the surface stress during the epoxy filling was one of the intentions of this study. However, the stress chip's ability in recording the flow induced shear stress is restricted only to an observable but insignificant change in stress data and does not provide any further information about the exact magnitude of friction on the chip's surface and on the other delicate components like the wires. The required sensitivity to detect the wall shear stress is at least two orders of magnitude lower than the sensitivity of the sensors used in our experiment (for the epoxy melt surface stress see chapter 4).

7.6.1.3. Curing

The main part of the test data contains the cure stage which comprises the region between the end of packing and the start of cooling. This does not necessarily mean that the filling or cooling stages are cure-free. However, to emphasize the cure induced shrinkage and its contribution to the residual stress the stage where the isothermal cure is applied should be taken into account independently from the cooling and filling stages. The same assumption has been made by many researchers including the preliminary work of Hahn and Pagano as well [23]. So, the stages of filling, cure and cooling are separated. The cure time is 1100 seconds and at 140^{o}C the degree of conversion is estimated by the kinetic model as 88.5%. The crosslink polymerization starts a few seconds after inserting the pellets to the transfer pots and ends at the end of cooling. Nevertheless, the region where the polymerization is much faster and happens in a larger extent is considered as the cure stage. This region comprises the stress build-up after the gel point. The data between the green and the blue markers in figure 7.8b is the cure region and the markers around 680s within this region illustrate the time in which the gelation is started. As mentioned before, the recorded data for the cure stage cannot be evaluated directly due to the existence of high out-of-plane stresses.

Although it was not possible to monitor the stress build up during cure, we can use the stress data directly after mold opening to get the in-plane cure induced stresses at the end of curing. In figure 7.9 the cure induced in-plane shear and in-plane normal stresses on the chip surface are shown by the iso-stress lines based on the stress data of the sensors after mold opening. The chip surface sensor positions are already shown in figure 7.6. The cure induced stress is determined as the stress difference between the uncured and the cured stages where the temperature and pressure values are the same. The uncured stress data is selected from the start of the filling and the cured data is obtained from just after the mold release. Hence, the cure induced stress profile on the chip surface is determined as the difference in stress values between the two states with a mutual temperature (140^{o}C) and

pressure (atmospheric pressure) values. The maximum in-plane normal stress of 0.8MPa was obtained at the back edge of the chip. Besides, a small region at the front edge (gate side) is around 0.55MPa, which is close to the maximum value. The in-plane normal stress σ_x decreases towards the chip center to 0.3MPa.

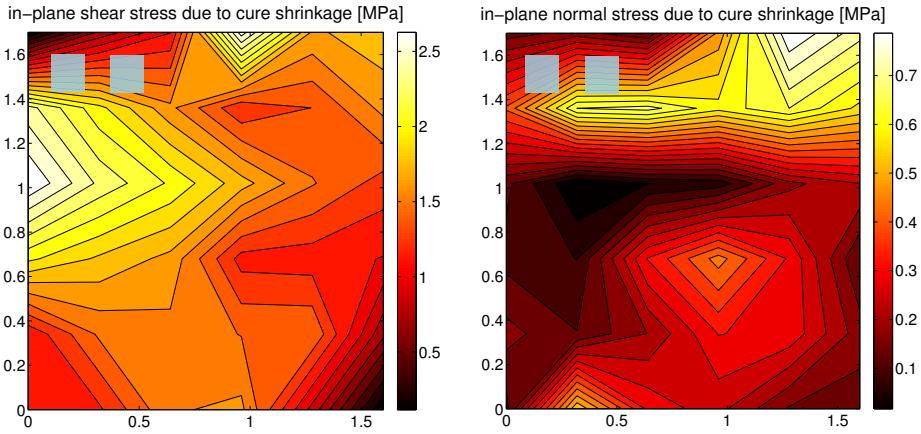

Fig 7.9 Cure induced in-plane shear and in-plane normal stress distributions on the area representing the region covered by the sensors on the chip surface for 140°C cure temperature molding experiment (the white squares indicate non-functioning sensors)

7.6.1.4. Cooling

The cooling stress difference is calculated between the final state at room temperature (just before putting the weight at 1640 sec) and the end of cure stage, just after the mold clamp release. The figures of the in-plane shear stress and the in-plane normal stress distributions are given in figure 7.10. The in-plane shear stress on the chip surface is highest at the corners and it decreases towards the region indicated by the blue dashed lines. The maximum cooling induced in-plane shear stress is 11MPa. On the other hand, the maximum in-plane normal stresses were observed at the edges facing the flow and at the opposite end. Note that this is the flow direction and the bending of the board also took place on this axis. The low stress regions are illustrated using the two blue oval dashed lines in each figure. The highest detected in-plane normal stress is 16.5MPa. The positive data do not necessarily mean a tensile stress since all the data are expressed in absolute values. Starting from the top edge where the stress is highest coming 0.2mm downward towards the center the stress becomes lower than 3MPa. Then at the center it rises again to 8MPa and this pattern continues to the front edge almost symmetrically.

In all of the tested chips some of the sensors were either unresponsive at all or giving inaccurate data. These faulty sensors are detected and the data collected from these sensors are eliminated. The positions of the faulty sensors for the tested case are given in figure 7.10 in the form of white squares. It is realized that the sensors at the last row are somehow much more vulnerable. The broken sensors interrupt the continuity and the symmetry of the stress distribution shown in the respective figures. In order to show the stress distribution in a more realistic manner the stress data for the unresponsive sensors were determined by interpolating the data of the working sensors.

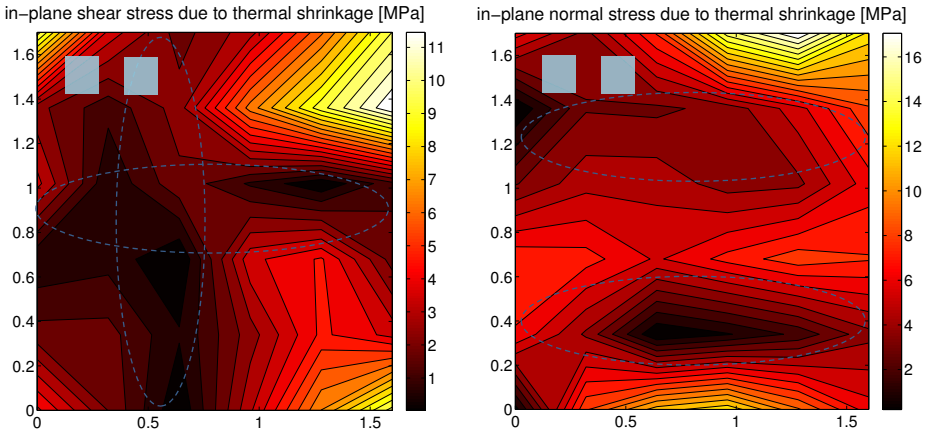

Fig 7.10 Thermal induced in-plane shear and in-plane normal stress distributions on the area representing the region covered by the sensors on the chip surface for 140^{o}C cure temperature molding experiment

The experimentally obtained cooling induced in-plane normal stresses can be compared with the results obtained by the 1D and 2D numerical studies given in figures 5.8 and 6.9, respectively. The last simulated stress profile at 1200s in figure 6.9 must be compared to the surface plot of the experimental in-plane normal stress in figure 7.10. The maximum stress is calculated as 16MPa by the numerical study, at the chip surface edges which compares well with the experimentally determined maximum value of 16.5MPa. Besides, the chip centre stress magnitude is obtained as 10MPa by the simulation which agrees with the experimentally measured data of 8-10MPa. In chapter 5 the cooling induced stress is calculated as 13 and 18MPa depending on the applied approach. As a result both numerical studies provided reliable results when compared with the experimental stress data. In order to compare the cure-end stresses, figures 5.8 and 6.8 should be compared with figure 7.9.

The cure-end stress is calculated as 1MPa in the one dimensional incremental elastic study of chapter 5, and 0.73 is the maximum magnitude of the in-plane normal stress determined in the two dimensional study of chapter 6. The maximum stress is obtained at the chip edges and the chip center stress is simulated as 5MPa. Therefore, the calculated stress distribution pattern on the chip surface also compares well with the experimental observation.

7.6.2. Molding measurement conducted at 120^{o}C cure temperature

The cure time for the 120^{o}C experiment is 2800 seconds which is corresponding to 83.5% degree of conversion. The in-plane stress distributions at the end of the cure and cooling stages are given in figure 7.11 and 7.12. Since the detailed analysis was performed for the 140^{o}C cure temperature, here only a brief interpretation of the in-plane normal stress data is given.

At the end of cure stage the measured maximum in-plane normal stress is 0.7MPa which was recorded by the sensor at the left edge of the chip. Unlike the cure stress data of 140^{o}C, at 120^{o}C the maximum stress was obtained at the center and not at the gate front or back edges. The shear stress, on the other hand is lowest at the corners and a gradual rise in the iso-line values, propagating towards the chip center can be observed.

At the end of the cooling stage the maximum stress is 14.5MPa (see figure 7.12) and detected at the front corner like the previous measurement. As it can be observed the pattern is similar as the stress is decreasing initially starting from the front edge towards the back edge. Then at almost one fourth of the chip length it becomes zero and later starts rising towards the chip center and this symmetric pattern is repeated for the rest of the chip length. The average stress at the center is just above 0.6MPa. The front and back edge stresses in average are around 0.3MPa. The two zero stress regions can be observed at the top and the bottom of the chip center. Note that the broken sensor nodes probably affected the symmetry patterns.

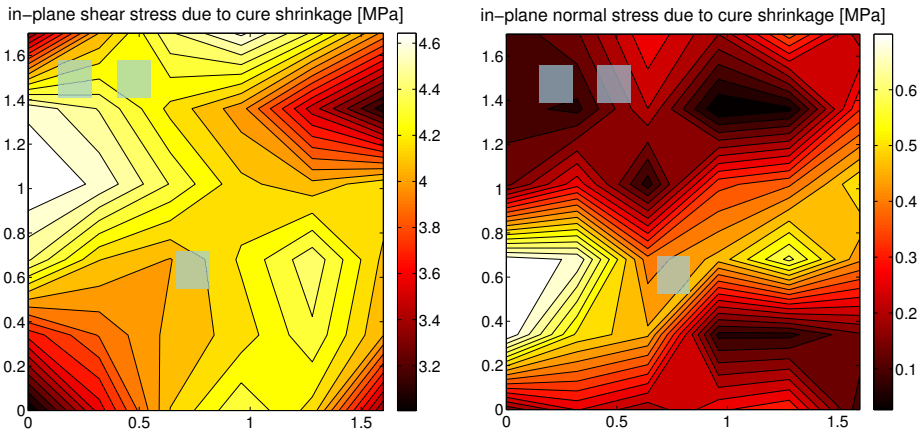

Fig 7.11 Cure induced in-plane shear and in-plane normal stress distributions on the area representing the region covered by the sensors on the chip surface for 120^{o}C cure temperature molding experiment

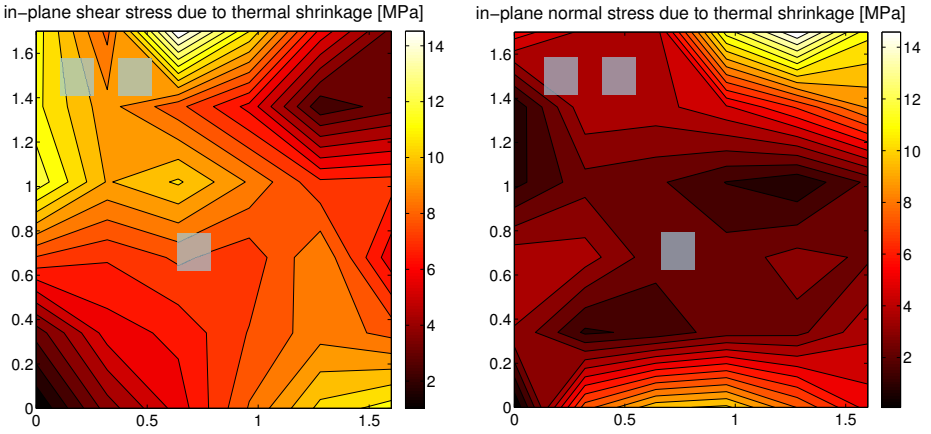

Fig 7.12 Thermal induced in-plane shear and in-plane normal stress distributions on the area representing the region covered by the sensors on the chip surface for 120^{o}C cure temperature molding experiment

The results can be compared with the analytically and the numerically estimated stress values shown in figures 5.11, 6.13 and 6.14. The cure induced stress is calculated as 0.85MPa using the incremental elastic approach and the maximum cure-end stress is determined to be 0.65MPa in chapter 6. The cooling-end stress is 15MPa based on the

incremental elastic study and 14MPa is the maximum stress value detected at the chip corner obtained by the viscoelastic 2D simulation in chapter, 6 which agrees well with the maximum experimental in-plane stress of 14.5MPa as well as its position on the chip surface.

7.6.3. Molding measurement conducted at 160°C cure temperature

In the molding experiment of 160°C the cure time which is 400s is much shorter than the previous measuements due to the higher mold temperature. The estimated conversion degree is 85% based on the kinetic model and the addition of the initial conversion results in 91% EMC conversion at the end of cure. Note that the initial conversion is calculated by considering the elapsed time between the loading of the EMC to the transfer pots and the start of filling. The higher the mold temperature the larger the effect of this time period on the degree of cure.

The maximum cure induced residual in-plane normal stress is obtained at the top right and bottom left corners of the chip according to figure 7.13 and a gradual decrease towards the chip center is detected. Based on the kinetic model the conversion degree is 91% which leads to a maximum cure induced stress of 1.3MPa. The cooling induced stress distribution with an initial temperature of 160°C is given in figure 7.14. The maximum cooling induced stress is measured as 22.5MPa which compares well with the predicted value of 21MPa from chapter 6. The cooling in-plane normal stress is highest at the front and back edges and it decreases gradually in between the two boundaries.

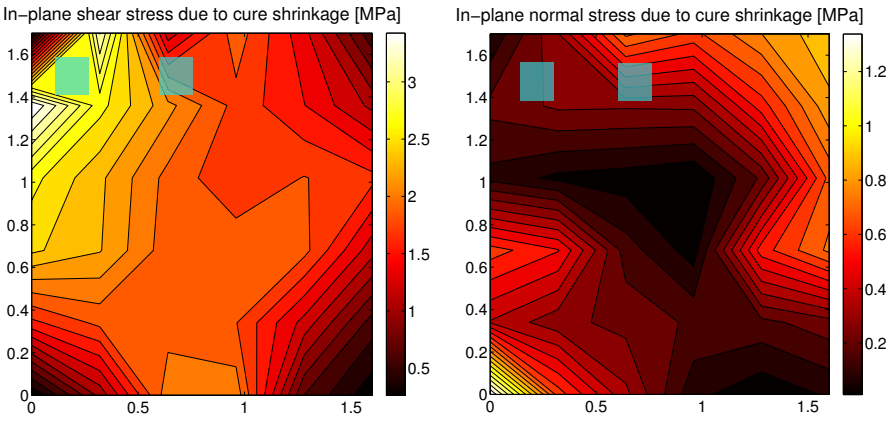

Fig 7.13 Cure induced in-plane shear and in-plane normal stress distributions on the area representing the region covered by the sensors on the chip surface for 160^{o}C cure temperature molding experiment

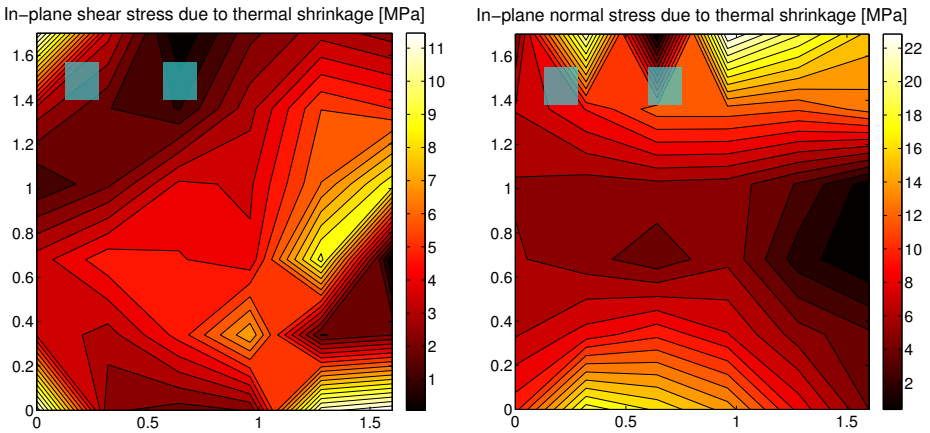

Fig 7.14 Thermal induced in-plane shear and in-plane normal stress distributions on the area representing the region covered by the sensors on the chip surface for 160^{o}C cure temperature molding experiment

7.7. Warpage

Warpage of packages after encapsulation is a major concern in electronic packaging. Extreme bending of the package may cause to board or chip cracking at the end or leads to installation issues when mounting the encapsulated package to a pcb or into another package like a package on package (PoP). The problem is more severe in the case of thin packages where the tensile stresses have profound impact on the robustness and reliability of the encapsulated electronic components and interconnections [24].

The warpage of the encapsulated boards in this study were measured using the Taylor Hobson surface profiler "Form Talysurf-120" shown in figure 7.15. Figure 7.16 gives the surface deflection over the transfer axis (flow axis) of the encapsulated package cured at 140^{o}C cure temperature. The maximum deflection at the center of the encapsulated region is recorded close to 4mm. This warpage is the result of the total shrinkage which is the sum of the cure induced constrained shrinkage of the epoxy compound and the free thermal shrinkage of the whole package.

The deflection estimated for the 140^{o}C process conditions obtained by the incremental elastic study in chapter 5 is 1.65mm. This value is less than the value obtained by the Profilometry measurement which is about 4mm at the midpoint. The curvature obtained by the Profilometry is calculated as 6.5m^{-1} based on equation 5.29 while the analytically calculated curvature by equations 5.23 and 5.26 is calculated as 2.2m^{-1} at the end of cooling. This is the total curvature obtained by addition of both stages' curvatures. On the other hand, using the viscoelastic numerical study in chapter 6 the deflection is predicted to be 3.5mm. The larger deflection determined by the Profilometry measurement can be attributed to the length of the board. The unencapsulated portion of the PI boards is not included in numerical studies. In reality, the expected bending of the encapsulated package is more symmetrical rather than being in one axis. However, the boards tend to bend on shorter edge and the longer edge deflection is restricted which is measured as 2.7mm.

Fig 7.15 Warpage measurements conducted using the Taylor Hobson surface profiler "Form Talysurf-120"

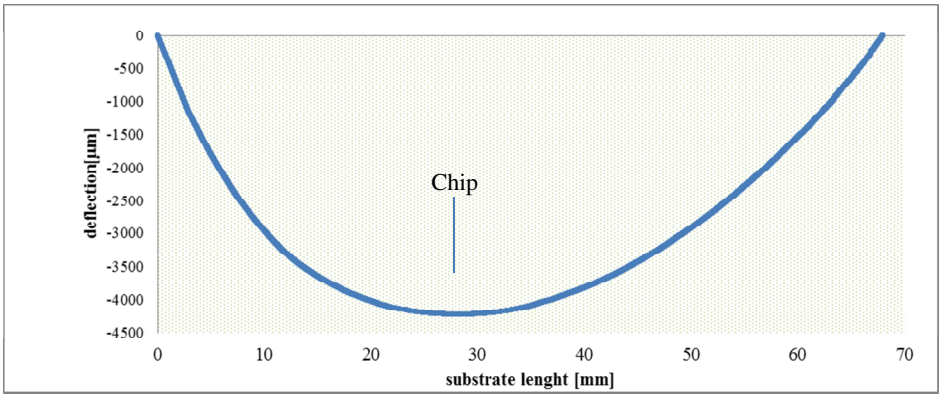

Figure 7.16 Curvature measurement of the encapsulated board used in the 140°C cure temperature molding experiment

7.8. Conclusion

A novel experimental method was investigated to study the residual stresses building up during and after the encapsulation of microelectronics. A chip with piezoresistive sensing elements was used for a real-time in-situ stress recording during molding. The chip was connected to a flexible polyimide board. The molding experiments were conducted at various isothermal cure temperatures. Due to limitations and sensitivity of the test set-up only three of the test results are investigated with an emphasis given on the measurement conducted at 140°C. The stages of the molding were determined based on the temperature and stress data analysis. The in-plane normal and shear stress distributions on the chip surface for each stage were obtained, independently. The maximum cure and cooling induced in-plane normal stress values are given in table 7.2.

Table 7.2 Experimental cure and cooling induced stress values

	120°C	140°C	160°C
Max. in-plane cure stress [MPa]	0.7	0.8	1.3
Max. in-plane cooling stress [MPa]	14.5	16.5	22.5

The effect of cure shrinkage is much smaller when compared to the thermal shrinkage effect on the in-plane stress. As it is given in table 7.2 the cure induced stress values in all of the measurements are found to be 5% of the cooling induced stresses of the respective experiment. The stress detected at the chip edge and center agrees well with the numerically obtained results. Moreover, the same pattern of sudden stress drop close to the edges and then the stress rise towards the chip surface center is also observed in the two dimensional

numerical study in chapter 6. The experimental chip surface stress distribution pattern is much more visible in the cooling stage since the stress range is much wider compared to the cure stage. The experimental stress profile matches quite well with the stress profile in numerical study of chapter 6 for both cure and cooling stages, independently. The experimental data determined by this approach provided a fair and reliable method for verification of the numerical and analytical stress studies performed in chapters 5 and 6.

The warpage of the encapsulated board (140^{o}C) is measured using a surface profilometer. The measured surface deflection is 4mm in flow direction. This is higher than the analytically calculated (1.65mm) and numerically obtained (3.5mm) values.

It is experimentally observed that the stress chips cannot be used during molding at elevated pressures. However, they can still be used to determine cure induced stresses by comparing the stress values just before and directly after the curing where the hydrostatic pressure is released and the cooling not started. Moreover, the magnitude of the measured maximum and minimum cure and cooling stresses compare very well with the simulated results of the previous chapters.

The simulated and experimentally determined surface stress distribution patterns of 140^{o}C cure temperature are compared in figure 7.17. The experimental data are determined from the sensors lying on a straight line from [1,4] to [6,4] (see figure 7.6). The experimental data are in good agreement with the numerical results and the same symmetrical pattern on the chip surface determined from both studies independently can be clearly seen in this figure.

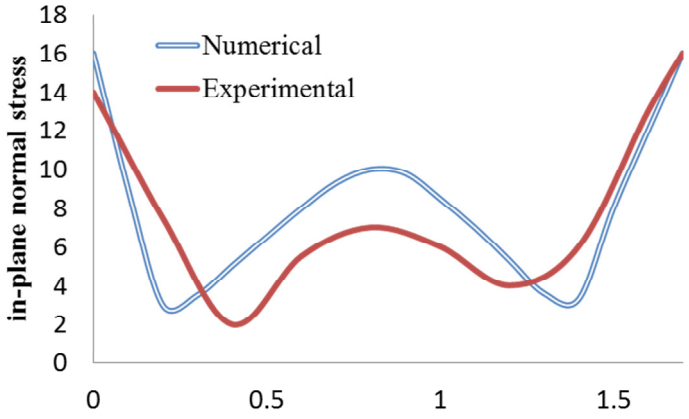

Figure 7.17 Numerical and experimental in-plane normal stress distribution on the chip surface

References

[1] K. Oota and M. Saka, "Cure Shrinkage Analysis of Epoxy Molding Compound," *Polym. Eng. Sci.*, vol. 41, no. 8, pp. 1373–1379, 2001.

[2] A. A. Barlian, W. Park, J. R. M. Jr, A. J. Rastegar, and B. L. Pruitt, "Review: Semiconductor Piezoresistance for Microsystems," in *Proceedings of the IEEE Institute of Electrical and Electronics Engineers*, 2009, vol. 97, no. 3, pp. 513–552.

[3] S. Hirsch, S. Doerner, P. Hauptmann, and B. Schmidt, "A New Test Device for Characterization of Mechanical Stress Caused by Packaging Processes," *J. Phys. Conf. Ser.*, vol. 34, pp. 39–44, 2006.

[4] R. C. Jaeger, J. C. Suhling, R. Ramani, A. T. Bradley, and J. Xu, "CMOS stress sensors on (100) silicon," *IEEE J. Solid-State Circuits*, vol. 35, no. 1, pp. 85–95, 2000.

[5] H. Kittel, S. Endler, H. Osterwinter, S. Osterle, and F. Schindler-Saefkow, "Novel Stress Measurement System for Evaluation of Package Induced Stress," in *Integration Issues of Miniaturized Systems - MOMS, MOEMS, ICS and Electronic Components (SSI), 2008 2nd European Conference & Exhibition on*, 2008, pp. 1–8.

[6] D. Meunier, S. Tardu, D. Tsamados, and J. Boussey, "Realization and simulation of wall shear stress integrated sensors," *Microelectronics J.*, vol. 34, no. 12, pp. 1129–1136, Dec. 2003.

[7] J. C. Suhling and R. C. Jaeger, "Silicon piezoresistive stress sensors and their application in electronic packaging," *IEEE Sens. J.*, vol. 1, no. 1, pp. 14–30, Jun. 2001.

[8] T. von Papen, U. Buder, H. D. Ngo, and E. Obermeier, "A second generation MEMS surface fence sensor for high resolution wall shear stress measurement," *Sensors Actuators A Phys.*, vol. 113, no. 2, pp. 151–155, Jul. 2004.

[9] T. Schreier-Alt, K. Unterhofer, F. Ansorge, and K.-D. Lang, "Stress analysis during assembly and packaging," in *2011 IEEE 61st Electronic Components and Technology Conference (ECTC)*, 2011, pp. 1684–1690.

[10] F. Schindler-Saefkow, O. Wittler, T. Schreier-Alt, H. Kittel, and B. Michel, "Package Induced Stress Simulation and Experimental Verification," in *Íntegration Issues of Miniaturized Systems - MOMS, MOEMS, ICS and Electronic Components (SSI)*, 2008, pp. 3–6.

[11] H. Kittel, C. Gebhardt, A. Bartos, T. Schreier-Alt, T. Walther, H. Osterwinter, W. Schneider, and U. Kutgens, "Abschlussbericht zum Verbundvorhaben iForceSens Entwicklung eines integrierten Stressmesssystems zur Quantifizierung der 3D-Verformung von Sensor- Bauelementen in Abhängigkeit des Verpackungsprozesses"," 2008.

[12] A. R. Rezaie Adli, K. M. B. Jansen, F. Schindler-Saefkow, and F. Rost, "Experimental Investigation and Interpretation of the real time, in situ Stress Measurement during Transfer Molding using the Piezoresistive Stress Chips," in *International Conference on Thermal, Mechanical and Multiphysics Simulation and Experiments in Microelectronics and Microsystems, EurosimE*, 2014, pp. 1–4.

[13] F. Rost, F. Schindler-Saefkow, A. R. Rezaie Adli, D. Vogel, K. M. B. Jansen, S. Rzepka, B. Michel, J. Schaufuß, A. Tsapkolenko, and P. Nossol, "Material parameter identification by combination of stress chip measurements and FE-simulation in MERGE," in *Smart System Integration*, 2014, vol. 2, no. 1, pp. 2–9.

[14] F. Schindler-Saefkow, F. Rost, A. R. Rezaie Adli, K. M. B. Jansen, B. Wunderle, J. Keller, S. Rzepka, and B. Michel, "Measuring the Mechanical Relevant Shrinkage during In-Mold and Post-Mold Cure with the Stress Chip," in *International Conference on Thermal, Mechanical and Multiphysics Simulation and Experiments in Microelectronics and Microsystems, EurosimE*, 2014, pp. 1–5.

[15] Y. Sun, S. E. Thompson, and T. Nishida, *Strain Effect in Semiconductors*. 2010.

[16] Y. Kanda, "A graphical representation of the piezoresistance coefficients in silicon," *IEEE Trans. Electron Devices*, vol. 29, no. 1, pp. 64–70, 1982.

[17] Y. Chen, "CMOS stress sensor circuits," 2006.

[18] L. T. Nguyen, "Reactive Flow Simulation in Transfer Molding of IC Packages," in *Electronic Components and Technology Conference*, 1993, pp. 375–390.

[19] J. W. Naughton and M. Sheplak, "Modern developments in shear-stress measurement," *Prog. Aerosp. Sci.*, vol. 38, no. June 2000, pp. 515–570, 2002.

[20] K. Noda, K. Hoshino, K. Matsumoto, and I. Shimoyama, "A shear stress sensor for tactile sensing with the piezoresistive cantilever standing in elastic material," *Sensors Actuators A Phys.*, vol. 127, no. 2, pp. 295–301, 2006.

[21] J. Shajii, K.-Y. Ng, and M. a. Schmidt, "A microfabricated floating-element shear stress sensor using wafer-bonding technology," *J. Microelectromechanical Syst.*, vol. 1, no. 2, pp. 89–94, 1992.

[22] J. C. Suhling and R. C. Jaeger, "Silicon piezoresistive stress sensors and their application in electronic packaging," *IEEE Sens. J.*, vol. 1, no. 1, pp. 14–30, 2001.

[23] H. T. Hahn and N. J. Pagano, "Curing Stresses in Composite Laminates," *J. Compos. Mater.*, vol. 9, no. January, pp. 91–106, 1975.

[24] G. Hu, S. Chew, and B. Singh, "Cure shrinkage analysis of green epoxy molding compound with application to warpage analysis in a plastic IC package," in *Proceedings of the Electronic Packaging Technology Conference, EPTC*, 2007, pp. 7–11.

Chapter 8

Conclusions & Recommendations

8.1. General conclusions

This thesis covers the various aspects involved in stress development in the microelectronics encapsulation (packaging) process which is investigated in five consecutive interdependent stages:

- The mechanical, thermal and kinetic behavior of the epoxy molding compound which is used as an encapsulant material in the packaging process is determined.
- The filling stage is studied thoroughly for free cavity and stacked die array models.
- An analytical approach for a two layer simple model is used to predict the residual stresses.
- A two dimensional simulation is conducted using a commercially available finite elements software package, in which the cure and cooling induced stresses are determined independently.
- A novel experimental approach for the stress estimation in packaging is designed and the previously determined analytical and numerical stress values are verified.

8.2. Conclusions on the experimental characterization and modeling of the EMC

Cure dependent and fully cured behavior of the epoxy molding compound is determined by the volumetric, kinetic and mechanical measurements using DSC, PVT, DMA and rheometer test set-ups. Reliability of the stresses is largely affected by the accuracy of the material models. Therefore, in this study two EMCs with different filler contents are analyzed and the one with the higher accuracy is selected to be used.

- Differential scanning calorimeter is used to characterize the kinetic behavior. The conversion degree as a function of time and temperature is determined by the multiple heating rate method (fig. 2.8).
- The cure rate is modeled by the autocatalytic Kamal and Sourour model (eq. 2.7) in which the model parameters are determined using the Friedman method (tab. 2.4).
- The model parameters are also verified using the heating scans of the partially cured samples which are heated for various curing times isothermally. Hence, the model parameters are double-checked (fig. 2.5) and a satisfactory fitting of the model representing the conversion of the EMC is obtained.
- A direct relationship between the degree of conversion and the glass transition temperature is observed in the isothermal DSC data which is modeled by the Di Benedetto fit (fig. 2.4).
- A linear model is proposed for the cure shrinkage based on the volumetric experiment conducted with an initially uncured sample curing isothermally above its T_g to full conversion. As a result 1.27% of total volume shrinkage is measured (fig. 2.13).
- CTE and bulk modulus of the fully cured EMC sample is determined experimentally by incremental pressure and temperature rise. The modified Tait model provided a fair fit to the temperature and pressure dependent specific volume change of the epoxy compound. The derivative of the specific volume modeled by the Tait equation with respect to temperature resulted in CTE and with respect to pressure yielded Bulk modulus (fig. 2.16).

8.3. Conclusions on the dynamic mechanical behavior of the EMC

- The DMA shear sandwich test of an initially uncured sample reveals that the modulus is negligibly small even after the gel point and therefore it is assumed that the stress relaxes fully below the gel point (fig. 6.2).
- Dynamic properties of the fully cured EMC as a function of frequency is determined by a heating scan in the tensile DMA test set-up (fig. 3.17-3.18). The

master curve (fig. 3.19) for the storage modulus in the transient region is modeled by the Prony series covering the range of 25 decades (tab. 3.2).

- The investigated thermosetting compound is assumed as thermo-rheologicaly simple and the time-temperature superposition principles is applied numerically using the reduced time concept (eq. 3.44-3.45) by the WLF and polynomial of second degree formulas for above and below T_g, respectively. This approach results in a much accurate numerical approximation of the transition region (fig. 3.20).
- Parallel plate viscometer at a constant frequency is used to determine the dynamic viscosity of the EMC which is liquid at higher temperatures below its gel point. By the Cox-Merz rule the dynamic data is converted to the steady state viscosity (eq. 3.42). And the data modeled by the temperature and conversion dependent Castro Macosko equation (eq. 3.39 and 3.43) leads to a satisfactory description of the viscosity (fig. 3.9).
- A new empirical based approach is implemented to determine the gel point. In this method the viscosity data is correlated to the degree of conversion using the previously obtained autocatalytic model and the gel point for each isothermal cure temperature is approximated as the unset of the last linear intersection in the "S" shape curve in the logarithmic plot (fig. 3.14). The average of these points is taken as the gel point, which is calculated as 45% for the corresponding EMC.

8.4. Conclusion on the encapsulation Analysis

- The filling stage of encapsulation process of the two different cavity geometries (fig. 4.2-4.3 and eq. 4.13-4.15) are simulated based on the Navier-Stokes equations (eq. 4.1-4.3) in Moldex 3D. The flow front advancement of the free cavity model is determined to be more symmetrical and smooth (fig. 4.4), while the void and air trap phenomenon is observed in stacked die encapsulation due to the flow retardation at the small gap regions between the dies and die-cavity gap (fig. 4.16).
- It is determined that for the studied temperature and initial conversion degree conditions, the effect of temperature is much dominant compared to the effect of conversion on the viscosity of the polymer melt (fig. 4.5-4.6). Hence, the wall shear stress is calculated to be higher for the lower temperature.
- The positions of the gates dictate the maximum pressure and conversion regions even in a simple cavity (fig. 4.9). Considering the delicate components that are supposed to be protected by the encapsulation, they may be affected by the improper selection of the gates.

- The stacked dies at the gate front region are more vulnerable to higher conversion and higher viscosity (fig. 4.17).

8.5. Conclusions on the numerical analysis of the residual stresses

- The stress study is done by splitting the whole process in two stages of cure and cooling (fig. 5.1). The constitutive modeling at each stage is based on the process conditions, degree of conversion and the boundary conditions surrounding the epoxy polymer.
- In analytical stress study it is assumed that during curing the curvature and plain strain of the whole package is in its initial state due to the constrained boundary condition imposed by the mold platens. Whereas the boundary conditions are assumed free after the mold release that indicated the start of cooling period.
- In analytical model the stress in cure stage is assumed as cure shrinkage induced, and in cooling stage it is taken as a function of temperature. The cure shrinkage is modeled by a linear equation (eq. 5.30) and the modulus is determined using the Adolf and Martin scaling theory (eq. 5.9). The cooling induced shrinkage and modulus change, on the other hand, are calculated based on the Tait model (eq. 2.21-2.23 and 6.15).
- The mechanical behavior of the thermosetting polymer during cooling is assumed to be viscoelastic in the numerical simulation which is performed by Comsol Multiphysics software package.
- The two dimensional numerical model comprised all of the five layers designed for the molding experiment (fig. 6.3), whereas the analytical model is based on a bilayer composition (fig. 5.2).
- The cure and cooling induced residual stresses are calculated for four process conditions at which three of these are dictated based on the experimental molding conditions (tab. 5.2). The cooling induced residual stresses are calculated to be much larger than the cure induced stresses in all testing conditions. The maximum curing induced stress is determined in 140^{o}C simulation as 0.73MPa by the numerical model. Likewise, the maximum cooling induced stress is obtained as 16MPa.
- The stress maxima are obtained at the chip edges and center. The minimum values, on the other hand, are detected in between these two peak points (fig. 6.8, 6.9, 6.13, 6.14, 6.17, 6.18, 6.21 and 6.22).
- The EMC is never fully reacted at the end of cure stage in any of the studies (tab. 6.2).

8.6. Conclusion on the experimental analysis of the molding process

- The microchips with 36 piezoresistive stress measuring elements (fig. 7.1) are used to measure the stress variations during the packaging process. The in-plane normal and shear stresses along with the temperature can be measured by these chips.
- The chips are connected to the polyimide boards which are designed specifically to measure the stresses during the whole encapsulation process (fig. 7.3). The flexible polymeric material of the board let us to monitor the data during the molding when the cavity is clamped. The chip connections which are sandwiched between the PI layers are extended to the outside of the cavity and connected to a PC for data acquisition.
- The stages of the molding are determined by analyzing both the temperature and stress data (fig. 7.7-7.8). The filling stage stresses are difficult to obtain due to the lower sensitivity of the chips. The cure and cooling stages stresses are determined independently and comparison of the stresses with the analytical and numerical ones showed that the results are verifiable for each molding and material conditions.
- The chips should be used at atmospheric pressure to be able to determine the in-plane normal stresses. If the chips are subjected to compressive force the results are not reliable.
- The similar pattern of stress distribution on the chip surface which is obtained using the finite elements simulation is determined by the experiments as well (fig. 7.9, 7.10, 7.11, 7.12, 7.13, 7.14).
- The chips are unresponsive above 160^{o}C. As a result, the standard transfer molding which is conducted mostly at 175^{o}C cannot be studied by the chips used in this study.
- The highest cure temperature of 160^{o}C yielded the maximum cure induced residual stress of 1.3MPa (fig. 7.13) and cooling induced stress of 22.5MPa (fig. 7.14). These maximum stresses in both stages which are obtained at the chip's surface edges agree well with the numerically simulated (fig. 6.17-6.18) and analytically calculated (fig. 5.14) stresses.
- In all of the molding experiments the measured in-plane stresses in cure stage are 5% of the cooling induced stresses. This pattern is confirmed by the instantaneously elastic and viscoelastic 2D numerical studies as well.

8.7. Recommendations, highlights and limitations

- Among the model free iso-conversion methods the Friedman method provided the most accurate estimation of the activation energy and hence the most reliable representation of the kinetic model.
- Curing reaction of the polymer is assumed to be the main factor in stiffness build-up during the isothermal cure stage. The transient time dependent response of the material is neglected. The consequences of this assumption are assumed to be negligible. However, a cure dependent viscoelastic model can be implemented if the cure temperature is below the equilibrium plateau.
- The Poisson's ratio is calculated to be temperature dependent based on the interrelation of the material function (fig. 5.4).
- In this study it is clearly shown that the reliable material models provide a fair prediction of the stresses even using a simple constitutive modeling approach without considering the viscoelastic behavior of the encapsulant.
- Viscosity of a thermosetting polymer is found to be the most difficult property to be modeled. In this thesis, various testing techniques have been implemented including the slit viscometer, shear sandwich and parallel plate test setup to provide a fair estimation for the viscosity of the EMC during filling.
- Stacked repetitive array of dies would lead to air traps during filling (encapsulation). The gates would be designed in different arrangements, positions and shapes to reduce the risk of air traps. Moreover, the longer the filling time, the higher the risk of air traps due to the higher viscosity.
- The flow front advancement can also be detected experimentally by connecting multiple chips such that they are distributed on the surface of the board in the cavity.

Samenvatting

Thermohardende polymeren worden vaak gebruikt om micro-elektronische componenten te verpakken vanwege hun unieke mechanische, thermische en elektrische eigenschappen. De term verpakken wordt gebruikt voor het proces van vullen en inkapselen van geïntegreerde schakelingen. Het proces veroorzaakt restspanningen, zowel tijdens fabricage als tijdens de cyclische thermo-mechanische belasting gedurende de functionele levenscyclus van de elektrische en de electro-mechanische schakelingen die ingekapseld zijn binnen de genoemde verpakkingen.

In deze studie zijn de spanningen veroorzaakt door het vullen en inkapselen onderzocht door het proces in drie stappen op te delen: viskeus vullen, isothermisch uitharden en afkoelen. De residuele spanningen worden geïnitieerd door crosslinking(uitharden) van het epoxy polymeer. Crosslinking is een eigenschap van de thermohardende polymeren en is gekoppeld aan een verhoging in stijfheid en een volume krimp. Het process van inkapselen vindt op een hoge uithardingstemperatuur plaats (± 175^{o}C). De navolgende afkoeling tot de omgevingstemperatuur leidt tot het verder krimpen van het materiaal samen met de overige ingekapselde componenten in de verpakking. De mechanische eigenschappen van het uitgharde polymeer veranderen dan van een rubberachtige toestand naar een glasachtige toestand.

Het inkapselprocess gebeurt met het “transfer molding” process waarbij de epoxy op een hoge temperatuur smelt en in een mal geperst wordt waar de chip en het substraat zich bevinden.

De vroegste studies naar restspanningen waren gebaseerd op tijdrovende trial-ad-error methodes. Deze inefficiënte en oude methoden zijn tegenwoordig vervangen door meer betrouwbare numerieke methoden. Door gebruik te maken van deze methoden kunnen restspanningen sneller, en kosten effectiever worden voorspeld. Door een parametrische analyse te gebruiken kunnen deze spanningen verminderd worden in iedere fase van het inkapselproces. Om dit virtuele prototyping op een betrouwbare manier te kunnen doen is een betyrouwbare representatie van het materiaalgedrag van het polymeer nodig. Het tijd, temperatuur en conversie afhankelijk gedrag van de epoxy molding compound (EMC) wordt in dit proefschrift experimenteel bepaald. De kinetische karakterisatie van de EMC is

verkregen na enkele verwarmingssnelheid scans van niet-verharde samples in een DSC (differential scanning calorimeter). Het autocatalytisch model van Kamal en Sourour wordt gebruikt om de conversiesnelheid van de gemeten data te modelleren. Daarnaast, wordt de conversie-glastransitie relatie vastgelegd door isothermisch verharde monsters te scannen met constante opwarmsnelheid. De totale volumekrimp wordt bepaald met een PVT-test waarin een EMC monster wordt verhit en vervolgens isotherm uitgehard op een temperatuur dichtbij de glasovergangstemperatuur. De specifieke volume verandering tussen het begin en het eind van het uithardingsproces wordt beschouwd als de totale uithardingskrimp. Het combineren van het kinetisch model en de volumekrimp data laat zien dat de krimp nagenoeg lineair met de conversie is. De uitzettingscoëfficiënt en bulkmodulus van het zelfde monster worden ook bepaald met het PVT apparaat. Een gemodificeerde versie van het Tait model wordt gebruikt om het verandering in volume als functie van druk en temperatuur in een model vast te leggen.

De eerder genoemde volumekrimp van het thermohardende polymeer gaat gepaard met variaties in mechanische eigenschappen. De epoxy is, in het begin van het proces, een cilindrische pellet die na opwarmen verandert in een laag viskeuse vloeistof. De lineaire groei van ketens wordt gevolgd door vertakking en crosslinking. Tijdens het proces van polymerisatie neemt het molekuulgewicht van de EMC toe. Op een bepaald punt verliest de polymeer de eigenschap om te vloeien en wordt een rubberachtige gel. Dit stadium wordt het gelpunt genoemd en voorbij dit punt relaxeert een deel van het de volumekrimp spanningen niet meer. De overgebleven spanning in de uitgeharde epoxy wordt ook wel de restspanning genoemd en bouwt zich op tijdens het uitharden en het koelen. Het gelpunt en de viscositeit van de EMC tijdens het uitharden zijn gemeten in een parallele plaat viscometer. Het bepalen van het gelpunt wordt in deze studie niet gedaan op basis van het kruisen van de opslag- en verliesmodulus curves maar er wordt een nieuwe methode voorgesteld die gebaseerd is op de vorm van de logaritmische viscositeits-conversiecurve. Deze benadering zorgt voor een reproduceerbare bepaling van de gel conversiegraad, onafhankelijk van de test temperatuur.

Een thermohardend polymeer zal zich anders gedragen bij verschillende verwerkingscondities en initiele conversieniveaus. Helaas zijn de materiaal datasheets die vaak door materiaalleveranciers verstreken worden ontoereikend in het laten zien van het totaalplaatje. Daarom zijn betrouwbare materiaalmodellen en de bijbehorende parameters een essentiele onderdeel voor een goede numerieke analyse van de verschillende processtappen. Nu, moet nog de vraag van nauwkeurig constitutief modelleren van de complete inkapselproces beantwoord worden. Het transfer molding proces bestaat uit een vul- uithardings- en koelfase en voor elk van deze stappen zullen de restspanningen moeten worden bepaald.

De schuifspanning van de epoxy smelt tijdens de vulfase kan worden berekend door uit te gaan van een newtonse vloeistof met conversie- en temperatuur afhankelijke viscositeit. De progressie van de vloeigrens is voor twee verschillende matrijsgeometriën berekend voor een aantal geselecteerde posities. De eerste geometrie is gebaseerd op de experimenele opzet die later in deze studie gebruikt wordt om de berekeningen te valideren. De tweede is een geometrie met twee gestapelde die in de industrie gebruikt wordt om de dichtheid van IC's te vergroten. In de simulaties worden de viscositeit van de epoxy smelt, afschuifsnelheid en afschuifspanningen aan de oppervlak van de matrijs en de substaat berekend alsmede de conversie en drukverdeling aan het eind van het vullen. Hieruit blijkt dat de kleine ruimte tussen de IC's de zwakke plekken zijn die gevoelig zijn voor ingesloten lucht door het langzame vulproces in deze gebieden. Deze lokale trage vulling resulteert in een hogere conversie en viscositeit.

Daarnaast is een versimpeld analytische model gebruikt om de uithardings- en afkoelspanningen te voorspellen. Hierin is aangenomen dat in de uithardingsfase het materiaal rubber-elastisch is met een conversie afhankelijke modulus. Dit is gemodelleerd op basis van de Adolf en Martin schalingstheorie. In de koelfase is uitgegaan van een constante modulus en een temperatuur afhankelijk uitzettingscoefficient die gebaseerd is op het bovengenoeme Tait model.

Daarna is een simulatie gedaan van een twee-dimensionale geometrie van een productconfiguratie bestaande uit een printplaat, lijmlaag, chip en epoxy molding compoud. In deze simulaties is in de koelfase het materiaal gemodelleerd als viscoelastisch, gebaseerd op het generalized Maxwell model. Vergelijking met voorspellingen van het analytische model laten zien dat de berekende restspanningen vergelijkbaar zijn.

Voor de experimentele verificatie is een nieuwe meettechniek gebruikt waarbij een stress chip wordt ge-encapsuleerd en de spanningen in-situe worden gemonitord. Hieruit bleek dat de stress chip bij de hogere temperaturen geen reproduceerbare resultaten produceerde maar voor de lagere temperaturen wel in staat was de spanningen tijdens vullen, uitharden en afkoelen te meten en dat bleef doen nat het openen van de matrijs. De normaalspanningen tijdens elk van de procesfases bleek goed overeen te komen met de voorspellingen van zowel het analyisch als het numerieke model.

Acknowledgments

I would like to take this opportunity to express my gratitude to all the people who have contributed to the completion of the research work in this thesis. First of all, I would like to express my sincere gratitude to my promotor, Prof. Kaspar M. B. Jansen for offering me the opportunity to conduct this PhD project. I am thankful for his guidance and support on every stage of this thesis, especially on coding and algorithm development which forms the backbone of this thesis, and for the many fruitful discussions we have had on evaluation and interpretation of the numerical and experimental data. His suggestions encouraged me to look for the many aspects of the matter and to cover the research much further than originally intended in the first place. I would like to express my gratitude to my promotor, Prof. Leo J. Ernst for his invaluable support and guidance during this thesis. I am thankful for the many challenging discussions which contributed to the finalization of this project.

I would like to thank Prof. A. Wymyslowsky, Prof. D. Yang, Prof. U. Staufer and Prof. G.Q. Zhang for accepting to be member of my defense committee and for reviewing my thesis.

I am highly indebted to Henk Wensink and Hans Venrooij from Besi, for their exceptional contributions in the early stages of this project and later on for their efforts during the setup of the molding measurements which were conducted at Besi's facilities. The technical supports of Frans de Vries and Chris Brouwer from Fico/Besi during the viscosity and molding experiments were also highly valuable and appreciated.

My special thanks to Florian Rost and Florian Schindler Saefkow. The molding measurements cannot be accomplished successfully without their skills and technical knowhow.

The design of the verification experiment is a significant milestone in this thesis. I owe a big thank to Amar Mavinkurve for his invaluable ideas and cooperation on wire bonding. I am also thankful to Peter Koch who performed all the chip to board connections manually that required a lot of time and effort.

My sincere thanks to Harry Jansen, Patrick van Holst, Rob Luttjeboer and Jos van Driel from 3ME for their technical support in material characterization experiments.

I am especially indebted to Will de Haas from Philips Innovation services at High Tech Campus for his contribution in the rheological characterization experiments that required promptness and high accuracy.

I would like to thank to my colleagues Jan de Vreugd, Xiaosing Ma, Muhammad Akram, Mahdi Sadeghinia, Berkan Ozturk and John Suman Nakka. They all contributed to the enjoyable work environment.

I am particularly grateful to Mecnun and İskender Çınar, Ismail, Erdal, Yavuz and Muhittin whose moral support helped me get through my years in Delft.

I wish to heartily thank my loving and thoughtful wife, Nil. I am thankful to her for being by my side even through the hardest times when I lost all my energy and hope.

I am deeply indebted to my parents Davud and Betül Rezaie Adli for their constant encouragement, inspiration and support not only during my PhD but throughout my whole life. Very special thanks to my beloved sister for having to shoulder more responsibility in my absence.

Last but not least, I would like to express my appreciation to all friends. I am especially thankful to Argun Cencen for translating the propositions and the summary in Dutch in a very short notice. Many thanks to my hard working friends Umut and Muammer for their friendship and help in this period. We were the night-workers of the department (sometimes till midnight), but I am not sure if that really paid off. And a special thanks to Hamed for his hospitality and support in my first year in Delft.

I have had so many memorable moments, especially in the first half of my PhD. Thanks to my friends Deniz, Vania, Cuzde, Sinan and Olgu for being the part of my PhD journey that was full of ups and downs like an emotional roller coaster ride. I will miss the coffee breaks, dinners and game nights we had together.

Ali R. Rezaie Adli

Curriculum Vitae

Ali R. Rezaie Adli was born in Tabriz on February 14, 1979. He completed his secondary education at Yeşilköy 50th year high school in Istanbul, Turkey. He enrolled in the mechanical engineering department in Boğaziçi University and received the "Bachelor of Science in Mechanical Engineering" in 2005. He pursued his Master's degree in mechanical engineering at the same university in the following year. In 2008 he received the "Master of Science in Mechanical Engineering" by completing his research project on "Computational Investigation of Non-Isothermal Lid-Driven Flow in Arc-Shape Cavities". In late 2009 he was employed as a PhD researcher in Technical University of Delft. The research which was a part of larger EU project "Jemsip-3D" was funded by ENIAC (European Nanoelectronics Initiative Advisory Council).